Cranfield University

Ahmed Abdullahi Shinkafi

Development of a Method to Study Aircraft Trajectory Optimisation in the Presence of Icing Conditions

SCHOOL OF ENGINEERING

Department of Aerospace Engineering

PhD Thesis

Supervisor: Dr. Craig Lawson

November 2015

Cranfield University

Ahmed Abdullahi Shinkafi

Development of a Method to Study Aircraft Trajectory Optimisation in the Presence of Icing Conditions

SCHOOL OF ENGINEERING

Department of Aerospace Engineering

PhD Thesis

Supervisor: Dr. Craig Lawson

November 2015

This thesis is submitted in partial fulfilment of the requirements for the degree of Doctor of Philosophy

"The most important thing about global warming is this. Whether humans are responsible for the bulk of climate change is going to be left to the scientists, but it's all of our responsibility to leave this planet in better shape for the future generations than we found it."

Mike Huckabee[1]

[1]Mike Huckabee was the 44th Governor of Arkansas, and a candidate for U.S. president in the 2016 election.

–Dedicated to the Memories of My Father

Abstract

There is a growing demand for new technologies and flight procedures that will enable aircraft operators to burn less fuel and reduce the impacts of aviation on the environment. Conventional approaches to trajectory optimisation do not include aircraft systems in the optimisation set-up. However, the fuel penalty due to aircraft systems operation is significant. Thus, applying optimised trajectories which do not account for systems off-takes in real aircraft Flight Management System (FMS) will likely fail to achieve a true optimum. This is more important in real scenarios where the ambient conditions influence the systems operation significantly. This research proposed an ice protection methodology which enables the development of a decision making process within the FMS dependent on weather conditions; thus transforming the conventional anti-icing method into a more intelligent system.

A case of a medium size transport aircraft flight from London - Amsterdam under various levels of possible icing was studied. The results show that fuel burn due to anti-icing operation can increase up to 3.7% between climb and cruise altitudes. Up to 5.5% of this penalty can be saved using icing optimised trajectories. A 45% reduction in awakenings due to noise was achieved with 3% fuel penalty. The novelty of the study was extended using 3D optimisation to further improve flight operations. It was found that the simulation successfully changed the lateral position of the aircraft to minimise the time spent and distance covered in icing conditions. The work here presents a feasible methodology for future intelligent ice protection system (IPS) development, which incorporates intelligent operation.

Acknowledgments

My first and foremost gratitude goes to the Almighty Allah for protecting me and granting me the health and ability to carry out this project. A special thanks goes to my supervisor, Dr. Craig Lawson, for his support and encouragement in this research work. This work would have been a nerve-racking experience without his continuous guidance and unreserved availability. His nice, friendly and ever smiling reassurances were a great source of motivation for me throughout the period of this work. I will also thank Profs Marin Guenov, Howard Smith, James Whidborne and David Mba for their support and guidance. I will also like to thank Dr. Roger Gent for finding time to answer my questions on the two occasions I visited him at his AeroTex UK office.

I have made many friends in Cranfield University and the Clean Sky team such as Dr Irfan Madani, Dr. Mudassir Lone, Dr. Devaiah Nalianda, Dr. Michael Cooper, Ravinka Seresinhe, Daniele Quaglia, Rukshan Navaratne and Farah Hashim. I will like to thank them for their individual contributions. A special thanks to you Ravinka; your invaluable assistance in GATAC simulation and Statistica post-processing has significantly improved the quality of this work. Thank you too Kryssy Zielinska for your assistance in proof reading the thesis. I am also grateful to the Nigerian Air Force for sponsoring most part of this research work, and the Clean Sky-JTI for providing part funding. A reserved special thanks goes to my family for supporting and encouraging me throughout the course of this work. Last but not the least, my thanks goes to both academic and non-academic staff of Cranfield University and those that I could not mention in this acknowledgment. The contributions of all of you are highly appreciated.

Table of Contents

List of Figures

List of Tables

Nomenclature

Symbols

α - Wing body setting angle (deg)

β - Local catch efficiency (dimensionless)

λ, k_0 - Thermal conductivity of air ($W/m.K$)

λ_A - Geodetic angle (deg)

μ - Absolute viscosity of air ($kg/s.m$)

μ_A - Bank role angle (deg)

μ_{icing} - Viscosity of air in icing condition ($kg/s.m$)

ρ_i - Density of ice (kg/m^3)

φ_A - Geodetic latitude (deg)

γ - Air specific heat ratio (dimensionless).

γ_A Flight path angle (deg)

χ_A - Heading angle (deg)

$\triangle H_{f,ice}$ - latent heat of fusion of ice (J/kg)

Where d_h,c_h and denote the heater thickness, specific heat capacity and density respectively.

where d is the ice thickness, and ρ_i are the and density of ice respectively.

ΔL_{fice} - Latent heat of fusion of ice (kJ/kg)

ΔT - Temperature difference (℃)

Af - Windscreen frontal area (m^2)

$C_{L_{max}}$ - Maximum lift coefficient (dimensionless)

c, C_p - Specific heat $(J/kg.K)$

c_h - Heater thickness (m)

d_i - Ice thickness (m)

d_{med} - Median droplets size (μm)

D - Drag magnitude (N)

DRR - Droplets range ratio (dimensionless)

e - Saturation pressure (hPa)

E_m - Overall collection efficiency (%)

f - Freezing rate (dimensionless)

g - Gravitational acceleration m/s^2

h - Altitude (ft)

h_0 - Local heat transfer coefficient $(W/K.m^2)$

h_proj - Aerofoil projected height (m)

h_s - Skin Heat transfer coefficient $(W/K.m^2)$

i, h - Subscripts i and h refer to ice and heater

K - Inertia parameter (dimensionless)

K_0 - Modified inertia parameter $(dimensionless)$

L - Aerofoil chord length (m)

L_e - Latent heat for water evaporation (kJ/kg)

L_{MAC} - Mean Aerodynamic Chord Length(m)

LWC - Clouds liquid water content (g/m^3)

m_{ac} - Mass of the accreted water (kg)

$m_{e,s}$ - Mass of the evaporated or sublimated water (kg)

m_{im} - Mass of the impinging water droplets (kg)

m_{in} - Mass of the runback-in water (kg)

m_{out} - Mass of the water (kg)

m_{ws} - Total water catch of windscreen ($kg/s.m^2$)

$\dot{m}_i$ - Icing rate (kg/s)

MVD - Medium Volumetric Diameter (μm)

m_w - Water mass flow rate (kg/s)

Nu - Nusselt number (dimensionless)

OAT - Outside Air Temperature (K)

P_∞ - Ambient pressure (Pa)

Pr - Prandtl's number (dimensionless)

q - Heat flow rate (kW) q_{ac} - Heat lost due to accretion

q_{air} - Heat lost due to airflow

$q_{e,s}$ - Heat lost due to evaporation or sublimation

q_{con} - Heat lost due to convection

q_{fri} - Heat gained due to the viscous or frictional heating in the boundary layer

q_{im} - Heat lost due to warming of the impinging droplets

q_{in} - Heat lost due to runback-in water

q_{ke} - Heat gained due to the kinetic energy of the impinging droplets

q_L - Heat gained due to the release of the latent heat of fusion

$\dot{q}$ - Power density (kW/m^2)

r - Recovery factor applying to kinetic heating (dimensionless)

R_c - Boundary recovery factor ($dimensionless$)

Re - Reynolds number ($dimensionless$)

Re_d - Droplets Reynolds number ($dimensionless$)

Rh - Relative humidity (%)

S_0 - Reference protected area (m^2)

S_L - Lower surface limit (m)

S_U - Upper surface limit (m)

t_{es} - Equilibrium surface temperature (K)

t_{ice} - Ice thickness to be melted (m)

t_{in} - Temperature of in-coming water (K)

t_{out} - Temperature of runback water (K)

t_s) - Surface temperature K

T - Temperature $(K,)$

T_A - Thrust magnitude (N)

t_{icing} - Time in icing encounter (s)

T_m - Melting temperature (℃)

T_{sk} - Skin temperature (℃)

V_∞ - Free stream air speed (kt)

V_{CAS} - Calibrated air speed (kt)

V_{TAS} - True air speed (kt)

w_{m_total} - Total mass of water collected per unit length (g/m)

x - Characteristic length (m)

X - Runback rate kg/s

Abbreviations

ACARE - Advisory Council for Aeronautics Research in Europe

ADF - Aircraft De-icing Fuids

ADM - Aircraft Dynamics Model

ADS-B - Automatic Dependent Surveillance-Broadcast

AFIT - Air Force Institute of Technology

AI - Anti-icing

AIPS - Active Ice Protection Systems

AIR - Aerospace Information Reports

AITA - International Air Transport Association

AMS - Sciphol Amsterdam Airport

ASM - Aircraft Systems Model

ATC - Air Traffic Control

ATFM - Air Traffic Flow Management

ATM - Air Traffic Management

ATS - Air Traffic Services

AWR - Airborne Weather Radar

BADA - Base of Aircraft Data

CAA - Civil Aviation Authority

CARATS - Collaborative Action for Renovation of Air Transport Systems

CFD - Computational Fluids Dynamics

CM - Continuous Maximum

CO-ATM - Co-Operative Air Traffic Management

DERA - Defence Evaluation and Research Agency

DoC - Direct Operating Costs

EASA - European Aviation Safety Agency

ECS - Environmental Control System

ED - Eco-Design

EEDS - Electro-Expulsive De-icing System

EESS - Electro-Expulsive Separation System

EIDI - Electro-Impulsive De-Icing

EMEDIS - Electro-Mechanical Expulsive De-icing System

FAA - Federal Aviation Authority

FMS - Flight Management System

GATAC - Greener Aircraft Trajectories under ATM Constraints

GHG - Greenhouse Gas

GPS - Global Positioning System

GR - Green Rotorcraft

GRA - Green Regional Aircraft

GUI - Graphic User Interface

HTEMS - Hybrid Thermal-Electro-Mechanical Simulation

HYOP - Hybrid OPtimiser

ICAO - International Civil Aviation Organisation

IFR - Instrument Flight Rule

IHB - Internal Heat Balance

IIPS - Intelligent Ice Protection System

IM - Intermittent Maximum

INS - Inertial Navigation System

IPS - Ice Protection System

ITD - Integrated Technology DEmonstrator

JPDO - Joint Planning and Development Office

JTI - Joint Technology Initiative

LHR - London Heathrow airport

LPED - Low Power Electro-thermal Deicer

MOGA - Multi-objective Genetic Algorithm

MOTS - Multi-objective Tabu Search

MTM - Management of Trajectory and Mission

NASA - National Aeronautics and Space Administration

NextGen - Next Generation Air Transport System

NGATS - Next Generation Air Transportation System

NOAA - National Oceanic and Atmospheric Administration

NPGA - Niched Pareto Genetic Algorithm

NPR - Noise Preferential Routes

NSGA - Non-Dominated Sorting Genetic Algorithm

NSGAMO - Non-dominated Search Genetic Algorithm Multi-objective Optimiser

NTSB - National Transport Safety Board

ONERA - Office National d'Etudes et de Recherches Aérospatiales

PBN - Performance Based Navigation

PIPS - passive ice protection systems

RAE - Royal Aerospace Establishment

RM-MEDA - Regularity Model Based Multi-Objective Estimation of Distribution Algorithm

RNAV - Area Navigation

RNP - Required Navigation Performance

SAE - Society for Automotive Engineering

SESAR - Single European Sky ATM Research

SID - Standard Instrument Departure

SLD - Super-cooled Large Droplets

SFWA - Smart Fixed-Wing Aircraft

SGO - System for Green Operation

SGE - Sustainable and Green Engines

SPEA - Strength Pareto Evolutionary Algorithm

STAR - Standard Terminal Arrival Route

TBO - Trajectory Based Operation

TMEDS - Thermo-Mechanical De-icing System

UIUC - University of Illinois Urban-Champaign

VEGA - Vector Evaluated Genetic Algorithms(VEGA)

VFR - Visual Flight Rule

WP - Way Point

Chapter 1

Introduction

Chapter 1 gives an overview of the research problem which is the effects of in-flight icing on aircraft energy usage and air quality of the environment. It also gives insight into the causes of in-flight icing and the level of losses it causes in terms of air transport resources and human lives. Thus, a case was made for the study in terms of the growing demand for new technologies/flight procedures that would minimise fuel burn and the impacts of aircraft emissions on the environment. The chapter further specifies the objectives and relevance of the study with respect to future Air Traffic Management (ATM) system.

1.1 Research Problem

Ice build-up on airframe surfaces disrupts the lamina flow of the air thereby decreasing the aerofoil's ability to generate lift. In many occasions aircraft icing have resulted in fatal air incidents. A total of 135 aircraft were involved in air crash due to icing encounter between 1993 and 2005 [28]. In the US alone, 228 icing related accidents occurred from 2006 to 2010 [29]. Major disasters caused by in-flight icing includes the October 31^{st} 1994 air crash involving an ATR72 regional airliner, and the 9^{th} of January 1997 crashing of Embraer EMB-120 in which all persons were killed. In a more recent development, a British Airways Boeing777 crashed at Heathrow on the 17^{th} of January

2008 due to ice accretion on cold surfaces, and the ATR42-320 regional airliner that crashed during approach to landing under freezing drizzle conditions at the Lubbock Airport Texas in 2009 (see Fig. 1.1) [30].

Fig. 1.1: Lubbock TX-ATR42-320 accident of 27 January 2009 [1]

Air mishap due to in-flight icing has become a reoccurring decimal and increasingly so in recent times. It is reported that nearly 10% of air disasters involve aircraft icing, Martenez [31]. Hence, in-flight icing has been on the National Transport Safety Board (NTSB) most wanted list of safety improvements from 1997 to 2011, NTSB [30].

Despite the risk imposed by in-flight icing, the current drive for ultra efficient propulsion systems in modern aircraft demands reduction in the amount of engine bleed air available for secondary power usage. By implications, all modern aircraft must accept some ice accretion on tolerant areas as part of a design compromise. Thus, typically, wing tips and roots may be left unprotected. However, the NASA study TM83564 [32],

shows that close to 50% of the total drag associated with icing remains after all protected surfaces were cleared. This 50% drag comes from unprotected surfaces such as flap hinges, control horns, fuselage frontal area, windscreen wipers, wing struts, fixed landing gear, antennae, etc. This indicates that the classical (thermal, mechanical and chemical) methods of protecting aircraft against in-flight icing are not as efficient as required. This poses three major research problems.

The first problem has to do with the current means of powering aircraft. Presently, transport aircraft depend mainly on fossil fuels and turbine technology for propulsion. Therefore secondary power off-take due to aircraft systems such as IPS further exacerbates fuel burn and associated emissions. In effect, this means extra weight, extra fuel burn and more environmental pollution. The second problem arises from the growing demand for air transport in recent years. The current increase in demand for air transport is pushing aircraft operators towards all weather operations, which the conventional methods may not be able to meet. At present, thermal anti-icing method is the leading ice protection technology on most of today's medium and large size transport aircraft. A large business aircraft requires between 200-400 kW bleed power for wing and engine ice protection, and a limited amount of electrical energy for windscreen and probes protection. Considering the negative impacts of such power off-takes on engine performance, certain tolerant parts of the aircraft such as the tail plain are left unprotected in many large transport aircraft, Gent et al [23]. This creates an inefficiency within the system due to the fact that the tail plane must to be over sized in order to cope with ice accretion thereby resulting in increased parasite drag. Thus, the efforts for ultra efficient propulsion systems in modern aircraft and the consequent reduction in the amount of engine bleed air available for ice protection is counteracted by the extra weight and drag imposed by the over sized structure.

The last research problem which is dealt with in the current scope, boarders on the inefficiency of the conventional aircraft trajectory methods under real adverse weather situations. The conventional approaches to trajectory optimisation do not take the effect of secondary power off-take into account. Neglecting these effects may be inadequate, especially when one considers the proportion of aircraft operations that have to be taken in real weather scenarios such as icing conditions. With reference to the above discussed problems, it can be noted that transport aircraft use hydrocarbon fuels inefficiently on non-weather optimised aircraft trajectories causing excessive fuel burn and emissions particularly in weather conditions such as icing. Therefore there arises the need for a more efficient, greener and safer method for dealing with in-flight icing risk.

1.2 Proposed Solution

In the past, efforts to reduce air transport costs and the negative impacts to the environment have been primarily focused upon aircraft and engine design optimisation. This led to the design of advance and efficient aircraft and power plants. The focus is now shifting towards Trajectory Based Operations (TBO) as one of the most significant solutions for achieving greater overall air transport efficiency. Using today's cutting edge technologies such as the Automatic Dependent Surveillance-Broadcast (ADS-B), Performance Based Navigation (PBN) and shared network-enabled real time weather data links, TBO could be employed for more efficient operations in icing conditions. Thus, transforming the conventional ice protection method into a more intelligent system where the amount of energy used can be controlled based upon the mission's operating conditions. In the present work, a method has been developed in which a huge improvement can be realised by operating aircraft at low power levels by incorporating icing conditions in

aircraft trajectory optimisation schemes. The ability to fly trajectories optimised for aircraft performance in real weather scenarios would greatly reduce unnecessary fuel consumption and associated green house gas (GHG) emissions. The details of the work cover the development and validation of a tool for estimating the total anti-icing (AI) system power and a theoretical analysis of the effects of icing parameters on AI energy to establish critical cases for the study. The core of the study encompasses simulation of optimised aircraft trajectories in order to assess the fuel penalties, emissions and noise impacts to the environment.

1.3 Objectives of the Research

The primary objective of this work is to develop a consistent and cohesive strategy for managing in-flight icing in a future Air Traffic Management (ATM) environment. This approach would enable a greater efficiency in flight planning, and use of optimised aircraft trajectories. It could also be used to investigate other efficient ways to operate aircraft in icing conditions. Furthermore, this approach shall develop a tool for estimating anti-icing power requirements for a controllable IPS operation so that potential savings associated with routing could be investigated.

To achieve the above objective, a concept for controllable IPS has to be developed for trajectory optimisation in icing conditions. This is necessary as the conventional approaches to trajectory optimisation do not take into account the effect of aircraft systems power off-take. With this, the possibility of minimising IPS power demand based on routing in icing conditions could be investigated. Secondly, a tool had to be developed in MATLAB/Simulink environment for simulating anti-icing power requirements under

a wide range of icing conditions. The model was integrated with GATAC[1] for independent assessment of fuel penalty and emissions due to IPS operation. This was necessary in order to demonstrate environmental gains that can be achieved by flying optimised routes. Thirdly, to achieve the above objectives, a sensitivity analysis had to be carried out on the various parameters affecting AI energy in order to determine the most critical icing conditions with regard to anti-icing power requirements. Lastly and most importantly, selected multi-objective aircraft trajectory optimisation cases were simulated to assess the impacts of flying trajectories obtained with and without consideration to the icing conditions on fuel burn, emissions and noise.

1.4 Motivation for the Research

Aviation has become an important instrument for economic growth which resulted in a global rise in demand for air transport services. Based on the current annual projection of about 5%, the annual passenger total is expected to increase from 3.1 billion in 2013 to 6.4 billion by 2030 [33]. Aircraft emit gases and particles directly into the atmosphere where they impact negatively on the environment. These gases and particles alter the concentration of atmospheric greenhouse gases, including carbon dioxide (CO_2), carbon monoxide (CO), ozone (O_3), water vapour (H_2O) and methane (CH); trigger formation of condensation trails (contrails); and may increase cirrus cloudiness - all of which contribute to climate change [2].

The CO_2 is a product of complete combustion and a key component of the greenhouse gases. It is estimated that more than 300,000 tonnes of CO_2 are generated per day from aircraft operations in Europe [34]. The CO_2 depletes the ozone layer thereby by causing

[1]Greener Aircraft Trajectories under ATM Constraints- a tool which has been developed by Cranfield University Clean Sky Reserach team, see section 3.2.3

global warming. Although emissions due to air transport account for only 2% of CO_2 emissions through the burning of fossils fuels, it is expected to increase to 3% by 2050 with the continuous and steady growth of air traffic [35]. Consequently, the Intergovernmental Panel on Climate Change (IPCC) developed a range of scenarios, IS92a-f, [2], for future greenhouse gases and aerosol precursor emissions based on assumptions concerning population and economic growth, land use, technological changes, energy availability, and fuel mix during the period 1990 to 2100. The study [2] shows that global emissions of CO_2 by aircraft were 0.14 Gt C/year in 1992 which is about 2% of total anthropogenic CO_2 emissions in 1992. It is projected that aircraft emissions of CO_2 will continue to grow and by 2050 will be 0.23 to 1.45 Gt C/year [2] as shown in Fig. 1.2. The right-hand side scale of the figure represents a projected percentage growth of global aviation CO_2 given in Tables 1.2 and 1.1.

1.2.

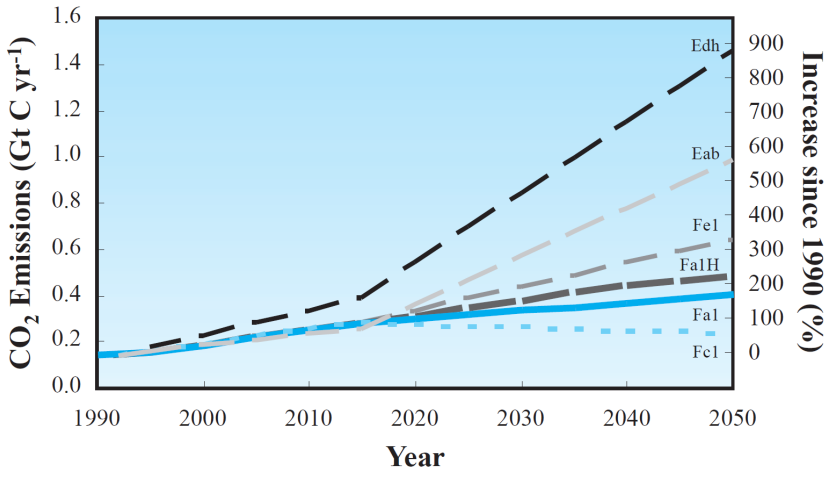

Fig. 1.2: Total Aviation CO_2 Emissions from Six Different Scenarios for Aircraft Fuel Use [2]

The Nitrogen-Oxide (NOx) is produced by the engine from the reaction of Nitrogen and air during high temperature combustions. The global NOx emissions from sub-

Table 1.1: Definitions of the IPCC Environmental Reference Scenarios (reproduced from [2])

Scenario	**Note**
Fa1	Reference scenario developed by ICAO Forecasting and Economic Support Group (FESG); midrange economic growth from IPCC (1992); technology for both improved fuel efficiency and NOx reduction
Fa1H	Fa1 traffic and technology scenario with a fleet of supersonic aircraft replacing some of the subsonic fleet
Fa2	Fa1 traffic scenario; technology with greater emphasis on NOx reduction, but slightly smaller fuel efficiency improvement
Fc1	FESG low-growth scenario; technology as for Fa1 scenario
Fe1	FESG high-growth scenario; technology as for Fa1 scenario
Eab	Traffic-growth scenario based on IS92a developed by Environmental Defense Fund (EDF); technology for very low NOx assumed
Edh	High traffic-growth EDF scenario; technology for very low NOx assumed

sonic aircraft in 1992 were estimated to have increased ozone concentrations at cruise altitudes in northern mid-latitudes by up to 6%, compared to an atmosphere without aircraft emissions. This is projected to rise to about 13% by 2050 in the reference scenario. NOx reacts with moisture and ammonium to form smog (smoke fog) and rain acid. Acid rains are those that are unusually acidic (elevated hydrogen ions) caused by emissions of compounds such as SO_2 and NOx into the atmosphere. The NOx from aircraft exhaust reacts with water molecules in the atmosphere to form nitric acid (HNO_3) which has harmful effects on aquatic life, plants and infrastructures.[36]. In 1992, aircraft engine condensation trails (contrails) covered about 0.1% of the Earth's surface, and is projected to grow to 0.5% by 2050 in the reference scenario (Fa1), see Table 1.4. Contrails are formed when water vapour condenses and freezes around small particles contained in aircraft exhaust gases. The water vapour is partly due to high humidity and partly from the aircraft exhaust gases. Contrails affect the environment by blocking heat generated by the Earth from escaping into space, thus contributing to global warming. Whilst trapping radiated heat from escaping to space, contrails do also block sunlight from reaching the Earth (serving as reflective clouds) thereby aiding the global cooling effect. Therefore, contrails can be said to be good or bad for the environment depending on which aspect is considered or rather, which aspect dominates which.

The above discussed issues sparked a series of public outcries on the negative impacts of air transport with respect to the environment and air quality. The desire to combat this trend led to the setting up of major global initiatives, research and development (R&D) projects such as NextGen of the USA, Single European Sky ATM Research (SESAR) of Europe and Collaborative Action for Renovation of Air Transport Systems (CARATS) of Japan, etc. These initiatives were introduced to modernise the present Air Transportation System (ATS) and cater for air transport demands in the foreseeable future

Table 1.2: Summary of Future Global Aircraft Scenarios (reproduced from [2])

Scenario - -	***Traffic growth per year 1990-2050***	***Annual growth rate of fuel burn 1990-2050***	***Annual economic growth rate***	***Annual population growth rate***	***Ratio of traffic 2050/ 1990***	***Ratio of fuel burn 2050/ 1990***
Fa1	3.1%	1.7%	2.9% 1990-2025 2.3% 1990-2100	1.4% 1990-2025 0.7% 1990-2100	6.4	2.7
Fa1H	3.1%	12.0%	2.9% 1990-2025 2.3% 1990-2100	1.4% 1990-2025 0.7% 1990-2100	6.4	3.3
Fa2	3.1%	1.7%	2.9% 1990-2025 2.3% 1990-2100	1.4% 1990-2025 0.7% 1990-2100	6.4	2.7
Fc1	2.2%	0.8%	2.0% 1990-2025 1.2% 1990-2100	1.1% 1990-2025 0.2% 1990-2100	6.4	2.
Fe1	3.9%	12.5%	3.5% 1990-2025 3.0% 1990-2100	1.4% 1990-2025 0.7% 1990-2100	10.1	4.4
Eab	4.0%	3.2%	-	-	1 10.7	6.6
Fa1	4.7%	3.8%	-	-	15.5	9.4

[37]. The European Union (EU) initiated three stream comprehensive projects to mitigate the impacts of aviation on the environment and fuel resources. These are R&D for greener technology, modernisation of air traffic management systems and market based measures. This led to set-up of the Clean Sky Joint Technology Initiative (JTI) was introduced as the flagship of the R&D projects for the greening of air transport in Europe.

The Clean Sky JTI involves six technology evaluators. These are: Green Regional Aircraft (GRA), Smart Fixed-Wing Aircraft (SFWA), Green Rotorcraft (GR), Systems for Green Operations (SGO), Sustainable and Green Engines (SGE), and Eco Design (ED) as described in Fig. 1.3. These evaluators are set to be achieved through identification, development and validation of key technologies necessary for the realisation of ACARE[2] Flightpath 2050 environmental goals. The key objectives as defined by ACARE were the reduction of CO_2 by 75%, NOx by 90% and perceived noise by 65% by 2050 referenced to 2000 standard [38].

The aim of the GRA is to deliver low-weight aircraft using smart structures with low external noise configurations and integration of other technological components delivered by the other divisions within the technology evaluator such as engines, energy management and new system architectures. The SFWA is aimed at delivering light wing technology and new aircraft configuration whereas the GR aims to deliver innovative rotor blades and engine installation for noise reduction, lower airframe drag, integration of diesel engine technology and advanced electrical systems for elimination of noxious hydraulic fluids and fuel consumption reduction. The SGE is aimed to produce five engine demonstrators which would integrate technologies for low noise, lightweight, low NOx and low weight novel configurations such as open rotors and inter-coolers. The EC

[2]Advisory Council for Aeronautics Research in Europe

focuses on the whole product life cycle based on optimal and efficient use of raw materials and energies. While, the SGO is directed towards all electric aircraft equipment and system architectures and, thermal management for greener trajectories and mission which is of particular interest to this work. In this work both the flight trajectory and the anti-icing system are considered part of the global aircraft icing protection system that require effective management as illustrated in Fig. 1.3. The benefit of this is to assist commercial aircraft operators manage excessive fuel burn and emissions imposed by power off-takes while operating in real weather conditions.

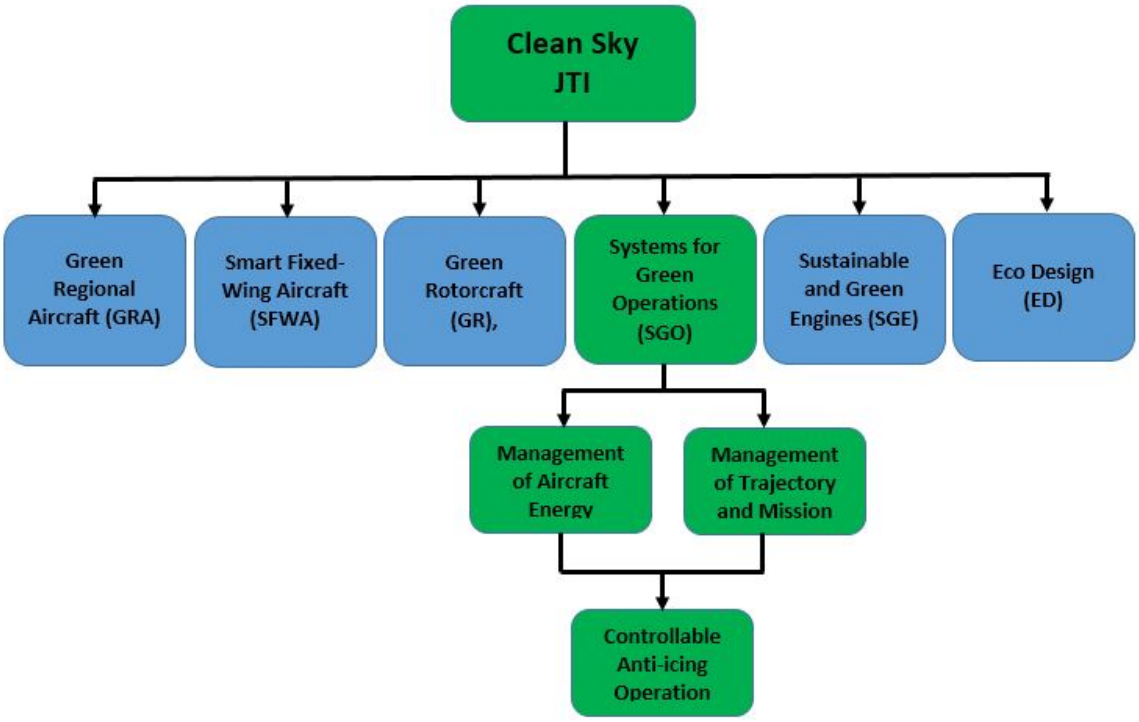

Fig. 1.3: Clean Sky Setup (Modified from [3])

In view of the Clean Sky JTI discussed above, the European Council in partnership with the aeronautics industry granted funding under the 7th Framework Program for research in Europe (including the one undertaken in this work) to mitigate the impacts

of aviation on the environment. Consequently, the environmental concerns, the project funding and the level of collaboration with the industrial partners have served as a great source of motivation for this work.

An overview of aircraft icing risk and its impacts on flight safety, economy and the environment further buttresses the desire for this work. This discussion includes the factors influencing in-flight icing and the effects of ice formation on aircraft performance.

1.5 Overview of Aircraft Icing Risk and Effects

Aircraft icing is caused by the freezing of super-cooled water droplets found in clouds when they come into contact with aircraft unheated surfaces. The rate and amount of ice accretion on the surface depends on the shape, surface finish, size, the speed at which the body is travelling, and the free stream temperature. Liquid Water Concentration (LWC) and the size of the water droplets in the clouds [23] also contribute to ice accretion. The worst continuous icing conditions are found near the freezing level in heavy stratified clouds, or in rain, with icing possible up to 8,000 ft high. There are basically four types of clouds that could affect aircraft icing. These are Cirrus, Nimbus, Stratus and Cumulus. Sometimes, different cloud types can come together in the atmosphere forming a mixed cloud such as Cumulus-nimbus and Cirro-cumulus. Depending on the operating altitude, clouds may be classified as low, medium or high. Typically, icing occurs from sea level to about 20,000 ft. Above this altitude, high clouds such as Cirrus, Cirro-cumulus and Cirro-stratus are encountered which contain little water droplets and more of ice crystals. At mid-altitudes for example between 6,000 to 20,000 ft, middle clouds such as Alto-cumulus and Alto-stratus are encountered which usually contain a mixture of water droplets and ice crystals. Below 6,500 ft, low clouds such as

Nimbo-stratus and Cumulus are mostly encountered which are rich in water content and hardly any crystals. Icing is rare above 8,000 ft as the droplets in the clouds are already frozen. However, in Cumuliform clouds with strong updrafts, large water droplets may be carried to high altitudes and structural icing is possible up to very high altitudes. [27]

Table 1.3: Icing Risk (modified from [27])

Altitude	**Cumulus Clouds**	**Stratiform Clouds**	**Rain and Drizzle**
High	0°C to -20°C	0°C to -15°C	0°C and below
Medium	-20°C to -40°C	-15°C to -30°C	
Low	< -40°C	< -30°C	

The distinct types of ice that can build on and adhere to aircraft surfaces in flight are the Rime and Glaze or clear ice. Literature [5] shows that over 50% of ice accretion occurs between -12℃ to -8℃ with Rime occurring at -12℃ and glaze ice occurring at temperature close the freezing point, whereas, mixed ice occurring in between this range. Rime ice is rough, opaque and whitish with trapped air inside it. Much of Rime ice can be removed by de-icing or prevented by anti-icing. Normally, Rime ice has single horned shape, whereas Glaze or clear ice usually has two horns shape as illustrated in Fig. [4]. Glaze ice is smooth at microscopic level and generally follows the contours of the surface closely, and can form ridges on further accumulation. Unlike Rime ice, Glaze ice is a smooth, glossy and clear ice that forms on impact with large water droplets at temperatures near 0℃. Glaze ice freezes slowly on an aircraft's surfaces, which allows the water to run and air bubbles to escape resulting in clear and dense ice structure. Glaze is harder to remove and is far more damaging to aerodynamic properties than the Rime ice. In a real life situation, ice formation on aircraft surfaces is not as distinct as expressed above [39]. Sometimes both Rime and Glaze ice may build-up simultaneously

with one type dominating the other as conditions favour it. This situation gives rise to a mixed type of ice which exhibits Glaze ice characteristics around the stagnation line and Rime ice characteristics away from it.

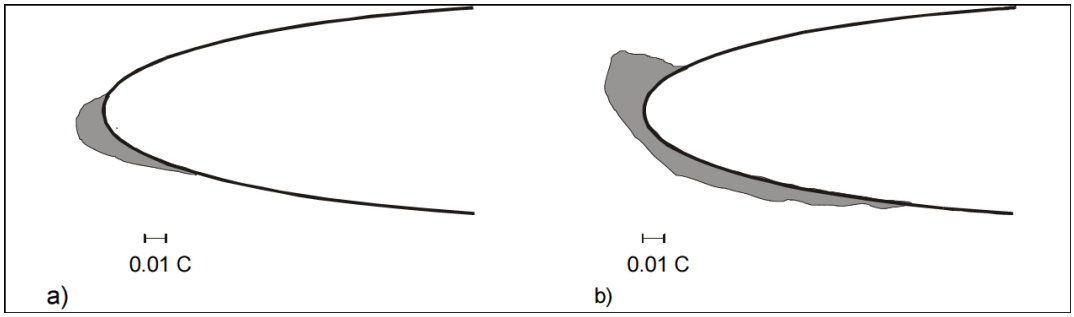

Fig. 1.4: Types of Ice: (a) Rime ice, (b) Glaze ice [4]

Ice distorts a lamina flow of air over the wing, diminishing the wing's maximum lift and reducing the angle of attack for maximum lift. The upper horn of the Glaze ice is particularly damaging to $C_{L_{max}}$. Aircraft icing also adversely affects aircraft handling qualities, and can significantly increase drag [27]. Ice may also accumulate on control surfaces such as flaps and ailerons which could lead to loss of control. Other aircraft parts that are affected by ice accretion include the windscreen, empennage and probes. Factors responsible for icing and those influencing its onset are discussed below.

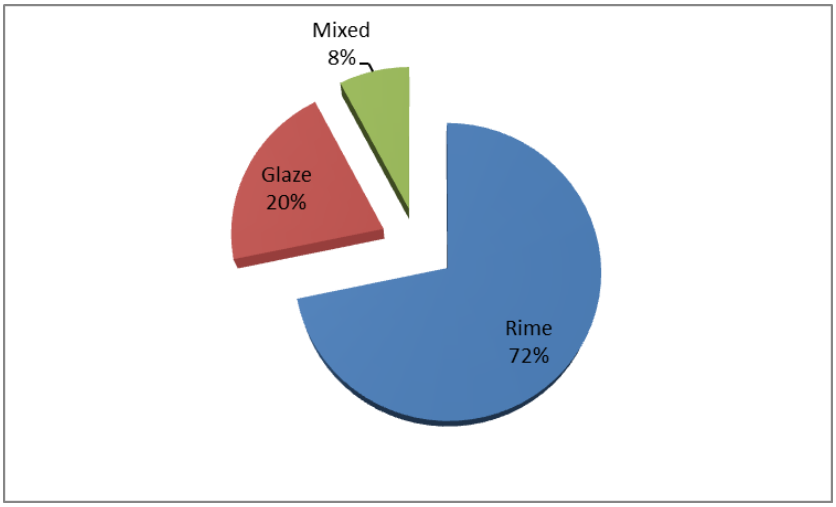

Fig. 1.5: Icing Type Frequency of Occurrence, modified from NOAA

1.5.1 Factors Affecting Aircraft Icing

The factors affecting aircraft icing are categorised into atmospheric, mission and aircraft related. The atmospheric factors include ambient temperature, cloud's LWC, mean droplet size, free stream air density and airspeed [40]. The major aircraft geometrical parameters are the aerofoil shape/size, wing leading edge sweep and body setting angle. The mission-related factors include mission route and duration of icing encounters.

The outside air temperature (OAT) affects both the icing severity and the type of ice formed. The OAT is by far the most influencing parameter as far as ice accretion is concerned [23]. Mostly icing occurs between -20 to 0 ℃, with -40 ℃ being the limit. At -40 ℃ droplets can freeze even without icing nuclei [41]. The lower the OAT, the higher the de-icing power required. Design atmospheric conditions used in aircraft ice protection certification reflects a relationship between OAT and a cloud's LWC. The rate of ice accumulation is directly related to LWC for a given temperature. The LWC gives an indication of how much water is available for icing. A generic icing severity

index defined in terms of cloud LWC is contained in Table 1.4. In can be seen in Fig. 1.6 that airframe icing potential rises with cloud's water concentration and accretion rate.

Table 1.4: Icing Severity Index

Category	**LWC** (g/m^3)	**Accretion**
Trace	< 0.1	$< 1g/cm^2/hr$
Light	0.11 to 0.6	$> 1g/cm^2/hr$
Moderate	0.61 to 1.2	$> 6g/cm^2/hr$
Severe	>1.2	$> 12g/cm^2/hr$

By definition, trace and light icing do not pose any specific restraints on aircraft behaviour whereas the moderate and severe icing does, and thus requires mitigating action. The water droplet size given in microns (μm) is the measure of mean droplet size often referred to as Mean Volumetric Diameter (MVD). Appendix C icing envelope accounts for conditions below $50\mu m$. Aircraft geometry and water droplet size are two parameters affecting collection efficiency and the overall water catch of a body. The aircraft wing section has a significant impact on the IPS operational requirement such as the anti-icing energy whereas the chord size influences the projected height it generates. Another factor affecting anti-icing power requirement is the impingement limits of the aerofoil section. The impingement limits describe the upper (S_U) and lower (S_L) limits of the protected area. Though not crucial like temperature and LWC, droplet size can affect the ice shape as well. This is because droplet size is important in the calculation of the modified inertia parameter (K_0), which gives an indication of the collection efficiency (E_m). Basically, (E_m) is a measure of the ability of a body to collect water along its flight path. The Relative Humidity (RH) also has great influence on airframe icing. High RH in low temperatures increases icing potential.

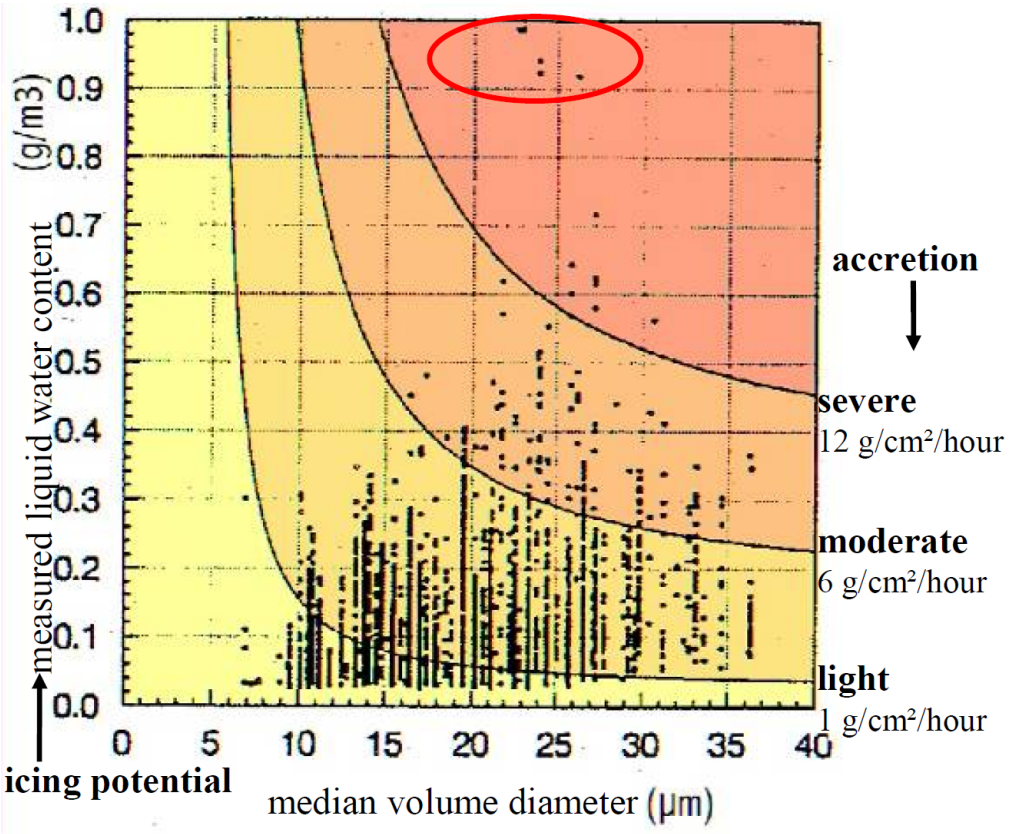

Fig. 1.6: Icing Potential vs MVD [5]

Mission route is also a fundamental factor affecting fuel burn due to the IPS operation. Thus, optimal overall performance is influenced by many factors, including dynamic route optimization, accurate flight plans, optimal use of re-dispatch. According to Altus [42], an optimal flight planning scenario for saving fuel and emissions involves calculating multiple routes or operating approaches for each flight, ranking these scenarios by total cost, choosing the scenario that best accomplishes the airline's cost objectives, and providing summaries of the other scenarios for operational flexibility. While the scenario chosen by the system might be used most of the time, dispatchers and operations managers at an airline's control center may choose another scenario to meet the airline's operational goals, such as routing of airplanes, crews, and passengers. This means that every commercial airline flight begins with a flight plan. Over time however, small adjustments to each flight plan can add up to substantial savings across a fleet. [42]

1.5.2 Effects of Ice Formation on Aircraft and Engine Performance

The most critical locations where ice can accumulate include the leading edges of wing and empennage, propellers and hub on a fixed wing aircraft, engine nacelles, rotor blades on helicopters and windscreens [43], [44]. Wind tunnel and flight tests have shown that ice accretion (no thicker or rougher than a piece of coarse sandpaper) on the leading edge or upper surface of a wing can reduce lift by 30% and increase drag up to 40%, [4]. Larger accretions can reduce lift even further and increase drag by 80% or more. Other ways ice can affect airfcraft is when it strikes the airframe as hailstones. At high speeds, large ice particles may cause structural damage on impact. Accumulation of

ice on aircraft surfaces can affect the performance in many ways. Generally, cing has detrimental effects on aircraft performance, instrument readings, windscreen vision and engine health. Thus, ice accretion on critical flight surfaces can negatively affect safe and efficient operation of aircraft. Ice build-up on aerofoil surfaces could change the aerodynamic properties of the aerofoil, potentially leading to reduced lift and increased stall speed. It can cause flow separation which could lead to loss of effectiveness of control surfaces as demonstrated in Fig. 1.7(c). In fact, airflow disruption over control surfaces can alter the aerodynamic balance of the controls, which could render the aircraft uncontrollable. Similarly, handling abnormalities could lead to both roll and pitch upsets in a wing or tail stall. Overall, icing results in decreased lift, increased drag, reduced stall angle and thrust leading to alteration of handling qualities. [4]

Ice accretion on wing leading edge reduces the maximum lift coefficient ($C_{L_{max}}$) and Angle of Attack (AoA) for stall leading to an increase in stall speed. Icing degrades aircraft longitudinal stability and control [45]. The effect of ice on lift is illustrated in Fig. 1.7, where lift coefficient is plotted against angle of attack for a clean and an iced aerofoil. In turbine engine aircraft, ice build-up on intake could restrict air flow into the engine; the ice may break up and enter inner engine parts, which could result in loss of the engine. For a propeller driven aircraft, ice on propellers or rotor blades can cause propeller vibration, increase in drag and decrease in lift of the blades thereby leading to an overall reduction in efficiency. This places further burden on the engine to maintain the blade speed. In aircraft equipped with carburettors, ice can accumulate on the venturi and throttle plate which occludes airflow, or impedes the fuel flow thereby starving the engine of fuel and airflow. In aircraft equipped with stall warning vanes, icing on these sensors could lead to false angle of attack indication. Therefore, to prevent icing on air data sensors such as pitot pressure sensor, communication and navigational sen-

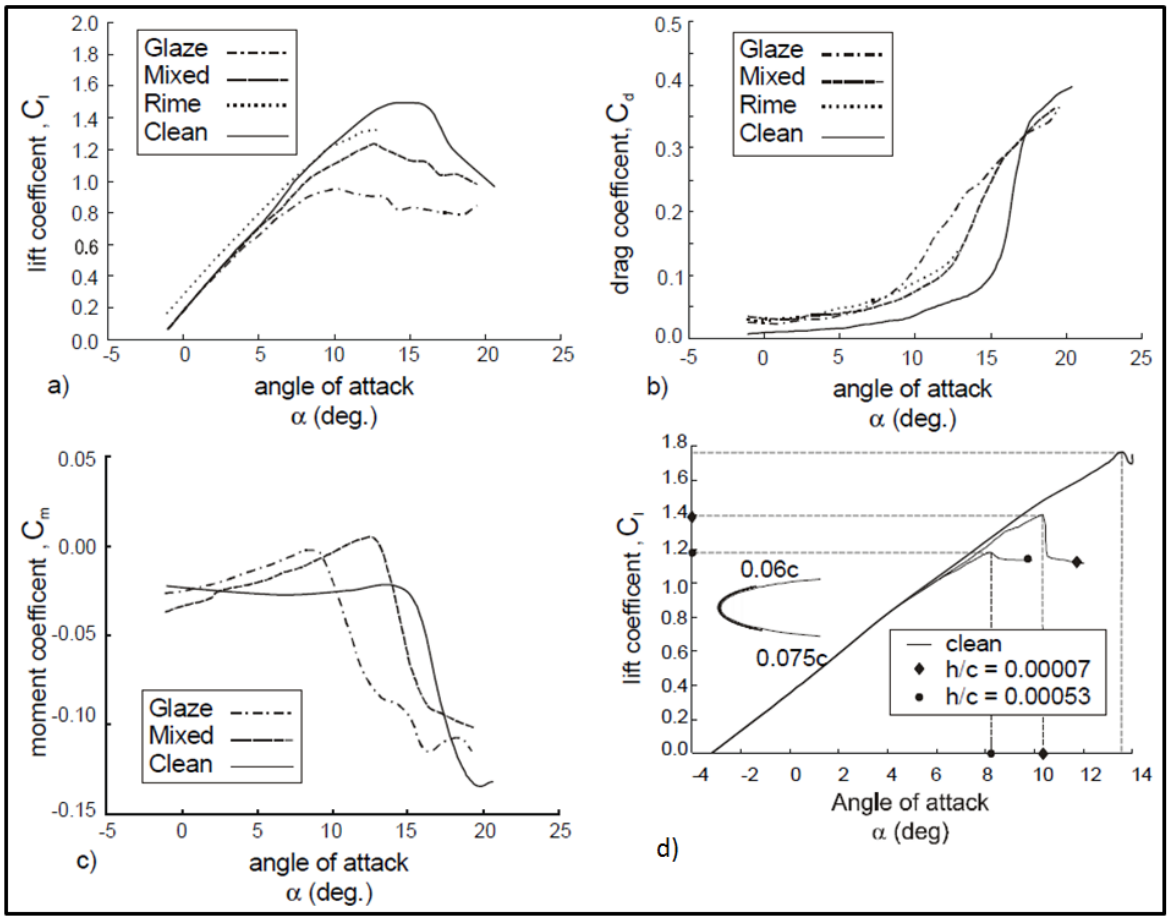

Fig. 1.7: Aerodynamic Performance Degradation: (a) C_L Vs α for glaze, mixed, rime and clean configuration; (b) C_d Vs α; (c) C_m Vs α; (d) C_L Vs α clean for different projected heights [4]

sors, electrical heating is provided. Ice does also build up on forward-facing windscreen panels while flying in icing conditions, posing risk to the pilot's vision. Consequently, windscreens are normally equipped with ice protection systems to allow pilot visibility in case of icing encounter. In some windscreens, thin and narrow rows of conductive film are embedded, through which electric current runs to heat the windscreen. Conversely, in smaller aircraft, anti-freeze fluids or hot air jets are generally used. It therefore costs a significant amount of energy to protect aircraft against in-flight icing.

Because of the inherent danger and risk involved in icing encounters, flying in icing conditions are highly controlled by national and regional aviation safety agencies. In effect, the Federal Aviation Authority (FAA) of the USA, European Aviation Safety Agency (EASA) of the EU, Civil Aviation Authority (CAA) of China and similar other regional regulatory bodies have provided standards for certifying aircraft for operation in known icing conditions.

1.6 Airworthiness Standards for the Design and Certification of Aircraft Operation in Icing Conditions

The current airworthiness FAR/EASA CS standards governing aircraft certification for operation in known icing conditions are Parts 23, 25, 27, 29 and 33. To be certified for flight into icing conditions, an aircraft must demonstrate its capability to cope with the FAR/CS25 Appendix C icing conditions for large aircraft, FAR/CS23 for commuters, FAR/CS27 and CS29 for small and large rotorcrafts, while CS33 for engines. The

Appendix C icing envelope prescribed the icing environment in terms of cloud's water mass concentration and droplets size.

1.6.1 Appendix C Icing Envelope

The *Appendix C* gave two sets of conditions: the Continuous Maximum (CM) for Stratiform clouds, and the Intermittent Maximum (IM) for Cumuliform clouds icing envelopes; each as a function of LWC vs MVD, and ambient temperature vs pressure altitude as shown in Appendix A to this thesis. The objective of *Appendix C* is to provide maximum probable (99.99%) icing conditions that could be encountered with which the IPS must be able to cope [46]. Currently, no aircraft is certified to fly in icing conditions outside *Appendix C* envelope, i.e., beyond $50\mu m$ cloud water droplets size or freezing drizzle and freezing rain [47]. Meanwhile, as at 2011, 6 accidents were recorded that occurred in severe icing conditions including Supercooled Large Droplets (SLD) outside the *Appendix C* envelope. As a result, three draft proposals were advanced for Appendices D, O and P covering those conditions.

1.6.2 Other Proposed Standards

The 1994 ATR72 crash resulted in an NTSB recommendation to expand the *Appendix C* icing envelope to include freezing drizzle/freezing rain, and mixed water ice conditions. Thus, FAR Part 33 Appendix D has been proposed to cope with conditions outside such extreme conditions. Appendix D extends the temperature/altitude range to -60 ℃/45,500 ft for certification test concerning SLD and mixed phase clouds conditions (see Appendix A to this thesis). Appendix O SLD icing conditions are those in which the aircraft must be able to either safely exit following their detection or safely operate without restrictions. The SLD freezing drizzle conditions have a droplet diameter

range of 100-500 μm, pressure altitude range of 0 -22,000 ft, maximum vertical extent of 12,000 ft and horizontal extent of 17.4 nm [48].

The EASA also proposed Appendix P that is identical to FAA Appendix D, encompassing all the known occurrences with a minimum temperature of -75 ℃. The proposal was based on an experience of an incident due to a temporary erroneous airspeed indication at high altitude at a static air temperature below the current -60 ℃ proposed Appendix D limit. Both the Appendix D and P proposals were widely circulated for contributions by specialised research organisations and individuals. Till this moment however, the method of compliance is yet to be circulated. It is obvious from the above discussions that next generation aircraft need to have capabilities to operate in conditions outside present *Appendix C* envelope if it were to meet the growing demands for air transport services.

1.7 Contents of the Work Done

The European Commission aerospace industry set-up the Clean Sky programme to mitigate the impacts of air transport on the environment and on fuel resources. The work reported in this thesis is part of the stream of activities carried out under the Clean Sky programme towards the realisation of the ACARE objectives. The Clean Sky JTI and air transport is a collaborative effort involving industry, research organisations and academia to introduce novel technologies to improve the environmental impact of aviation. As part of the activities, more environmentally friendly aircraft trajectories are studied under the SGO Integrated Technology Demonstrator (ITD). The classical aircraft trajectory optimisation approach defines the problem by using the aircraft dynamics and engine performance thus neglecting the airframe systems power

requirement. Airframe systems are vital in commercial aircraft and their operation incurs a fuel penalty (herein singularly referred to as 'penalties' thereafter) on the aircraft engines from which the energy is extracted. Presently, the airframe systems penalties have not been considered within the classical trajectory optimisation problem definition. However, the effects of these penalties on typical trajectories flown today are significant which necessitated the need to identify methods of making the overall secondary power system work more efficiently.

In this work therefore, the effects of secondary power off-take penalties on aircraft trajectory optimisation were studied. The study focused on identifying these penalties on current aircraft trajectories when compared with trajectories optimised without considerations to power off-takes. The work involves the development and evaluation of GATAC through optimised trajectory simulations. The models required for GATAC evaluation include the Aircraft Dynamics Model (ADM[3]), Aircraft Systems Model (ASM[4]), Air Traffic Management (ATM), atmospheric, engine and emissions models. I the author personally developed the ant-icing model algorithm within the ASM. The purpose of the anti-icing model is to provide quantitative estimates of fuel penalty due to anti-icing which would allow the evaluation of fuel burn, noise and emissions from aircraft fitted with future air navigation systems in line with the Clean Sky activities (see Fig. 1.8). The figure shows the set-up for identification, development and evaluation of key technologies through the use of demonstration models for the concept of greener and lighter next generation aircraft.

At the time of this work, the weather model was yet to be developed, therefore, an artificial cloud algorithm was implemented within the scope of the icing cases ran. The

[3]Developed by the Cranfield University Clean Sky team.
[4]Developed by the Cranfield University Clean Sky team with the contributions of the author.

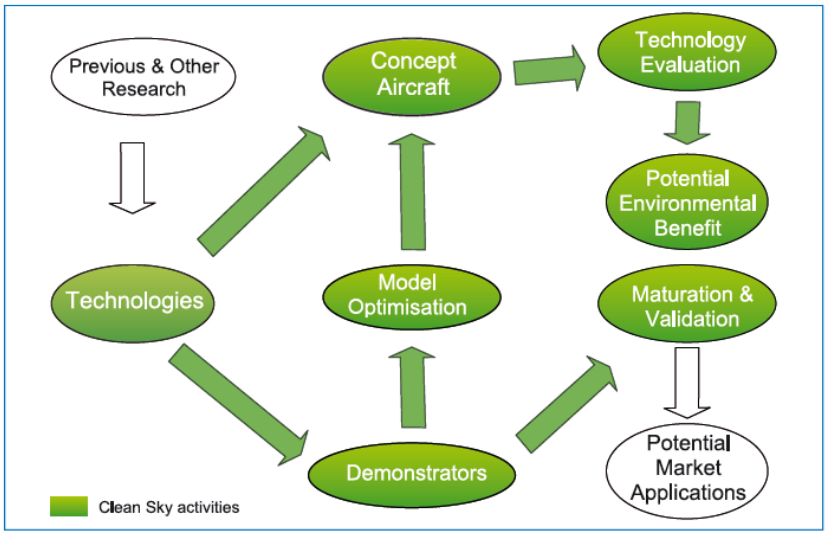

Fig. 1.8: Scope of Clean Sky Activities [6]

artificial icing model could simulate hundreds of icing scenarios based on the Appendix C icing conditions; however, only 48 cases (see Table 5.1) were of significance to this work. The simulations were ran and analysed, and the results have been presented in section 6. The primary case study for the analysis is:

- A short haul flight from London (Heathrow) to Amsterdam (Schiphol) was used as the case study route.
- A medium size, 180 passenger twin turbo-fan engine aircraft.
- Each segment was optimised with and without consideration to power off-take penalties.
- NSGAMO[5] was used.
- GATAC tool was used for generating the optimised trajectories.

The subsidiary cases include the departure, cruise and arrival under icing conditions. In each case, the trajectory was optimised based on trade-off between fuel burn and

[5]Non-dominated Search Genetic Algorithm Multi-objective Optimiser developed by Cranfield University

flight time. Consequently, a multi-objective trajectory optimisation based on Pareto efficiency method was used to minimise fuel burn, emissions and noise using GATAC tool. A vertical profile mission was simulated with the aim to obtain trajectories optimised for minimum fuel burn, flight time and emissions. A 3D mission was also simulated for the three objectives as well as minimum noise. It is worth noting that in Pareto method, a trajectory optimised for one parameter would not be the same as that optimised for another parameter. The objectives functions are in conflict such that minimising one objective leads to increase in the other; hence, a compromise trade-off is sought. This trade-off is defined as the Pareto optimum. To narrow down the search domain, certain constraints such as altitude, speed and stopping criteria were imposed relative to the mission and baseline aircraft profile.

A total of 60,000m ground distance was covered during departure from the ground level to FL100. The cruise simulation covered a range of 360,000m operating from FL100 to FL390 while the arrival covered a distance of 60,000m from FL100 to the ground level. In addition to minimum fuel and minimum time optimality problem, cases for noise mitigation were simulated in the 3D case departure. This is because during departure and arrival noise is of a great concern to the people living around airports. Above FL100, noise is actually no longer an issue to the ground population, therefore, was not considered in the cruise case. Noise minimisation was also not considered in the arrival case because arrival is viewed as a reversal of departure in this work. In each case, 250 generations were ran for a population of 100, and initialisation factor of 50 which gives a total of 30,000 generations. Usually, a simulation of this nature would require very long running time except unless done on a grid system. Consequently, a high speed cluster of five computers each running three daemons[6] was used in order to

[6]A small computer program running in the background on every host [49].

speed up the simulation. A typical cruise case takes between 36 to 48 hours run time using the cluster. However, in departure and arrival which require less computational effort, local multiple daemons in the host computer were used to attain convergence within reasonable time.

The results (see section 6) showed that flying theoretically optimised trajectories with systems can cause unexpected fuel penalties up to 11%. By including the penalties of airframe systems within the optimisation loop however, fuel savings of up to 4% could be achieved. Thus, this work helped in evaluating the relationship between fuel burnt during flight and the amount of emissions generated by the classical and weather optimised aircraft trajectories. The approach used in this work could therefore, assist commercial aircraft operators manage excessive fuel burn and emissions imposed by power off-takes while operating in real weather conditions.

1.8 Relevance of the Study

Development and Evaluation of GATAC (Greener Aircraft Trajectories under ATM Constraints): This work is a collaborative research funded by Clean Sky involving three universities and leading aerospace industries in Europe. These are Cranfield University, Delft University of Technology and The University of Malta; and the industrial partners are Airbus, Thales and DLR among others. One of the Clean Sky activities is the Management of Trajectory and Mission (MTM) work package under SGO Integrated Technology Demonstrators (ITD). Within this work package, Cranfield University is tasked with GATAC evaluation, development of optimisers and key models required for GATAC validation as illustrated in Fig. 1.9. The work done in this research contributes towards the development and evaluation of GATAC through the

development of a method for generating optimised aircraft trajectories for real weather conditions in line with MTM work package. The simulation cases ran also helped in evaluating the performance of GATAC tool for MTM, both of which are aimed at defining environmentally sustainable aircraft trajectories.

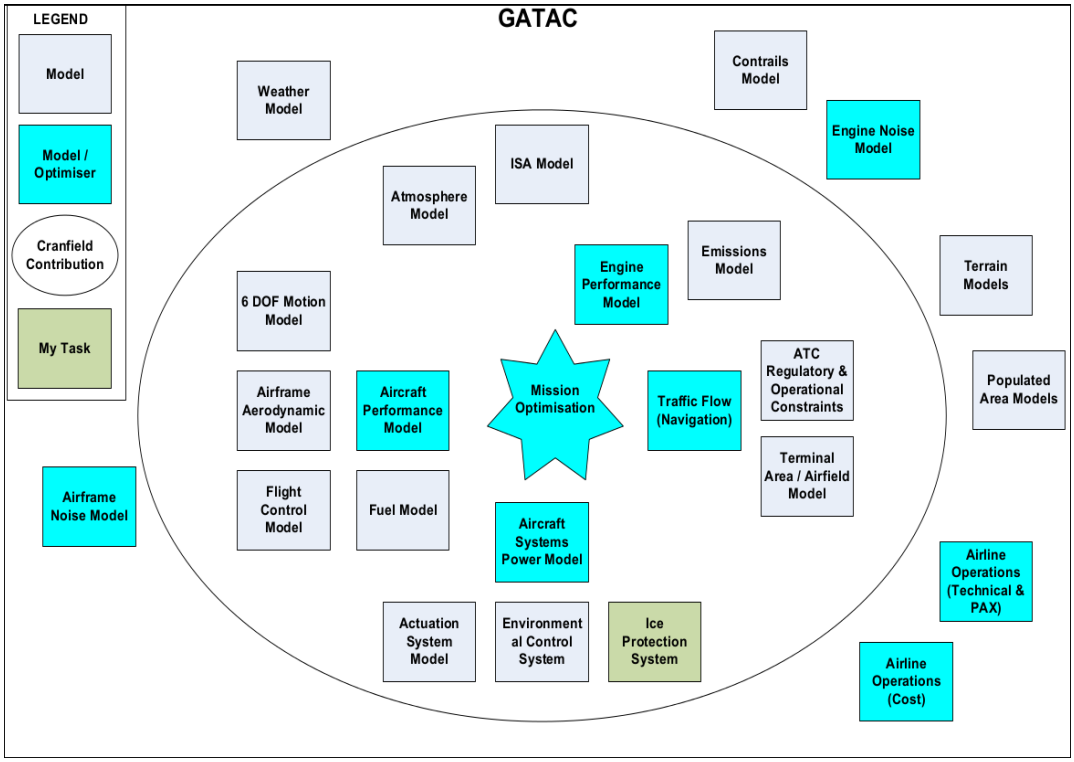

Fig. 1.9: GATAC Schematic Diagram (Modified from Dr. C. Lawson and Dr. H. Jia's materials)

Towards the Accomplishment of ACARE Goals: This work enabled the development of a method for efficient aircraft operation in real weather scenarios in line with ACARE objectives. Flying optimal aircraft trajectories for minimum fuel burn, emissions and perceived noise of a flying aircraft is in line with ACARE Flightpath 2050[7].

[7]Reduction of CO_2 emission by 75%, NOx emission by 90% and perceived noise emission of a flying aircraft by 65% relative to a typical new aircraft flying in 2000 [50].

Supporting Efficient Aircraft Operations in a Future Air Traffic Environment: At present, integrated aircraft routing and crew scheduling consisting of a minimum-cost set of aircraft routes and crew pairings (such that each flight leg is covered by one aircraft and one crew) are used to cope with the high air transport demand. The objective of such approach is to achieve customer satisfaction with least direct operating cost (DoC). Environmental benefits are marginal in the current flight scheduling procedures which caused the need for new technologies and operational strategies for minimising energy usage. In this research work therefore, a controllable anti-icing method has been developed that combines the operational aspects of aircraft with weather conditions to achieve more efficient missions in the next generation aircraft. Current technologies such as the PBN, enabled by satellite positioning are enablers of the anti-icing approach proposed in this work. The PBN enables more direct, fuel efficient routes and provides alternatives for routing around airspace disruptions, such as bad weather or unexpected congestion [51]. Thus, the anti-icing method developed in this work would help in simulating migration from the constrained flight procedure of the current ATM system to optimised flight trajectories in the future ATM environment.

Academic Use: MSc Aerospace Vehicle Design (AVD) is one of the largest courses undertaken in the School of Engineering. The course runs a double stream each year and involves the design of different aircraft including all airframe systems. This work would help students with a validated tool for analysing the anti-icing power requirements of different aircraft design configurations. The tool could also be used for further studies within and without the department.

Nigerian Air Force (NAF) Research and Development: In the field, over 70% of first line to third line maintenance works are on aircraft systems. The doctoral research

training in aircraft systems will advance the NAF R&D projects usually imported from field maintenance units to the Air Force Institute of Technology (AFIT) research centre. The knowledge and research training gained from this research work would help the author in further aerospace related projects undertaken by the NAF.

1.9 Thesis Structure

Chapter 1: Introduction. Chapter 1 gives a general overview of the in-flight icing problem, the proposed solution, motivation for the research and the structure of the thesis.

Chapter 2: Literature Review. Chapter 2 discusses a literature survey carried out on relevant subjects of the research. The survey covers the following areas:

- Effects of Ice Formation on Aircraft Performance
- Factors Contributing to Aircraft Icing
- Airworthiness Standards for the Design and Certification of Aircraft Operation in Icing Conditions
- Current Ice Protection Technologies
- Icing Simulation and Analysis Tools
- Recent Progress in Novel IPS Technology and Next Generation Aircraft
- Aircraft Trajectory Optimisation
- Previous Studies on Aircraft Operation in Icing Conditions

Chapter 3: Methodology. Chapter 3 presents the methodology applied in this work. The tools and techniques used in modelling and simulations of the AI model and aircraft trajectory optimisations are explained. An overview of the nature and capabilities of GATAC optimisation framework and integration principles were also discussed in this chapter.

Chapter 4: Development of a Tool to Study Aircraft Trajectory Optimisation in the Presence of Icing Conditions. This chapter describes the development of a tool for simulating aircraft AI energy demand based on the aircraft, mission and atmospheric parameters.

Chapter 5: Theoretical Analysis of Icing Parameters. Chapter 5 describes a sensitivity analysis carried out on the various parameters with a view to determine important test cases that are used for the simulation.

Chapter 6: Discussion and Analysis of Results. Chapter 6 presents the results of the simulation cases and analyses the impacts of the method on aircraft fuel burn, noise and greenhouse gas emissions for operations involving icing.

Chapter 7: Conclusion and Recommendation for Future Work. Chapter 7 draws some conclusions from the results obtained. At the end of the Chapter, recommendations were made for future work.

Chapter 2

Literature Review

This chapter reports on literature review carried out on relevant subjects concerning aircraft icing and ice protection technology, the effects of icing parameters on de-icing energy, engine power off-take performance, and intelligent anti-icing operations. The chapter also discusses the leading icing codes available today for icing simulation and analysis including different trajectory optimisation methods. The chapter concludes with a case for this research based on the identified areas that require further investigations.

2.1 Ice Accretion Studies

The first stage in any aircraft icing issue is to determine whether there is an accretion or not, and how serious it is. The second stage is to use icing codes to analyse the water droplet trajectories, collection efficiency and any resulting growth of ice on the surface [52]. Significant experiments and flight test were carried out between 1940 and 1960s which laid the foundation for most of the ice accretion codes in use today. However, significant progress in theoretical studies of aircraft ice accretion was not achieved until the advent of computer age during the late 1970s [23]. Prominent among the early concepts of modern anti-icing systems includes the works of Johnson [53] and Hardy [54] in 1940 and 1946 respectively. Johnson described the effects of wing loading, aircraft icing and associated aspects into modern transport design whereas Hardy developed one

of the modern concept for protection of aircraft against ice for the Defence Evaluation and Research Agency (DERA)[1]. Around the same time, a dimensionless droplet size distribution was established by Langmuir and Blogett [55] which introduced the use of natural-icing cloud measurements in analysis of aircraft icing. These developments led to further studies on aircraft encounter with super-cooled water droplets in flight. The earlier experimental works on droplets impingement were pioneered by Lewis [56] in 1955 and, Von Glahn [57] and Gelder [58] in 1956. However, the fundamental principle of mass and energy balance calculation method used for aircraft icing analysis was founded by Bernard Messinger [12] in 1953. The Messinger's model [12] (see section 2.4.4 for further details) utilised convection, sensible heating, evaporation/sublimation, kinetic energy, and viscosity terms in the conservation energy equation to find the equilibrium temperature of an unheated icing surface. In the Messinger model, the heat transfer coefficient and the rate of water catch are the two essential parameters for computing the fraction of the non-freezing water and the balance temperature. The key parameters affecting the water collection efficiency are droplet size, angle of attack, chord, and flow speed. However, where the flow speed exceeds Mach 0.3, compressibility effects are normally considered significant. Thus, one of the major limitations of the Messinger model is that it applies to non-compressible flows alone in its original form.

To mitigate the shortfall of the classical Messinger model, in 1983, Cansdale and Gents [59] extended Messingers model to cover compressible flows and water local concentration. Another fundamental limitation of the Messinger model is that the ice and water layers are isothermal, and so conduction through these layers cannot be accounted for. The substrate is assumed insulated which removes conduction through the substrate which is far from ideal. For this reason, the Messinger model would always predict a

[1]Previously known as the Royal Aerospace Establishment (RAE)

lower rate of ice accretion than occurs in practice. In 2001, Myers [60] developed both two and three-dimensional mathematical models for describing ice growth due to supercooled fluid impacting on a solid substrate. With this, the Messinger method was improved by the addition of an energy source at the substrate. Similarly, Özgen and Canibek [61] in 2009 developed an extended version of the Messinger model suitable for the runback mass estimation. In 2013, Ryosuke [62] compared the two approaches and came to the conclusion that the extended Messinger model is far more superior to the original Messinger model in simulating glaze icing. In addition to the works credited to the early individual researchers, some major icing research centres have contributed to the analysis and understanding of the cause and effects of aircraft icing through development of several icing codes and standards. Major research agencies involved in the development of the foundation of icing simulations codes in use today are discussed in the succeeding sections.

The Lewis Research Center in the US, and the DERA in the UK [23] were the first contributors in the resurgence of aircraft-icing analysis based on computer icing modelling and simulation. During the International Workshop in Aircraft Icing in July 1978, USA, participants observed that the expanding private aircraft fleet wanted all weather capability for their expensive investment; military and civilian helicopters needed rotor-blade ice protection and the large transport aircraft sought more energy efficient systems. It became clear that it was time to apply modern computers and instrumentation to the icing problem. The new icing program began with three NASA-funded study contracts to develop computer codes that would: a) predict water droplet collection on aircraft surfaces, b) model the ice build-up on aircraft surfaces, and c) provide design tools for various ice-protection systems [63]. French research establishment, Office National d'Etudes et de Recherches Aérospatiales (ONERA) joined in the 1980s. Italy, Spain,

Germany and Canada joined in many collaborative researches in the 1990s which saw to the development of icing codes that are use by aircraft manufacturers today.

Computer based aircraft-icing analysis have transformed the certification process of aircraft for flight into known icing conditions. The ability to analyse cases with the use of computers has reduced the number of experiments and flight tests where they are now predominantly used for the verification and validation phase - thereby inevitably reducing the certification costs. In more recent years, computer icing codes have allowed the analysis of many complex icing problems that were hitherto hard or impossible to analyse using rig and flight test. Presently, aircraft anti-icing analysis and certifications are performed by a combination of computational simulations, icing tunnel experiments and flight tests using tanker, Gent [23]. A combination of the above tools is not always applicable on the entire Appendix C icing envelope, due to inherent individual deficiencies associated with each method. In many instances, numerical modelling makes possible the study of some processes which might be difficult or economically unprofitable with a direct experiment. Icing analysis using computer codes also eliminates experimental assumptions and measurement errors.

Despite the enormous advantages of icing analysis using computers, icing codes have 3 major shortfalls. First, the mathematical equations that govern their operation do not reflect all physical processes of a natural process. Secondly, instability of numerical calculations and inaccurate discretisation sometimes affects their results [64]. Nonetheless, computational simulations are important for analysing icing encounter worst case scenarios and estimating ice accretion rate and patterns. They are fast and cost effective tool for aircraft icing analysis. Computational simulations could be used to determine temperature distribution over the surface vis-à-vis heating requirements.

2.2 Review of Existing Icing Codes

The leading algorithms available for icing simulation today include LEWICE [65], TRAJICE2 [66], ONERA [67]. Others are AID [52], ICECREMO2 [68], CANICE [69] and FENSAP-ICE3D [70]. These codes utilised internal solvers that utilizes Navier-Stokes fluid flow equations to simulate droplet trajectories and surface water catch rate and collection efficiency. The LEWICE icing code was developed based upon the Messinger model in 1982 for NASA-Lewis Research Centre for ice accretion modelling and simulation. The code was further developed to LEWICE/Thermal for simulating electro-thermal de-icing and anti-icing systems. The TRAJICE (Trajectory Ice Accretion) code was developed for the DERA, UK. Similarly, ONERA icing code developed for the French Aerospace Research Centre, uses Messinger equations to determine the local freezing fraction and Langrangian method for calculating droplets trajectories and impingement locations. The ICECREMO2 was developed through partnership collaborations between Cranfield University, BAE Systems, Airbus UK, Rolls Royce, and Dunlop Aerospace. The FENSAP-ICE is a multi-purpose icing code that can be employed for single and multi-step simulation based on Navier-Stokes CFD modules dubbed DROP3D, ICE3D and CHT3D (conjugate heat transfer). The AID algorithm is a suite of icing codes developed by the AeroTex UK for aircraft icing analysis.

Most of these codes are complex and focused heavily on ice growth and a variety of parameters must be computed before commencing the icing analysis. Due to these complexities and the computational penalties, none of the main stream icing codes can be easily integrated into trajectory optimisation frameworks. Some of the mainstream codes such as TRAJICE and AID may not be not large. However, they do not possess plugins for trajectory optimisers. Therefore, to couple those with the ASM and the

aircraft dynamics model, an interface model requiring a lot of mathematical equations have to be coded and integrated. Since the objective of the anti-icing model is to simulate the heat load, a simplified icing model which focuses mainly on power requirement had to be developed. To arrive at a suitable theoretical framework for anti-icing power modelling, the ice detection mechanisms were reviewed and reported below.

2.3 Ice Detection Methods

Ice accretion on critical aircraft surfaces has been identified as a primary contributor to many commercial and military aircraft accidents. Hence, the demand for flight in all weather conditions has necessitated the need to correctly detect icing and taking reasonable measures against it [71]. Many researches have been conducted in improving the accuracy of the present inflight ice detection methods. The leading recent novel methods that are relevant to this work include the University of IIlinois smart-icing management systems (SMS) [17], ice detection using Kalman filtering [71] and, ice detection via neural networks and Kohonen Self Organizing Maps (SOMs). With NASA support, the University of Illinois under the leadership of Prof Michael Bragg developed a smart in-flight ice management system (IMS) that can be used to sense the effects of ice build-up on aircraft performance [17] (see section 2.6.2 for details). In 2005, Aykan *et. al* [71], developed a method for detecting and identification of airframe icing using Kalman filtering based on statistical properties of aircraft. The work introduced a neural network structure that uses the aircraft estimated measurements as inputs and generates the icing parameters as outputs. Similarly, Johnson and Rokhsaz [72] and Schuchard *et. al* [73] developed developed an algorithm for the detection of airframe icing using neural networks and self organising maps method and, detection & classifi-

cation of aircraft icing using neural networks respectively.

Presently, inflight ice detection systems are in great demand [74] in order to improve aviation safety and reduce operating cost as well as the negative impacts of air transport to the environment. Most of the commercial aircraft nowadays carry an Airborne Weather Radar (AWR) system that is most often built into the aircraft nose. The on-board weather radar provides the pilots with a local weather picture ahead of the aircraft which allows the pilot to identify and avoid specific, undesirable weather formations as illustrated in Fig. 2.1. Some of these radars have a maximum range of up to 180 nm. At present, the on-board weather radar is used for the detection of thunderstorm, areas of strong precipitation and turbulence. Precipitations are associated with clouds formation, hence a weather radar, if used in combination with other meteorological information such as temperature and clouds LWC, can provide valuable information for the identification of aircraft icing areas. In spite of equipping commercial aircraft with AWR, there is still the lingering need for a sensitive, reliable and aerodynamically efficient ice detection systems that meet the growing demand of air transportation.

Ice detectors can be used in a primary or advisory role. In general terms, ice is detected in flight using devices that can detect the presence of ice and send advisory signal to the pilot in some cases trigger an de-icing action. In a primary role, an ice detector can be part of a fully automated AI system with capability to activate or de-activate anti/de-icing process based on the icing status. In an advisory role however, the ice detector is connected with several warning systems in the cockpit such as ice warning lights, de-icing action switch and system failure indication. Different ice detectors have different modes of operation. Some detect icing conditions, others detect ice accretion while some other ones detect aerodynamic degradation, etc. In any case, the primary function of

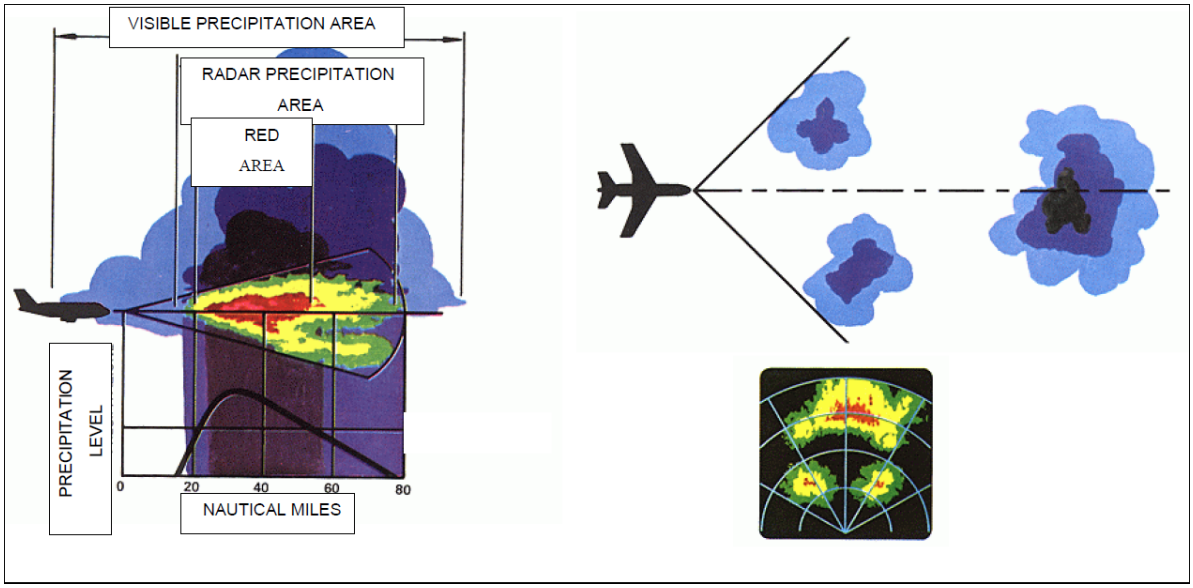

Fig. 2.1: Weather Radar Principles [4]

all of them is the detection of onset of icing, ice presence and its thickness. In almost all commercial aircraft however, ice detection is backed by crew visual observations. Common example of the current ice detectors include the electro-mechanical ice sensor detector (also known as vibro-meter) [7] and optical transducer ice detector sensor. Vibro-meters use continuous vibration to detect the presence of ice and water based on the different frequencies generated by the sensor diaphragm. Ice build up on the diaphragm increases its mass and stiffness causing it to vibrate. The device can activate de-icing sequence from a couple of millimeters of ice build up to 2-3cm. The problem with this device is that unlike the optical senses it is affected fatigue due the to repetitive icing and de-icing cycles. A schematic illustration of a vibro-meter sensor is shown in Fig. 2.2. In a more recent development, ON-WINGS [8] have developed a fixed-point optical ice-detector sensors that could be embedded in heater mat electro-thermal de-icers for composite structures as illustrated in Fig. 2.3. The advantage of this technology is the full integration of the detector with the ice protection system enabling real time control. It could also be applied to both the big and small aircraft. The NASA/Innovative

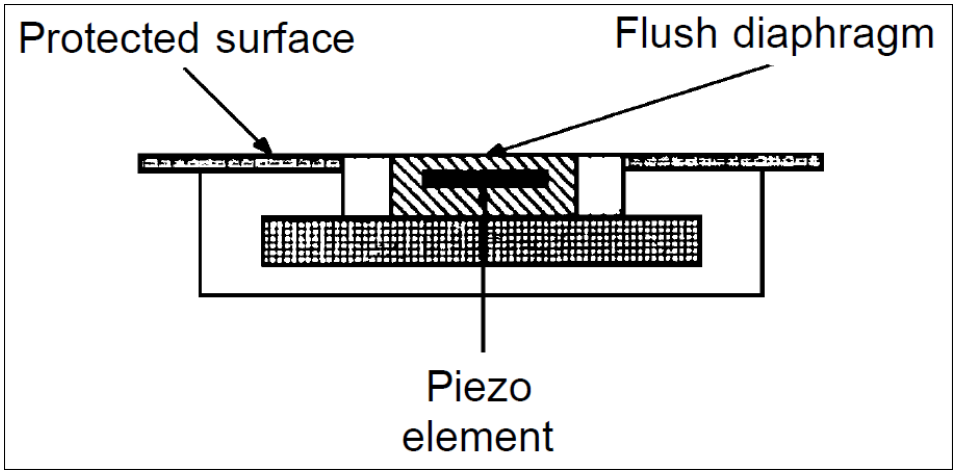

Fig. 2.2: Electro-mechanical Sensor Operating Principle [7]

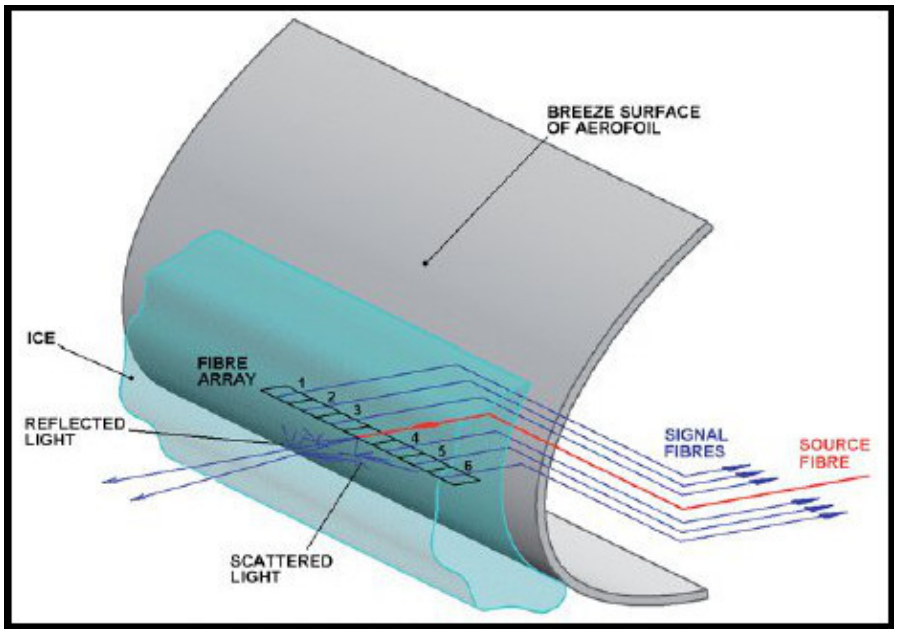

Fig. 2.3: Optical Ice-detector Sensors Experimental Arrangement [8]

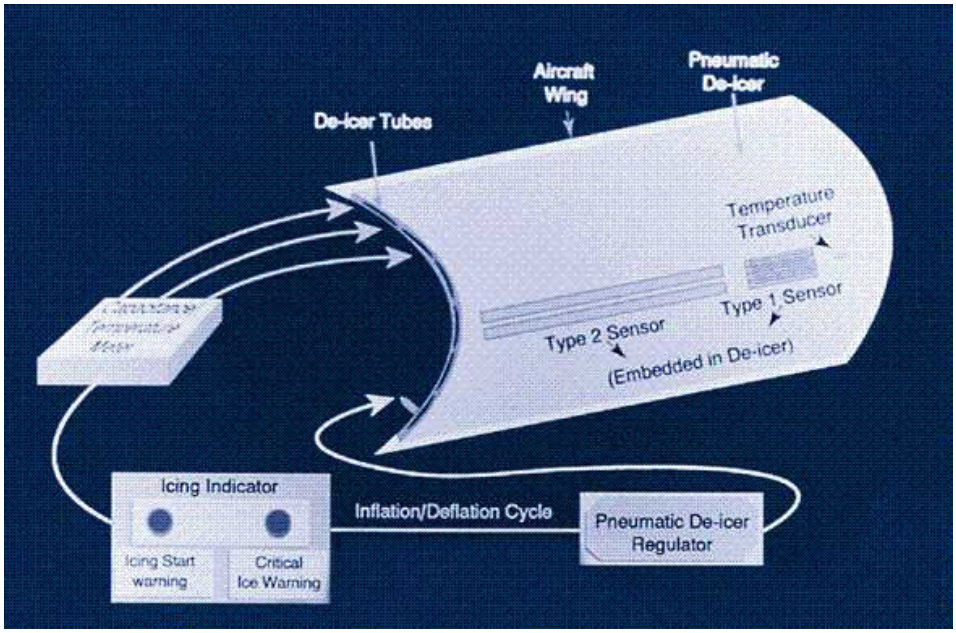

Fig. 2.4: Optical Ice Detectors for Pneumatic Deicers [9]

Dynamics Inc. have developed similar technology that would be used on Goodrich pneumatic deices as illustrated in Fig. 2.4.

2.4 Current Ice Protection Technologies

Aircraft icing issues are divided into two broad categories; that is according to whether they prevent an aircraft taking off (ground icing) or impede its subsequent flight (in-flight icing),[75]. On the ground generally, aircraft are de-iced before take-off by the spray of warm water or glycol based fluids, or taking shelter in warm hangars. For in-flight icing however, there are basically three methods of coping with ice accretion ie: thermal, mechanical and chemical methods. Sometimes two or more methods are employed to give rise to what is referred to as a hybrid system. A division of the different methods of ice protection is presented in Fig. 2.5. Aircraft IPS is operated either in anti-icing mode or de-icing mode. In anti-icing mode, the system is operated

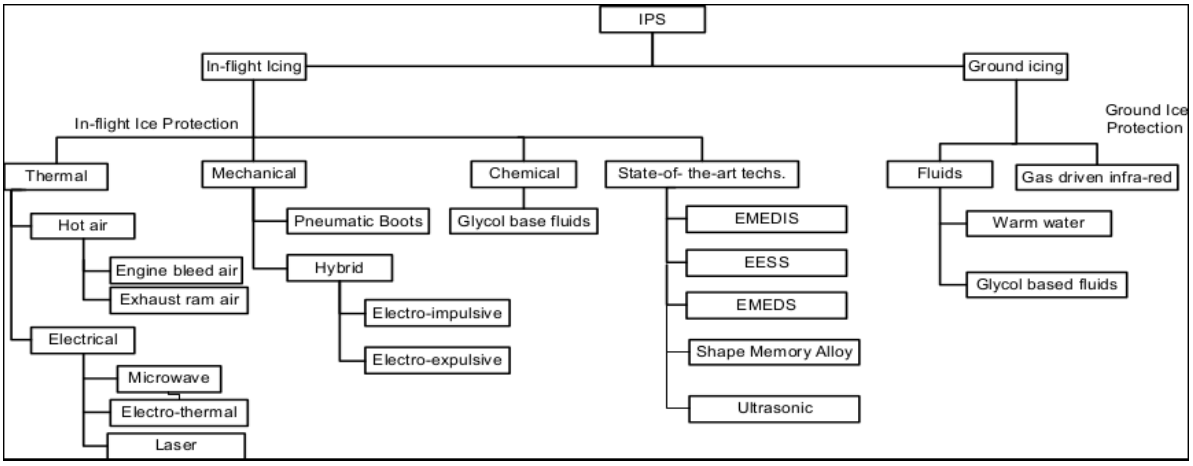

Fig. 2.5: Aircraft Ice Protection Technologies

continuously or intermittently whereas in de-icing mode, the system is operated only when the accretion passed a pre-determined level.

2.4.1 Chemical

Chemical de-icers work by applying aircraft de-icing fluids (ADF) such as TKS[2] on the surfaces to inhibit or delay the reformation of ice. The fluids serve as icing inhibitors by preventing the adhesion of ice to the protected surface or making mechanical removal easier. There are several drawbacks associated with using chemicals for in-flight ice protection. Firstly, their operation relies on a supply of de-icing fluids which is inherently limiting as only a finite amount of fluid can be stored on board, thus compromising mission time. Secondly, the chemical IPS incorporates a porous medium on the surface to be protected, which degrades aerodynamic efficiency [76]. A typical example of a chemical de-icer can be found on a Cessna 210 aircraft.

[2]TKS stands for Tecalemit-Kilfrost-Sheepbridge Stokes

2.4.2 Mechanical

Mechanical de-icers work on the principle that ice is naturally stiff and brittle, and slight distortion therefore fractures it. For this reason, mechanical de-icers operate in de-icing mode only once the ice has been allowed to build up to an acceptable limit before breaking its adhesion to the surface. A pneumatic boot is the commonest example of a mechanical de-icer (see Fig. 2.6. A pneumatic boot consists of an inflatable rubber sheets bonded to the surface which when inflated shatters the ice cohesion. The shattered ice residues are then swept away by aerodynamic forces [77]. This technology has the least energy requirement among all in-flight anti/de-icing systems. One of the disadvantages of this technology is that they are inefficient relative to thermal IPS as they leave the protected areas un-properly cleared. Fig 2.6 illustrates boots de-icer operation.

The rubber boots are affected by solar radiation, mineral oils and other chemicals which causes them to deteriorate with time. Hence, a high level of skill supervision, maintenance and operation are required. They are also associated with high drag penalties when operated which could counteract the gains made from their low energy requirement. Similarly, chances are that the shattered ice pieces may hit and damage part of the airframe. Because of these numerous dis-advantages, boots de-icers are normally limited to low-to-mid speed application up to Mach 0.5 because of fear of deformation on the wing aerofoil or intake leading edge [78].

Pneumatic boot deicers can be found on mostly smaller and turboprop aircraft such as ATR 72. Other novel mechanical methods include Electro-Impulsive De-Icing (EIDI) and Electro-Expulsive De-icing System (EEDS) technologies. These technologies utilize electricity to energize the deicers instead of pneumatic power, (see section 2.5 for details).

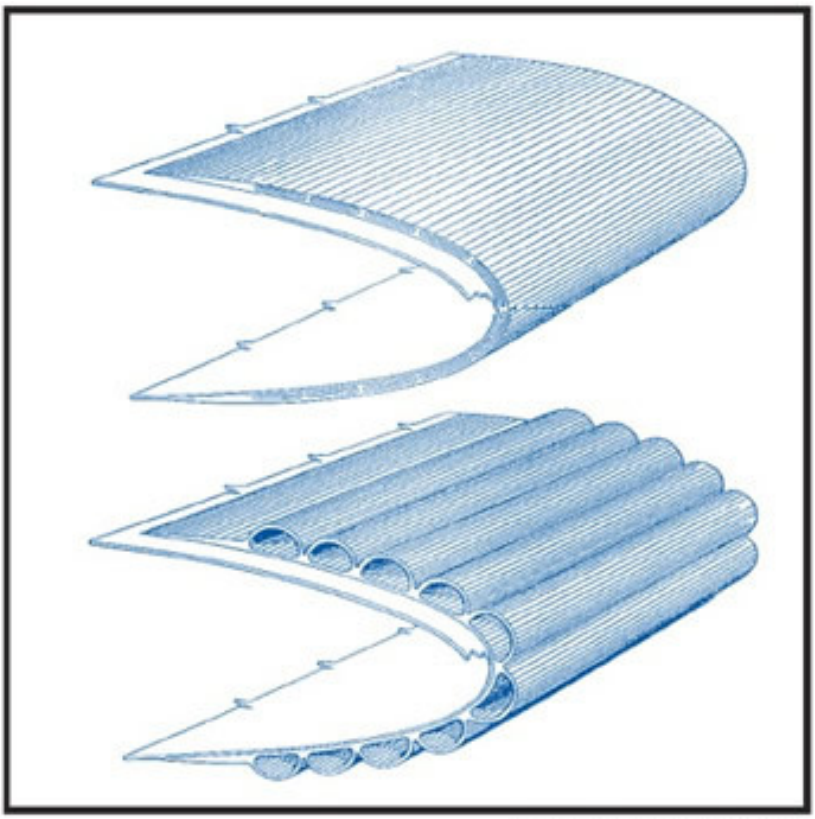

H

Fig. 2.6: Pneumatic De-icer Boots Operation [10]

2.4.3 Thermal

In the thermal method, heat is used either to prevent ice from building up or to remove it once it accumulates over the protected surfaces [79]. Thermal IPS can be bleed hot air or electrically operated. In the hot air type systems, hot air is generally drawn from an intermediate or high stage compressor bleed port or provided by a heating system through a heat exchanger. The air is then ducted through passages to the leading edges of wings, empennages, engine nacelles or other critical areas [80].

The principle of the electro-thermal IPS is to transfer the energy required for anti/de-icing to the protected areas in electrical form [81]. There are three major classifications of this technology, namely microwave energy, heater mats and laser de-icers. The earlier versions of microwave technologies (US Patent nos. 4,060,2112, 4,365,131 and 5,061,836) claim to work by raising the droplets temperature such that they do not freeze on contact with aircraft surface. Energy losses are great in this method because only a fraction of the microwave energy is intercepted by the protected surface. In recent designs, the microwave is absorbed in a propagation tube inside the leading edge and turned into thermal power, before being conducted to the skin through thermal transfer vanes [82]. In heater mat de-icers, heater elements are installed on the protected surfaces and energised by electricity to produce the desired heat. The advantage of this technology is that the heater element can be tailored to suit the application, which minimises wastage as heat is directed at the protected surfaces alone. Its disadvantage is that it is relatively heavy and expensive because large electrical power is required to activate the system. The Northcoast Technologies [83] have introduced a more efficient use of this technology through the use of graphite based heating elements. Because, the flexible expanded graphite foil is a monolithic structure that may be shaped, sculptured or layered to dif-

ferent thickness over different areas, only a single control mechanism is required which reduces the overall deicing energy. By replacing the normal heating elements with a laminate of flexible expanded graphite foil, only one-third of the energy would be required to achieve de-icing temperatures. [83]

Aircraft de-icing using lasers is a recent technology. In this technology, beams of radiant energy are generated and directed towards critical surfaces to create a footprint on that surface of the aircraft. The beams are manipulated so that the footprint is moved about on the aircraft surface to remove ice. Laser beams have wavelengths that are preferentially reflected by aircraft surface and absorbed by ice. The absorbed beams generate heat that removes the ice as the beam footprint is moved about. Laser beam generators could be heavy but the advantage is that mirrors can be used repeatedly to reflect the beam unto a wider area than can be covered by the generated beam. Presently, thermal anti-icing method is the leading ice protection technology on most of the today's medium and large transport aircraft [84].

A thermal AI system can be wet running or fully evaporative, or even cyclic de-icing. In a fully evaporative system, airflow requirements are determined based on the assumption that all the impinging water droplets under the severest condition will be evaporated. In wet running systems however, heat requirement is based on maintaining a surface temperature just above freezing allowing for the impinging water to run back for another round of freezing. This technique is mostly applied on areas where ice build up aft of the heated area can be tolerated such as turbine engine inlet duct and propeller spinners.

The major difference between the evaporative and run wetting calculating methods is that the evaporative anti-icing requirements are based on average quantities, whereas

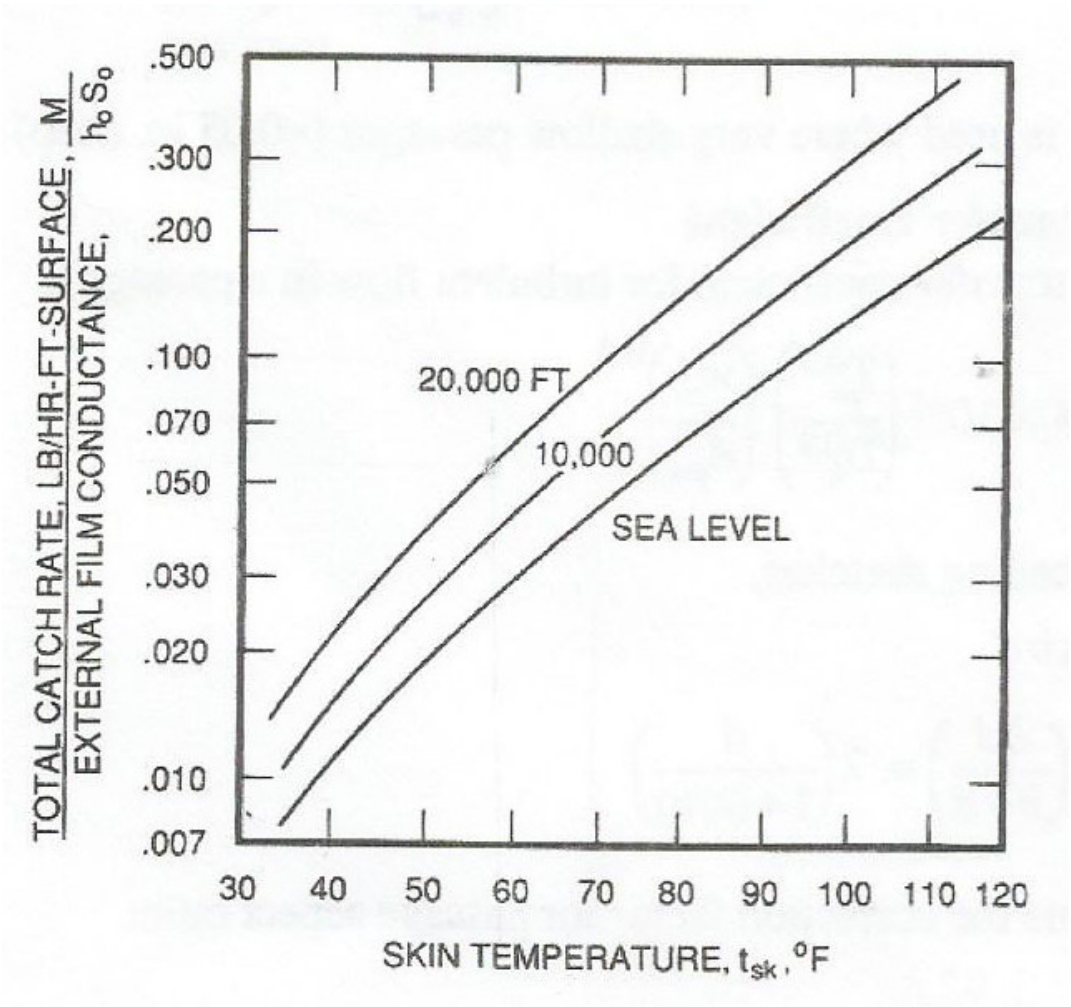

Fig. 2.7: Skin Temperature Required for Evaporative Anti-icing [11]

running wet anti-icing requirements are computed using local values of water catch rate and heat transfer. [11] In addition, a desired skin temperature (usually between 1.7 to 10 ℃) has to be selected before hand to compute the energy requirement of a running wet system. This approach is rather conservative and good only for initial estimates as it negates the contribution of the energy gains due to kinetic energy of incoming water and the heat gained due the passage of fluid over a body (aerodynamic heating). One of the key benefits of this method however, is that it allows the estimation of the required skin temperature based on the rate of water catch as shown in Fig. 2.7.

In the cyclic de-icing system, high energy is used for periodic melting of inter-facial ice which is blown away by aerodynamic forces [11]. Under this method, ice is allowed to build up to a predetermine thickness (usually small and not detrimental to aircraft performance) before the ice-surface interface is melted using a high rate heat input thereby rendering the interface adhesion zero. In this method, electrothermal energy is normally used for heating the inter-facial ice in a heat-on/heat-off cycles. The leading edge area which is to be protected is divided into several spanwise and chordwise areas such that each area can be energised sequentially or simultaneously with corresponding area on opposite sides of the aircraft. For partially swept wings, a parting strip area (typically about 2-3cm width) is provided for continuous heating of the stagnation line to prevent bridging of the upper and lower parts of the leading edge. The parting strip also provides access to the aerodynamic forces for removing the top layer ice once the ice-surface interface is melted.

The basic heater construction consists of electrical resistant elements sandwiched between two layers of dielectric material and coated with water resistant material on the external surface. This method requires the least amount of energy among all thermal ice protection methods. This advantage is however, partially offset by drag penalties incurred during ice build up (heat-off period). The efficiency of this method depends on the heater construction and the leading edge geometry. The most optimum design is that which provides higher de-icing efficiency and light weight. A cross section of a typical heater construction is shown in Fig. 2.8. [11] The thermal anti-icing is the most efficient of the three classical anti-icing methods (mechanical, chemical and thermal), and thus is currently the standard ice protection method on most of the large size transport aircraft. And among the thermal systems, the cyclic method has relatively the least heating requirement. This advantage is however, partially offset by the drag

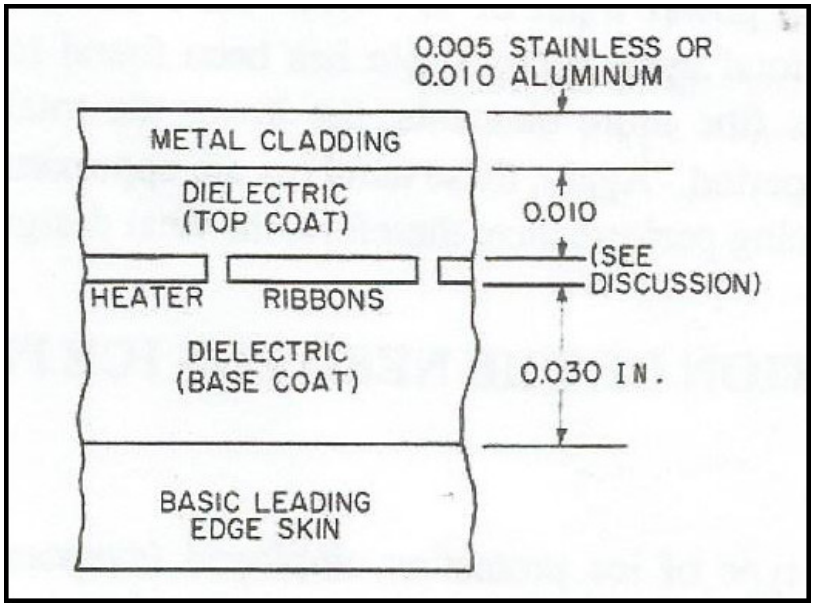

Fig. 2.8: A Typical Heater Construction Layout [11]

penalties incurred during heat-off period. [11]. Currently, Boeing 787 is the only large commercial aircraft to use cyclic de-icing technology based on heater mats developed by GKN Aerospace (see Fig. 2.13). With the exception of the cyclic de-icing system, the problem of a thermal system is that it has great potentials for runback ice which may require yet another cycle of de-icing [85]. Therefore, this technology is not applied on areas where runback may lead to refreezing on the control surfaces. Similarly, they are not applied on engine intakes because of the complexities involved. Among the important literatures for the analysis of runback ice are the FAA runback documentaion [86] and, Al-khalil *et. al* [87] and Alegre [88] works. The FAA document [86], described extensively the characteristics of ice accretion and their aerodynamic effects whereas Al-khalil *et. al* [87] developed an anti-icing runback model describing heat transfer procedures in a running wet system while Alegre [88] developed a one-dimensional model for predicting heating requirements in a runback ice accretion study. Other literatures dealing with anti-icing heating requirement are discussed in the following section.

2.4.4 Anti-icing Power Estimation Methods

Several methods have been developed for AI power estimation that could be learnt from. The most prevalent of these methods based on the literature survey conducted in this work are the Messinger, SAE, Roger Gent, Petrenko and Krammer/Mieir/Scholz methods. These methods are similar in the sense that they are all based on thermal anti-icing solution. Their major differences come in the number and physics of the energy terms used in the analysis, and the level of their complexities. Basic principles of these methods are discussed in the following sections.

Messinger Method

The Messinger model gives the energy balance between cooling due to convection, sensible heating requirement, evaporation/sublimation, kinetic energy, and viscosity terms in the conservation energy equation. The sensible heating refers to the energy required to raise the temperature of the impinging water droplets to the skin temperature, and the evaporative heating is that due to the variation of the saturated vapour pressure over water at the surface equilibrium temperature whereas, convective cooling accounts for energy loss due to temperature difference between the surface and the impinging water droplets. The kinetic energy term accounts for heat gains due to the kinetic energy of the incoming droplets, and the viscosity term refers to heat gains due to the resistance of fluid (friction) due to the passage of a body in it. Thus, for an icing surface having a steady state temperature, t_{e_s}, of less than 0℃, the actual value of t_{e_s}, will be largely dependent on the result of an energy balance involving the simultaneous interchange of the terms as illustrated in Fig. 2.9

In the Messinger model, the heat transfer coefficient and the rate of water catch are

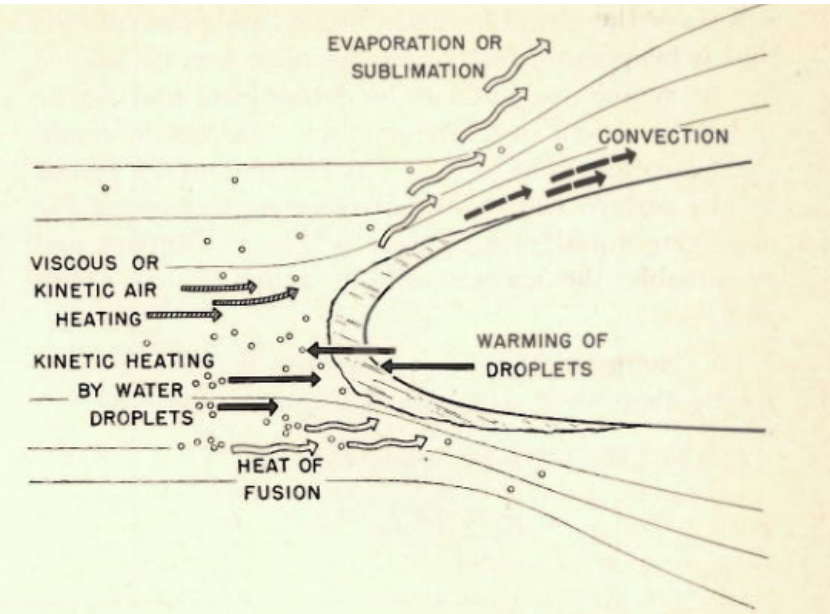

Fig. 2.9: Modes of Energy Transfer for an Unheated Airfoil in Icing Conditions [12]

the two essential parameters for computing the fraction of the non-freezing water (f) and the balance temperature. The governing equations for the original Messinger model based on the mass and energy balance in a control volume are expressed as:

$$m_{im} + m_{in} = m_{ac} + m_{e,s} + m_{out} \tag{2.1}$$

$$q_{im} + q_{in} + q_{air} + q_{fri} = q_{ac} + q_{e,s} + q_{out} + q_{con} \tag{2.2}$$

Where

The freezing rate is expressed as:

$$f = \frac{m_{ac}}{m_{im} + m_{in}} \tag{2.3}$$

$$m_{out} = (1 - f)(m_{in} + m_{in} - m_{e,s}) \tag{2.4}$$

If $f = 1$, all mass in the control volume accretes, if however, $f = 0$, all mass in the control volume runbacks to the next cell. Further readings on the above equations can be found in Ryosuke [62] and Messinger [12]. Many anti-icing power calculation methods have been evolved based on the mass and energy balance principle. These include:

SAE Method

The Society for Automotive Engineering (SAE) Aerospace submitted among its regular Aerospace Information Reports (AIR), the AIR1168/4 [11] for recognition as an American National Standard for ice, rain, fog and frost protection. The document gave good examples to follow using the three methods (evaporative anti-icing, wet running system and cyclic de-icing) of thermal ice protection. It presented basic equations for computing ice protection requirements for both transparent and non-transparent surfaces including simplified equations for preliminary design. These equations which were given in imperial units gives the evaporative anti-icing heat load as:

$$\frac{q}{h_0 S_0} = (t_{sk} - t_w) + [\frac{M}{h_0 S_0} c_w (t_{sk} - t_w)] + [\frac{M}{h_0 S_0} L_e] \tag{2.5}$$

The right hand side of the equation accounts for the convection, sensible and the evaporation terms. For a wet running system, the equation is given as:

$$\frac{q}{h_0 S} = (t_{sk} - t_{aw}) + \frac{M_\beta}{h_0} c_w (t_{sk} - t_w) + \frac{2.9 L_e (p_{sk} - P_w)}{p_{amb} - P_{sk}} \tag{2.6}$$

Roger Gent Method

The classic Messinger approach assumes incompressible flows on the icing surface. Where the flow speed exceeds Mach 0.3 however, compressibility effects are normally considered significant. Hence, Cansdale and Gents [59] extended the analysis to compressible flows by combining the convective and kinetic terms, and adding a new evaporative cooling term which allows for the effect of pressure distribution around the aerofoil on the local water vapour concentration. [23] Thus:

$$q_{con} - q_{ke} = h_C(t_s - t_r) \tag{2.7}$$

where h_c is the convective heat transfer coefficient, t_s is the surface temperature and t_r is the dry adiabatic recovery temperature. The recovery temperature can be evaluated from the following equation:

$$t_r = \left(t_\infty + 273.15 + \frac{V_\infty^2}{2C_p}\right)\left(\frac{1 + r(\frac{1}{5}M_L^2)}{1 + r(\frac{1}{5}M_L^2)}\right) - 273.15 \tag{2.8}$$

The subscripts ∞ and L denote freestream and local respectively. Thus, the new expression for evaporative cooling for a compressible flow is given by [59]:

$$q_e = \frac{0.622 h_c L_v}{C_p H_0 Le^{2/3}}\left(e_s\left(\frac{T_T}{T_s}\right)\left(\frac{P_L}{H_0}\right)^{-1/\gamma} - e_\infty\left(\frac{H_0}{P_\infty}\right)\right) \tag{2.9}$$

The subscript s refers to the properties at the surface and T_T refers to the total temperature. The total energy balance within a small control volume is thus given as:

$$q_c - q_{ke} + q_e + q_{im} = q_L + q_{ke} + q_{out} \tag{2.10}$$

where,

$$q_{im} = m_w C_{pw}(t_f - t_\infty) \tag{2.11}$$

$$q_L = N_f(1+X)M_w L_F \tag{2.12}$$

$$q_{ke} = 0.5 m_w V_i^2 \tag{2.13}$$

$$q_{out} = X m_w C_{pw}(t_{out} - t_s) \tag{2.14}$$

The the freezing rate (N_f) is given by:

$$N_f = \lambda\vartheta(e_{th}(\frac{T_T}{273.15})\beta^{\frac{1}{7}} - e_{t_\infty}\chi) - \lambda(t_r + b(\frac{V_\infty^2}{2C_{pw}} + t_\infty + X t_{out})) \tag{2.15}$$

where,

$$\lambda = \frac{C_{pw}}{bL_f(1+X)} \tag{2.16}$$

$$b = \frac{m_w C_{pw}}{h_C} \tag{2.17}$$

$$\vartheta = \frac{0.622 L_v}{C_p H_0 Le^{2/3}} \tag{2.18}$$

In this method, the impact speed V_i can be approximated to the freestream speed V. The term X represents the runback rate expressed as a fraction of the directly impinging water mass catch rate, [11]. The method was applied on the AeroTex UK [52] code, Internal Heat Balance (IHB), for the calculation of ice growth rates on the surface and initial sizing of heating power requirements for anti-ice systems.

Victor Petrenko Method

In 2000, Prof Victor Petrenko [89] patented a method for modifying the ice adhesion strength (US Pat Nos. 6027075, 6427946, 7034257) which paved way for further re-

searches into low power electrical de-icing. Petrenko went ahead in 2003 [90] to develop a simple Pulse Electro-thermal De-icing model based on the method. Using same model, Petrenko demonstrated that the de-icing energy is linearly proportional to the inverse power density. The method was further used for optimising thickness of complex shapes for pulse electro-thermal de-icing systems [91]. In this method, a temperature distribution and range, and a freezing time produced by the de-icing pulse were modelled. Thus, the total energy required to de-ice an aircraft wing of certain geometry is given as:

$$q = q_{warm} + q_{min} + q_h \tag{2.19}$$

The total time (t) it takes to raise the temperature of ice from temperature T to the melting temperature T_s is expressed as:

$$t = \frac{\pi(T_{melt} - T)^2}{4 \cdot \dot{q}_{anti}^2}(\sqrt{\lambda_i \rho_i c_i} + \sqrt{\lambda_s \rho_s c_s}) \tag{2.20}$$

The actual energy required to melt the inter-facial ice is given by:

$$q_{min} = d \cdot \triangle H_{f,ice} \rho_i \tag{2.21}$$

In the case of a thicker heater, a term (q_h) to account for heater thermal capacity is added as follows:

$$q_h = d_h \cdot c_h \cdot \rho_h \tag{2.22}$$

Where d_h,c_h and ρ_h denote the heater thickness, specific heat capacity and density respectively. Therefore, total energy required to de-ice the surface is given by:

$$q = \frac{\pi(T_{melt} - T)^2}{4 \cdot W^2}(\sqrt{\lambda_i \rho_i c_i} + \sqrt{\lambda_s \rho_s c_s}) + d \cdot \triangle H_{f,ice} \rho_i + d_h \cdot c_h \cdot \rho_h \tag{2.23}$$

Petrenko's model is only applicable to heater mat electro-thermal technology. Further readings on this method can be obtain in Petrenko [90] and [91]

Krammer, Meier and Scholz Method

Based on a method for estimating de-icing power developed in Krammer and Scholz [92], and Meier and Scholz [84], thermal balance over the surface is performed satisfying the following relationship:

$$\dot{q}_{anti} = \dot{q}_{sensib} + \dot{q}_{conv} + \dot{q}_{evap} - \dot{q}_{ke} - \dot{q}_{aero} = 0 \tag{2.24}$$

where, for full surface de-icing in a fully evaporative system,

$$\dot{q}_{conv} = \bar{h}(T_{sk} - T_\infty) \tag{2.25}$$

$$\dot{q}_{sens} = \dot{m}_{imp} \cdot c_{p_{liq}} \cdot (T_{sk} - T_\infty) \tag{2.26}$$

$$\dot{q}_{evap} = 0.7 h_0 L_e \left[\frac{R_h e_\infty - e_{surf}}{P_\infty C_{P_{air}}}\right] \tag{2.27}$$

$$\dot{q}_{ke} = \dot{m}_{imp} \cdot \frac{V_\infty^2}{2} \tag{2.28}$$

$$\dot{q}_{aero} = R_c \bar{h} \left[\frac{V_\infty^2}{2 c_{p_{air}}}\right] \tag{2.29}$$

For a wet running system, same equations as above are applied except that the equilibrium temperature is kept low, just over the freezing point. For cyclic de-icing however,

$$\dot{q}_{sens} = \dot{q}_{cycl} = \frac{\dot{m}_{ice}}{t} \left[\Delta T \cdot c_{ice} + L_f\right] \tag{2.30}$$

where, m_{ice} is given by:

$$m_{ice} = t_{ice} \cdot \rho_{ice} \tag{2.31}$$

The term t_{ice} denotes the thickness of ice to be melted, and the impingement mass flow per unit area is given by:

$$\dot{m}_{imp} = \dot{m}_{localimp} \tag{2.32}$$

$$= \frac{\dot{m}}{A} = V \cdot \rho_{LWC}.E_m \tag{2.33}$$

The average heat transfer coefficient ($\bar{h}$) is expressed as:

$$\bar{h} = \bar{N}u_L \cdot \frac{k}{L} \tag{2.34}$$

The symbol k represents the thermal conductivity of air whereas x stands for the leading edge characteristic length, and Rc represents the recovery factor. The Nusselt number Nu, is expressed as [93]:

$$\bar{N}u = (0.037Re_L^{4/5} - 871) \cdot Pr^{1/3} \tag{2.35}$$

Where Prandtl (Pr) and Reynolds (Re) numbers are dimensionless quantities that could be calculated from the following relationships:

$$Pr = \frac{C_p \cdot \mu}{k} \tag{2.36}$$

$$Re = \frac{\rho_{MSL} \cdot V \cdot l}{\mu} \tag{2.37}$$

For a cyclic deicing system, Mieir and Scholz [94] presented a simple method for assessing the cyclic power demand. For $20\mu m$ droplets size, the collection efficiency is given as [94]:

$$E_m = 0.00324 \cdot (\frac{v}{t})^{0.619} \tag{2.38}$$

$$\dot{m} = v \cdot t \cdot LWC \cdot E_m \tag{2.39}$$

$$\tag{2.40}$$

whereas,

$$\dot{q}_{sensible} = \dot{q}_{cycle} \tag{2.41}$$

$$= \frac{\dot{m_{ice}}}{t}[\triangle T c_i + L_f]\dot{m}_{ice} = t \cdot \rho \tag{2.42}$$

Therefore, the average specific heat flux is given by:

$$\dot{q}_{total} = \dot{q}_{PS} \cdot k_{PS} + \dot{q}_{cycl} \cdot k_{cycl} \tag{2.43}$$

Where parting strip power, $\dot{q}_{PS}$ is given by Eq. 4.5, k_{PS} is the ratio of the area to be de-iced by the parting strip to the total protected area (for initial design this is taken as 19%). K_{cycl} is the ratio of the cyclic heat on time to the total cycle time. Further reading on the Krammer and Scholz calculation method can be found in references [92],

[94] and [84].

It can be noted that the Messinger model does not cover incompressible flow condition which makes it unsuitable for use in its original form in this work while the SAE method covers only the principal energy loosing terms and ignored the contribution of the energy gaining terms such as friction and kinetic energy. Though small in comparison, the energy gaining terms tend to generate significant amount of heat that may reduce the anti-icing power requirement. The Gent's method is quite rich and detailed, however, it is found to be too complex for the level of application required in this work which is icing power estimation. The method would be most appropriate for icing codes involving droplets trajectory calculation and ice growth analysis. The Petrenko's model is still under development for application in large commercial transport aircraft and therefore not suitable for application on the baseline aircraft too. The Krammer/Mieir/Scholz method however, is simple and applicable to the type of anti-icing system on the baseline aircraft. Hence, the Krammer *et. al* [92] method was applied for modeling the anti-icing power module of the aircraft systems model.

In the course of the literature survey, other newer and energy efficient ice protection technologies that are yet to attend maturity for commercial transport application were discovered. Major ones among these state-of-the-art ice protection technologies include the Electro-Mechanical Expulsive De-icing System (EMEDIS) and Thermo-Mechanical De-icing System (TMEDS). A brief details of these technologies are discussed below.

2.5 State-of-the-Art Ice protection Systems

The state-of-the-art hybrid de-icers combine electric, thermal and mechanical effects for aircraft icing protection [14]. The EMEDIS invented by Gerardi et al [95] is among the leading state-of-the-art ice protection systems. The EMEDIS is an off-shoot of the Electro-Impulse De-Icing (EIDI) system with improved actuator coil and electronics. The other method known as Electro-Expulsive Separation System (EESS) was invented by L.A. Haslim and R.D. Lee [96]. The EESS, work by dis-tendering elastomeric material placed on the leading edge for ice shed off. There are other similar projects developed based on this method such as the Electro-Mechanical Expulsion De-icing System (EMEDS) developed by Olson et al [97]. The sizing and mechanism of operation of some typical examples of this technology are discussed below.

2.5.1 Electro-Magnetic Expulsion De-icing System

A typical EMEDS coil is illustrated in Fig. 2.10. Sizing of EMEDS is carried out by determining the electromagnetic force of the coil translated into power consumption of the system [98]. The electromagnetic force of each actuator is given by:

$$F = \frac{C_1 N^2 I^2}{b}\left[\tan^{-1}\frac{b}{d_m} - \frac{d_m}{2b} ln \frac{d_m^2 + b^2}{d_m^2}\right] \tag{2.44}$$

where b is the width of the conductive strip, C_1 is $4 \cdot 10^{-7}$, d_m is the mean separation between the winding bundles, I is the current in the coil, L is the length of the coil and N is the number of turns in the coil. This approximation is only valid if the mean separation d_m is much greater than the thickness of the upper and lower individual

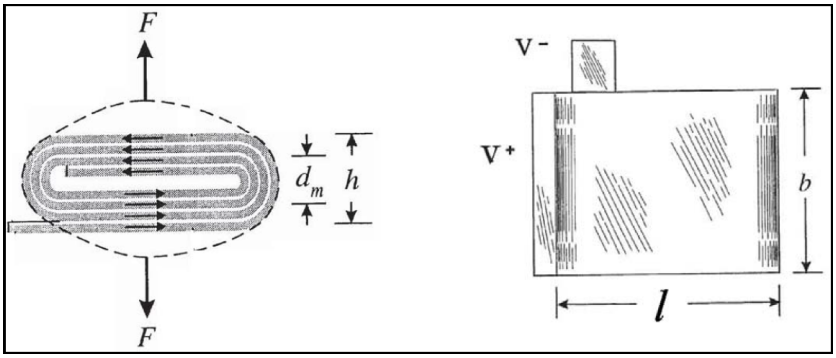

Fig. 2.10: EMEDS Coil Properties [13]

winding layers. This shows that F strongly depends on the number of turns in the coil, N. However, care is required as high N would lead to increase the mean winding bundle separation, d_m, thereby tending to decrease the actuation force. Therefore, according to Geraridi and Ingram [13] the maximum number of turns is given by:

$$N_{max} = \frac{h_{max}}{(2(a_{min} + I_{min})} \tag{2.45}$$

$$h_{max} = 2 \cdot d_{max} \tag{2.46}$$

where a_{min} is the minimum available thickness of the conductive strips t_{min} is the minimum available thickness of the dielectric and h_{max} is the maximum allowable coil height. The resistance of the coil, R is given by:

$$R = 2\frac{NL}{ab}R_c \tag{2.47}$$

The length ab is the cross-sectional area of the conductor and L , the inductance of the coil. L can be obtained from:

$$L = \frac{N^2 \mu_0 l d_m}{b} \tag{2.48}$$

where l is the coil length and μ_0 is the permeability of free space. The circuit is closed

by connecting switch S to point a which causes the capacitor to start charging from the electric source. When de-icing mode is activated, switch S moves from point a to c thereby discharging to generate electromagnetic force in the actuator. Circuit oscillation is avoided by applying over-damped response configuration. The current in the coil is given:

$$i(t) = A_1 e^{s_1,t} + A_2 e^{s_2,t} \tag{2.49}$$

where $s_1 and s_2$ are given by:

$$s_{1,2} = \frac{2R}{L} \pm \sqrt{\left(\frac{R}{2L}\right)^2 - \frac{1}{LC}} \tag{2.50}$$

Therefore $u_c(t)$ is given by:

$$u_c = \frac{1}{C} \int_0^{t_0} i(t)dt \tag{2.51}$$

and the power consumed by each actuator is given by:

$$P = \frac{1}{t_0} \int_0^{t_0} u_c(t) \cdot i(t)dt \tag{2.52}$$

Current application of this technology is limited to the wing tips and stabilizers of general aviation military transport aircraft such as Raytheon and Boeing P-8A. However, this technology is a potential low energy ice protection system for the next generation large commercial transport aircraft wings. Further details can be obtained from the work of Geraridi and Ingram [13].

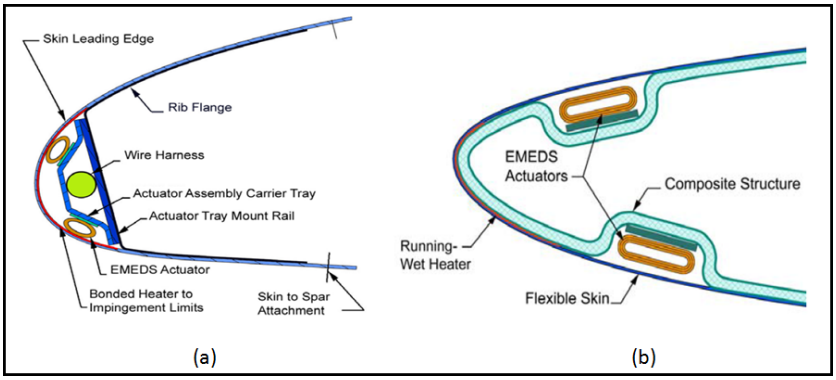

Fig. 2.11: Diffenrent Configurations of the TMEDS [14]

2.5.2 Thermo-Mechanical Expulsion De-icing System

A thermo-mechanical de-icing system (TMEDS) consists of an electro-thermal or hot gas anti/de-icer and a mechanical de-icer operated in harmony to limit inter-cycle ice accumulation thickness to below a prescribed limit and or to prevent runback icing [14]. The TMEDS can be mounted at the same place or different positions depending on the design as illustrated in Fig. 2.11. When mounted at the same position, the heating and flexing are synchronised locally to achieve efficient operation. Heat is applied to raise the inter-facial ice temperature in order to weaken the adhesion of ice to the skin. Hence, once the heat is added the ice layer could be easily dislodged by flexing the actuators. In an anti-ice configuration, the thermal device is mounted at the leading edge whereas the mechanical device is mounted aft of the thermal anti-icer. When operated, the anti-icer prevent icing of the leading edge by flexing from to time, and the thermal component melts any run-back ice. This reduces the power required to operate the system if the entire area has to be thermally anti-iced [14]. Current application of this technology include the Lear Jet 85 horizantal stabilizer and, North Grumman Triton MQ-4C wings and horizantal stabilizers. Using a typical layout as shown in Fig. 2.12, the power requirement of TMEDS is given by:

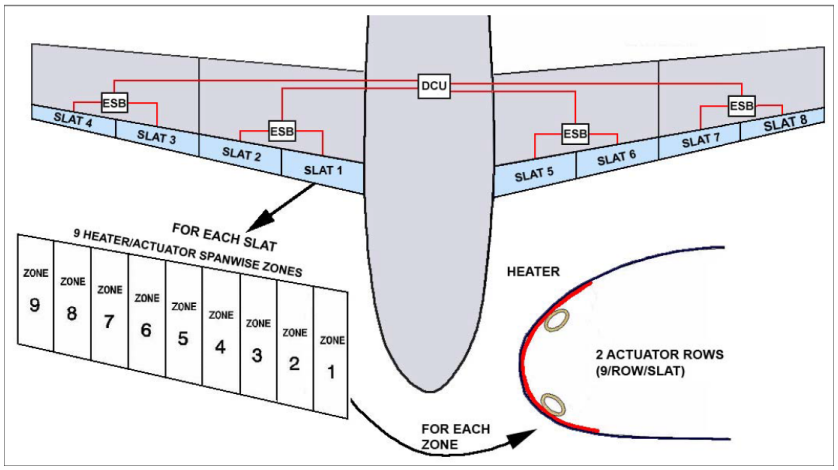

Fig. 2.12: Typical TMEDS Layout of Spanwise Segments[14]

$$\dot{Q}_{TMEDS} = \frac{q}{S_0} \cdot S_{zone} \cdot n_{zone} + \dot{Q}_{EMEDS} \tag{2.53}$$

The TMEDS is another potential low energy IPS for consideration in the next generation large transport aircraft. It combines the efficiency of the thermal system and the low energy operation of the mechanical system. Further reading on this technology can be obtained from [14].

2.6 Other Novel IPS Technologies

There is a lot of progress towards the development of new and more efficient de-icing systems that are compatible with next generation composite airframe structures. These include the heater mat technology, smart IPS and icephobic coatings among others. Botura *et. al* [99] developed a low thermal mass and low energy system with an average power density of less than 1.5 W/in^2 at -4 °F. Paul Stoner *et. al.* [100] describe a methodology for fabricating a Ti-Ni heater element and its electrical energy controller.

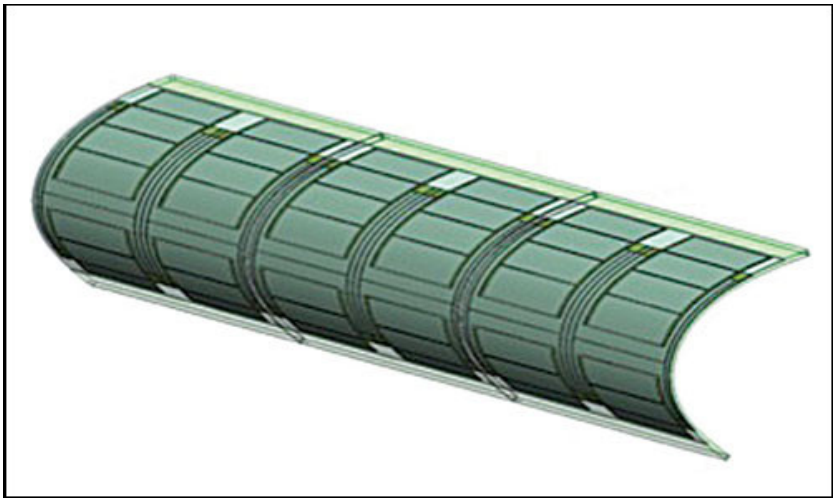

Fig. 2.13: GKN Electro-thermal Heater Mat [15]

In 2001, Rutherford and Dudman [83] developed the Zoned Aircraft De-icing System and Method on behalf of Northcoast Technologies. The B787 heater mats were developed by GKN Aerospace using composite material (see Fig. 2.13). According to the report [15], the B787 power consumption was reduced to between 45 to 75 kW using this technology compared to 150 to 200 kW required if classical technology was used. A more efficient 'low power electro-thermal deicer (LPED)' technology (same as pulse deicer) has been developed in which the thermal energy is concentrated directly on the ice impinging surface at the ice/skin interface, minimizing the energy losses. Goodrich Corp tested this technology on a Cessna 303T wing leading edge during the 2003/4 winter, and reported that between 20-50% energy was saved compared to the conventional methods [99].

In 2010, Habashi [101] introduced volumetric source term within the conduction layer in FENSAP-ICE CHT module for heater pads energy simulation. In mid-2010, Meier and Scholz [84] developed a simplified method for a quick estimation of power requirements for electrical de-icing systems. The AeroTex UK developed the HTEMS (hybrid

electro-thermal-electromechanical simulation) tool under the Clean Sky, JTI for complex icing analysis including electromechanical and electro-thermal systems. The AeroTex also conducted environmental icing tests on acoustically protected, electrically powered, scoop intake and channel [102]. Petrenko et al [91] predicted that a pulse de-icer may require just 1% of the energy requirement of a conventional thermal de-icer when fully optimised. This further shows that a lot is required to be solved about electrical de-icing systems.

2.6.1 Icephobic Coating

Conventional methods of protecting aircraft against inflight icing involve use of active ice protection systems (AIPS). However, AIPS are characterised by complexity and high fuel consumption. Hence, there are on-going research efforts aimed at developing passive ice protection systems (PIPS) that are easy and require less energy to replace AIPS. Prominent among PIPS is the use of icephobic coatings on aircraft parts prone to inflight icing to reduce ice adherence to the surfaces. At present, there are numerous materials, coatings, and paints that have low friction properties which are marketed as icephobic. Research has shown that these materials will not prevent ice build up. In fact, ice often builds on these materials at the same rate as on any other material, which indicates high failure rate [103].

Previous experiments have shown that icephobic coatings have the potential to significantly reduce AIPS power consumption [104]. However, these coatings must have certain chemical and physical properties to withstand an aircraft's harsh operating environment. Thus, their durability, costs and expected service life have not yet been established as compared to AIPS. Erosion, corrosion and reaction with atmospheric

substances vis-a-vis its effects to the environment are a great challenge to understand at the moment. It is also yet to be established whether icephobic coatings alone could safely be used on the entire Appendix C envelope as well as other proposed appendices. Response to lightening, electrostatic properties, interference with electromagnetic signals and avionic components are all issues that are not yet resolved. The safety of AIPS has been established and is therefore certified by FAR/EASA for use in flight in known icing conditions.

2.6.2 Smart Ice Protection Systems

The icing sensors currently in use primarily sense ice accretion, but not its effect on aircraft performance and control. Icing related accidents could be avoided in two ways: avoiding icing conditions or designing and operating aircraft systems in an ice tolerant manner. However, in commercial aircraft where schedules must be maintained and DoC must be kept to the barest minimum, ice tolerant designs/procedures may be preferred options except for severe icing conditions [105]. Aircraft accident investigations showed that in many cases aircraft accident could have been survived in non-standard set of flight conditions if proper control procedure was used [71].

According to, Prof Bragg, the SMS[3] would detect the onset then alert the pilot and prevent dangerous manoeuvres based on the effects such a manoeuvre will have on the smart system. The system will then adapt the FMS for a safer operation mode [105] as illustrated in Fig. 2.15. To accomplish these objectives, the IMS receives inputs from the traditional ice sensors, the IPS system, flight crew, the aircraft flight dynamics and other aircraft state information. The IMS was designed to control the IPS and analyse

[3]The concept of Smart-icing Management System (SMS) has been introduced in section 2.3, page 38

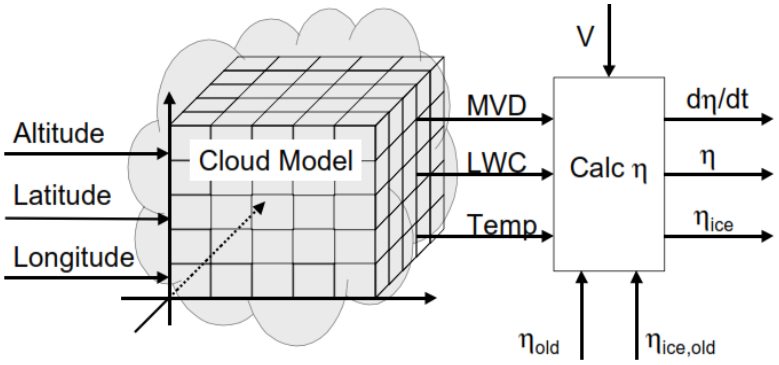

Fig. 2.14: Ice Accretion Effects Simulation [16]

the available information to determine the effect of the ice accretion on the aircraft performance, stability and control. [17] The ice accretion effects was modelled based on the following equation:

$$C_{(A)iced} = (1 + \eta_{ice} k'_{C_A}) C_{(A)} \tag{2.54}$$

where

$$k'_{C_A} = \frac{\eta}{\eta_{ice}} k_{C_A} \tag{2.55}$$

In this model [17], the η_{ice} represents the icing severity of the icing encounter whereas, η is an aircraft specific icing severity parameter and k represents the relative effect ice has on a particular stability and control parameter $C_{(A)}$. The η_{ice} is calculated based on aircraft speed and size, and the icing conditions as illustrated in Fig. 2.14.

It is expected that this technology would prevent pilots from making bad decisions in the absence of adequate information. An icing encounter flight simulator has thus been developed to integrate and test different components of this technology [16]. The simulator is to perform the function of a systems integrator by bringing together the various flight simulator components composed of an aircraft model, flight mechanics,

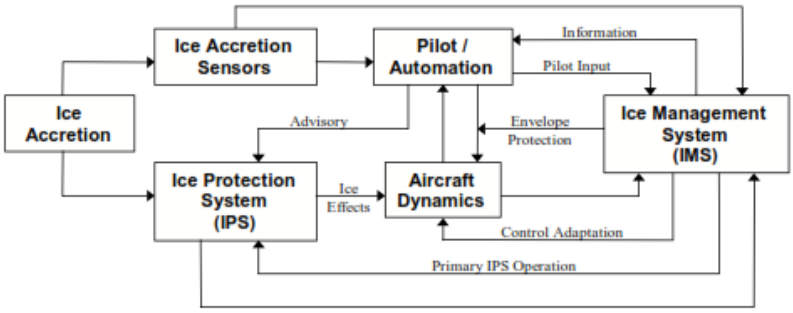

Fig. 2.15: Schematic of the Functions Performed by the Ice Management System [17]

aerodynamics, propulsion, controls, sensors, the ice protection system, the smart icing system, and human factors. Also to perform virtual flight tests to examine the effects of icing on aircraft operations under various icing conditions. [16] The team want the ice-management system to automatically adapt the flight control system to make an aircraft controllable and safe to fly when iced. For larger, newer aircraft , the system could operate autonomously, while keeping the pilot properly informed. Still yet, the above proposed solutions did not address the lingering impacts of emissions due to air transport and the increasing demand for all-weather air transport. However, trajectory based operations involving adverse weather conditions such as aircraft icing could minimise the environmental impacts aviation by including those factors influencing aircraft icing in the current trajectory optimisation method. Therefore, taking advantage of on the current advances in performance navigation systems, a method has been developed in this work for operating aircraft at low power levels by incorporating icing conditions in aircraft trajectory optimisation schemes. This would greatly enhance aircraft performance in real weather scenarios as well as the reduction of unnecessary fuel consumption and emissions. In addition, this objective is in line with the Clean Sky system for green operations Work Package 3 (SGO WP3) for management of trajectory and mission (MTM), and the management of aircraft energy, (see Fig. 1.3 for details). Consequently, a literature review of the different optimisation methods including air-

craft trajectories, and future Air Traffic Management (ATM) system as well as next generation aircraft were carried out and discussed below.

2.7 Optimisation Methods

Optimisation through mathematical analysis was first independently developed by Sir, Isaac Newton, Gottfried Leibniz and Pierre de Fermat in the 1600s. [106] In particular, Fermat defined the basis of most analytical optimization through the computation of local minimums and maximums of functions by solving for the derivative and setting it to zero. In addition Fermat, along with Blaise Pascal, founded the theory of probability that is critical to today's Monte Carlo techniques and the recently developed evolutionary/genetic optimisation algorithms. Another major break-through was the concept of Pareto optimality developed by Vilfredo Pareto [106]. The graphical representation of Pareto optimality is widely used to define two or more objective optimality. The Pareto set gives trade-off solution between multiple objectives for the current generation which means any improvement to one objective is possibly only through a reduction in performance in another. Optimisation techniques have been used to solved many real life problems:economical, environmental, social, technical, etc. These kind of results which are based on trade-off, are often referred to as the best compromise solutions [107].

Within the new generation optimisation algorithms, Schaffer developed the first multi-objective evolutionary algorithms dubbed Vector Evaluated Genetic Algorithms(VEGA) [108]. According to [109] VEGA sometimes have bias toward some regions in multi-objective optimisation problems. Other forms of multi-objective optimisation algorithms that followed after include Multi-objective Genetic Algorithm (MOGA) by Fonseca

and Fleming [110]; Niched Pareto Genetic Algorithm (NPGA, NPGA2) by Horn et al. [111]; Non-Dominated Sorting Genetic Algorithm (NSGA, NSGAII) by Srinivas and Deb [109], and Strength Pareto Evolutionary Algorithm (SPEA, SPEA2) by Zitzler, Laumanns [112], and Thiele. Most recent ones which are distinct from the traditional Pareto-dominated mechanisms includes Pareto-Adaptive ε-dominance by Hernandez-Diaz et al. [113]; and Regularity Model Based Multi-Objective Estimation of Distribution Algorithm(RM-MEDA) by Zhang and Zhou [114]. For very complex problems, the Gradient Based, Direct Search and Hybrid methods are usually employed. In the Gradient Based, the optimal solution is found by calculating the gradient information of the objective function and the constraints given for the test case whereas, the Direct Search method work independent to the gradient information of the objective, but they do depend on the value of the objective function. On the other hand, the hybrid methods combine the traits of two or more optimisation techniques to optimise the complex problem. [107] The optimal control theory is widely accepted as the standard approach in solving trajectory optimisation problems. However, optimal control theory requires parameterisation for controls and states of the problem and typically uses gradient based techniques to find the solution. This level of analysis is usually required for complex design problems where local minimums are required. The goal of this study is not to find optimal solutions but rather to find efficient solutions (Pareto optimal) which can prioritise multiple objectives based on given sets of criteria. Hence, the approach to this study is to use genetic algorithms optimisers for trajectory optimisation.

2.7.1 Trajectory Optimisation

Every optimisation problem falls into one of two broad categories: constrained optimisation and unconstrained optimisation. A constrained optimisation is the minimisa-

tion of an objective function subject to constraints on the possible value of the design variable, and can either be equality or inequality constraint. An unconstrained optimisation problem, on the other hand, is the minimisation of an objective function that is not subject to any restriction on the values of the design variables. The goal of an unconstrained optimisation problem is to find the global optima whereas the goal of a constrained optimisation is to find the local optima satisfying the constraints [106]. The constraint approach imposes search boundaries which reduces search domain and computation time. For example in the case of the mission route used in this work, the en-route phase starts after the aircraft has reached London Heathrow BPK SID and ends when the aircraft enters the Amsterdam Schiphol STAR procedure. During this phase a minimum altitude of FL100 and a maximum of FL390 were maintained. These bounds give the optimiser the freedom to choose an optimum flight level and achieve convergence within affordable platform power and acceptable computation time. The unconstrained approach however, eliminates constraints such as speed and altitude in a trajectory optimization problem which broadens the scope of the search domain thereby making convergence difficult to achieve. Any solution obtained outside convergence will not be an exact solution to the original problem; therefore cannot be considered optimal or efficient. Perhaps, t he most significant advantage of unconstrained approach over the constraint approach is that, one does not need to worry about finding an initial feasible point which reduces the complexity of the algorithm. Trajectory optimisation uses these processes to choose a route with minimum fuel burn or time depending on the objective. In this study, the optimiser search domain is limited in terms of altitude and speed. These two constraints limits the computation time and the number of daemons (search programs) required per case.

An aircraft trajectory can be optimise for emissions by introducing fuel as an objective

to be minimised in trade-off with flight time. Various studies have been conducted on commercial aircraft trajectory optimisation which paved way for this work. Pisani [3] used GATAC for multi-parameter trajectory optimisation in the presesnce of wing and Calise [115] worked on extended flight performance optimisation methods. Howe [116] talked about removing the current ATC restrictions which is a requirement for implementing a free flight system. Sridhar et al. [117] developed a trajectory optimisation algorithm for computing minimum-time routes and an aircraft fuel burn model for generating fuel-optimal vertical profiles. Wickramasinghe et al. [37] developed a 4D optimal flight trajectory based on aircraft performance, weather forecasts, Air Traffic Control (ATC) databases and aircraft operational data. Romero [118] proposed a method for solving direct operating cost based on parametric optimisation theory. Mache [119] and Armanini [120], in a separate but closely related study, developed decision-making algorithms for UAV flight in icing conditions. Tang and John [121] developed a tactical conflict detection algorithm which would be required for free flights in a future air traffic system.

The above discussed literatures enabled the understanding of different optimisation approaches and set-ups. They provided an insight into the various methods for solving direct operating cost based on parametric optimisation theory, and a trajectory optimisation algorithm for computing fuel-optimal 2 and 3 dimensional profiles. Although these studies served as a spring board for the present study, they have a common flaw. They use aircraft dynamics models coupled with engine performance models to optimise for different objectives such as fuel, time, noise and emissions. All of the studies that performed trajectory optimisation in the presence of weather, limited the definition of weather to wind and, atmospheric pressure and temperature. There is the need to consider other atmospheric parameters such as clouds water concentration and super-cooled

water droplets size, which give rise to safety issues such in-flight icing.

2.7.2 Current ATM Environment

The current ground-based systems have served the aviation community well since inception; however, as the demand for air transportation services increases, they do not permit the flexibility of point-to-point operations required for the future ATM environment [122]. Numerous restrictions are imposed on the ATC system by the regulatory bodies such as CAA and FAA. The primary purpose of these regulations is to maintain the safety of every aircraft in traffic; whether on the ground or in the airspace [116]. The ATM constraints are a mandatory part of aircraft trajectory optimisation as they give the tactical limitations in terms of speed, altitude and heading. Essentially, ATM constraints are a collection of all airborne and ground-based functions required to ensure safe and efficient flight operation. The ATM comprises of the Air Space Management, Air Traffic Flow Management (ATFM), Air Traffic Services (ATS) and flight operations. The Air Space Management prevents mutual interference from air space users, whereas ATFM maintains an orderly flow of air traffic, and ATS prevents air collision by maintaining a tactical safety separation between aircraft and terrain. The ICAO defines three basic air space control areas namely: positive controlled, controlled and uncontrolled air space.

In a positive controlled air space, separation between all flights both IFR and VFR are maintained by the ATC, whereas in a controlled air space only the IFR flights are separated by the ATC. In an uncontrolled air space however, separations are achieved by pilots in both IFR and VFR flights. In IFR flights, Standard Instrument Departure (SID) charts guide the pilot in the departure segment. Similarly, during arrival, Stan-

dard Terminal Arrival Route (STAR) charts are used to guide pilots in arrival segment. These constraints limit aircraft speed, altitude and course. Inadvertently, the current ATC procedures are quite restrictive and are far from being efficient. While some of the restrictions are necessary to maintain safety, many of the restrictions imposed on individual flight plans are due to outdated technology and the inability of the current ATC system to plan and track complete trajectories [116].

2.8 Concept of Next Generation Aircraft

The next generation aircraft is required to be 'extremely efficient' by design, light weight (composites structures) with lower maintenance and overall operating costs, and reduced impact on the environment based on the global JTU such as SESAR, ACARE[4] and NextGen as well as the International Civil Aviation Organization (ICAO) policy on PBN optimised flight routes. This led to the development of new and more efficient systems that are compatible with next generation composite airframe structures, and ATM procedures for efficient aircraft operation and cleaner environment.

2.8.1 Development of the Performance Based Navigation System

The ICAO has adopted the PBN system in principle to address the challenges posed by the current ATM environment [123]. The PBN system defines performance requirements for aircraft navigating on an Air Traffic Service (ATS) route, terminal procedure or in a designated airspace. One of the major advantages of PBN system is that it permits optimal trajectory based operations by providing very precise lateral and vertical flight

[4]The ACARE environmental goals includes the reduction of CO_2 by 75%, NOx by 90% and perceived noise by 65% by 2050 referenced to a new aircraft flying in 2000. [38]

paths. Through the application of Area Navigation (RNAV) and Required Navigation Performance (RNP) specifications, PBN provides the means for flexible routes and terminal procedures [123]. The International Air Transport Association (IATA) estimated that shorter PBN routes globally could cut CO_2 emissions by 13 million tonnes per year. Thus, emissions are reduced by as much as 3.19 kg of CO_2 for every kg of fuel saved [124].

In the past, the efforts to reduce air transport cost and negative effects to the environment have mainly focused on aircraft and engine designs. This led to the design of advance and efficient aircraft and power plants. The focus is now shifting towards TBO as one of the most significant solutions for achieving greater overall air transport efficiency. Recent advances in computer based automation has made it possible to develop new approaches to solving these problems. The next generation air traffic control system is required to be capable of handling a safe and efficient high density traffic volume three times today's capacity [125]. Research and Development (R&D) projects such as NextGen of the USA, SESAR of Europe and CARATS of Japan are introduced to modernise the present ATS and cater for these demands in the foreseeable future [37]. Using today's cutting edge technology such as the ADS-B and PBN, TBO could be employed for more efficient operations in icing conditions. Thus, transforming the conventional ice protection method into a more controllable system where the amount of energy used can be controlled based on the operating conditions.

The NASA Ames Research Centre is also exploring Co-Operative Air Traffic Management (CO-ATM) concept for the transformation of aircraft and ATM operations towards the Next Generation Air Transportation System (NGATS). This is aimed at increasing the NGATS capacity and efficiency and according airspace users more flexibility of operations while maintaining safety [126]. In Europe, the EU has initiated three streams

of comprehensive projects/measures to mitigate the impacts of aviation on the environment and fuel resources. These are research and developments for greener technology, modernised air traffic management systems and market based measures. From 2030, aircraft are expected to fly optimal trajectories that are defined in the form of three dimensional way points plus associated required times (4D) of overfly [18].

2.8.2 SESAR

The Single European Sky ATM Research (SESAR) is an EU programme, which aims to develop the new generation air traffic management system capable of ensuring the safety and efficiency of air transport throughout in Europe by 2030, as shown in Fig. 2.16. These are to enable reduction in overall costs and CO_2 emissions, increase safety and economic growth for Europe. The line-up activities includes operational improvements of airport platform safety, airborne operations, ATC operations and network management. The goals are to improve air transport safety ten folds, enabling a 10% reduction in the environmental impacts of aviation and reduce air transport cost by 50% [18]. The environment and flight efficiency is to improve by 0.75 points on the horizontal-flight efficiency indicator as compared to 2009. The cost-efficiency to achieve an average en-route Determined Unit Rate of 53.92 euro in 2014, as against 59.97 euro in 2011 (in euros at 2009 prices); and the reduction of ATFM delay to 0.5 minutes per flight [18]. The I-4D represents a key element in the transition from constrained flights in the current ATM system to optimised flights in the future Single European Sky [34].

2.8.3 NextGen

Under Vision 100 Century of Aviation Reauthorization Act (P.L. 108-176), the Joint Planning and Development Office (JPDO) was charged with creating an integrated plan

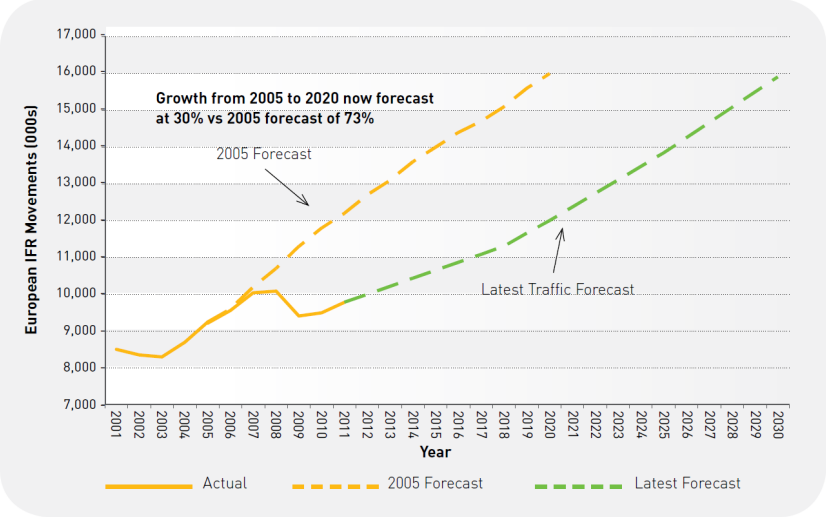

Fig. 2.16: Growth from 2005 to 2020 now Forecast at 30% vs 2005 Forecast of 73% [18]

for the Next Generation Air Transportation System (NextGen).[127] The Federal Aviation Administration (FAA) was charged to (in collaboration with industry) deploy procedures/technologies and policies on the ground and in the air for increased safety and capacity, savings in flight time, fuel burn and GHG emissions. Technologies such as ADS-B, PBN and data communications, and common weather systems have been used to further increase NextGen, enabling the sharing of real-time data on weather, aircraft location and condition, which are essential to future air transportation needs. NextGen projects include alternative fuels, more precise flight paths, new equipment and procedures for a more efficient and environmentally friendly aviation. The NextGen estimates reduction to delays by 41% by the year 2020 compared with what would happen if no further NextGen improvements were made beyond what was already done. This will translate into an estimated 1.6 billion gallons of fuel use and 16 million metric tons of CO_2 reductions. The delay reduction and fuel efficiency improvements will provide an estimated $38 billion in cumulative benefits to aircraft operators, the travelling public and the FAA [127].

2.9 Chapter Summary

A critical review of the various aircraft icing protection mechanisms shows that the successful operation of the thermal method of protection in current aircraft has proved to be practicable and desirable for application in a future ATM environment in terms of performance, efficiency and impacts on the environment. The review also shows that recent advances in computer automation and digital control have paved way for efficient air navigation. The TBO is a promising technology for minimising air transport cost and environmental impacts. It was however, observed that all the trajectory optimisation researches undertaken in previous studies did not consider the effect of icing conditions on aircraft fuel burn, noise and GHG emissions despite the pressing demand for improved air quality and all weather operations by commercial aircraft. This gap is important and needed to be filled. This work therefore adds to the body of knowledge by bridging this gap and proving answers to the research problems as evident in the succeeding sections.

Chapter 3

Methodology

This chapter discusses the methodological framework used to describe the approach to the research problem, and the principles of methods and tools used in achieving the objectives of this research. The major subjects of the discussion are the optimisation frame work, optimisation methods and setup, the optimiser selection and the airframe systems model.

3.1 Methodological Framework

Literature has shown that the recent advancements in technology have provided opportunities to investigate the use of optimal flight routes around disturbances which have the potential to decrease fuel burn and improve the environmental impacts of aviation. Literature has also shown that while maintaining the use of today's cutting edge technology, icing optimised trajectories could be employed for more efficient operations in icing conditions. However, conventional approaches to trajectory optimisation do not take the effect of aircraft systems into account. Neglecting these effects may be inadequate, especially when one considers real aircraft operations in real weather scenarios. While continuing to have safety as a primary objective, this work utilises future aircraft's PBN concept to investigate possible ways of minimising IPS power demand that would lead to greater efficiency and capacity. The approach in this work, therefore, is to include the icing conditions in the trajectory optimisation loop to demonstrate the environmental

gains that can be achieved if such optimised flight profiles are flown. This would enable the development of a decision making process dependent on weather within the flight management system; thus, transforming the conventional ice protection method into a more intelligent system. The difference between this method and the baseline aircraft AI method is in the operation. In this model, the IPS penalises the engine based on icing inputs from sensors/weather data and aircraft mission parameters such as air speed and altitude. In this way, the system demands only that much energy required for the current operation in contrast to the baseline AI system that is operated on an on/off basis, and a fixed value of kg/s and kW are demanded for ice protection once the system is on.

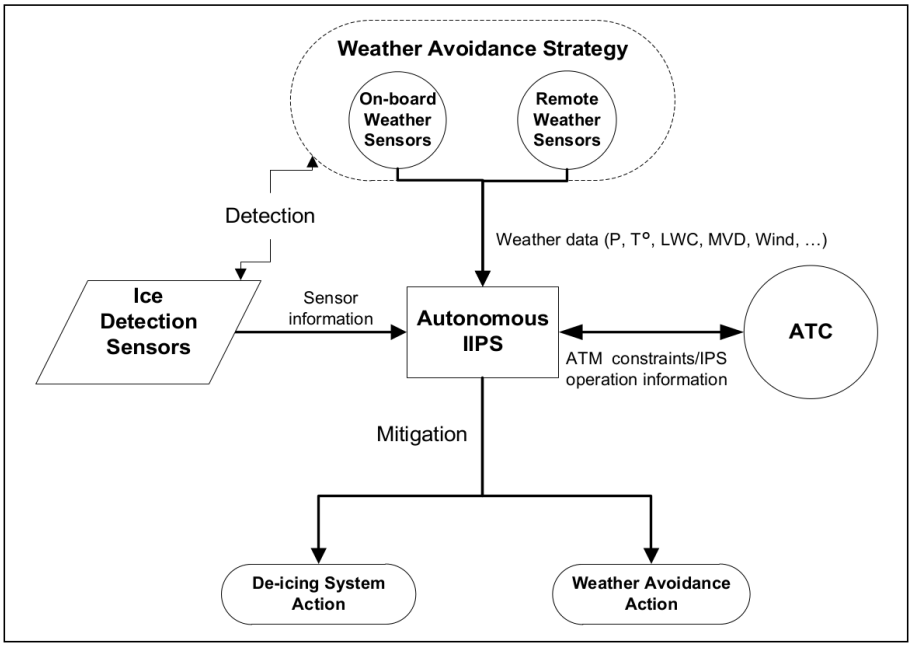

Fig. 3.1: IIPS Functional Diagram

This approach is an improvement on the conventional approach of representing only the aircraft dynamics and engines system neglecting aircraft systems impacts. Based on this approach, the autonomous IPS comprises four major modules, namely: sensors/ weather data, intelligent ice protection system (IIPS) and the ATC constraints as illus-

trated in Fig. 3.1. This approach is a technology driven strategy for future aircraft. In fact, NASA has been pursuing a research activity to develop remote sensing technologies for the detection and measurement of icing conditions aloft. Remote sensing of the clouds with the help of polarimetric radar can detect the super-cooled water droplets in clouds [128]. Utilising radar, radiometry, and lidar, a region of supercooled liquid can be identified [129].

This approach will depend on a common weather and system status information, and on-board equipment such as the ADS-B and Data Comm. There would also be the need for an enabling navigation policy such as the implementation of the ICAO initiated the PBN programme. The overall objective of this approach is to apply a multi-objective and multi-disciplinary optimisation methods to evolve an improved aircraft operation strategy that takes into account optimised flight routings due to icing/weather conditions.

3.2 Optimisation Method

A two-object optimisation scheme based on Pareto method was used to optimise the fuel burn, flight time and noise. Two variables are used; x_1 and x_2. The theoretical optimal Pareto front solutions are thus defined as:

$$x_1 \epsilon [0.1, 1.0] \tag{3.1}$$

and,

$$x_2 \epsilon [1, 60] \tag{3.2}$$

3.2.1 Objective Functions/Constraints

The objective functions to be minimised are:

$$f_1(x) = x_1 \tag{3.3}$$

$$f_2(x) = \frac{1 + x_2}{x_1} \tag{3.4}$$

The $f_1(x)$ refers to the minimum fuel objective whereas, $f_2(x)$ refers to the minimum time objective. The applied constraints are given by:

$$g_1(x) = x_2 + 9x_1 \geq 6 \tag{3.5}$$

$$g_2(x) = -x_2 + 9x_1 \geq 1 \tag{3.6}$$

3.2.2 Optimisation Benefits Calculations

The overall impacts of icing conditions on fuel consumption, and fuel savings on the total fuel burn due to the improved optimisation approach (considers weather in the optimisation set-up) are calculated as expressed in Eqs. 3.7 and 3.8. Let,

A = Trajectory optimised without IPS

A' = Traj A flown on-board with IPS

B = Trajectory optimised with IPS in the loop

F = Fuel burn

F' = Fuel penalty due to IPS (%)

F" = Advantage due to IPS in the loop (%)

$\Longrightarrow$

$$F' = \frac{F_{A'} - F_A}{F_A} \cdot 100 \tag{3.7}$$

$$F'' = \frac{F_B - F_{A'}}{F_{A'}} \cdot 100 \tag{3.8}$$

3.2.3 Optimisation Framework

GATAC trajectory optimisation software was used to run the simulation. The architecture is made up of four system level components, namely the GATAC core, the graphical user interface (GUI), the post-processing suite and the model suite as illustrated in Fig. 3.2.

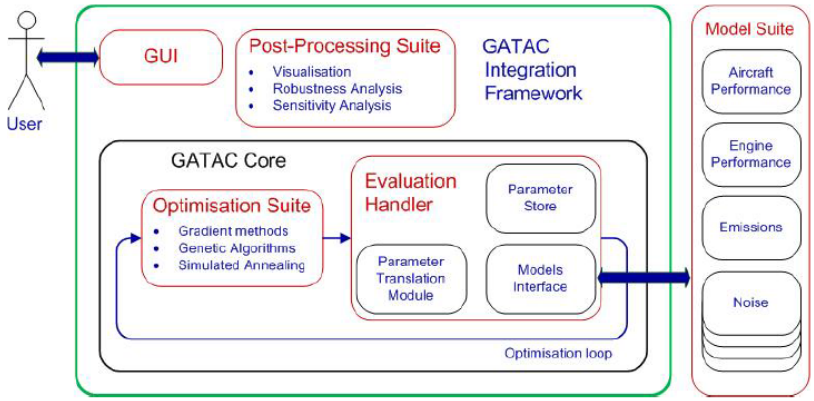

Fig. 3.2: GATAC Integration Framework Architecture [19]

The GATAC core supports the optimisation process whereas the model suite services the GATAC core on request by executing models and transferring data to the GATAC core. The post-processing suite processes the results of the optimisation. The GUI, as usual, provides the user with a window for setting up the case. Currently there are

three optimisers implemented in GATAC. These are the Multi-Objective Tabu Search (MOTS), Hybrid Optimiser (HYOP) and the Non-dominated Sorting Genetic Algorithm Multi-Objective (NSGA) [49].

NSGA. GAs are particularly suited for multi-objective optimisation problems because they can handle large populations of solutions, which they drive towards optimality through a generational process of selection and elimination [130]. For each generation, a ranking approach is used to evaluate the relative dominance of each solution and to determine the set of non-dominated, with the first rank solutions known as Pareto sets [131].

MOTS. Generally, GAs can experience difficulties on highly constrained problems. Thus, MOTS algorithms have been developed for optimising complex and highly constrained problems such as shapes of aerodynamic systems [132]. The optimiser combines a systematic local search with a stochastic element and intelligent coverage of the entire search space [133]. Because of this, MOTS algorithms require long computational run time.

HYOP. The HYOP is a new class of compiler heuristics invented to achieve either a good running time performance at the expense of increased allocation time, or a reduction in allocation time at the expense of performance [134]. The HYP integrates a GA global and Nelder-Mead local search methods.

Both MOTS and HYOP are mostly suited for handling more than two objectives. The NSGAMO has been designed for lower computational complexity during non-dominated sorting. As the objectives in this work are limited to two in all cases, it will add no value in using either MOTS or HYOP. Moreover, NSGAMO has proved [49] to be the most stable of the three optimisers when dealing with bi-objective problems with or

without constraints. The properties of GAs to optimise problems with local minimums perfectly fits to the needs of this work. Consequently, NSGAMO was used in this work for a bi-objective simulation. The NSGAMO optimisation set up is given in Fig. 3.3 and the general set-up is given in Table 6.1.

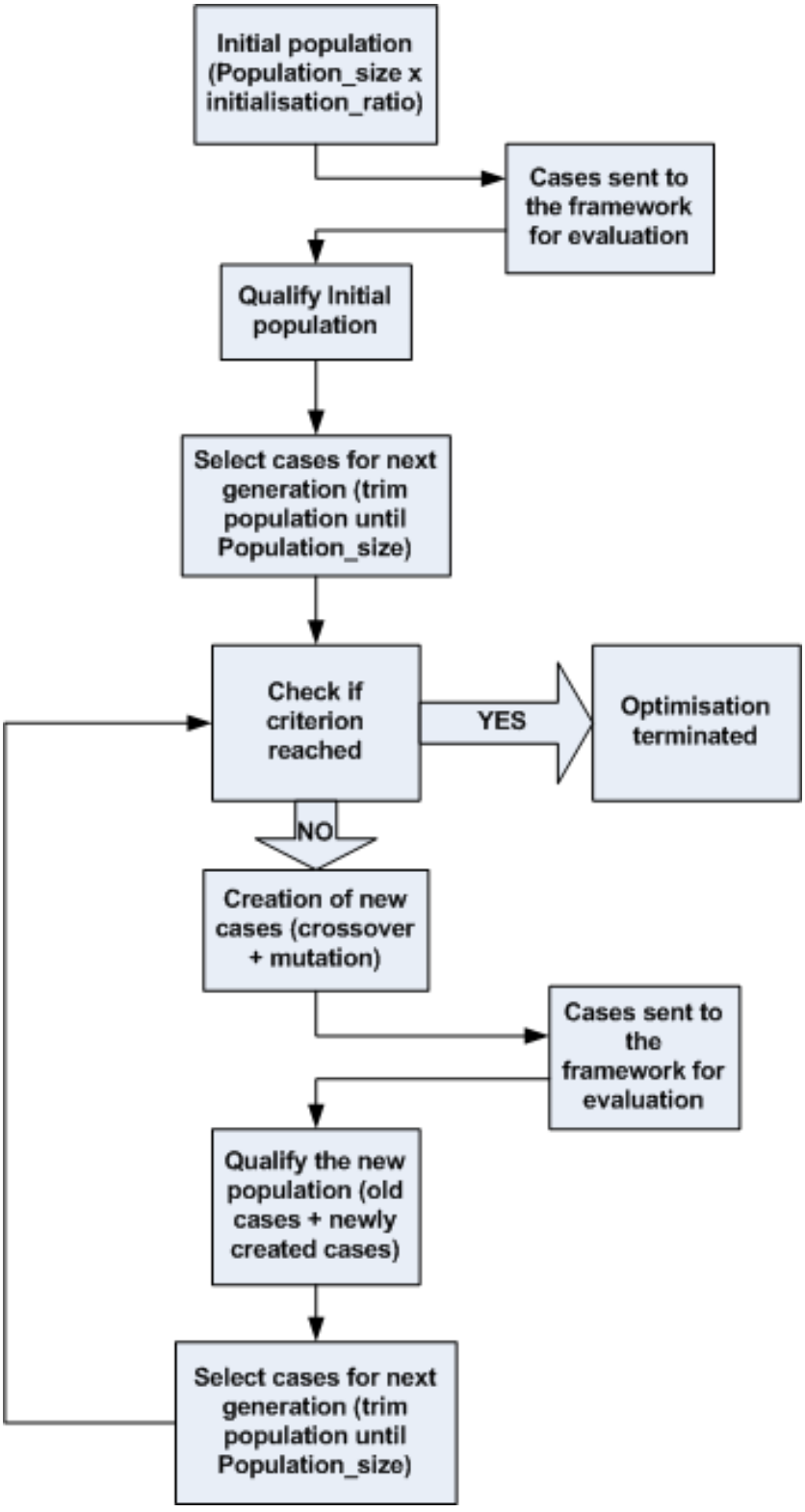

Fig. 3.3: NSGAMU Optimisation Flowchart [19]

3.3 General Settings

The objectives and the minimum/maximum allowable values are shown in Table 3.1.

Table 3.1: The Objectives and Constraints for the Simulations

Objective/ Constraint	**Description**	**Min**	**Max**	**Obj/Constraint type**	**Normalistaion function**
f_1	Total fuel consumption	0	15000	Minimisation	ObjectiveMin
f_2	Total flight time	0	15000	Minimisation	ObjectiveMin
g_1	Constraint 1	6.0	14.0	Greater than min	GreaterThan
g_2	Constraint 2	1.0	9.0	Greater than min	GreaterThan

The NSGAMO optimiser main settings:

- Population size = 100.0
- Initialisation factor = 50.0
- Creation schemes: Trilinear and Simulated Binary Crossover (SBX) crossover and Dynamic vector Mutate
- Creations selectors: Stochastic universal sampling for both crossover for the mutation operator item Creation rates: 0.45, 0.45, 0.10 respectively
- Stopping criteria set as maximum generation only (max generation = 250)
- Selection pressure = 2.0
- Validity check: Min = 0.5, Max = 2

Population Size: The population size is a factor which controls the number of design variables. Thus, as the number of variables increases, the population should also increase. Therefore, a large population size will increase the number of possible solutions. ***Initialisation Factor***: The initialisation factor is a number obtained by multiplying population size with initialisation ratio. A higher initialisation ratio will allow a higher density of possible solutions within the search space, which helps in finding a solution. ***Selection Pressure***: The selection pressure is the parameter that defines the convergence speed. A high selection pressure leads to premature convergence, and a low selection pressure could lead to a genetic drift in the population.

The simulation process was designed in the same manner as conventional aircraft flight phases: departure, cruise and arrival. Thus, the set-up is a direct take-off/climb initial phase referred to as departure followed a relatively longer flight segment termed cruise (or en-route) and finally a descent/approach segment referred to as arrival. In each phase an in-flght icing encounter was simulated through an artificial icing cloud coded within the aircraft systems model. Each phase is optimised separately for fuel burn/flight time after which the emission indices are analysed and the results post processed. The primary simulation tools used are discussed below.

3.4 Simulation Tools

The optimisation problem entertained in this work is a multi-disciplinary in nature as it involved aircraft dynamics, engine/emissions, aircraft systems and weather. Therefore, the models used for the simulation are the aircraft dynamics model (ADM), aircraft systems model (ASM), weather model, engine model, power off-takes and the emissions models. The author developed the IPS model which forms a part of the ASM, and run

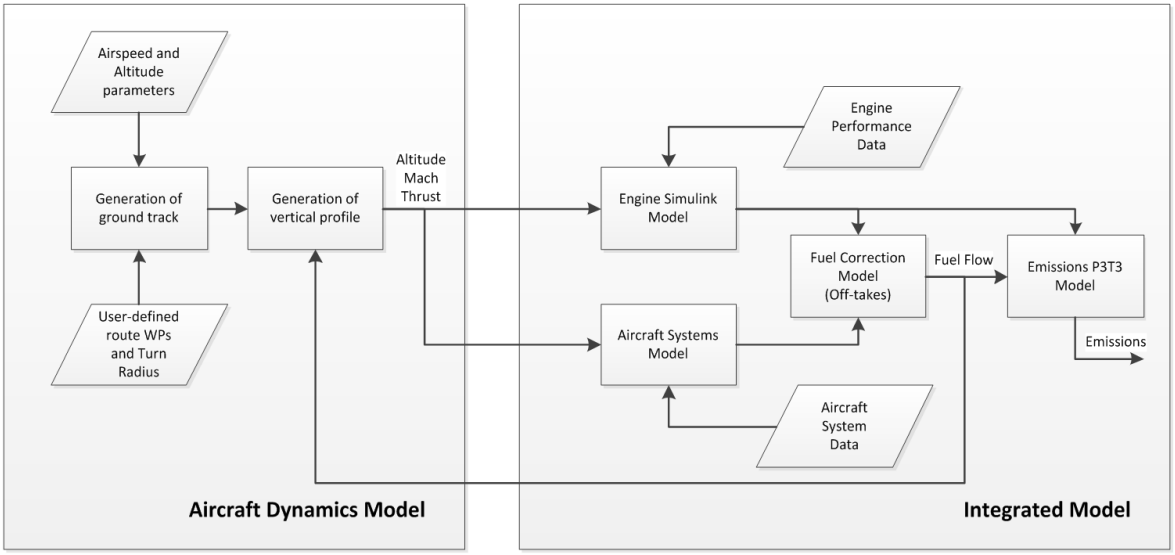

Fig. 3.4: ADM and ASM Interface

the simulation cases on the GATAC framework. Fig. 3.4 shows a block diagram of the models interface.

3.4.1 Aircraft Dynamics Model

The ADM is developed by Cranfield University as one of the core modules in the trajectory optimisation problem. It was designed to generate aircraft trajectory for a generic aircraft between two pre-defined positions in 3D space [135]. The ADM defines the altitude, speed and aircraft location to be used by the weather and IPS models. Thus, the method applied does not constrain the altitude; rather, it enables changes to the aircraft weight at specific points in order to reflect the rate of fuel burnt during a specific time segment. The aircraft motion was described using point mass with three degrees

of freedom and the resulting differential algebraic equations are listed:

$$m\frac{dV}{dt} = T - D - mgsin(\gamma_A) \tag{3.9}$$

$$mVcos(\gamma_A)\frac{dX}{dt} = Lsin(\mu_A) \tag{3.10}$$

$$mV\frac{dy}{dt} = Lcos(\mu_A) - mgcos(\gamma_A) \tag{3.11}$$

$$\tag{3.12}$$

$$mV\frac{dy}{dt} = Lcos(\mu_A) - mgcos(\gamma_A) \tag{3.13}$$

$$(R_E + h)\frac{d\varphi_A}{dt} = Vcos(\gamma_A)cos(\chi_A) \tag{3.14}$$

$$(R_E + h)\frac{d\lambda_A}{dt} = Vcos(\gamma_A)sin(\chi_A) \tag{3.15}$$

$$\frac{dh}{dt} = Vsin(\gamma_A) \tag{3.16}$$

The aerodynamic forces were modelled based on drag polar characteristic provided by BADA dataset [136] and the gravitational forces were modelled based on International Standard Atmosphere (ISA) datum value (9.81 ms^{-2}). The ADM generates 3D trajectories based on variables provided by the optimiser regarding way-point positions, altitude and airspeed information along the trajectory. Several input parameters such as initial and final positions and speed and aircraft initial mass are required to support the optimal variable to generate the trajectory and evaluate the overall fuel consumption and flight time, and emission indexes [135]. The engine and emissions model are coupled within the ADM in order to minimise the simulation time.

3.4.2 Airframe Systems Model

The aim of building and incorporating the ASM in the optimisation scheme is to simulate the combined power requirement of on-board systems at aircraft level. It provides a framework for evaluating the impacts of the various airframe systems on the vehicle performance and opportunity to investigate novel technologies. At present, the ASM is composed of the Environmental Control System (ECS), the IPS, actuators and electrical component [137] models. The tool is designed with a modular architecture and has the capability for expansion to include additional systems. The ECS was modelled to represent the bleed air requirements for the pressurisation, ventilation and thermal regulation of the cabin [138]. The icing model provides the off-take penalties due to anti-icing. An artificial icing cloud representing weather is encoded within the ASM. The purpose of the artificial icing cloud model is to generate local atmospheric conditions such as the air density, pressure and humidity based on the ICAO and ISA standards; and icing conditions such as OAT, LWC and MVD through a look-up table built based on Appendix C. The choice of the baseline aircraft and level of protection (see section 4.2.1 for details), and weather options for the development process for the icing model are discussed in the next chapter.

Chapter 4

Development of a Tool to Study Aircraft Trajectory Optimisation in the Presence of Icing Conditions

This chapter describes the development of a tool for simulating aircraft ice protection power requirements. The tool was developed based on Messinger mass and energy balance method for thermal anti-icing. The tool can calculate the total water catch and evaluate power requirements due to icing under a wide range of meteorological conditions.

4.1 Modelling Strategy

4.1.1 Design Standards

For an aircraft to meet airworthiness requirements for flights into icing conditions, it must be equipped with a certified ice protection system. At present, the primary safety regulation is provided by Appendix C of 14 CFR Part 25/CS 25.1419. Appendix C gives two sets of conditions: the Continuous Maximum (CM) for Stratiform clouds, and the Intermittent Maximum (IM) for Cumuliform clouds icing envelopes each as a function of LWC vs MVD, and ambient temperature vs pressure altitude. The sets of parameters shown in Table 4.1 applicable to Stratiform and Cumuliform clouds were used in this work.

Table 4.1: Appendix C Icing Envelope

Cloud Classification	**Horizantal Extent (nm)**	**Pressure Altitude (ft)**	**MVD(μm)**	**LWC (g/m_3)**	**T_∞ (℃)**
Stratiform	17.4	0-22,000	15-40	0.04-0.8	-30 to 0
Cumuliform	2.6	4,000-22,000	15-50	0.25-2.9	-40 to 0

4.2 Design Point

Based on the above standards, the design limits of the aircraft IPS are as follows:

- the cloud LWC is above $0.14g/m^3$
- the air or aircraft surface temperature is below 0℃
- the air temperature is above -40℃
- $15\mu m \leqslant MVD \leqslant 50\mu m$

However, there is the possibility of encountering Super Cooled Large Droplets (SLD) which refer to super cooled droplets with mean diameter $\geqslant 50\mu m$ including freezing drizzle drops and freezing raindrops. It is regulated that an aircraft must exit such conditions as soon as possible if ice protection system is certified in accordance with CS/FAR part 25 Appendix C [139].

4.2.1 Baseline Aircraft Description

The baseline aircraft of this study is a medium size, 180 passenger twin engine short haul, twin turbofan engine, transport transport similar to the Airbus A320. The A320 aircraft was chosen as a model because it is one of the Clean Sky baseline aircraft for technology demonstration. In addition, the aircraft (A320neo) offers advanced navigation technology such as Required Navigation Performance (RNP) capability and Future

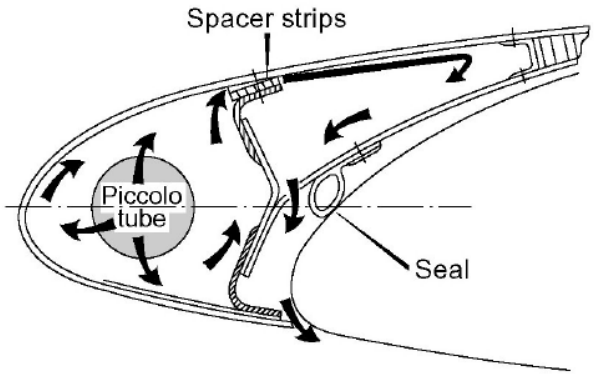

Fig. 4.1: Airbus Aircraft Wing Anti-icing (Airbus, [20])

Air Navigation System (FANS) which are part of the requirements for the use of the methodology developed in this work. The RNP reduces approach distances for landing while reducing fuel consumption and CO_2 emissions, while FANS enables the optimization of flight path and the reduction of aircraft spacing.

Generally, Airbus aircraft use the engine bleed air system for wing and engine protection against ice accretion. Engine bleed hot air is distributed along leading edge and into slat interior. Heat transfer via direct impingement of hot air from piccolo tube through slots which direct the heat onto the interior wall of the slat as illustrated in Fig. 4.1. The A320 aircraft uses bleed hot air from the engine for the protection of the three outboard slats (slats 3, 4 and 5) of each wing (see Fig. 4.2, two engine nacelles and electrical energy for de-icing the windscreen, probes and waste water drain mast.[1] Most of the current Airbus and Boeing (with the exception of B707) aircraft do not possess tail plane ice protection which led to oversizing of the structure (stabilizer) to carry the ice. The operating empty masses demonstrate acceptable stability and control with 3 inches artificial ice shapes on all unprotected wing and tail leading edges as part of the basic certification process. The results are confirmed by at least one natural icing

[1]This level of protection was adopted for the IPS model built in this work.

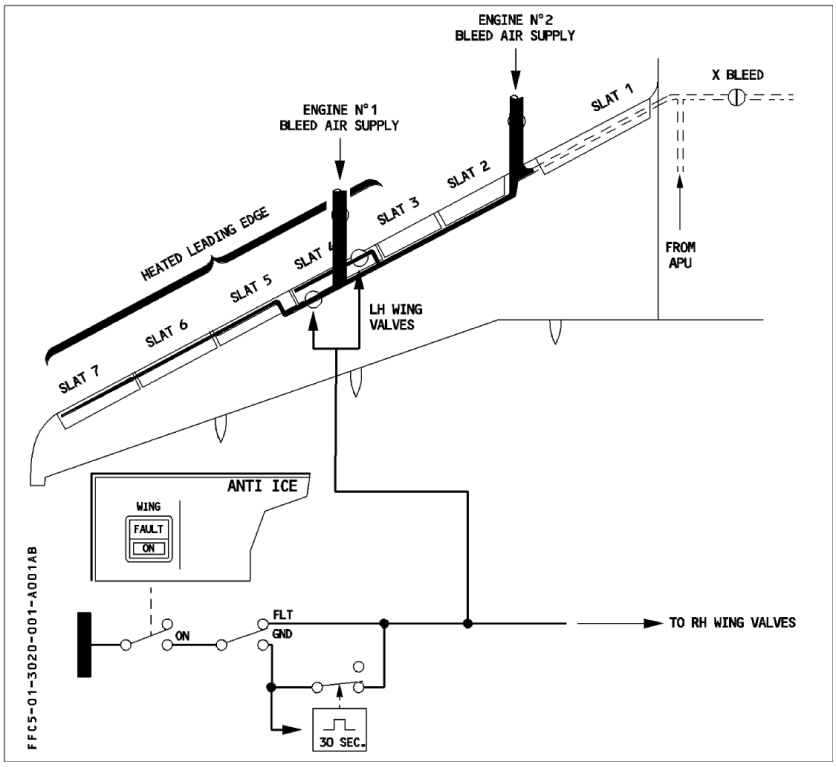

Fig. 4.2: A Schematic Diagram of A320 Wing Anti-icing System [21]

test. In addition, both the horizontal and the vertical tail planes are symmetrical which minimizes the impacts of ice accretion on their performance.

Although the parameters shown in Table 4.2 were used in developing the mode, the model is reconfigurable for any medium to large fixed wing aircraft.

4.2.2 Protected Areas

Large transport aircraft normally utilise engine bleed air for the wing and engine ice protection, and a limited amount of electrical energy for windscreen and probes protection. These areas are those mostly affected by ice formation in flight. Wing icing could lead to complete loss of control and/or insufficient lift to keep the aircraft airborne. In turbofan engines, laminar airflow is required at the face of the fan, hence they are

Table 4.2: Baseline Aircraft Configuration Control-Airbus A320-200

Parameter	**Value**	**Source**
Engine model	CFM56-5A3	Open source data
Engine max continuous thrust	23800lbs	Open source data
Engine pod diameter	1.7m	Calculated
Engine take-off thrust	26500lbs	Open source data
Engines total protected area	$1.12m^2$	Calculated
Flight deck windows area	2.6 m^2	Estimated
Medial wing Leading edge sweep (φ_{LE})	26.9°	Open source data
Probes protected area	$0.47m^2$	Estimated
Slat 4 L_{MAC}	2.5m	Calculated
Slat span (3,4,5)	3.18m	Calculated
Wing body setting angle (α)	3.66°	Open source data
Wing gross area	$122.4m^2$	Open source data
Wing Mean Aerodynamic Chord (L_{MAC})	4.19m	Open source data
Wing L_{MAC} thickness	12.50%	Open source data
Wing Span	33.91m	Open source data
Wing total protected area	$5.7m^2$	Calculated

provided with anti-icing systems to prevent ice formation. This is because ice formation on engine intakes can cause engine stall or damage to the compressor blades when ingested by the engine. Ice accretion on navigational and communications equipment such as probes and antennae can cause erroneous readings or loss of signal, which could lead to the loss of the aircraft. Therefore, the areas considered for protection against ice formation in the modelling process include the aircraft wing and engine cowl leading edges, windscreen and probes.

4.3 Wing and Engine Anti-ice Modelling

The wing and engine anti-icing systems were modelled based on empirical approaches as illustrated in Fig. 4.3.

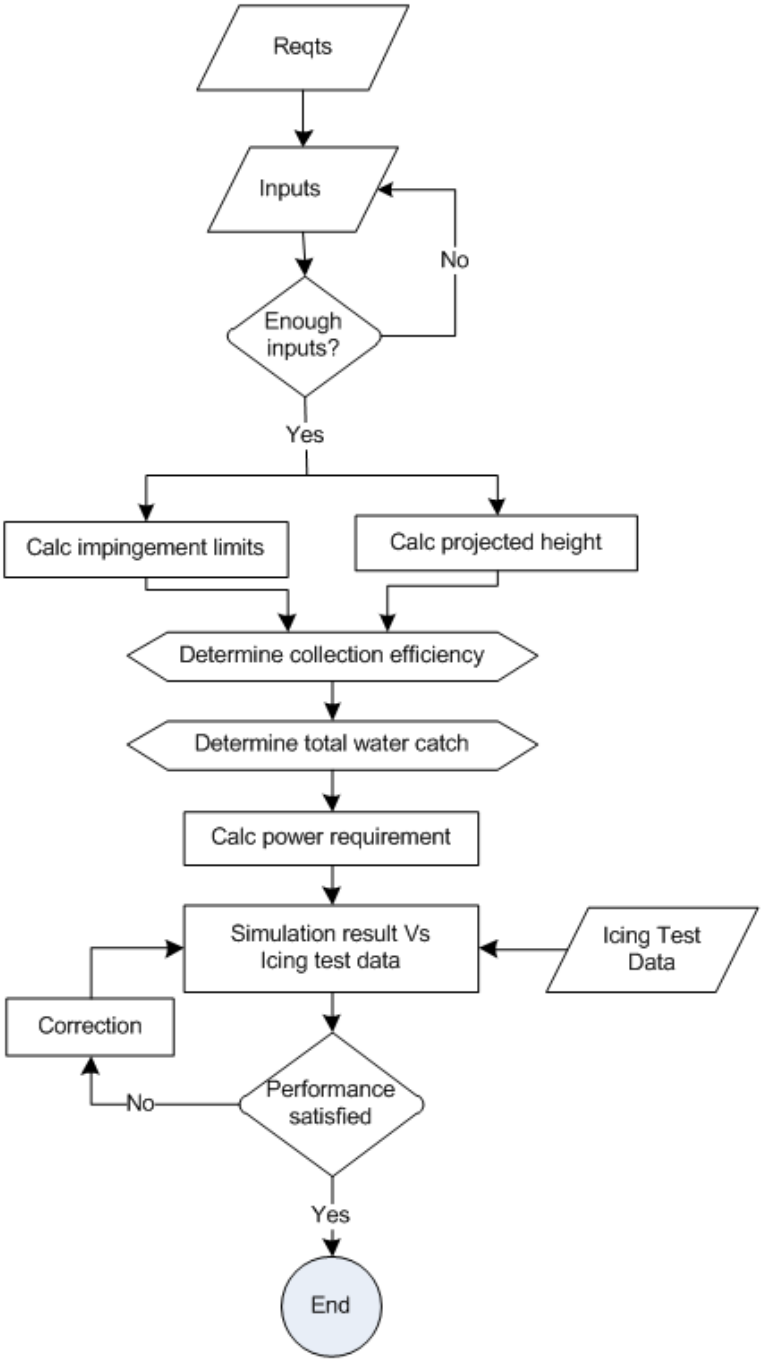

c

Fig. 4.3: Modelling Flow Chart

4.3.1 Choice of Aerofoil Section

Information on aerofoil data is an important part of aircraft anti-icing system sizing. It gives an indication of the wing collection efficiency and total water catch per unit time. The A320 and B737 were the closest aircraft models to the baseline aircraft whose aerofoil information could be used for the analysis. Aerofoil data on A320 was not available whereas B737 aerofoil data can be obtained from the University of Illinois Urban-Champaign (UIUC) Airfoil Data site [140]; although, icing parameters data on it were not as readily available. However, Alege [88] have used B737 aerofoil coordinates with icing data on a hybrid aerofoil which provided useful information on B737 aerofoil icing characterisation. Similar aerofoils whose icing data was available in the Engineering Summary of Airframe Icing Technical Data [22] include NACA 23012, NACA $64_1 - 212$ and NACA $65_1 - 212$. Fig. 4.4 shows a comparison of the different aerofoil sections.

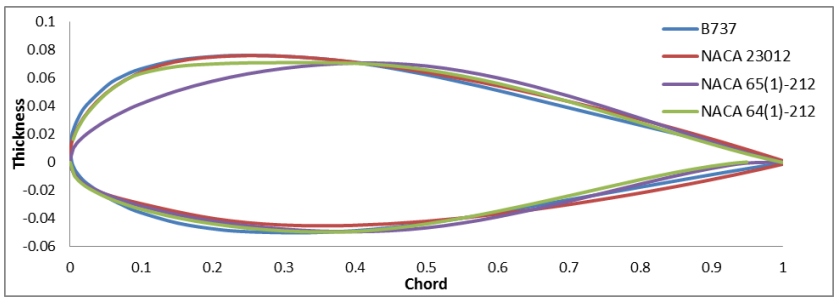

Fig. 4.4: Comparison of Aerofoil Sections

The NACA 23012 and NACA $64_1 - 212$ aerofoils are quite similar to B737 aerofoil in terms of leading edge radius, camber, maximum thickness (12-12.5% chord) and its position (about 30% chord). Any of these two would have been the ideal for the study aircraft except data icing data was not available on them. Meanwhile, NACA $65_1 - 212$ has same maximum thickness as B737 but at a different position (40% chord). It also has a smaller leading edge radius than the rest of the aerofoil sections, which means higher

impingement efficiency. In addition, because the maximum thickness is positioned at a higher percentage chord, NACA $65_1 - 212$ will have higher impingement limits.

The more the maximum thickness, the less the collection efficiency and the better for airflow in icing encounter. However, the further aft of the leading edge is the maximum thickness, the longer the impingement limit which means more accretion and less aerodynamic efficiency. The smaller the leading edge radius, the more the impingement efficiency which means more accretion and therefore less aerodynamic efficiency in icing encounter. For these reasons, the choice of NACA $65_1 - 212$ aerofoil will give a conservative estimate of the icing parameters.

4.3.2 Impingement Limits Calculations

In estimating the anti-icing power requirement, it is mandatory to establish the limits of water impingement on the surface. To determine how far aft of the leading edge the surface requires protection, the surface upper (S_U) and lower impingements limits (S_L) were derived as a function of the impingement parameter K_0 from a NASA experimental data [22]. The graphical data presents curves for determining the impingement limits for several aerofoil sections at various angles of attack. Therefore, the corresponding values of the Droplets Range Ratio (DRR) were read relative to the calculated droplet Reynolds number (Re_d) from Fig. 4.5. The (S_U) and (S_L) depend primarily on the droplets inertia factor K given as [22]:

$$K = \left[\left(\frac{1}{18} \right) \cdot \frac{D_d^2 \cdot V_{TAS} \cdot \rho_{water}}{\mu_{icing} \cdot L_{MAC}} \right] \tag{4.1}$$

The modified inertia parameter (K_0) can be calculated from Cassoni et al. [43] equation as follows:

$$K_0 = K(1 + 0.0967Re_d^{0.6397}) \tag{4.2}$$

It can also be obtained by multiplying K with the droplet range ratio (DRR) taken from Fig. 4.5.

$$K_0 = DRR.K \tag{4.3}$$

To determine the DDR however, the droplets Reynolds number has to be determined using the following equation:

$$Re_d = \frac{d_{med} \cdot \rho_{icing} \cdot V_{TAS}}{\mu_{icing}} \tag{4.4}$$

It is the K_0 that influences the water collection efficiency as well as the rates of water catch ($\dot{m}$). The $\dot{m}$ can be expressed as:

$$\dot{m} = V_{TAS} \cdot H \cdot L_{MAC} \cdot E_m \cdot LWC \tag{4.5}$$

Further reading on Eqs. (4.1) - (4.5) can be obtained from Cassoni et. al [43] and Rouffie [141].

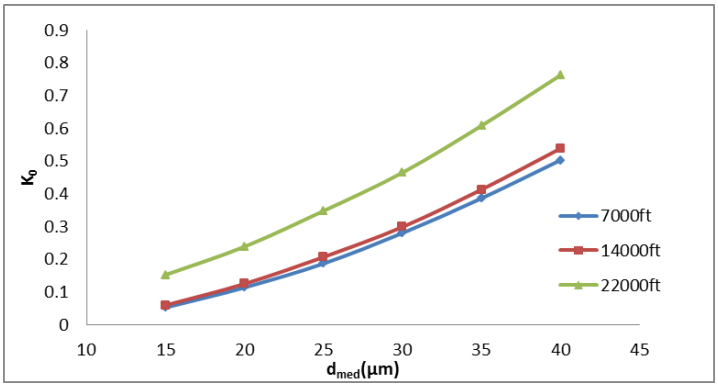

Fig. 4.6: Modified Droplets Inertia

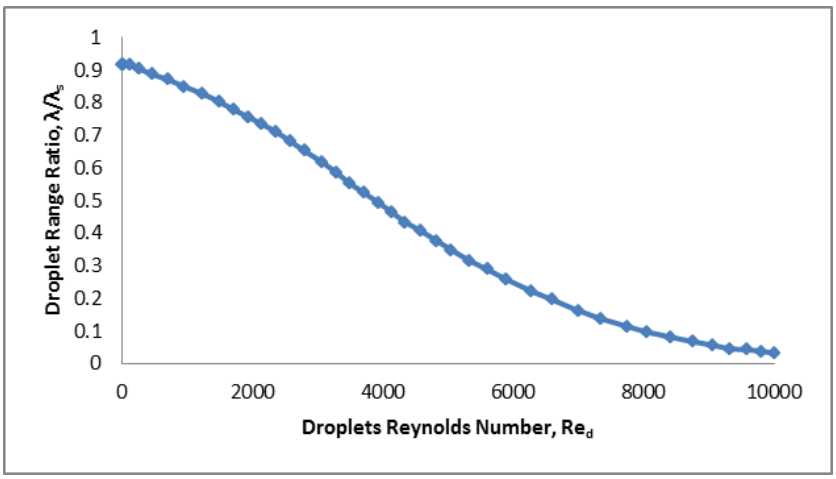

Fig. 4.5: Droplets Reynolds Number vs Range Ratio at $\alpha = 4°$(reproduced from Bowden et. al [22])

Literature [11] shows that the K_0 factor evaluation method discussed above is correct within ± 5 %. The K_0 for different droplet sizes was evaluated for the 3 altitudes of interest and represented graphically in Fig. 4.6 . In estimating the anti-icing power required it is necessary to establish the limits of water impingement on the surface. The values of the surface upper (S_U) and lower limits (S_L) were evaluated based on the study aircraft data, mission case and NACA $65_1 - 212$ at $4°$ α provided in the Engineering Summary of Airframe Icing Technical Data [142]) shown in Appendix B to this report.

A Therefore, to determine the chord-wise extent of impingement, the absolute values of S_U and S_L were obtained as a function of the impingement parameter K_0 from Figs B.3 and B.4 respectively.

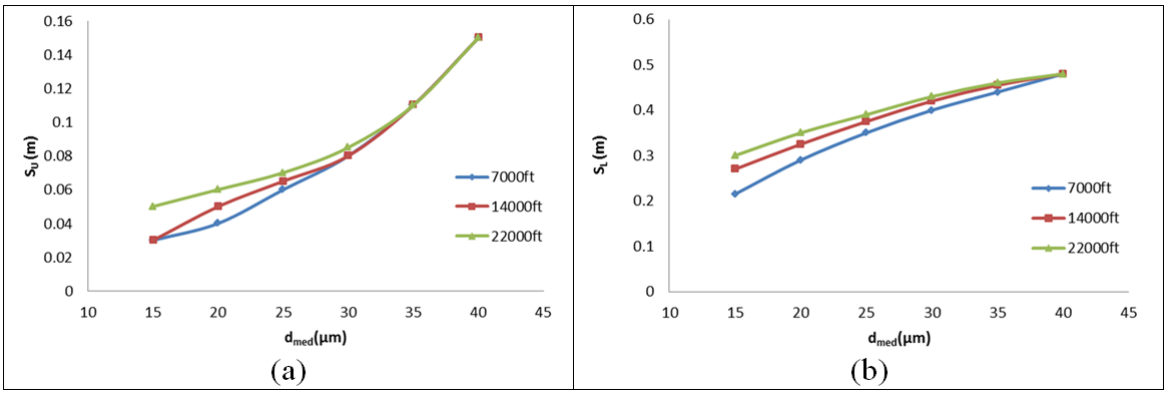

Fig. 4.7: Surface Impingement Limits (m)

Fig. 4.7 shows that increase in droplets size is accompanied by increase in the impingement limits for both the upper and lower surfaces.

4.3.3 Assumptions

To simplify the problem, the following assumptions were made:

- ***The anti-icing system is fully evaporative***. This implies that all impinging water droplets are evaporated, and no run-back icing. The evaporative system has higher thermal requirements than the running wet or cyclic de-icing systems. Therefore, to arrive at a universally conservative estimate, a fully evaporative model had to be assumed in this work.

- ***Ice melts at temperature of 0.01***℃. This assumption indicates that melting and freezing do not occur at the same temperature. In general terms however,

the melting point and freezing point of water are taken to be the same. The melting point of water depends slightly on pressure; in which case, there is not a single temperature that can be considered to be the melting point of water. In some cases, the melting point of water is considerably higher than its freezing point. For instance, in the absence of nucleating agents, water could super-cool down to –40 ℃ before freezing. Thus, the assumption of 0.01 ℃ melting point of water is valid and necessary for ease of computation especially when using Matlab environment.

- ***The skin temperature is fixed and known***. Fixing the skin temperature in the model means that only the internal flow thermal and pressure properties change during simulation. Aside limiting the heat load requirement, this assumption simplifies the calculation process.

- ***The windscreen is assumed to be near vertical and heated electrically***. The SAE AIR1168/4 [11] provided a well validated model for estimating slant windscreens anti-icing requirements. Since most the modern aircraft pilot windscreens (including the baseline aircraft) are this type, it is only reasonable to assume this configuration in the calculation process. In addition, the baseline aircraft utilises electrical energy for protection of the pilot windscreen against inflight icing; hence, an electrical anti-icing system is assumed in the calculation process of the windscreen anti-icing.

- ***The probes anti-icing electrical power requirement is assumed to be 10% that of windscreen***. Similar to the windscreen, the baseline aircraft uses electrical heating system for the protection of the sensors, pitot probes and static ports as well as the waste water drain mast. Although, the fraction of energy use for this purpose is grossly minimal, it needed to be accounted for in the

calculation scheme. Drawing from past experience in the MSc AVD course in Cranfield university, a 5-10% value in relation to the flight compartment windows is normally applied.

The above assumptions were necessary for ease of simulation. The energy consumption is a function of the heating intensity and the duration of exposure. Therefore, in all simulations, skin temperature to maintain an icing free surface was defined.

4.4 Windscreen/Probes Protection

Sometimes ice builds up on forward-facing windscreen panels while flying in icing conditions, posing a risk to the pilot's vision. Hence, windscreens are normally equipped with ice protection systems to allow pilot visibility in case of an icing encounter. The windscreen could be de-iced electrically or through the use of hot air. However, the baseline aircraft uses electrical energy for windscreen ice protection which informed the use of electrical energy on the windscreen. Usually, electric current is passed through transparent rows of conductive films located on the inner surface of the outer ply of the windscreen to heat it. In smaller aircraft or where electric power is not available, antifreeze fluids or hot air jets are normally used for windscreen ice protection [143]. The number and total probes area exposed to icing is a function of the aircraft type and mission as well as user choice. In this case, an across the board conservative estimate has been applied in the absence of the total probes area protected in the baseline aircraft: 10% of the windscreen ice protection power. To estimate the electrical power required for anti-icing, the windscreen water catch rate and heat transfer coefficient have to be determined. The total water catch $m_{ws}(kg/s.m^2)$ of the windscreen projected area was

calculated from:

$$m_{ws} = V \cdot A_f \cdot LWC \cdot E_m \tag{4.6}$$

The windscreen projected area $A_f(m^2)$ perpendicular to the line of flight is given by:

$$A_f = 2L_x \cdot L_y \tag{4.7}$$

where L_x is the distance from the base to the centre of a nearly vertical windscreen, and L_y is the total protected width of the windscreen. The impingement efficiency E_m was determined from [143] for semi-infinite triangle. In this case, the windscreen ant-icing system is assumed wet running. Hence, the average external heat transfer coefficient over a distance L_x based on the assumption of a fully turbulent flat plate is given by:

$$h_0 = 0.64(T_m)^{0.3} \cdot \frac{[1.69(\rho g)_0 v]^{0.8}}{L_X^{0.2}} \tag{4.8}$$

Reference [11] which gives the guidelines for sizing anti-icing system for forward-facing windscreen panels recommends that power input must be adequate to maintain a running wet surface of 1.67℃ . Therefore, the total heat required for maintaining the windscreen at an equilibrium temperature of 1.67 ℃ is given by Eq. (2.6) whereas the probes and waste water drain mast anti-icing power requirement is assumed to be 10% that of windscreen.

4.4.1 Final Reconfigurable IPS Model

Out of the five anti-icing power calculation methods studied in Chapter 2, Meier, Krammer and Scholz's method [92][84] (see Section 2.5.4) was used in the in the MATLAB/Simulink environment to build the anti-icing model. Apart from encoding the

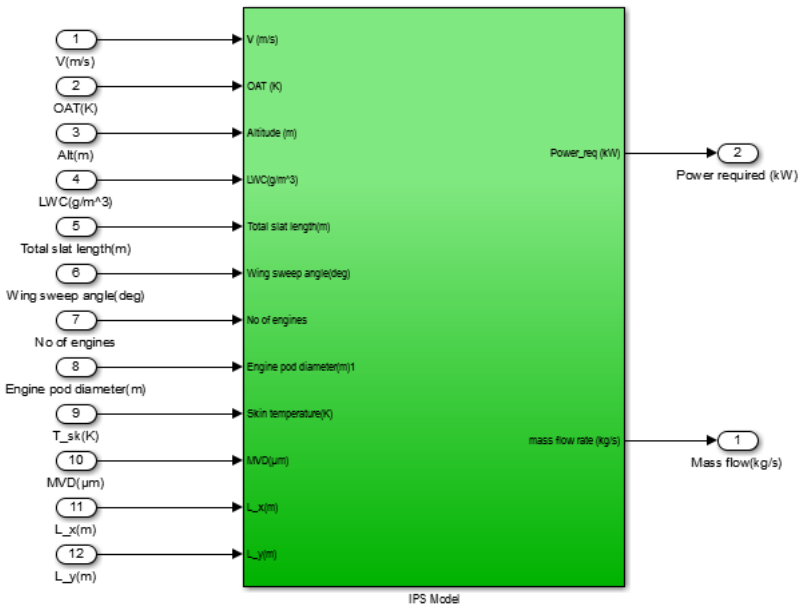

Fig. 4.8: Reconfigurable Aircraft Anti-icing Model

model in the Simulink environment, an artificial icing cloud was built in the model. In addition, the model was made reconfigurable for different sizes of fixed wing aircraft and weather conditions. The model can also be updated to include other terms such as radiation and gust effects if required. Presently, the model has twelve inputs which could be used to define the study aircraft parameters, atmospheric and mission parameters. These inputs include the speed, OAT, altitude, LWC, total slat length, wing LE sweep angle, and number of engines, engine pod diameter, skin equilibrium temperature droplets size, frontal windscreen length and breadth (L_x and L_y) as shown in Fig. 5. The outputs have being designed to suites the basic two anti-icing requirements: heat flux and bleed mass flow rate as shown in Figs 4.8. A snap shot of the the interaction of the energy terms within the model is shown in Fig. 4.9. To test the functionality of the model, an academic test case was created involving the baseline aircraft.

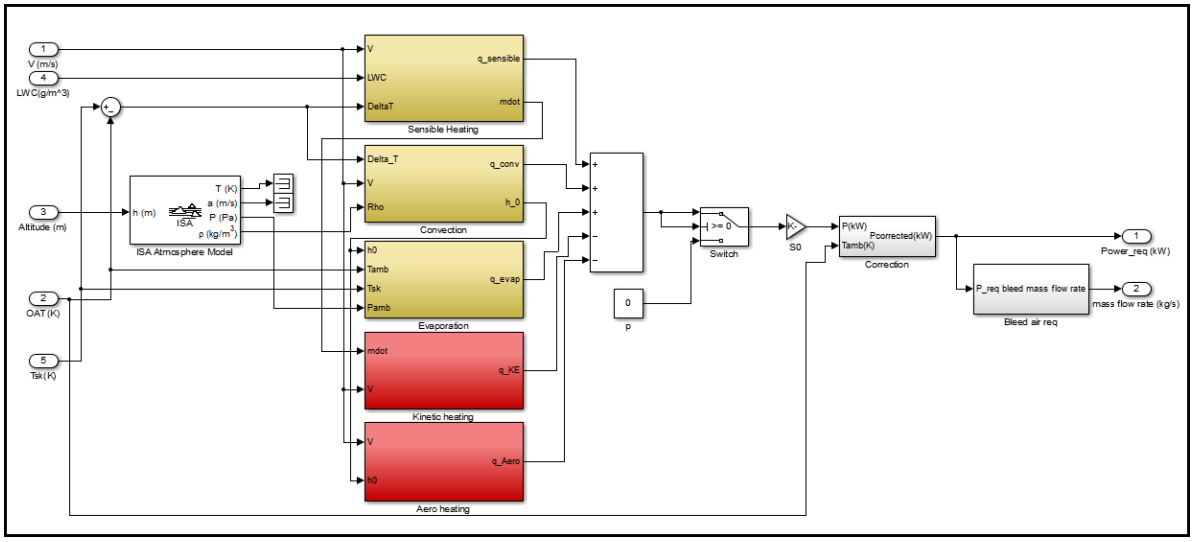

Fig. 4.9: A Representative Anti-icing Model for the Baseline Aircraft

4.5 Demonstration Test Case

Consider an A320 aircraft climbing to 20,000ft, in a known icing condition of OAT= -20℃, LWC=$0.5g/m^3$, MVD=$20\mu m$. By fixing the input parameters, the model allows the computation of power required to maintain the critical surfaces free of ice build up. To simplify the problem, the parameters that are peculiar to the case were defined as constants within the model. A list of the inputs, constants, and the outputs are listed in Table 4.3 below.

4.5.1 Test Results

Fig. 4.10 shows the energy requirement of the bleed air system on the baseline aircraft for three different speed configurations and skin temperature range of 0-5 ℃. The SAE AIR1168/4 presents curves for selecting skin temperature (T_{sk}) as a function of ratio of the total water catch to the relative film conductance. Aircraft encounter icing during climb to cruise altitude, and descent and hold. This is due the fact that the clouds that

Table 4.3: Baseline Aircraft Configuration Control-Airbus A320-200

Inputs		
Parameter	**Value**	**Units**
Altitude (h)	User define	ft
Ambient temperature (T_∞)	User define	℃
Surface heat transfer area (S_0)	User define	m^2
Flight speed (V_{TAS})	User define	kt
Clouds liquid water content (LWC)	User define	g/m^3
Internal constants		
Mean aerodynamic chord (L_{MAC})	2.2	m
Slat length (y_{SLAT})	3.14	m
Leading edge sweep (φ_{LE})	27.5	°
Skin temperature (T_{sk})	5	℃
MVD (d_{med})	20	μm
Pressure (P)	$f(h)$	hPa
Saturation pressure (e)	$f(T)$	hPa
Specific heat of air ($C_{P_{air}}$)	1005	$J/kg.K$
Specific heat of water ($C_{P_{water}}$) @ 0℃	1859	$J/kg.K$
Specific density of water (ρ_{water})	1000	Kg/m^3
Latent heat for water evaporation (L_e)	2257	kJ/kg
Latent heat of fusion (L_f) of ice	332.5	kJ/kg
Air density (ρ)	$f(h)$	kg/m^3
Absolute viscosity of air (μ)	$1.5636x10^{-5}$	$kg/s.m$
Thermal conductivity of air (k_0)	0.0228	$W/m.K$
Outputs		
Heat flux ($\dot{q}_{anti}$)	Result	kW
Bleed mass flow rate ($\dot{m}_{bleed}$)	Result	kg/s

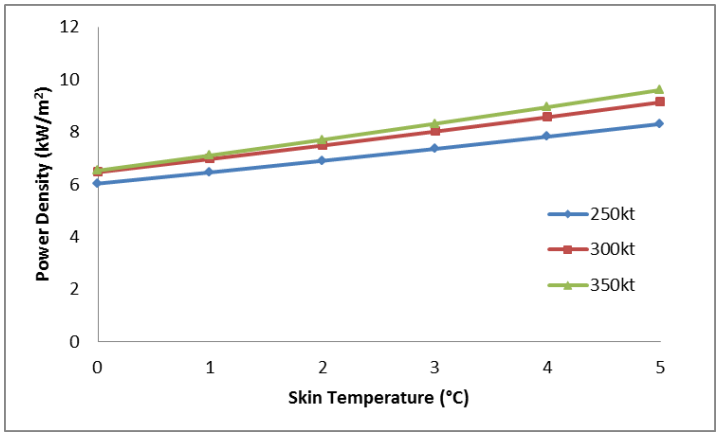

Fig. 4.10: Power requirement @ 20,000 ft, OAT= -20 ℃, LWC=0.5g/m3, $MVD = 20\mu m$ for different speeds

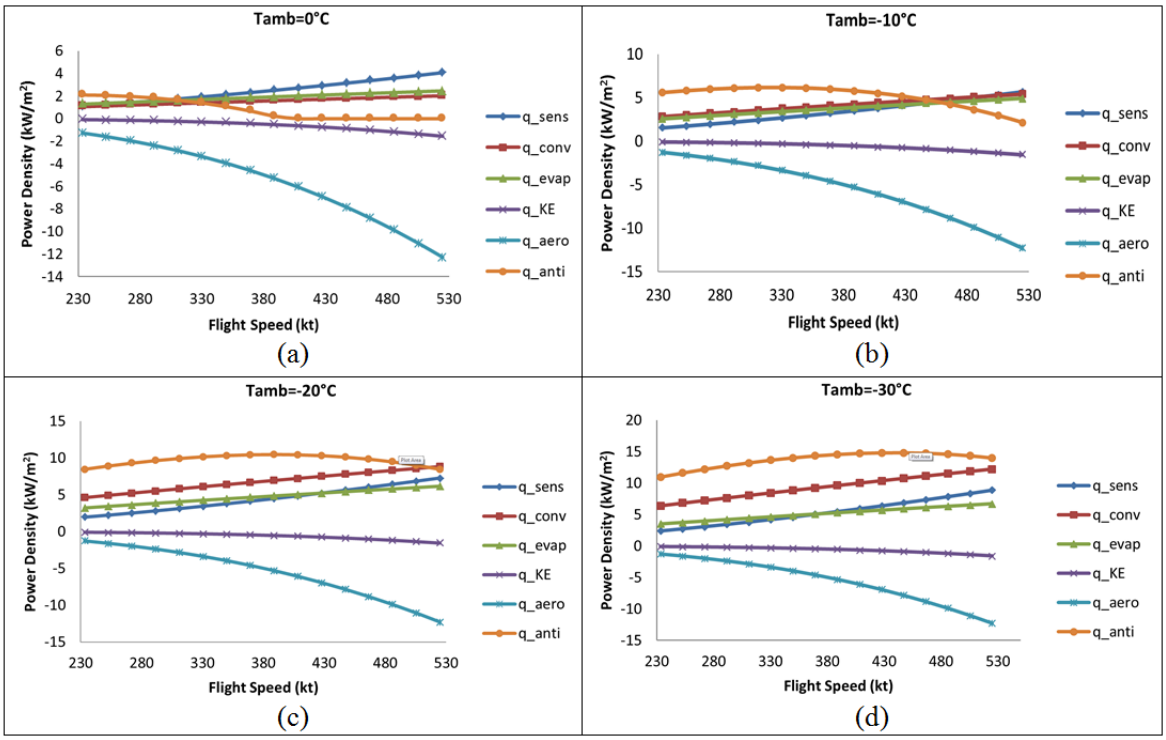

Fig. 4.11: Anti-icing Power Requirement

contain super-cooled water droplets exist at lower flight levels, and during descent and climb, aircraft reduces speed which lessens the effects of kinetic heating on the airframe. Thus, a further test was carried out for 7,000 ft altitude based on four temperature bands 0 ℃, -10 ℃, -20 ℃ and -30 ℃. In every case, a 5 ℃ skin temperature was maintained. The result (see Fig. 4.10) shows minimum power requirements of about $6kW/m^2$ at $250kt$ assuming that assumed that ice melt at a small fixed temperature point of about 0.01℃. At a maximum climb speed of 300-350kt, a maximum power requirement of between 7 to $9kW/m^2$ was obtained for a maximum 5℃ skin temperature based on SAE guidelines [11]. The skin temperature is bench marked at 5℃ due to the high power demand above that value (see Fig 2.7) and for the fact that maintaining such equilibrium would ensure full evaporation as can be deduced from Fig. 4.11. Fig. 4.11 shows the response of the power density to the changing ambient temperature and flight speed. In an evaporative system, the heat requirements for anti-icing depends strictly on the water catch as a

significant amount of energy is required to evaporate all the impinging water droplets. In running wet de-icing however, power consumption mainly depends on the ambient temperature. Speed is an additional parameter that needs consideration yet it is not part of the Appendix C. Speed determines the duration of the icing encounter and also has an influence on the wing angle of attack. Typically, thermal systems are designed for maximum energy requirements. The show that maximum energy requirements occur at between V_{TAS} of 250 kt to 350 kt for running wet systems, SAE [11]. Meanwhile, the test case results in Fig 4.11 show that the maximum energy requirement occurs at between 300 kt to 400 kt. This is expected as skin temperature for running wet systems are normally limited to between 0 to 1.67 ℃, SAE [11]. Thus, beyond these velocities, the kinetic heating outweighs convective losses and thus eliminates the need for anti-icing.

4.5.2 Model Verification and Validation

The ambient temperature has an important relationship with a cloud's water concentration. The lower the ambient air temperature, the lower the cloud's water concentration. The probability of encountering large amounts of super-cooled droplets reduces with decreased ambient temperature. As such, verification and validation processes were undertaken to investigate the performance of the model under a wide range of icing conditions. As a verification process, the sensitivity of the model to the inputs variation was checked to ensure that the results were not outside expected limits. Fig. 4.12 shows a Gaussian distribution of the simulated result compared to a value obtained from an experimental data of a large aircraft wing maximum anti-icing power off-take. Based on 1000 cases generated using a pseudo-Monte Carlo simulation method, the model was accurate to within 70% and the level of sensitivity was satisfactory. The observed mean is 1.4568, observed variance is 58.0193, and, the upper and lower limits are -20 and

25 respectively. The model performance was evaluated based on an icing experimental

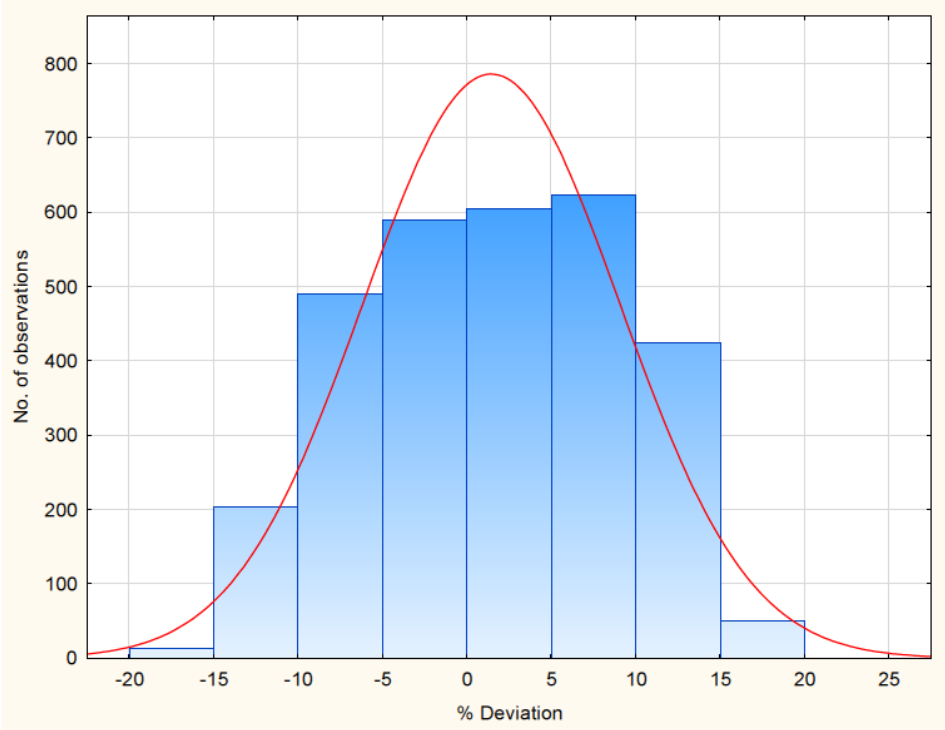

Fig. 4.12: Normal Distribution of Model Sensitivity to Inputs Variation

test conducted by Al-Khalil et al [144] on the engine intake of a turbine aircraft. The same test case was run with the model developed in this work and the results obtained compared very well with the experimental result as shown in Fig. 4.13. The percentage deviation of the model result from the experimental result in terms of total power plotted in Fig. 4.14 shows fewer than 20% discrepancies in all the six cases. Considering certain inputs related to aircraft level parameters being estimated conservatively, the less than 20% discrepancy is acceptable. In a second validation case, results of a specific parting strip power requirements are compared between the SAE AIR1168/4 [11] suggested value and the calculated value, Scholz [94] calculation result and the result obtain using the model. The comparison is presented in Fig. 4.15. The outcome of the evaluation using experimental data and the comparison with other calculation methods, suggest that the quality of the model developed here is more than sufficient for the

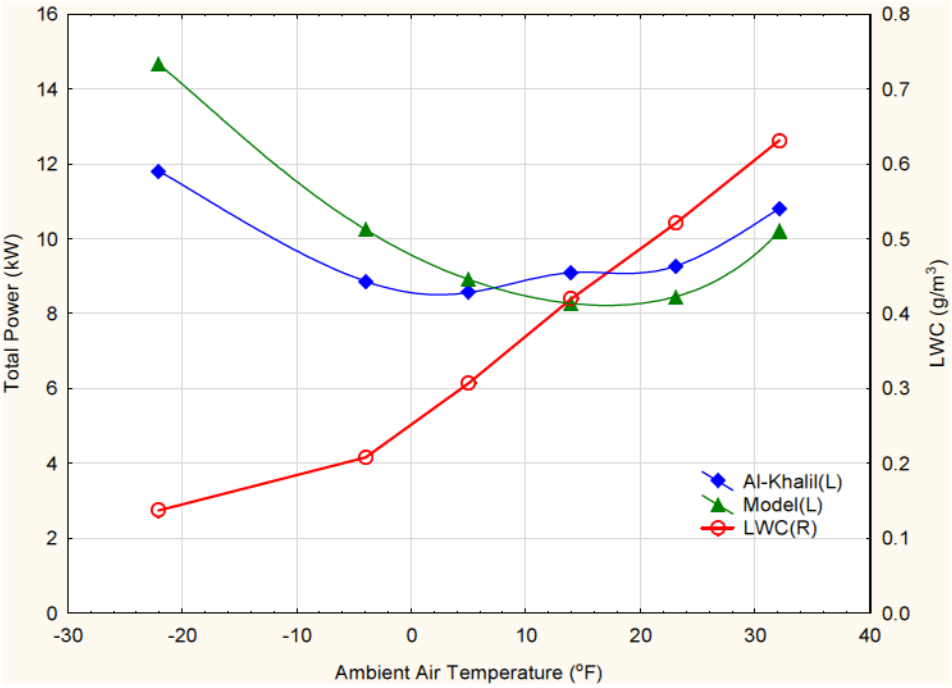

Fig. 4.13: IPS Model Validation with Experimental Data

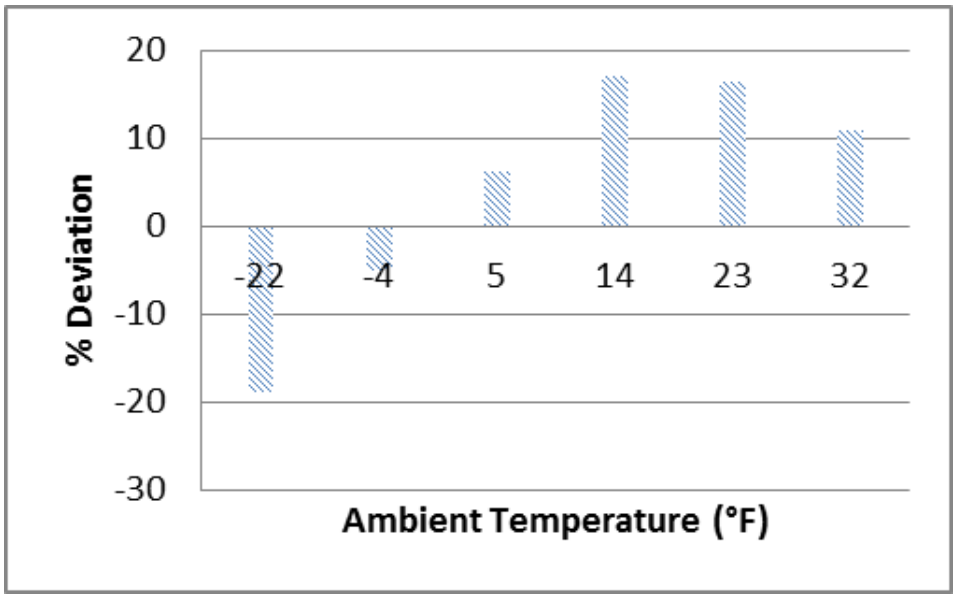

Fig. 4.14: Percentage Deviation from Experimental Data

optimisation study.

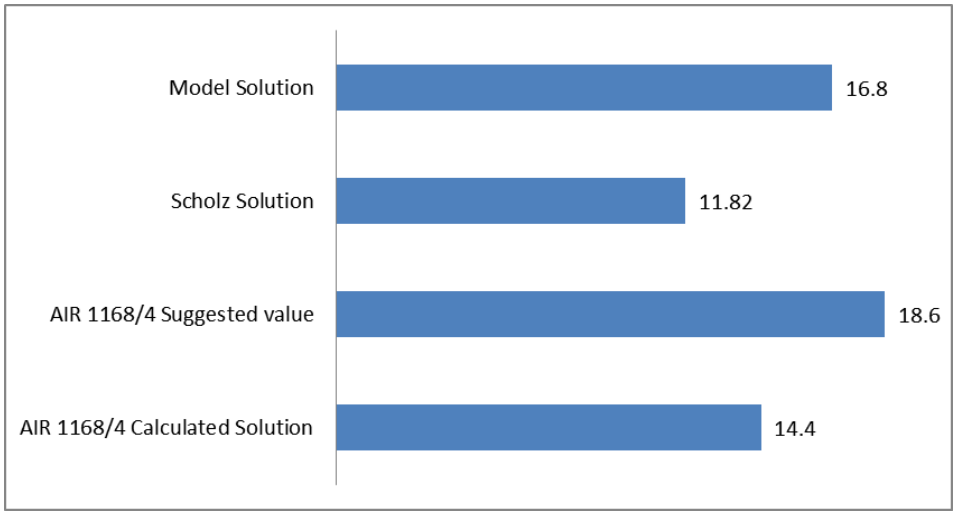

Fig. 4.15: Power Density (kW/m^2) Comparison

4.6 Modelling of a Cyclic Electrothermal De-icing System of an Aircraft Wing

Electro-thermal de-icing method is one the leading technologies considered for minimising aircraft in-flight ice protection power requirement.The electro-thermal power which is provided by the on-board generators could be quite excessive in terms of weight and fuel consumption. The concept of cyclic de-icing was developed in previous works and is still at different stages of investigation. At the moment there is no single commercial aircraft certified to use this technology for in-flight ice protection. This section discusses current approach to modelling an the electro-thermal de-icing system and its validation. The wing de-icing modelling process follow the same process as the baseline aircraft anti-icing model.

4.6.1 Cyclic De-icing Power Requirement

The cyclic de-icing method is basically used to decrease the continuous heated area, heat-on-time, and the heat drainage into ice or the structure. The method allow for the calculation of the relative portion of the parting strip area with respect to the overall area of the surface to be protected. De-icing power can be optimised by combining the cyclic de-icing and pulse electrical de-icing methods. The cyclic de-icing method is basically used to decrease the continuous heated area, heat-on-time, and the heat drainage into ice or the structure. The method allows for the calculation of the relative portion of the parting strip area for anti-icing with respect to the overall area of the surface to be protected. Eqs. 2.41 to 2.43 were used to calculate q_{total}.

The remaining is then de-iced cyclically. The problem with this method is to know the allowable ice thickness and the heat on and off periods for efficient performance. This problem could be solved using the pulse de-icing method. However, other important factors contributing to energy loss have to be accounted. The present work therefore utilises a combination of cyclic and pulsing de-icing techniques factoring radiation along with convection and conduction losses. The pulsing time was determined using Eq. 2.20.

Heater Model

Assuming the baseline aircraft model has facilities for electrothermal de-icing for flight in icing condition. In order to calculate the energy balance on the surface of the leading edge, a typical heater mat arrangement was modelled as shown in Fig. 4.16 and **??**. The upper surface of the heater is made of a thin layer of Neoprene which serves as electrical insulator and erosion shield. Neoprene excellent chemical, oil, water and solvent resis-

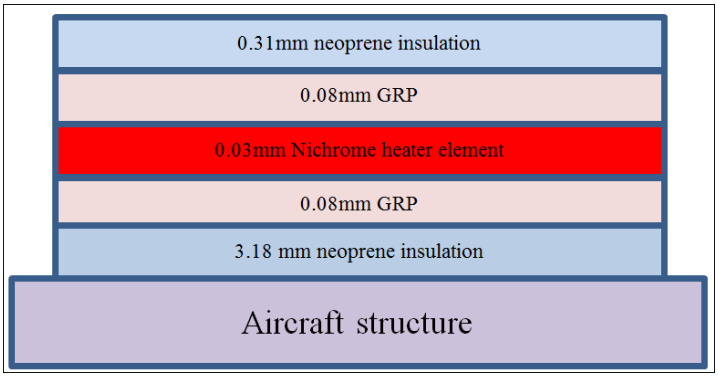

Fig. 4.16: Layout of heater mat model used for the calculation

tance made it a suitable erosion shield. The sprayed heater element is sandwiched by thin layers of GRP for stiffness. Another thick layer forms the inner layer of the heater mat. This layer doubles as electrical insulator and thermal insulator. The outlined lower layer represent the aerofoil structure. A maximum heater ribbon thickness of 6.35 mm was used with a gap of 1.27 mm analysis based on recommended heater design guidelines in [143] and [145]. The stagnation line does not have a fixed location over the leading edge. It is a function of the body setting angle and aircraft attitude in flight. Therefore, in order to cover the range of the stagnation line, a 30 mm parting strip width was used. Based on the a slat length shown in Table 4.3 and the impingement

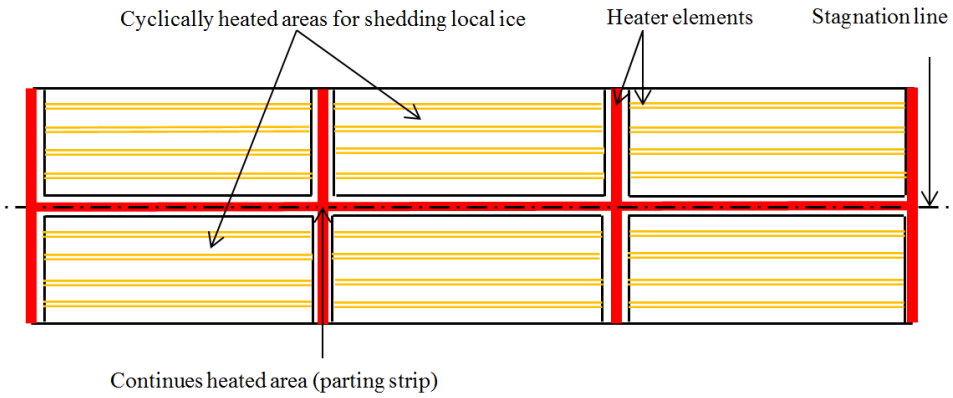

Fig. 4.17: Leading Edge Heater Mat Layout

limit analysis in Chapter 4, a total of 125 heating zones and 4 four break points per slat

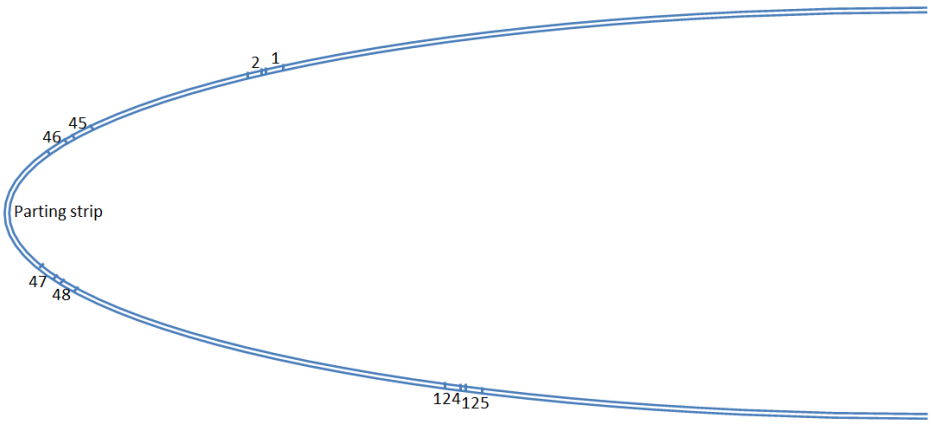

Fig. 4.18: Location of Heater Elements

were used in addition to the parting strip as illustrated in Fig. 4.18.

4.6.2 Factoring Radiation in the Current De-icing System Model

In the present study, the radiation term and conduction through composites was added and the process re-evaluated with a view to see the effect on the optimum de-icing power. The new approach is represented by Eq. 5.19.

$$P_{de-icing} = q_{conv} + q_{rad} + q_{cond} \tag{4.9}$$

The Newtons law of cooling states that the rate of cooling of the surface of a solid, immersed in a colder fluid, was proportional to the difference between the temperature of the surface of the solid and the temperature of the cooling fluid. In other terms this is referred to as convective cooling which can be expressed by the following equation:

$$q_{convec} = U(T_s - T_\infty) \tag{4.10}$$

Heat transfer from the heater due to net radiation exchange (q_rad) with the surroundings is given by:

$$q_{rad} = \epsilon\sigma(T_s^4 - T_0^4) \tag{4.11}$$

Thermal conduction is described by Fourier's law of heat conduction as follows:

$$\frac{\Delta q}{\Delta t} = -kA\frac{\Delta T}{\Delta x} \tag{4.12}$$

where A is the area of the cross section through which heat is conducted, k is the thermal conductivity, ΔT is the temperature difference between the two points that are separated by a distance x, and q is the transferred amount of thermal energy within time t. Hence heat transfer due to conduction from the heater to the laminates is given:

$$q_{cond} = \frac{(k(T_s - T_b))}{L} \tag{4.13}$$

Thus equation 5.19 becomes:

$$P_{de-icing} = U(T_s - T_\infty) + \epsilon\sigma(T_s^4 - T_0^4) + \frac{(k(T_s - T_b))}{L} \tag{4.14}$$

Overall Heat Transfer Coefficient

The overall heat transfer coefficient represented by U is expressed as:

$$\frac{1}{U} = \frac{1}{h_s} + \frac{x_{GRP(i)}}{k_{GRP}} + \frac{x_{GRP(0)}}{k_{GRP}} + \frac{x_{N(i)}}{k_N} + \frac{x_{N(i)}}{k_N} + \frac{x_c}{k_c} \tag{4.15}$$

The term h_s was calculated from Eq. 4.8. Using Eq. 5.25, the plot of the values U at different locations along the aerofoil for both laminar and transient flows is shown in

Fig. 4.19.

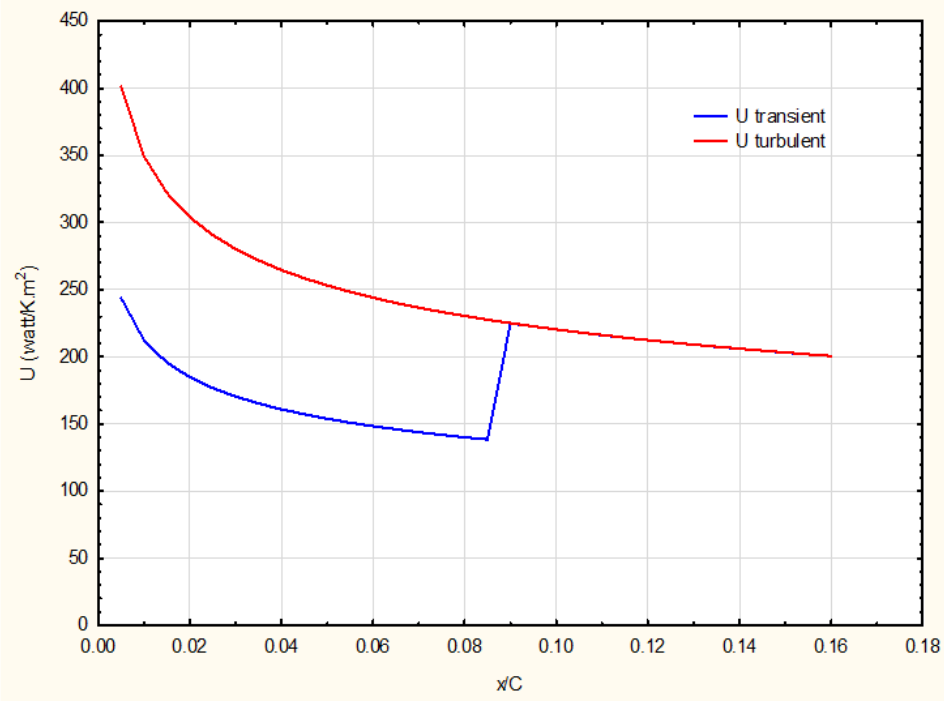

Fig. 4.19: Plot of overall heat transfer coefficient for both laminar and turbulent flows

4.6.3 Model Performance Verification and Validation

Consider a small aircraft flying in a known icing condition of -10℃at a speed of 100 kt. It would take the aircraft (t_{icing}) to exit the icing encounter. Using Eq. 2.5, it would take the aircraft 600 s to exit the icing encounter. Supposing ice has to be removed one it reaches 1mm thickness by a heater element of thickness 0.03mm on a composite aerofoil of thickness 2mm with the material values shown on Table 4.4.

Table 4.4: Material Properties

Layer	λ **(W/m .℃)**	ρ (kg/m^3)	**c(J/kg.℃)**	**d(mm)**
Ice	2.5	920	1882	1
Heater	11.3	8400	450	0.03
Neoprene	0.19	1250	1200	3.49
GRP_{out}	0.35	1900	670	0.18
GRP_{in}	0.35	1900	670	2

4.6.4 Variation of the surface heating intensity with distance along the chord

In estimating the heating intensity along the chord, two parameters have to be used simultaneously. These are the ambient temperature and clouds liquid water concentration. The ambient temperature has an important relationship with clouds water concentration. The cloud water concentration is directly proportional to the ambient temperature. The probability of encountering large amounts of supercooled droplets reduces with decreased ambient temperature. Thus in estimating the heating intensity along the chord, the two parameters have to be used simultaneously. Therefore, this section describes the energy balance at every point on the aerofoil, for three different icing conditions: 0°C/0.8gm^3, - 15°C/0.5gm^3 and - 30°C/0.2gm^3. Variation of the surface heating intensity with distance along the chord could be used to optimise the heater operation. This is because the maximum power is not required throughout the length of the aerofoil. To optimise the heater operation, we need to determine the heating intensity along the chord. Figure 4.20 shows how the heating requirement decays as air stream flows from the leading to the trailing edge. It should be noted that 0.8g/m^3 clouds water concentration corresponds to an ambient temperature of 0°C even though this level of surface heating does not provide 100% evaporation. Therefore, if we wish to evaporate all the surface water , it would correspond to the largest surface heating

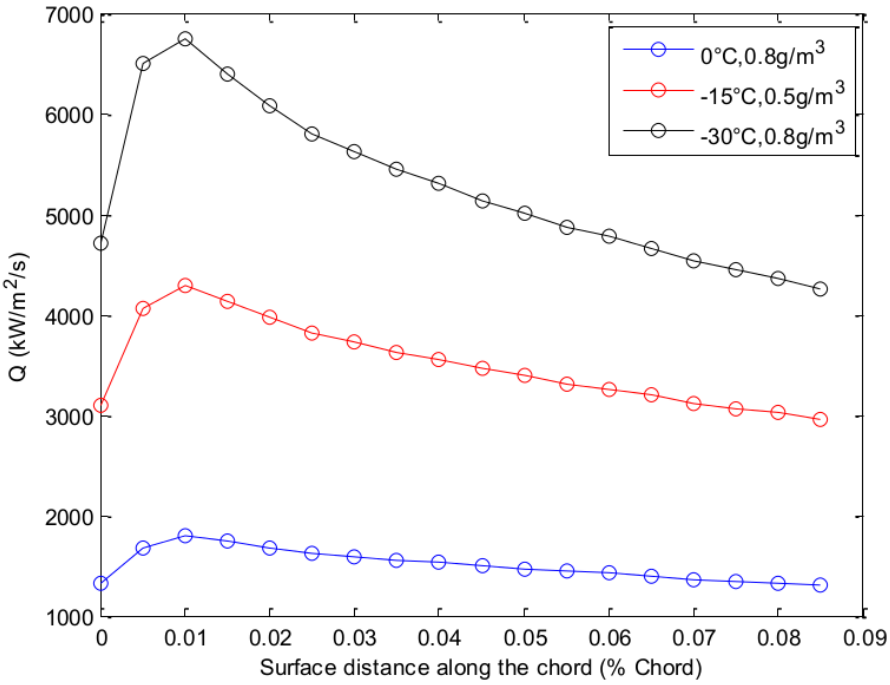

Fig. 4.20: Required heat intensity along the chord

intensity requirement.

4.6.5 Power Density

Fig. 4.21 shows the corresponding values of power density for convection term only and convection plus radiation and conduction for different chord-wise locations along the aerofoil. Laminar flows are more precise because turbulent flows needs exceptional accuracy for validation and data may be an issue. Therefore, the laminar flow HTC were used to determine the power density. The peak power is given by solving Eq. 5.27 and multiplying with the total area covered by cyclic de-icing. The total energy consumed was calculated from the sum of parting strip power and cyclic power. Using the matching plot technique, the peak power and energy curves were plotted on the same graph sheet as presented in Fig. 4.22. The point of intersection gives the minimum pulsing time. The region below each graph satisfies the performance requirements. The above approach

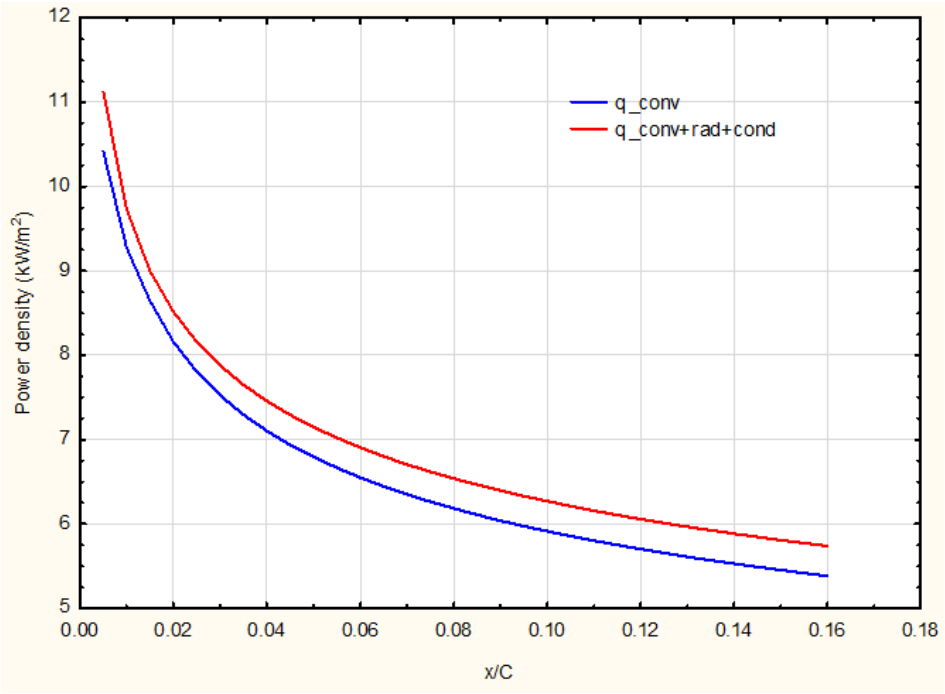

Fig. 4.21: Values of power density for laminar flow at different locations along the chord

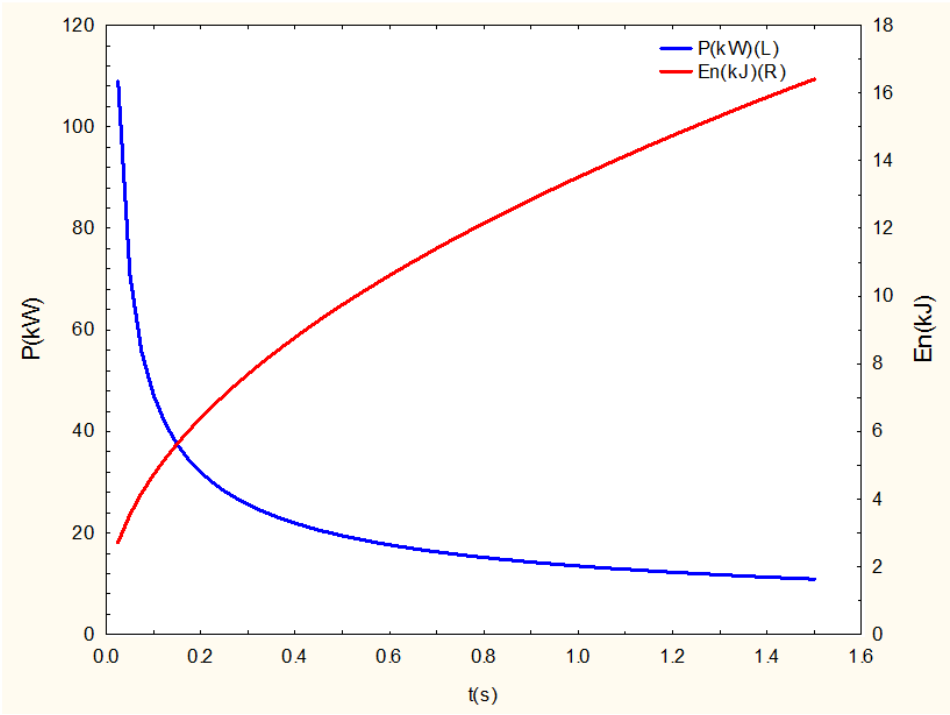

Fig. 4.22: Plot of de-icing power against energy consumption for different pulse rates

shows the variations of the power and energy costs with pulsing time. The point of intersection of the two curves gives the optimum pulse time for a given ice thickness and therefore makes the design point. From the design point, the corresponding value on y-axis gives the design power for the pulse de-icer.

4.6.6 Determination of Freezing Time

SAE standard recommends a heater on time of 9s against a heat off period of 180 seconds for a cyclic deicer. Having determined the pulsing time, we now need to know the equivalent pulsing time using the heat mat model parameters. The freezing time can be obtained using Planks equation as follows:

$$t_f = \frac{\lambda\rho}{(T - T_\infty)}\left(\frac{Pd_h}{h_s} + \frac{Rd_h^2}{k}\right) \tag{4.16}$$

Further reading on the tool can be obtained in [146].

4.6.7 Comparison of Heating Requirement Using Transient Heat Requirement

The performance of the model was compared with an experimental result presented in [65] using a one-dimensional transient heat conduction equation based on [98] model. The power equation is given by:

$$\rho c_p \frac{\partial T}{\partial t} = \frac{\partial}{\partial x}\left(k\frac{\partial T}{\partial x}\right) \tag{4.17}$$

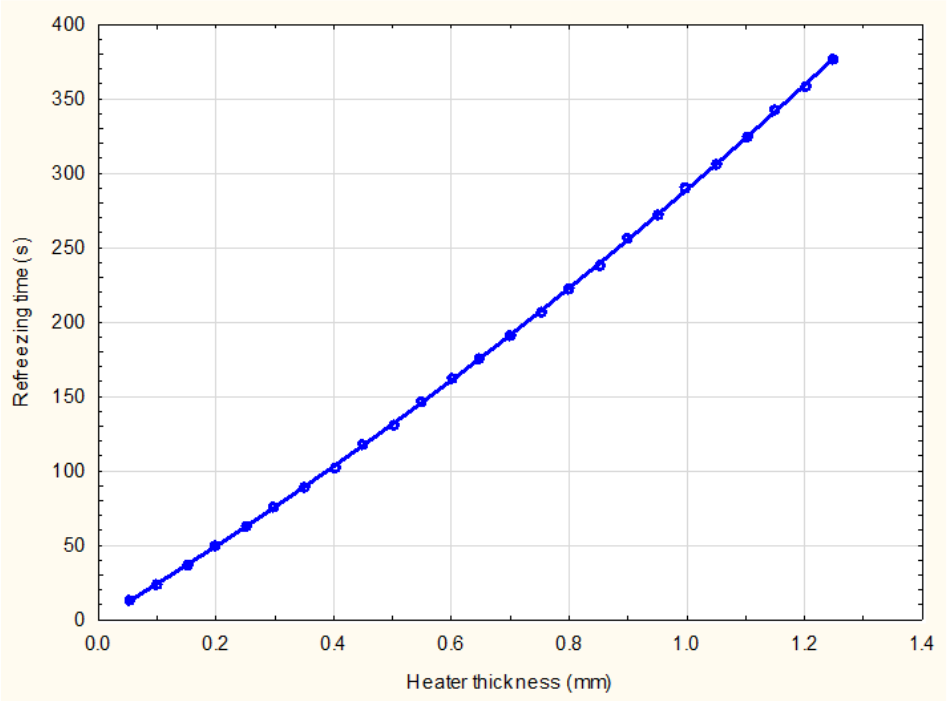

Fig. 4.23: Refrezeezing time against heater thickness

The thermal conductivity, density and heat capacity are constant over the model domain; hence Eq. 4.17 is simplified as:

$$\rho_j c_j \frac{\partial T_j}{\partial^2 T_j} = \lambda_j \frac{\partial^2 T_j}{\partial x^2} + q_j \tag{4.18}$$

For the interfacial ice layer, the mathematical model is given by:

$$\frac{\partial H_1}{\partial t} = \frac{\partial}{\partial x}\left(k_1 \frac{\partial T_1}{\partial x}\right) \tag{4.19}$$

Where H1 is the enthalpy, T1 is the temperature and k1 is the thermal conductivity of ice. The enthalpy is given as:

$$\begin{cases} \rho_s c_s T_1, & T_1 < T_m \\ \rho_L c_L (T_1 - T_m) + \rho_L (c_s T_m + \gamma), & T_1 > T_m \end{cases} \tag{4.20}$$

Where γ refers to the latent heat fusion, and the subscripts S and L refer to the solid and liquid states respectively.

There are two basic assumptions for this simulation. First there is a perfect thermal contact between ice and heater - all of which have constant layer properties. Secondly, the temperature and heat fluxes are continues at the layer interfaces. Thus, the boundary conditions at the interface are given by:

$$T_j \mid_I = T_{j+1} \mid_I \tag{4.21}$$

$$k_j \frac{\partial T_j}{\partial x} \mid_I = k_{j+1} \frac{\partial T_{j+1}}{\partial x} \mid_I^{j=1,2} \tag{4.22}$$

The subscript I refers to the interface. The boundary conditions at the interior and exterior surface are adiabatic, and the initial condition is given by:

$$T_j = T_0, \qquad j = 1, 2, 3 \tag{4.23}$$

The performance of the model compares very well in terms of cyclic de-icing process based on 0.2 s pulsing time in every 100s as shown in Fig. 4.24. Further reading on the transient heat method used in this simulation can be found in [98].

4.7 Chapter Summary

An aircraft anti-icing model was developed based on anti-icing mass and energy balance method for aircraft icing simulation. The aim of the work is to incorporate major aircraft systems into aircraft trajectory optimisation in order to demonstrate the environmental gains that can be achieved if such optimised flight profiles are flown. The

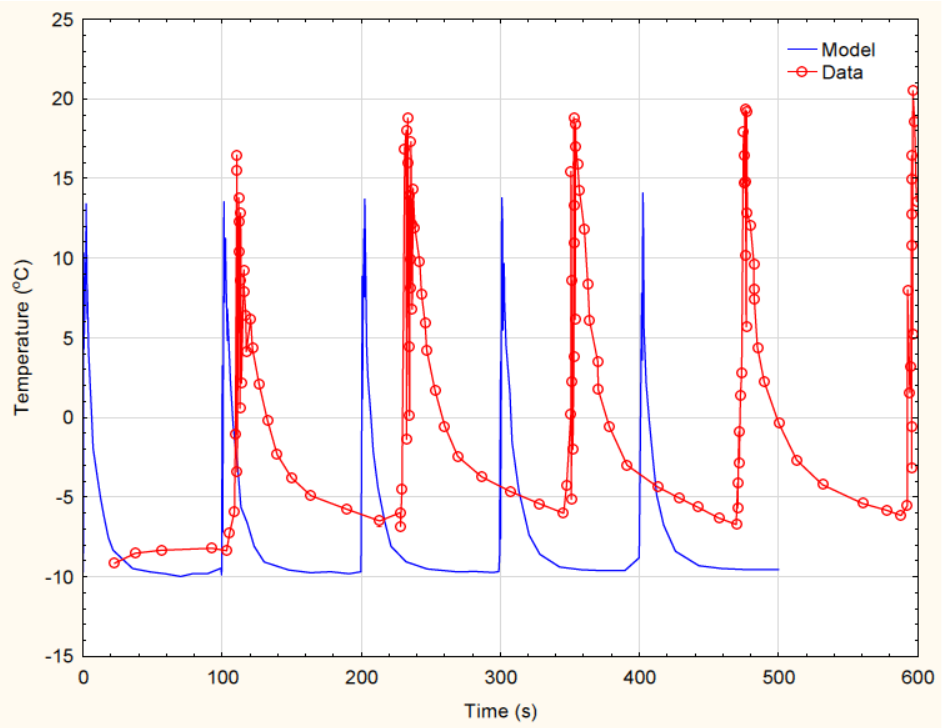

Fig. 4.24: Response of the skin temperature to heating time

reconfigurable version of the model developed in this work was successfully integrated with a trajectory optimization framework for independent assessment of fuel penalty due to icing and investigation of GHG emissions reduction through a mission profile optimisation.

Similarly, a cyclic deicing process accounting for radiation and conduction has been presented. The previous model did not account the effects of radiation term in the deicing energy calculation. However, this work shows that the energy loss due radiation can be significant in a cyclic deicing process. The method took into account the three primary heat transfer mechanisms (conduction, convection and radiation), and heater efficiency. The performance of the model compared well with experimental results.

Chapter 5

Parametric Analysis of Icing Parameters

This chapter describes a sensitivity analysis carried out on the various parameters affecting AI energy in order to determine the most critical cases. These parameters include aircraft geometry, ambient temperature, altitude, clouds LWC and droplets size, and flight speed. The effect of these parameters on AI energy is analysed based on standards established from experimental data and literature on aircraft icing. In order to determine the severity of icing, the need for protection, and the magnitude of the protection required, it is necessary to relate the meteorological conditions to the aircraft operating conditions and design characteristics. For this reason, the baseline aircraft, a typical flight plan, and probable meteorological conditions are used for this analysis.

5.1 Factors Affecting Heat Requirements

5.1.1 Ambient Temperature

For a fully evaporative system, it can be noted from Fig. 5.1 that the required power density for the wing increases as a result of decrease in ambient temperature.

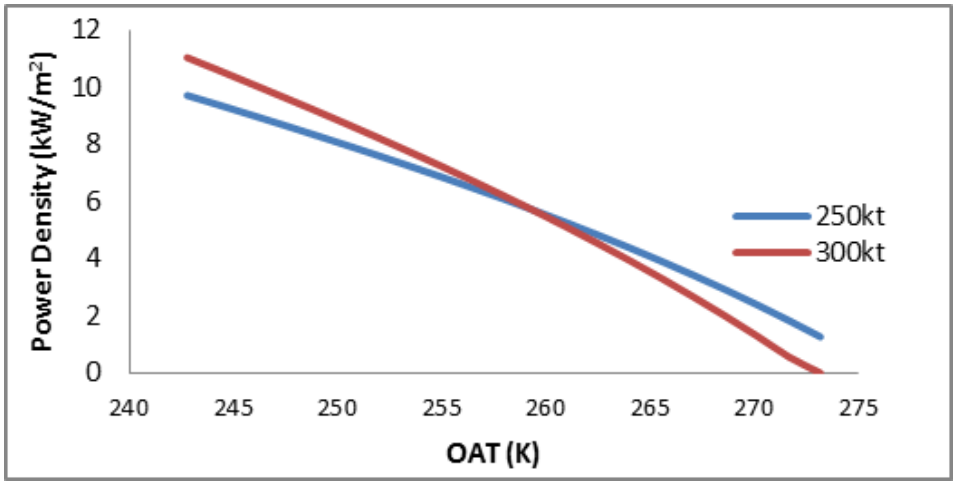

Fig. 5.1: Effects of Ambient Temperature on the Anti-icing Power Requirement

5.1.2 Cloud's Liquid Water Content

The work of Kilshaw [147] brings to fore the great relationship that exists between ambient temperature and a cloud's water content. Ice forms on aircraft surfaces when the ambient temperature is 0°or colder, and the clouds liquid water content is 0.2 g/m^3 or higher. The lower the temperature, the lower a cloud LWC because most of the supercooled droplets would have formed ice particles. This reduces the ice accretion rate relative to higher freezing temperatures such as -8 to 0℃. Typical values of LWC ranges between 0.2 to 1.4 g/m^3. The continuous maximum value of LWC that may be encountered in stratoform clouds at 0℃ is 0.8g/ m^3 which reduce to 0.2 g/m^3 at -30 ℃. This can however reach up to 1.7 g/m^3 in cumuli-form clouds. For the CM conditions, the 0.2 g/m^3 at -30 ℃set-up was used for the simulation whereas, 1.7 g/m^3 LWC was used for cases involving IM conditions.

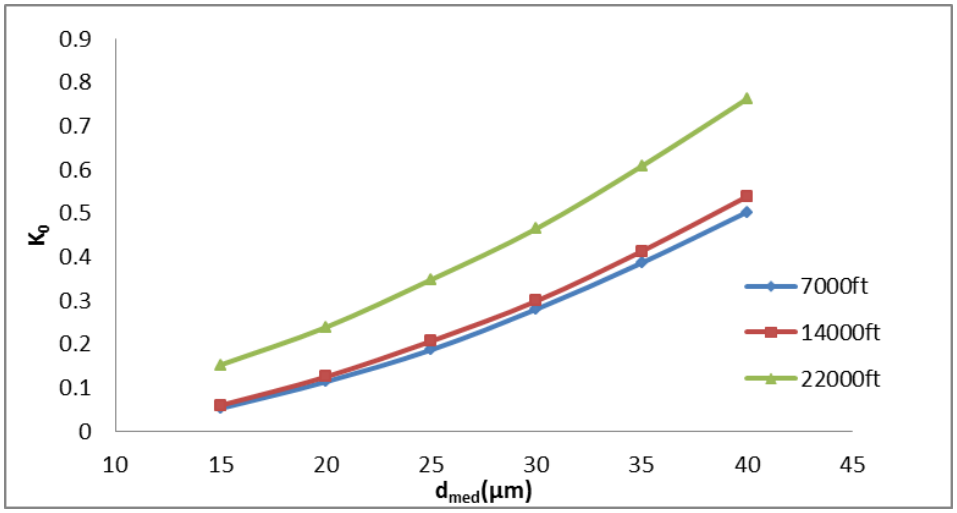

Fig. 5.2: Effects of Droplets Size on Modified Inertia Factor (K0)

5.1.3 Water Droplets Size

Aircraft geometry and water droplets size are two parameters affecting collection efficiency and the overall water catch. Though not important like temperature and LWC, droplet size can affect the ice shape as well. This is because droplet size is important in the calculation of the modified inertia parameter (K_0) which gives a measure of the collection efficiency. The K_0 for different droplet sizes was evaluated for the three altitudes that are critical to aircraft icing as represented graphically in Fig. 5.2. K_0 rises with increase in droplet size and altitude. This is because larger droplets are associated with higher inertia and therefore less affected by local aerodynamic forces whereas, droplets with small diameters hence low inertia are likely to flow along the air streamlines and do not impact the surface. This means that large droplets are more likely to collide with a body moving through the air, as opposed to following the streamlines around it.

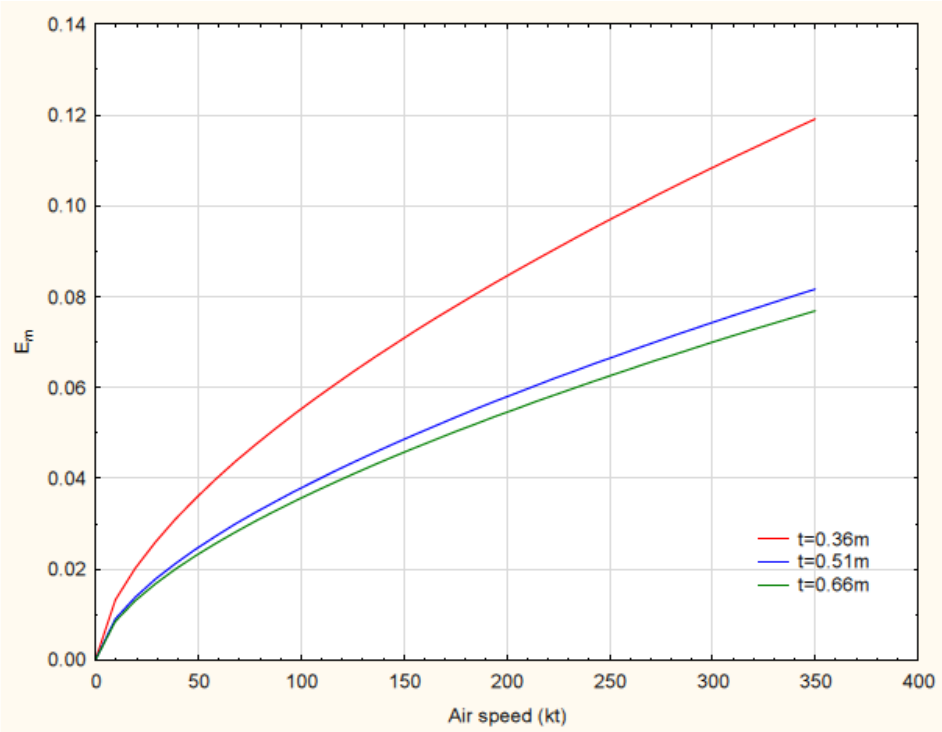

Fig. 5.3: Air Speed vs Collection Efficiency for Different Aerofoil Sizes

5.1.4 Aircraft Geometry

Fig. 5.3 shows the result of a simple test case involving three conceptualised aerofoils of different chord sizes subjected to same speeds. It can be noted that smaller aerofoils have higher collection efficiency than bigger ones. This is due the fact that the smaller the body the smaller the obstruction it creates against incoming droplets and hence the deviation of the droplets is not sufficient enough for them to avoid the body. As speed increases, water droplets have less time to flow around the surface which causes smaller droplets to deflect around the larger object. The droplet inertia factor K is given by:

$$K = \left[\left(\frac{1}{18}\right) \cdot \frac{D_d^2 \cdot V_{TAS} \cdot \rho_{water}}{\mu_{icing} \cdot L_{MAC}}\right] \tag{5.1}$$

In [23], E_m is defined as illustrated in Fig. 5.4.

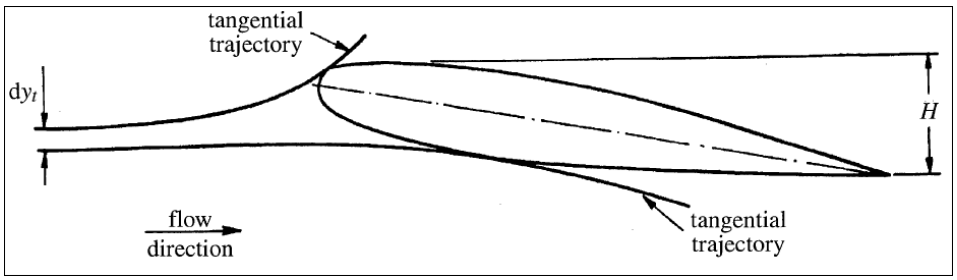

Fig. 5.4: Definition of Overall Water Catch [23]

Where:

$$E_m = \frac{d_{y_t}}{H} \tag{5.2}$$

The E_m being a function of aerofoil geometry, alpha (α) and K_0, can be read for the particular aerofoil from experimental data in [22].

5.1.5 Angle of Attack

Aerofoil projected height (h_proj) as seen in the x direction is a function of aerofoil geometry and angle of attack(α).

$$h_{proj} = f(\alpha) \tag{5.3}$$

The same experimental data provided the (h/C) ratios for various aerofoils at different angles of attack. Thus, parameter h_{proj} was obtained based on (h/C) from Fig B.1.

5.1.6 Collection Efficiency Calculation

The E_m was calculated for different altitudes and droplet sizes as shown in Fig. 5.5. The result shows that the collection increases with the droplet size and altitude. The

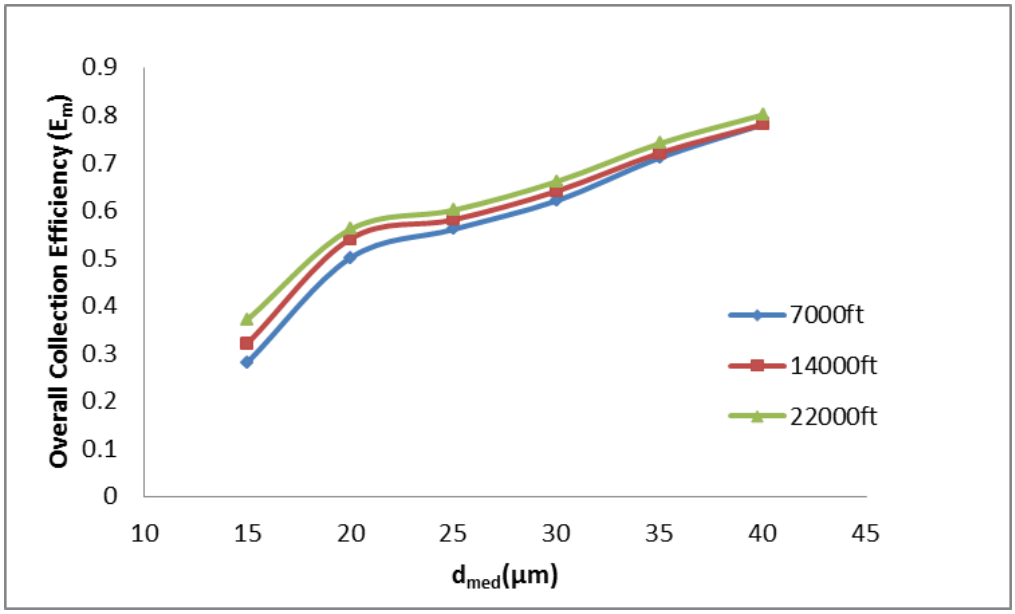

Fig. 5.5: Overall Collection Efficiency vs Droplets Size

E_m enables the determination of the total water catch rate of the wing. The overall collection efficiency enables the determination of the water catch rate of the wing.

5.1.7 Total Water Catch Calculation

Water and air are the only recognised substances in an anti-icing system analysis. Water flows on an aerofoil as a thin film, hence its proportions relative to that of the air need to be calculated in anti-icing performance. Therefore the difference between the wing surface temperature and the ambient temperature factored by the heat transfer coefficient and amount of water on the wing gives the total heat requirement and related power to generate this heat[148]. Due to the consideration of the wing leading edge sweep, the airspeed was multiplied by the cosine of the sweep angle.

$$V_{TAS} = V \cdot cos(\varphi L_E) \tag{5.4}$$

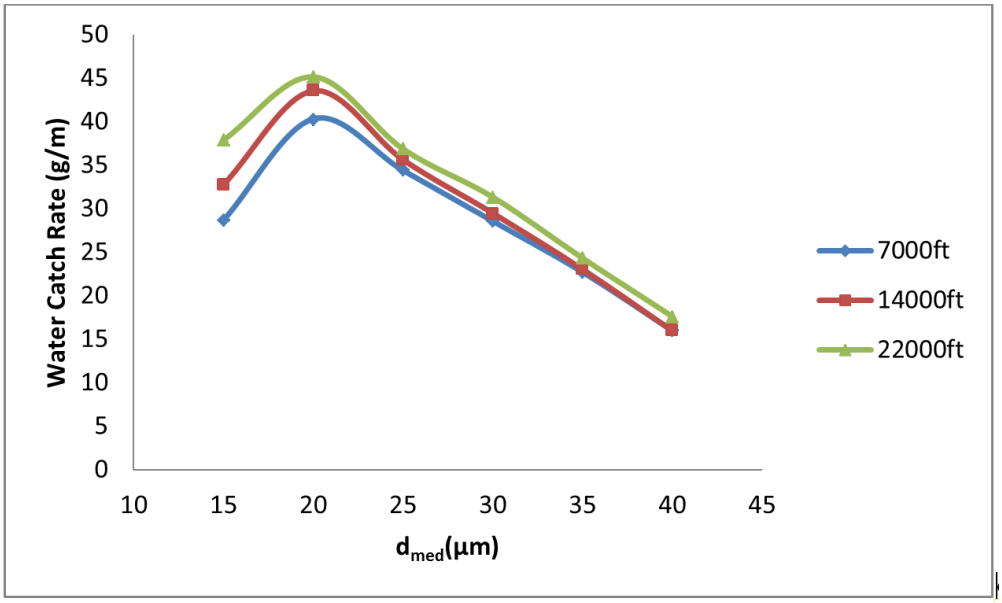

Fig. 5.6: Total Amount of Water Collected per Unit Span of the Wing for CM Icing Condition

The water catch $(g/s.m)$ is the product of the liquid water content, speed and the droplet collection efficiency for the heated area. Thus overall water mass flux is given by:

$$\dot{m}_w = LWC \cdot h_{proj} \cdot V_{TAS} \cdot L_x \cdot E_m \tag{5.5}$$

In the analysis of water catch for different droplet sizes in CM icing condition for the three altitudes under investigation, the results show that 20 μm is the most critical droplet size with the highest water catch and ice thickness as shown in Fig. 5.6 and Fig. 5.7 respectively. As a result of the higher inertia associated with larger masses, larger droplets are less affected by aerodynamic forces and therefore more likely to collide with an object moving through the air, as opposed to following the flow lines around it, resulting in a higher collection rate. If there is some reason to design for longer or shorter exposure duration, then the LWC originally selected may be reduced or increased by a factor obtained from [46] relating to non-standard operations in Appendix C. However,

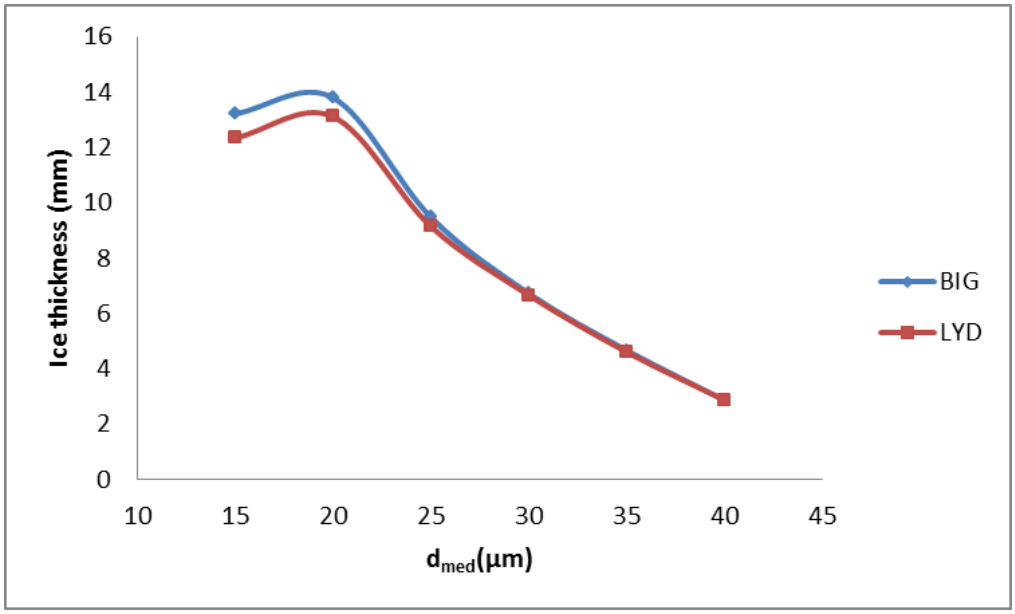

Fig. 5.7: Ice Formation Thickness for I Meter Span, Hold (45mins)

that was not required in this work as the methodology used in the modelling process yielded an expected result. Reading from Fig. 4.20 shows that the rate of ice accumulation is directly related to LWC for a given temperature.

During holding in icing conditions, an aircraft may be more vulnerable to ice accumulation because of the slower speeds and lower altitudes during this phase of flight. The general requirement for the design and analysis of inflight ice protection systems recommends a minimum of 45 minutes ice protection capability [149]. Thus, ice formation thickness for one meter span in a 45 minutes hold for 7000ft (BIG) and 14000ft (LYD) using London Heathrow airport standard arrival is shown in Fig. 5.7.

5.1.8 Altitude and Air Speed

The ambient temperature normally reduces with altitude, hence icing potentials increase with altitude as well. However, Fig. 5.8 shows that anti-icing power demand is higher at

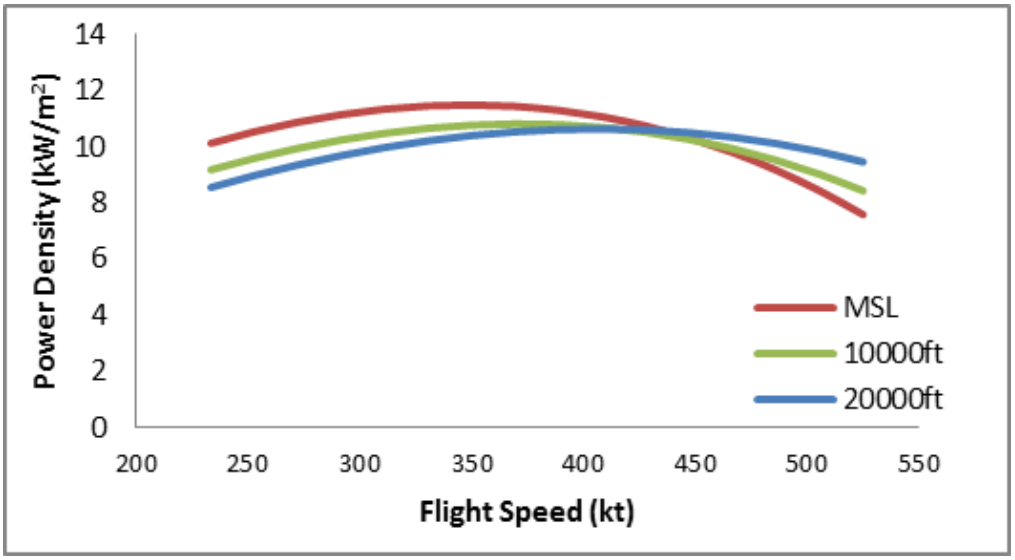

Fig. 5.8: Power Density as a Function of Flight Speed Altitude

low altitudes due the effects of density which is higher at lower altitudes and water rich clouds. An increase in the airspeed increases the volume of intercepted water per unit time, and aerodynamic and kinetic heating effects. It can be noted from Fig. 5.8 that power requirement increases with airspeed until about 430 kt when the aerodynamic and kinetic heating start to take effect. This means that as speed increases, the temperature range at which ice accretes starts to shift towards the low temperature region.

5.1.9 Duration of Exposure

The longer an aircraft stays in an icing encounter the more the accretion. Duration (t_{icing}) of icing encounter can be estimated by dividing the standard horizontal extent ($S_{horizantal}$) for the continuous and intermittent maximum conditions by the aircraft speed (V_{TAS}) [150]. Since the total water catch is a function of the time spent in icing condition, it is also speed dependent. Therefore, multiplying the exposure period with the calculated rate of water catch gives the total amount of water collected per unit

length of the wing span (g/m).

$$t_{icing} = \frac{S_{horizantal}}{V_{TAS}} \tag{5.6}$$

$$m_{w_{total}} = \dot{m}_w \cdot t_{icing} \tag{5.7}$$

5.2 Test Cases

It is known that most icing occurs at temperatures between 0 and -20℃ and more than 50% of that occurs between -8 and -12℃ [151]. But this range does not indicate the most critical design point. The critical design point for the IPS is when the power requirement is highest from an engine perspective the engine should be able to supply bleed air to satisfy this requirement. At each point the permissible bleed extraction should be adequate to supply the combine airflow requirement for both ECS and IPS. The whole Appendix C envelope was covered using 24 cases to determine the most critical weather conditions. The test cases are listed in Table 5.1.

5.2.1 Continuous Maximum Icing Conditions

Thermal AI systems are designed for maximum energy requirements which usually occur at between 250 kt and 350 kt V_{TAS}. At higher velocities, kinetic heating outweighs convective losses and thus eliminates the need for anti-icing. We know that most icing occurs at temperatures between 0 and -20 ℃ and more than 50% of that occurs between -8 and -12 ℃ [26]. But this range does not indicate the most critical design point. The

Table 5.1: Test Cases

Case		**CM**			**IM**	
-	**OAT**	**LWC**	**MVD**	**OAT**	**LWC**	**MVD**
	℃	g/m^3	$m\mu$	℃	g/m^3	$m\mu$
1.	0	0.8	15	0	2.8	15
2.	-10	0.6	15	-20	1.9	15
3.	-20	0.3	15	-30	1.14	15
4.	-30	0.2	15	-40	0.25	15
5.	0	0.63	20	0	2.6	20
6.	-10	0.43	20	-30	0.95	20
7.	-20	0.23	20	-40	0.23	20
8.	-30	0.15	20	0	1.75	20
9.	0	0.48	25	-20	1.18	25
10.	-10	0.3	25	-40	0.14	25
11.	-20	0.16	25	0	1.3	25
12.	-30	0.08	25	-10	1	25
13.	0	0.365	30	-30	0.45	30
14.	-10	0.23	30	-40	0.12	30
15.	-20	0.13	30	0	0.95	35
16.	-30	0.06	30	-20	0.57	35
17.	0	0.26	35	-40	0.1	35
18.	-10	0.16	35	0	0.75	40
19.	-20	0.07	35	-10	0.55	40
20.	-30	0.05	35	-40	0.1	40
21.	0	0.165	40	0	0.6	45
22.	-10	0.1	40	-40	0.1	45
23.	-20	0.065	40	0	0.38	50
24.	-30	0.05	40	-40	0.1	40

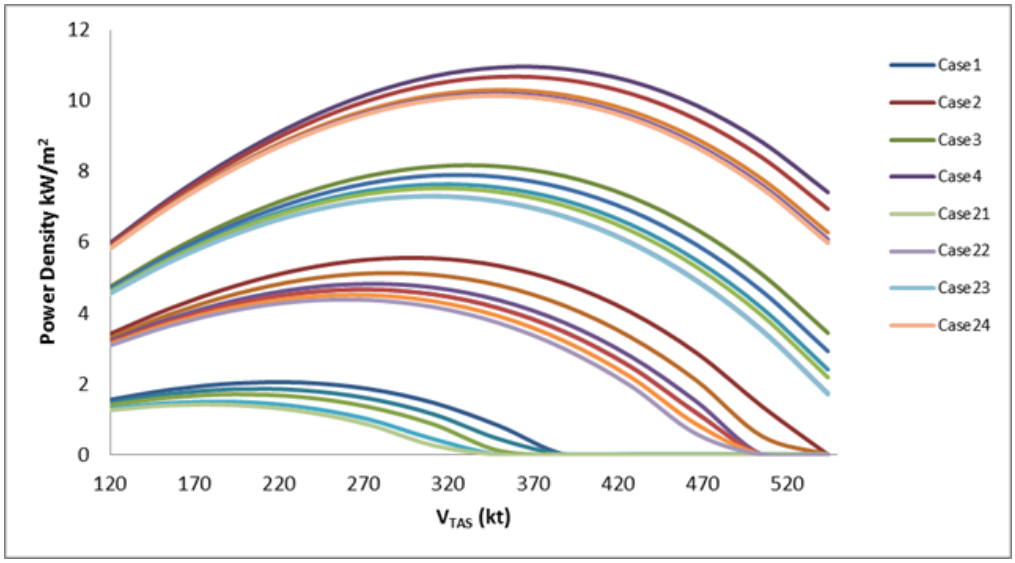

Fig. 5.9: Power Density for the CM Icing Envelope, MSL-22000 ft

critical design point is that with the highest power requirement. Therefore, the whole Appendix C envelope was covered using 24 cases to determine the most critical design point. Fig. 5.9 shows the response of the power density to different temperature bands (0 ℃, -10 ℃, -20 ℃and -30 ℃) at different speed settings. The result indicates a minimum power requirement of about 6 kW/m^2 at 250 kt assuming that ice melts at a low fixed temperature point of 0.01 ℃. At a maximum air speed of 300-350 kt, a maximum power requirement of between 7 to 9 kW/m^2 was obtained for a maximum 5 ℃ skin temperature. The clouds that contain super-cooled water droplets exist at lower flight levels, and during descent and climb, the aircraft flies at low speed which lessens the effects of kinetic heating on the airframe.

5.2.2 Intermittent Maximum Icing Conditions

The whole Appendix C envelope was covered and simulated to determine the most costly icing condition under the IM icing condition. A total of 24 cases were simulated and presented in Fig. 5.10. Case 3 representing -30 ℃, 0.2 g/m^3, 20 μm has the highest

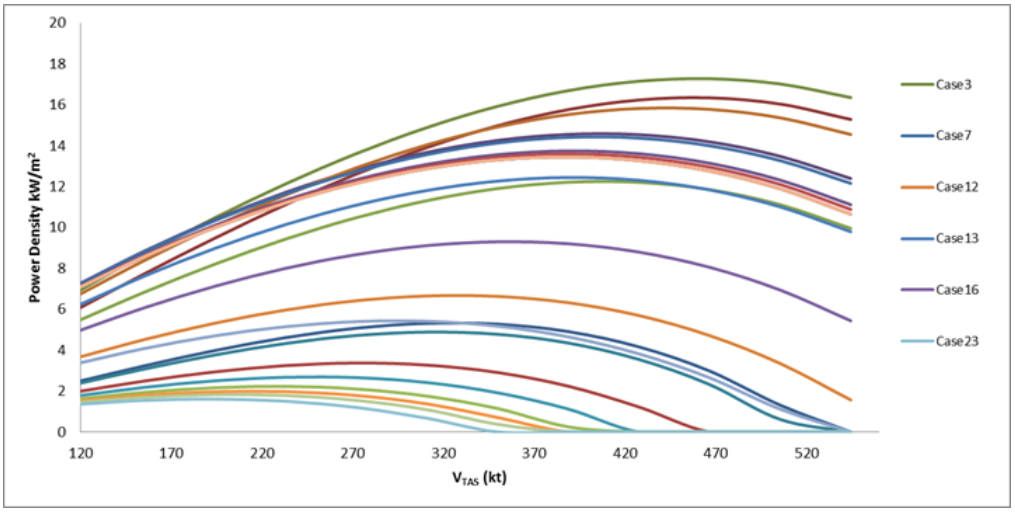

Fig. 5.10: Power Density for the IM Icing Envelope from 4000-22000 ft

power requirement whereas case 23, 0 ℃, 0.43 g/m^3, 30 μm has the lowest requirement. The upper and lower boundaries of the power demands were plotted in Fig. 5.11.

5.3 Chapter Summary

The above analysis shows that the probability of encountering large amounts of supercooled droplets reduces with decreased ambient temperature. The analysis further shows that icing does occur at 0℃ ambient temperature but anti-icing may not be necessary except for low climb speeds. Although, the power densities are closely entwined, however, the difference will manifest in overall power requirement which could lead to additional system weight and off-take penalties. The upper and lower boundaries of the power demands established in this analysis form an important part of the optimisation studies.

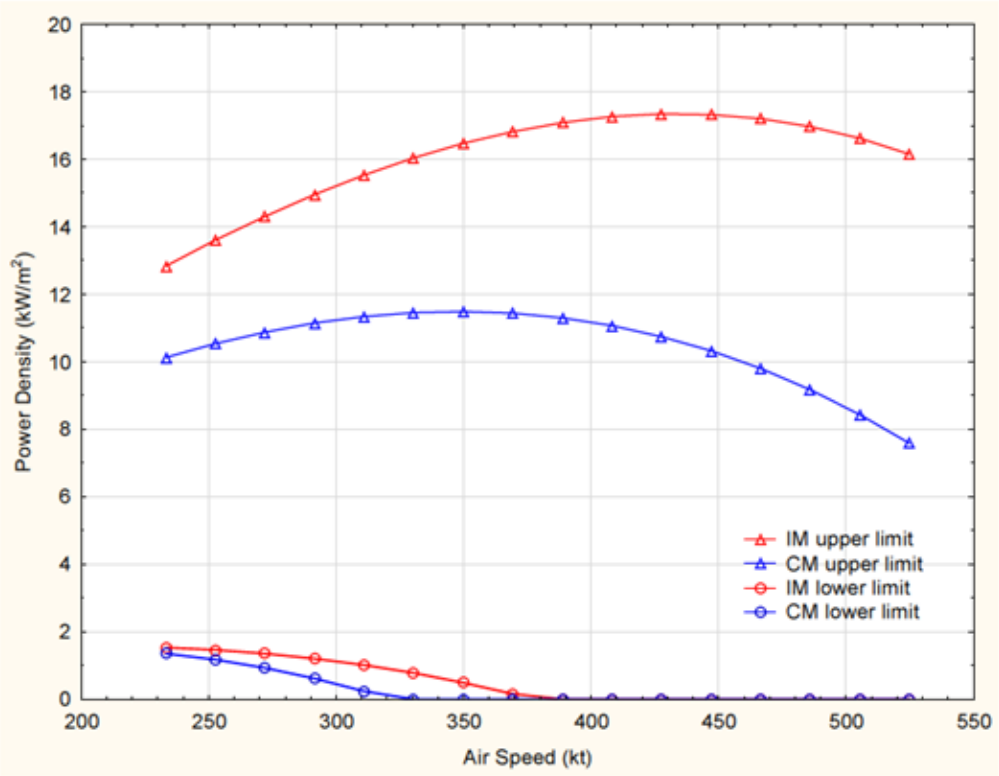

Fig. 5.11: Power Demand Boundaries

Chapter 6

Results and Discussions

Chapter 6 discusses the applications of all or part of the processes and tools described in previous chapters in a multidisciplinary and multi-objective trajectory optimisation. These processes and tools are applied in a trajectory optimisation problem involving icing conditions. Fuel burn, flight time, noise and GHG emissions are evaluated as cost functions for the departure, en-route and arrival phases by reviewing the aircraft performance in each case using the baseline aircraft model.

6.1 Introduction to the Cases

Recall that this work is a collaborative research involving three universities (Cranfield University, Delft University of Technology and The University of Malta), and industrial partners such as Airbus, Thales and DLR. Therefore, selected multi-objective trajectory optimisation cases are simulated to assess the impacts of including icing conditions in aircraft trajectory optimisation. This is to allow the assessment of effects of flying trajectories obtained with and without consideration to the icing conditions on fuel burn and associated emissions, and noise. It was agreed during one of the stakeholders meeting that Cranfield University and Delft University researchers should study the London Amsterdam short distance route, whereas The University of Malta studies the Malta-New York long Hall route. This decision was based on the accessibility of the

demographic data of the airport area and request of the sponsors. Consequently the London-Amsterdam route was chosen as a case study for this work.

At the top level, there is the London - Amsterdam flight route case, 3D optimisation case and the noise mitigation case. All cases involve icing encounters. The London-Amsterdam case is sub-divided into departure, en-route and arrival cases. Fuel burn, flight time and associated GHG emissions are assessed in the departure, en-route and the arrival phases. The 3D optimisation and the noise evaluation cases are performed on departure segment only as there would not be need for repeating these cases in cruise and arrival phases (see section 1.7, page 25). Each flight phase was optimised with and without considering airframe systems power off-take penalties with either fuel burn or flight time as the primary cost function. Hence, the results are presented in four distinct graphs: min fuel conventional, min time conventional, min fuel icing in the loop and min time icing in the loop. The 'minimum fuel - conventional' graph refers to the trajectory optimised for minimum fuel using the conventional approach (see section 3.1, page 78) whereas, the 'minimum time - conventional' graphs represents the trajectory optimised for minimum time using same method. On the other hand, the 'min fuel - icing in the loop represents the trajectory optimised for minimum fuel taking into account weather conditions (in this case icing) in the optimisation set-up; and the 'min time - icing in the loop' graph represents the trajectory optimised for minimum time using this approach.

6.1.1 London Airport Heathrow (EGLL/LHR) to Amsterdam Airport Schiphol (EHAM/AMS) Case

The British Airways and KLM Royal Dutch airlines are the major airlines operating this route. The BA uses A319 and A320 aircraft whereas KLM uses F70 and E190

Fig. 6.1: London - Amsterdam Typical Flight Route [24]

on this route. This analysis considers an aircraft similar to A320 aircraft flying this route in the presence of icing conditions. The simulated flight plan includes a Standard Instrument Departure (SID), Standard Terminal Arrival Route (STAR) and an RNAV-based Instrument Approach (IA). Fig. 6.1 shows a graphical projection of the flight trajectory obtained from FlightAware, a private flight tracking company [24]. The departure starts from 83 ft above ground level (AGL) to BPK VOR. The en-route phase starts after the aircraft has reached BPK VOR way point and ends when the aircraft enters the Amsterdam Schiphol STAR procedure. The arrival phase starts from 10,000 ft to landing. In all the cases, case 4 (see Table 5.1) was used as inputs to the artificial icing cloud algorithm in the ASM. The aim of running these cases is to evaluate the two optimisation approaches with a view to improving power-off efficiency in icing conditions.

6.1.2 Extended Departure from LHR in Icing Conditions: A 3D Case

The NextGen proposed improvements to lateral route planning in trajectory based operations, involves allowing an aircraft to operate in a 3D space. This will give the aircraft a wider latitude for efficient flight, rather than the current method of direct flight from one point to another at a constant altitude. Literature has shown that, by 2030, aircraft are expected to fly optimal trajectories that are defined in the form of 3D way points plus associated required times of overfly. This case considers departure from 83 ft to 23,000 with an icing encounter similar to case 4 from 12,000 ft to 18,500 ft. The aim of running this test case is to understand how the method developed in this work will perform in a 3D environment; a 3D optimisation problem was simulated and discussed.

6.1.3 Study of Alternative Noise Preferential Routing in Icing Conditions

Secondary power off-take due to aircraft systems operation places a burden on the engine. Meanwhile, the power produced by the engine is a function of the throttle setting, hence secondary power off-take raises the throttle setting. Thus, systems power off-take could increase noise generation. Therefore, there is the requirement to consider noise when using icing optimised trajectories. A standard departure from 83 ft to 10,000 ft was used with the addition of lateral movement. The population data around the Heathrow below the trajectory path within the greater London area was considered for the noise impacts assessment.

Table 6.1: Conditions of the Optimisation Studies

Flight phase	Objective1	Objective2	Initial mass(kg)	Generations	Population	Initialisation factor	Initial altitude(ft)	Initial airspeed (CAS)	Final altitude (ft)	Final airspeed(CAS)
Departure	Fuel	Time	66,000	250	100	50	83	140	10,000	310
Enroute	Fuel	Time	65,406	250	100	50	10,000	310	10,000	310
Arrival	Fuel	Time	63,000	250	100	50	10,000	310	0	140
Extended Departure	Fuel	Time	66,000	250	100	50	83	140	23,000	340

6.2 Fuel vs Time Problem

6.2.1 Set-up

The trajectory optimisation problem was set up including the presence of icing conditions. The solver was run with and without considering the icing conditions in the optimisation loop. The key settings for the different optimisation problems are shown on Table 6.1.

6.2.2 Simulation of the Critical Icing Conditions in terms of Fuel Burn

Case 4 which represents the most critical CM icing conditions was used for the optimisation. The Pareto front for this case for full route optimisation is shown in Fig. 6.2.

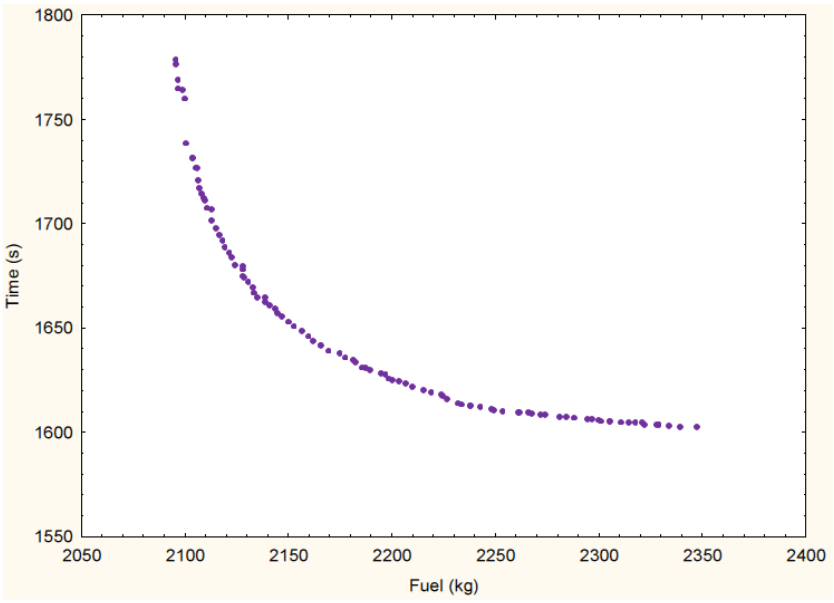

Fig. 6.2: Pareto Front for Case 4 Icing Conditions

The Pareto shows a difference of 252 kg between the minimum time and minimum fuel trajectories within 3 minutes difference of arrival time. A further simulation was carried out using Case 3 which represents the most probable icing conditions according to the literature [22]. The two Pareto fronts are compared in Fig. 6.3. A difference of 66 kg fuel burn was realised between the two cases. This implied that the most probable icing condition may not be the most critical in terms of AI power requirement.

6.2.3 Departure Case

At LHR airport, the ATC are responsible for routing all jet aircraft through Noise Preferential Routes (NPR) from take-off to 4,000 ft, except where there is safety concern. From 4,000 ft however, the pilot could be authorised to leave the NPR and fly a more direct heading to their destination [152]. In medium to large jet aircraft, departure phase is considered to begin with take-off and end at FL100 [153]. To accommodate the ATC constraints, an icing scenario between 4,000 ft and 10,000 ft was built into the

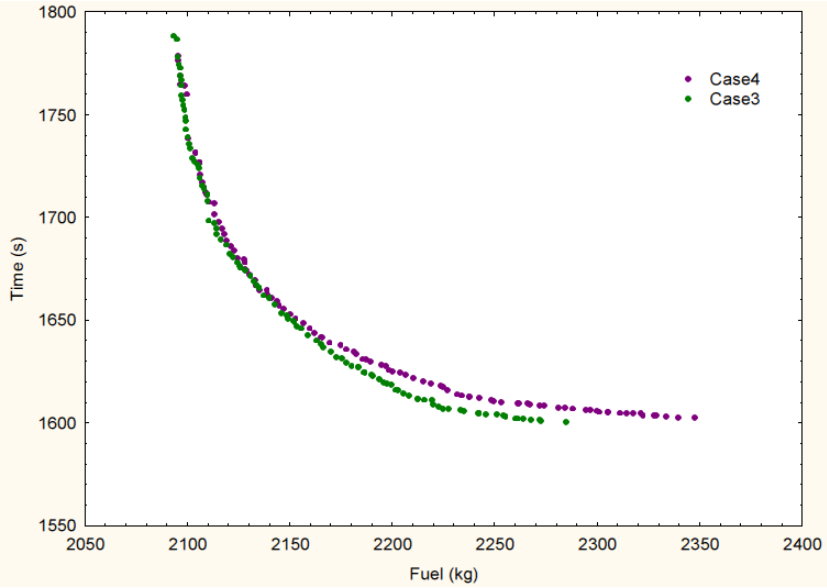

Fig. 6.3: Pareto Fronts for Cases 3 & 4 Icing Conditions

optimiser search domain based on Case 4 CM icing conditions.

The departure phase begins at 83 ft above ground level (AGL) with airspeed equal to V_2, and terminates at BPK SID. The SID selected for the departure phase is BPKGF from runway 27 (see Fig. C.1B) and the way points and related aircraft states used for the optimisation are listed in Table 6.2. Fig. 6.4 shows the trade-off between fuel

Table 6.2: Departure Phase

WP	**Latitude**	**Longitude**	**Altitude(ft) min/max**	**CAS(kt) min/max**
WP1	51 27 53.25 N	000 28 54.99 W	83	140
WP2	51 27 52.51 N	000 31 35.75 W	83/10,000	140/310
WP3	51 31 08.00 N	000 40 38.00 W	83/10,000	140/310
WP4	51 35 07.13 N	000 36 29.69 W	83/10,000	140/310
WP5	51 37 23.00 N	000 31 07.00 W	83/10,000	140/310
BPK	51 44 59.00 N	000 06 24.00 W	10,000	310

consumption and flight time for the different approaches. The associated trajectories and speed profiles are shown in Fig. 6.5 and Fig. 6.6. When icing was included in

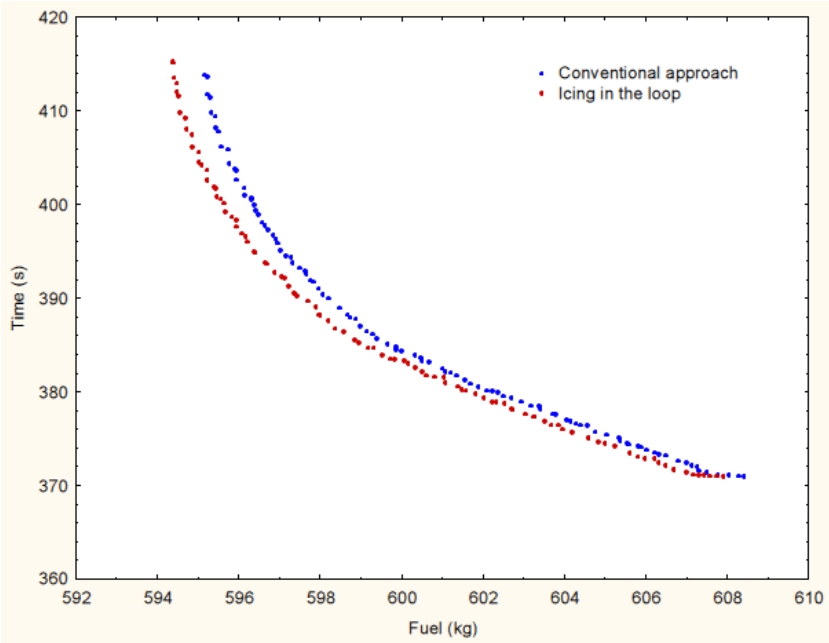

Fig. 6.4: Pareto Fronts of Fuel vs Time Optimisation for the Two Approaches

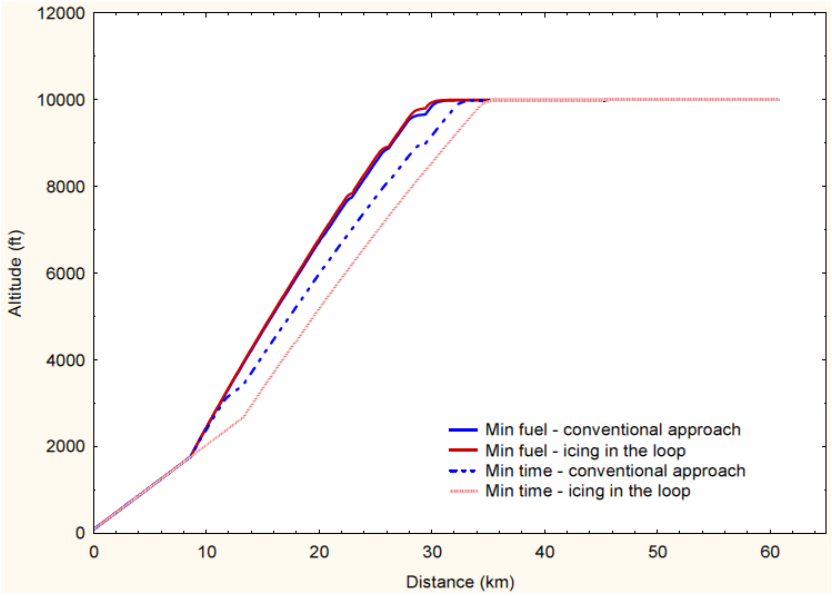

Fig. 6.5: Difference in Trajectories between the Two Approaches - Departure

the optimisation loop, the aircraft flew at a slightly higher altitude and lower speed than in the conventional approach for the minimum fuel result. This is expected as the optimiser finds points of low fuel consumption at higher altitudes and lower speeds

than lower altitudes, higher speeds. For the minimum time trajectories, the icing in the loop operated at a relatively lower altitude and higher speed pattern. The different projections of the different trajectories indicates that, there is the need to fly aircraft in a different way in the presence of icing conditions.

Air speed has a significant effect on AI system energy consumption. Faster aircraft are likely to consume less energy than slower ones due to kinetic and aerodynamic heatings. As can be seen in Fig. 6.6, including the AI conditions in the set-up made the aircraft to fly at a higher true air speed (TAS) than in the conventional approach. Because of the higher TAS in the enhanced approach, the kinetic heating is more; hence, requires less AI power. Fig. 6.8 and Fig. 6.7 show the bleed power demand and fuel flow to

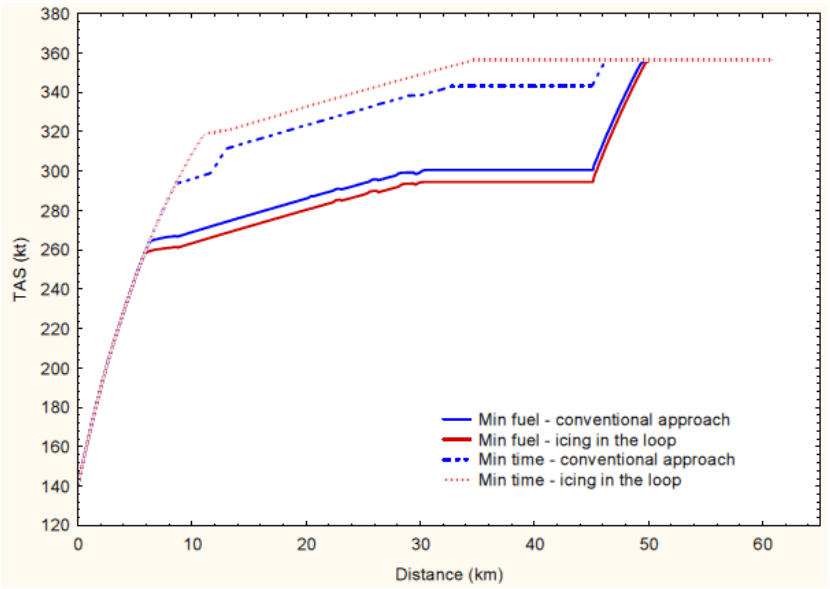

Fig. 6.6: Aircraft TAS for the Departure

engine respectively. The conventional trajectories show higher fuel flow rates than the icing optimised trajectories. This is because including icing conditions to the set up adds more arguments to the optimisation which changes the points of minimum cost. This has resulted in different bleed power demands. As the fuel flow is a function of

the speed, altitude, throttle setting and power off-take, it can be observed in Fig. 6.7 that reduction in the bleed power demand associated with the enhanced approach has helped to reduce the fuel flow to the engines. The production of the greenhouse gas

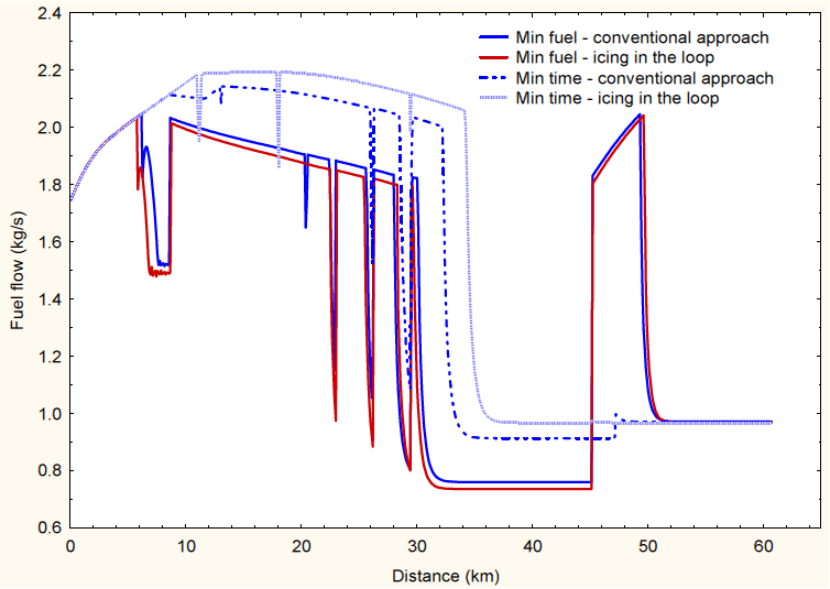

Fig. 6.7: Fuel Flow Requirement for the Departure

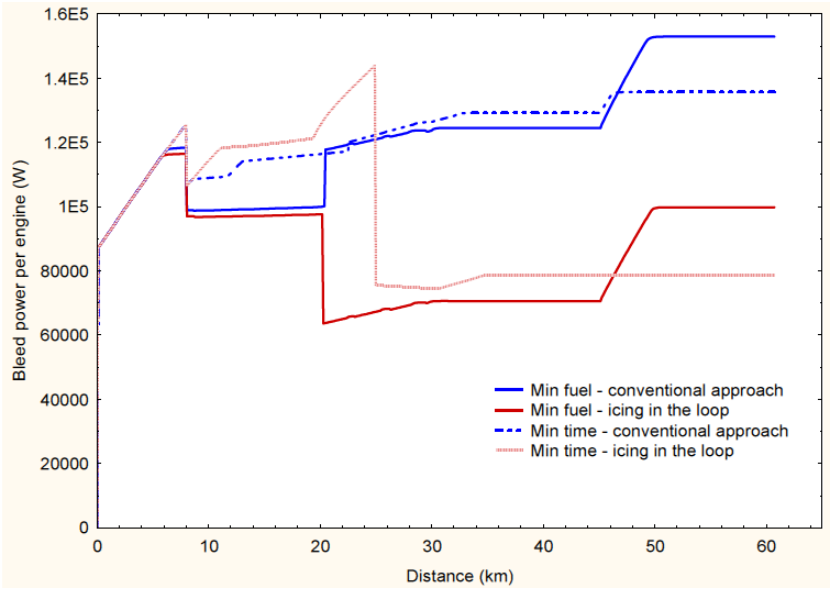

Fig. 6.8: Difference in Bleed Power Requirement for the Departure Phase

is directly correlated with fuel consumption [154]. Hence, savings on fuel results in

direct reduction on GHG emissions. Fig. 6.9 and Fig. 6.10 show the difference in total CO_2 and NOx emissions respectively, for the enhanced approach and the conventional approach to trajectory optimisation. The total H_2O emission is presented in Fig. 6.11. The time optimised trajectories generate higher GHG emissions than the minimum fuel trajectories. The minimum time, icing optimised trajectory records the highest amount of emissions because of the high true air speed. Conversely, the minimum fuel, icing optimised trajectory has the lowest emissions because of its relatively low speed and high altitude operation. Fig. 6.28 and Fig. 6.13 present the total CO and HC emissions

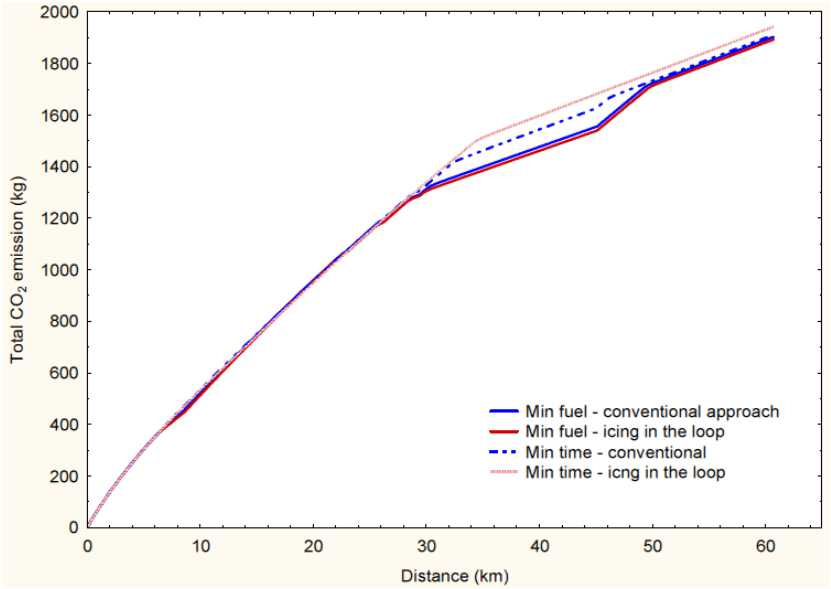

Fig. 6.9: Difference in the Total CO_2 Emission for the Two Approaches

respectively for the departure phase. The minimum fuel, icing optimised trajectory generated the highest CO and lowest HC emissions, whereas the minimum time, icing optimised trajectory generated the lowest CO and highest HC.

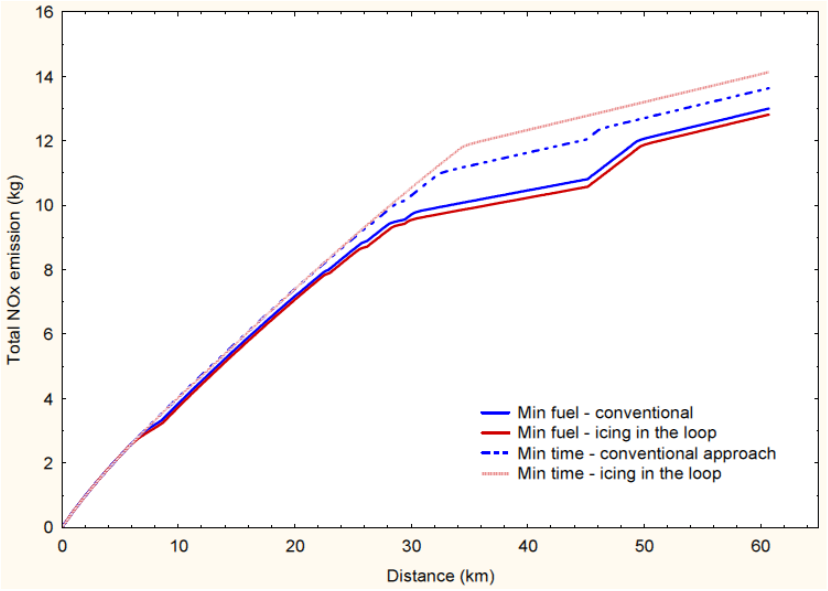

Fig. 6.10: Difference in the Total NOx Emission for the Two Approaches

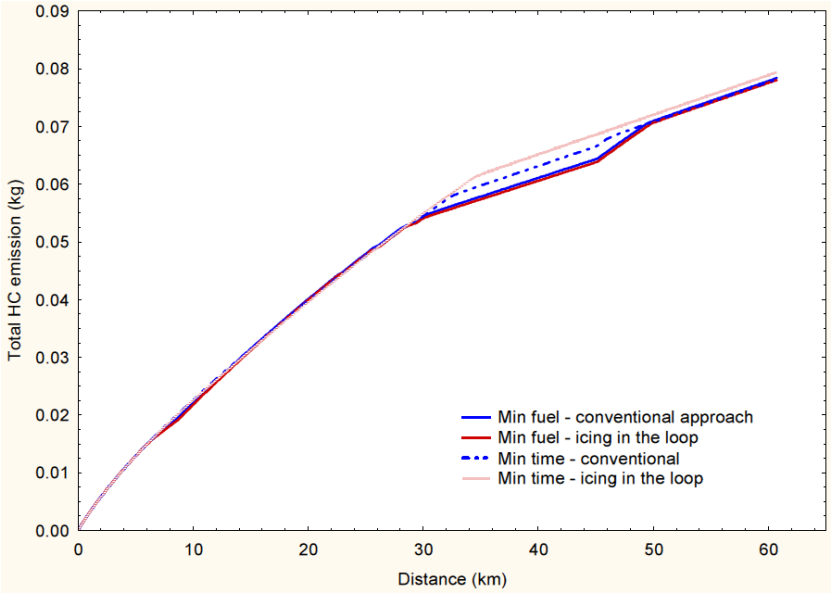

Fig. 6.13: Total HC Emissions for the Departure

Overall, it can be noted that there is more GHG savings in the enhanced approach than in the conventional approach which shows that there are environmental benefits in flying performance based trajectories when operating in known icing conditions. The

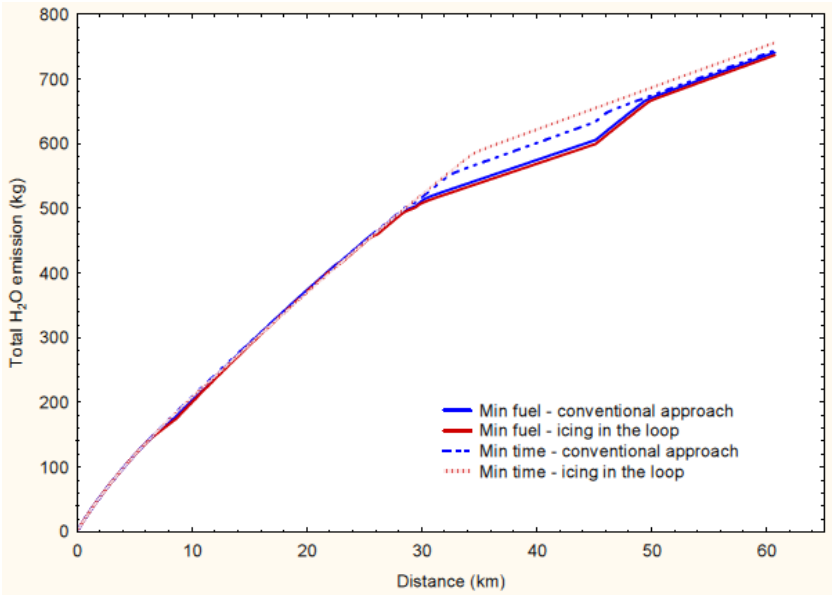

Fig. 6.11: Difference in the Total H_2O Emissions for the Departure Case

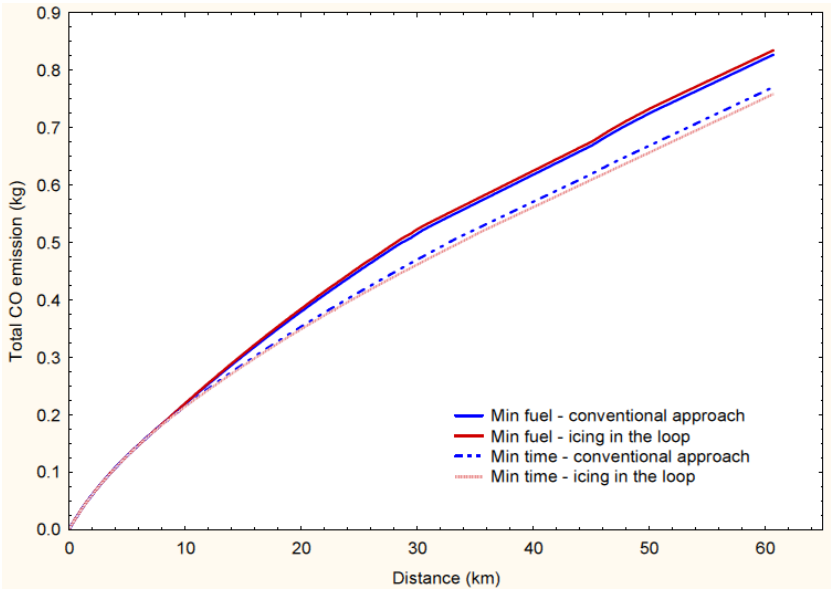

Fig. 6.12: Total CO Emissions for the Departure

Table 6.3: Summary of the Departure Optimisation Results

Trajectory definition	**Fuel burn (kg)**	**Flight time (s)**	**Impacts due to icing**	**Fuel savings due to strategy**
Fuel optimised without IPS	608	413	-	-
Fuel optimised with IPS penalty added	629	413	3.5%	-
Fuel optimised with icing in the loop	595	416	-	2.0%
Time optimised without IPS	619	374	-	-
Time optimised with IPS penalty added	612	374	1.1%	-
Time optimised with icing in the loop	609	371	-	0.5%

summary of the departure optimisation results are as shown on Table 6.3.

The overall result indicates a 1.1% savings on the fuel penalty due to IPS operation. Although the difference for a single flight segment is small and power off-take due to icing is small. However, considering that 83,000 departures [155] that take place globally every day and the appreciable number of these that encounter icing conditions, the combined effect of the global fleet is significant. Similarly, considering flights in non-standard icing condition for example of the extent of 200 nm; the relevance of this approach to ACARE objectives is apparent.

6.2.4 En-route Case

En-route phase starts after the aircraft has reached BPK SID and ends when the aircraft enters the Amsterdam Schiphol STAR procedure. During this phase a minimum altitude of FL100 and a maximum of FL390 were maintained. These bounds give the optimiser the freedom to choose an optimum flight level within both lower and upper airspaces.

The en-route way points are shown in Table 6.4.

Table 6.4: Enroute Phase

WP	**Latitude**	**Longitude**	**Altitude(ft) min/max**	**CAS(kt) min/max**
BPK	51 44 59.00 N	000 06 24.00 W	10,000	310
WP2	51 46 30.00 N	000 11 48.00 E	10,000/39,000	310/400
WP3	51 46 45.00 N	000 15 00.00 E	10,000/39,000	310/400
WP4	51 48 40.00 N	000 39 06.00 E	10,000/39,000	310/400
WP5	51 49 19.00 N	000 47 39.00 E	10,000/39,000	310/400
WP6	51 50 55.00 N	001 08 51.00 E	10,000/39,000	310/400
WP7	51 54 19.00 N	001 25 33.00 E	10,000/39,000	310/400
WP8	52 06 52.51 N	002 29 16.61 E	10,000/39,000	310/400
WP9	52 26 52.00 N	003 25 15.00 E	10,000/39,000	310/400
SUGOL	52 31 31.00 N	003 58 02.00 E	10,000	310

The minimum fuel and minimum time trajectories obtained from the two approaches are compared in Fig. 6.14. There is distinct difference between the fuel optimised trajectories whereas the time optimised trajectories are identical. This is because the fuel penalty due to IPS operation is not significant enough to change the trajectory when the setup is optimised for time. But when the objective is to fly with the minimum fuel burn, the effect of the systems are significant. The aircraft flew at a low altitude in the conventional approach than in the icing optimised trajectory. Obviously, the aircraft was made to fly at a higher altitude, simply due to the influence of the icing conditions which forms part of the optimiser search criteria. In search of points of low fuel consumption, the optimiser naturally selects the up higher altitude points within the simulation set up; a choice that is not available in the conventional optimisation set

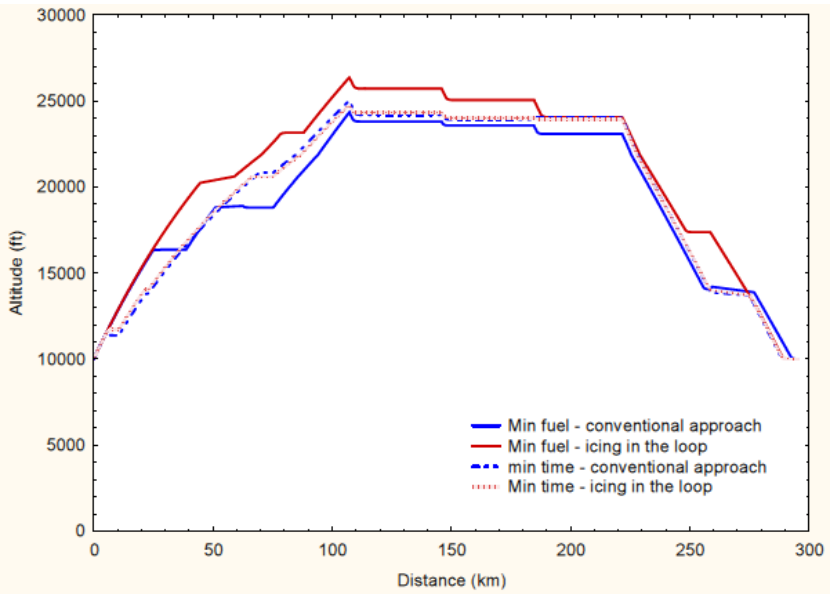

Fig. 6.14: Enroute Trajectories Comparison

up. The time optimised trajectories are similar and close to one another because the objective is not fuel burn but arrival time. Despite this fact, there are level of difference in the two profiles which can only be explained by looking at their true air speeds. The different trajectory profiles mean different aircraft performances. Consequently, further aircraft parameters are investigated in the following discussions. Fig. 6.15 shows the speed variation with distance.

The minimum time results are almost identical as expected and the overall airspeed is higher than in minimum fuel results because the optimiser tries to let the aircraft reach the final condition in the minimum time possible. On the other hand, the minimum fuel results have different values of airspeed because the optimiser finds the value of airspeed which reduces the overall fuel burn. True air speed is linked to the aircraft operating altitude. It is not surprising therefore that the speed profiles for time optimised trajectories are also close for both set ups, hence, the throttle setting for these cases is plotted in Fig. 6.16. to better understand where they differ and how. The throttle settings for

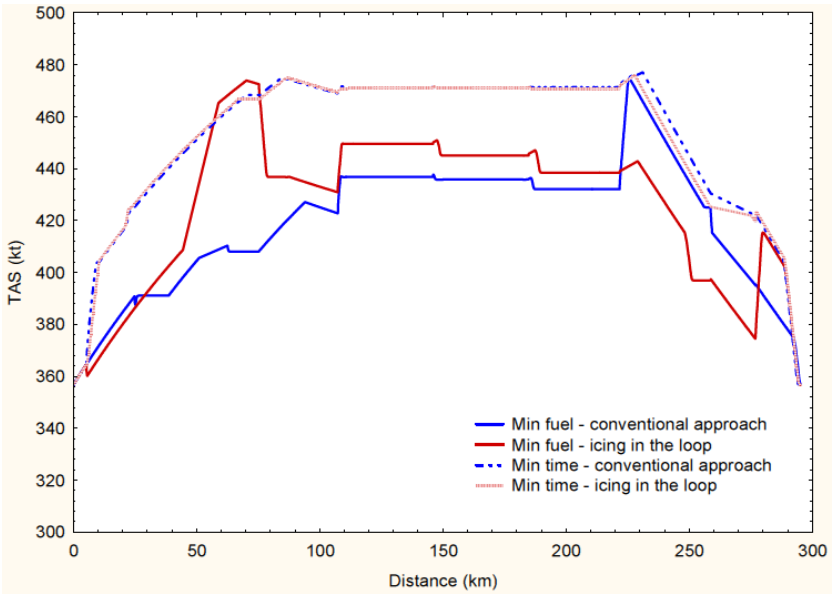

Fig. 6.15: TAS Comparison for Enroute Case

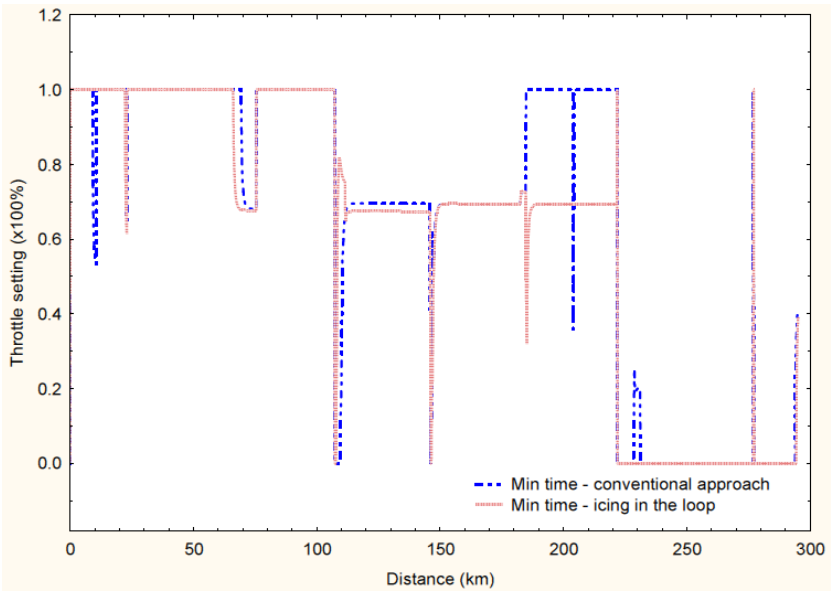

Fig. 6.16: Throttle Setting for Enroute Case

the two set-ups differ for the identical time optimised trajectories. Fig. 6.17 shows the response of the fuel flow to the two engines based on the different set-ups. The optimiser settings are set equal for both approaches. The effect created due to aircraft systems off-takes is proportional to the bleed power requirement as can be seen in Fig. 6.18.

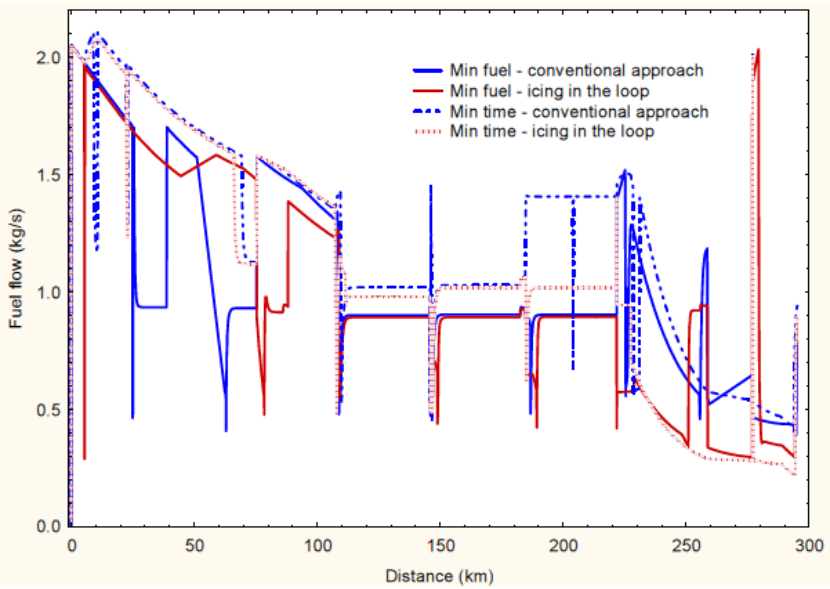

Fig. 6.17: Fuel Flow vs Distance

Fig. 6.17 shows the variations of fuel flow to the engines in the cruise phase. The results show an entwined trend, and it is therefore difficult to say which one is higher than the other. This happens because there are many parameters influencing fuel flow to the engine. In addition to IPS and ECS, there is the power and throttle setting, control surfaces, in-flight intertaiment system, etc. However, looking at Fig. 6.18, it can be noticed that the conventionally generated trajectories resulted in higher bleed off-takes than in icing optimised trajectories.

The en-route results of the GHG emissions are shown in Figures 6.19 to 6.23. In Fig. 6.19, 6.20 and 6.21 which show CO_2, NOx and H_2O emissions respectively, the conventionally time optimised trajectories have consistently topped the emission chart. Similarly, the minimum fuel - icing in the loop trajectories have consistently shown the least emission values. This could be due to the fact that these pollutants are products of complete combustion. This suggests that, GHG emissions could be reduced through

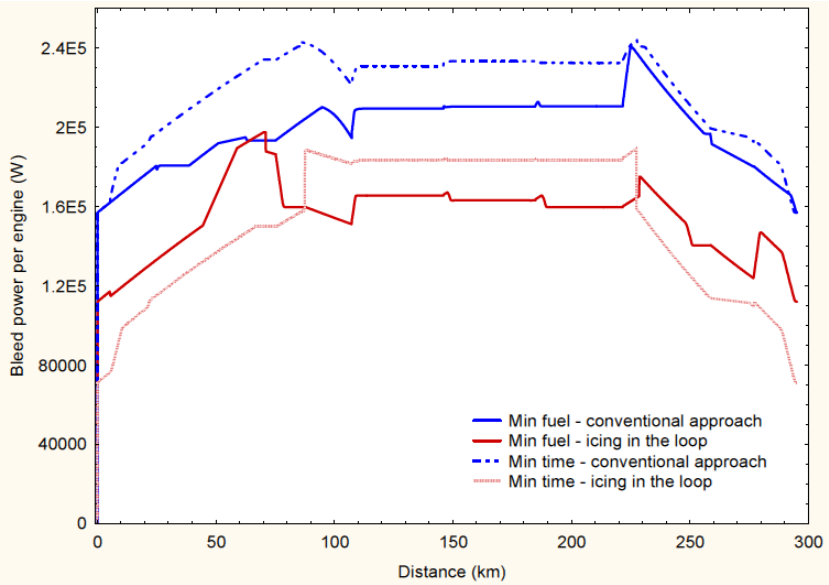

Fig. 6.18: Bleed Power Comaprison for Enroute Phase for Enroute

trajectory based operations. Literature shows that CO and HC are products of incomplete combustion, hence they are likely to be more influenced by engine efficiency. Results of CO and HC emissions in the en-route phase are shown in Fig. 6.22 and 6.23 respectively.

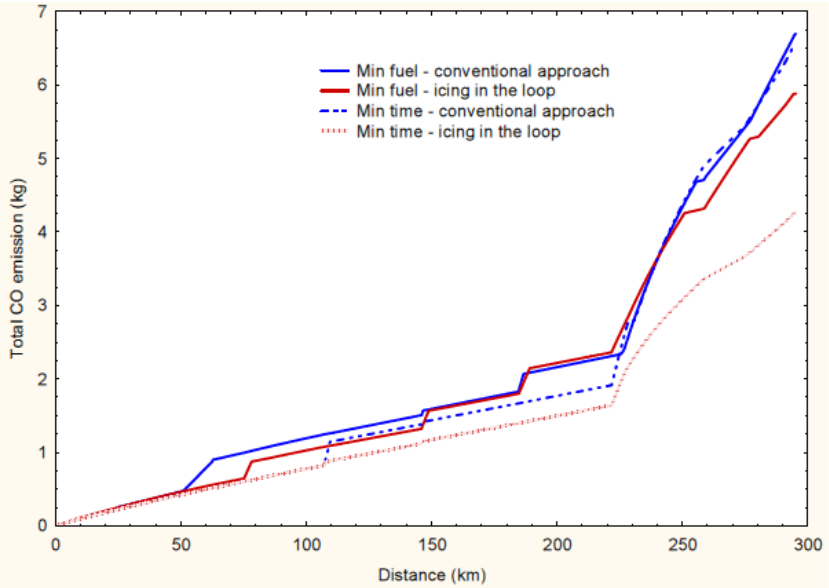

Fig. 6.22: CO Emissions Comparison for the Enroute Case

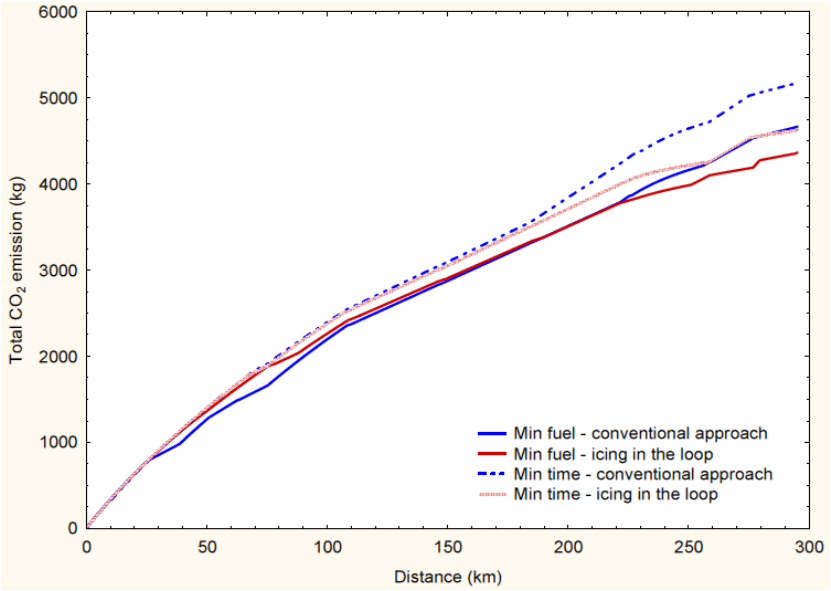

Fig. 6.19: CO_2 Comparison for the Enroute Case

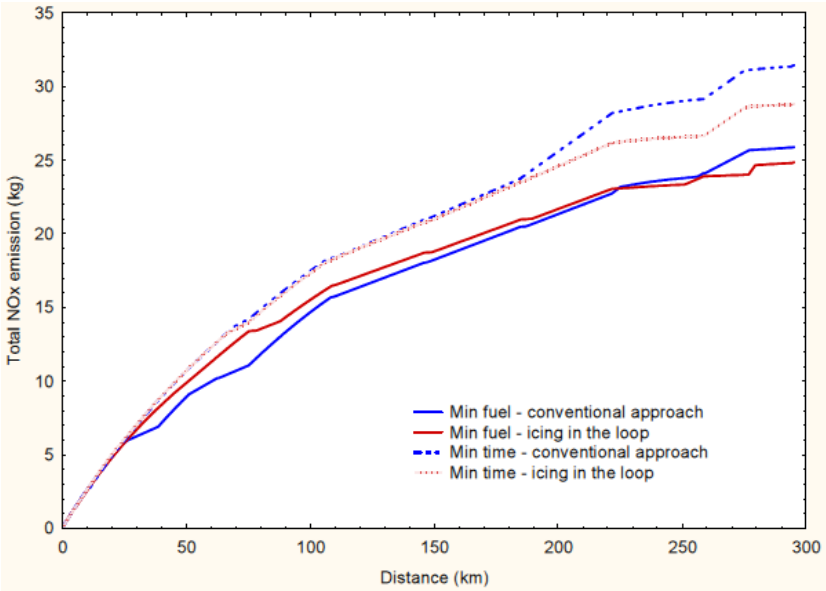

Fig. 6.20: NOx Comparison for the Enroute Case

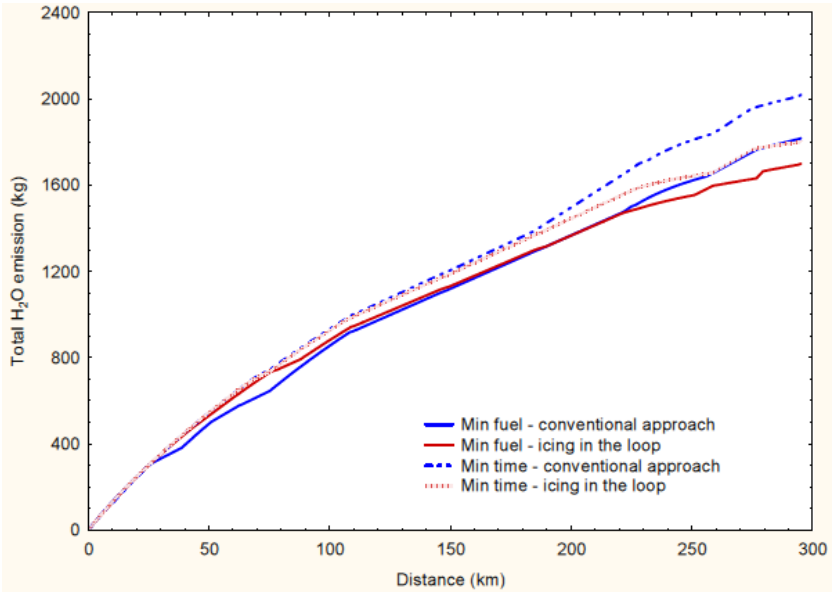

Fig. 6.21: Total H_2O Emissions Comparison for Enroute Case

H

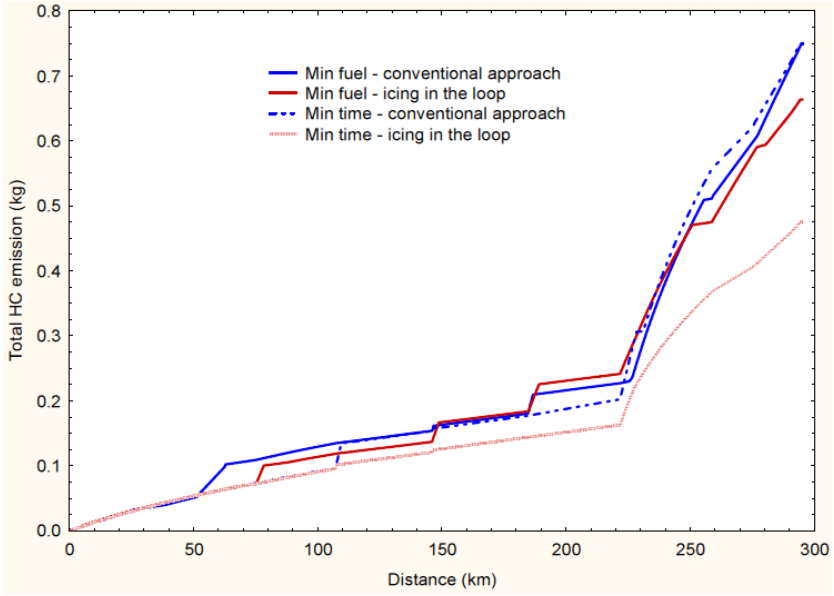

Fig. 6.23: HC Emissions Comparison for the Enroute Case

It can be noted that in contrast to the complete combustion products, the minimum time and minimum fuel trajectories are identical in the remaining gases. The results show that there are significant savings in CO and HC emission if icing conditions are accounted for in the optimisation settings. The overall en-route result is summarised in Table 6.5.

Table 6.5: Summary of the En-route Optimisation Results

Trajectory definition	**Fuel (kg)**	**Time (s)**	**Impacts due to icing**	**Fuel savings due to strategy**
Fuel optimised without IPS	1343	1376	-	-
Fuel optimised with IPS penalty added	1393	1376	3.7%	-
Fuel optimised with icing in the loop	1373	1378	-	1.5%
Time optimised without IPS	1465	1275	-	-
Time optimised with IPS penalty added	1554	1276	5.7%	-
Time optimised with icing in the loop	1469	1275	-	5.5%

The results show that there are benefits in including the icing conditions in the optimisation set up for flights in known icing conditions. Up to to 5.5% of fuel saving can be achieved by considering the icing conditions in the optimisation set up relative to non-icing optimised trajectories for operations in the presence of icing conditions.

6.2.5 Arrival Case

The arrival phase starts when the aircraft passes over SUGOL and terminates at the threshold of Runway 06. The STAR used in this phase for Amsterdam Schiphol airport is RNAV-Night RWY06 (see Appendix B) and the entry altitude is set to FL70. The route and the related parameters for the arrival phase are listed in Table 6.6.

Table 6.6: Arrival Phase

WP	**Latitude**	**Longitude**	**Altitude(ft) min/max**	**CAS(kt) min/max**
SUGOL	52 31 31.00 N	003 58 02.00 E	10,000	310
WP2	52 25 20.00 N	004 23 16.00 E	0/10,000	140/310
WP3	52 14 14.00 N	004 21 51.00 E	0/10,000	140/310
WP4	52 12 33.00 N	004 27 45.00 E	0/10,000	140/310
WP5	52 12 28.00 N	004 31 35.00 E	0/10,000	140/310
WP6	52 17 20.00 N	004 44 14.00 E	0	140

The optimised trajectories for the arrival case are presented in Fig. 6.24. The minimum fuel trajectory for icing in the loop simulation occupies the lower boundary of the altitude band and the conventional optimised minimum time trajectory occupies the upper boundary. Fig. 6.25 shows the speed profiles for the trajectories. While the minimum fuel trajectories decelerated rapidly, the minimum time trajectories show very little deceleration. Thus, the minimum time trajectories resulted in higher GHG emissions as can be seen in Fig. 6.26, Fig. 6.27 and Fig. 6.30 In each case, the minimum fuel trajectories generate less CO_2, NOx and H_2O emissions than the minimum time trajectories. This is because there is a direct relationship between the amount of fuel burnt and CO_2 and H_2O emissions. Fig. 6.27 shows similar trend for the NOx emission

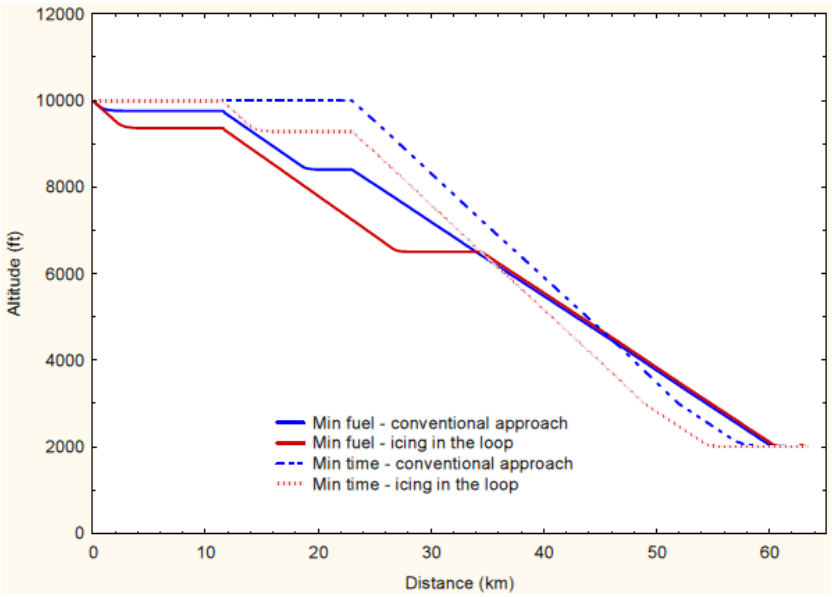

Fig. 6.24: Optimised Trajectories for the Arrival Case

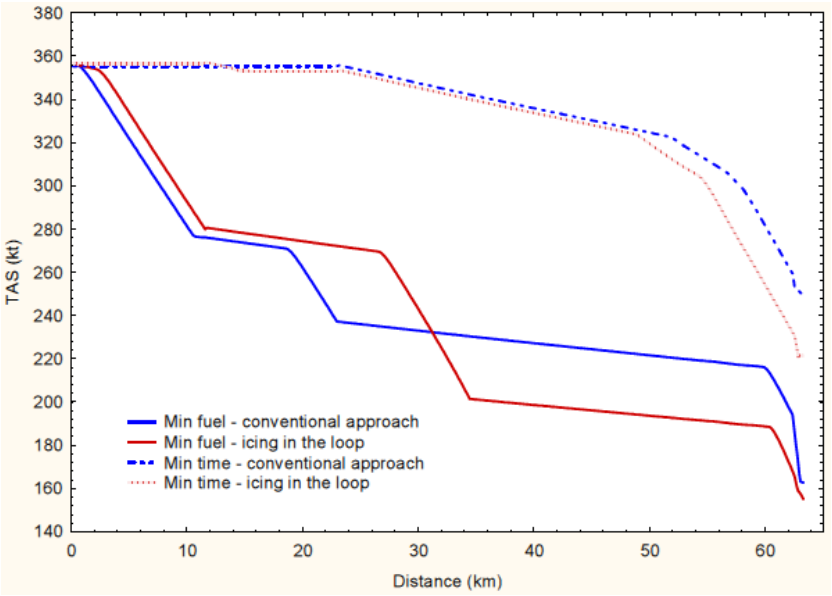

Fig. 6.25: TAS Comparison

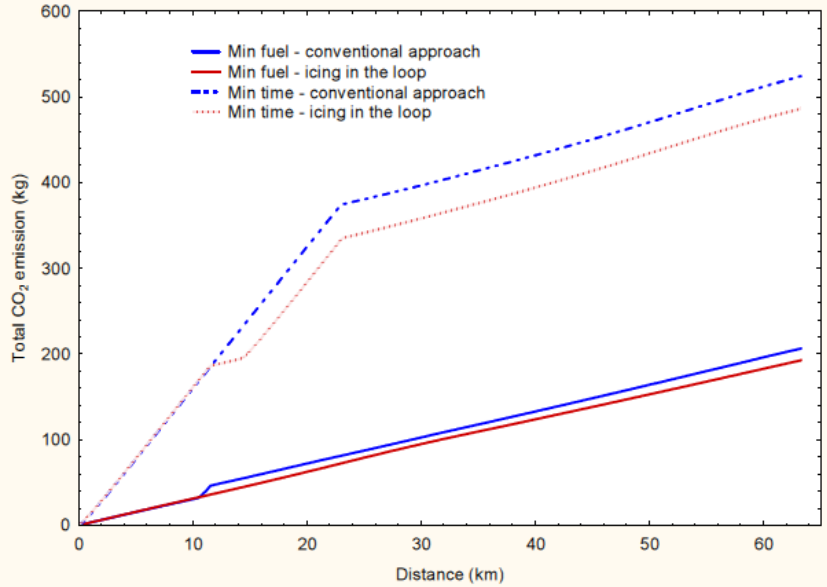

Fig. 6.26: Total CO_2 Emission for the Arrival Case

because the combustion chamber temperature has a link to the amount of fuel burn.

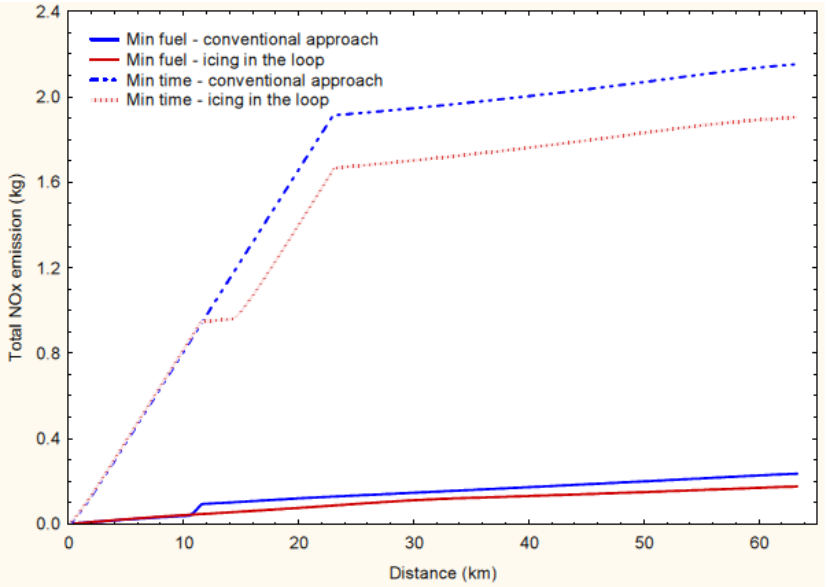

Fig. 6.27: Total NOx Emission for the Arrival Case

In Fig. 6.28 and Fig. 6.29 however, the results indicated that the respective CO and HC emissions are marginally higher in icing optimised trajectories. This is due to the fact that while the aircraft is accelarating through the departure and maintaining speed

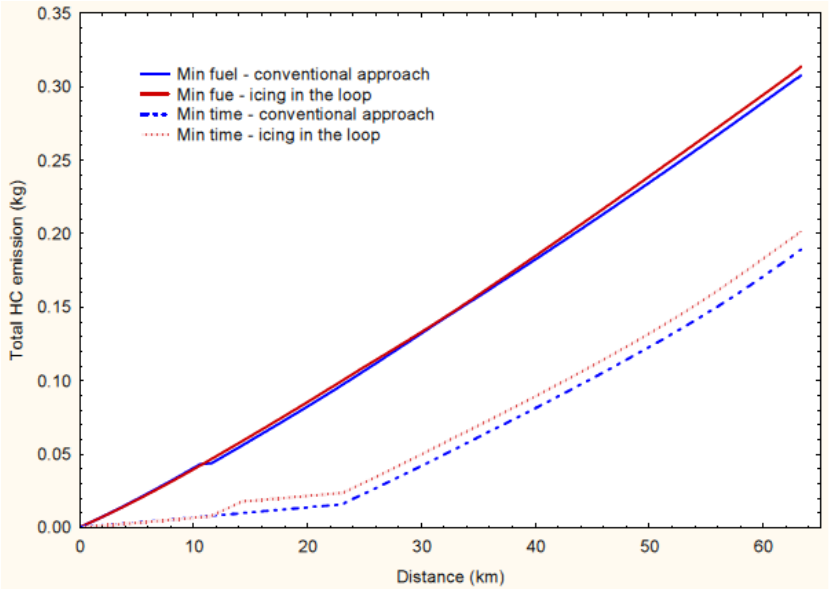

Fig. 6.29: Arrival Segment Total HC Emission

in cruise, it is decelerating in arrival; a totally different throttle setting. In any case, the emissions difference is not critical as it is only 0.4% higher as against the advantage 16% gained in departure and cruise.

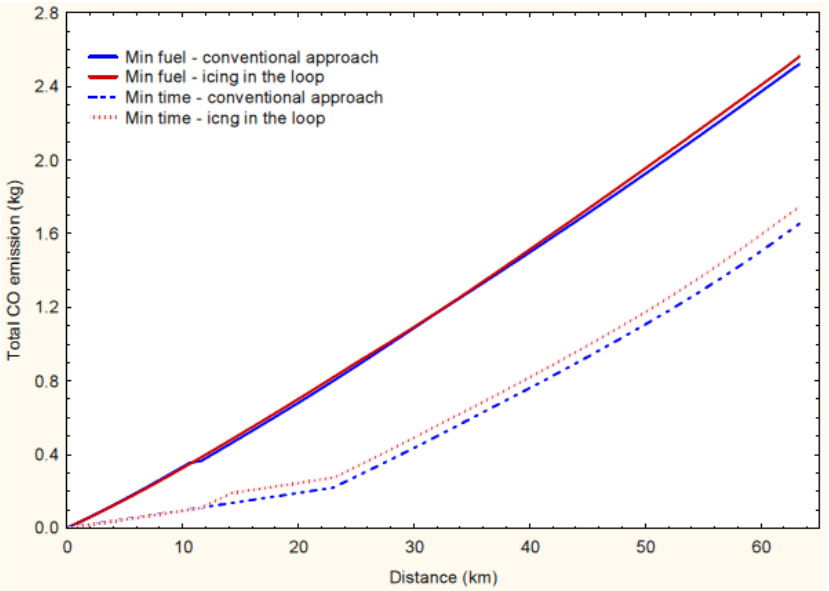

Fig. 6.28: Total CO Emission for the Arrival Case

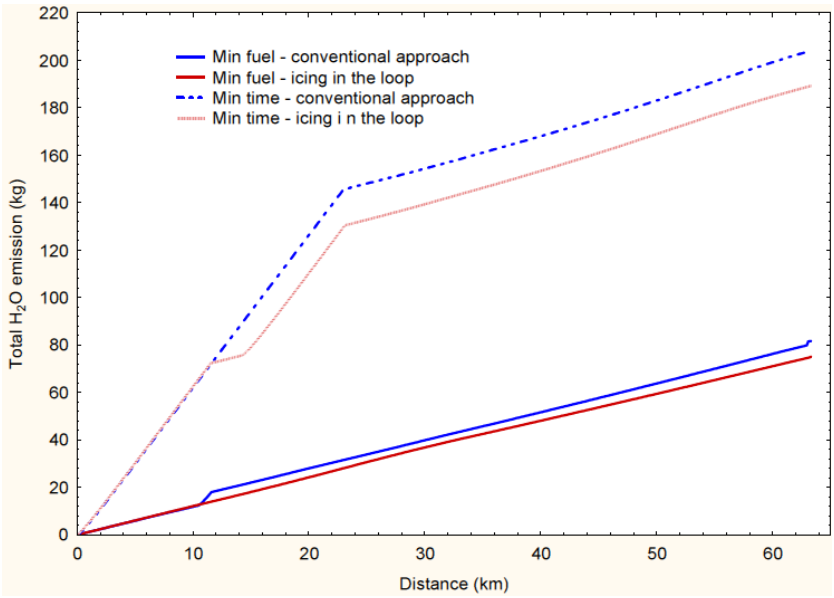

Fig. 6.30: Arrival Segment Total H_2O Emission

The overall arrival result is summarised in Table 6.7. There is more fuel savings using

Table 6.7: Summary of the Arrival Results

Trajectory definition	**Fuel burn (kg)**	**Flight time(s)**	**Impacts due to icing**	**Fuel savings due to strategy**
Fuel optimised without IPS	59.2	507	-	-
Fuel optimised with IPS penalty added	65.8	507	11.1%	-
Fuel optimised with icing in the loop	61.1	532.5	-	7.7%
Time optimised without IPS	151.4	367.9	-	-
Time optimised with IPS penalty added	167.5	367.9	10.6%	-
Time optimised with icing in the loop	156.9	375	-	6.8%

icing optimised trajectories during arrival than any other flight segment. This is becasuse, the fuel penalty due to icing is dependant on both the icing requirement as well as the corresponding throttle setting at those conditions. High icing power requirements

in lower throttle settings are more demanding than high icing requirements in lower throttle settings. Fuel penalty due to IPS operation can get up to 11% during arrival as shown in Table 6.7.

6.3 Comparison with a Typical Mission Profile for the Mission Route

The minimum fuel and minimum time trajectories for Case 3 were compared with a typical trajectory flown by commercial aircraft from EGLL/LHR to Amsterdam Airport Schiphol EHAM/AMS as shown in Fig. 6.1. It can be seen in Fig. 6.31. The minimum time trajectory was very close to the typical trajectory of the commercial aircraft. One of the lessons learnt from this result is that the typical aircraft finishes climb earlier than the simulated baseline aircraft. This could be associated with ATM operational requirement at LHR.

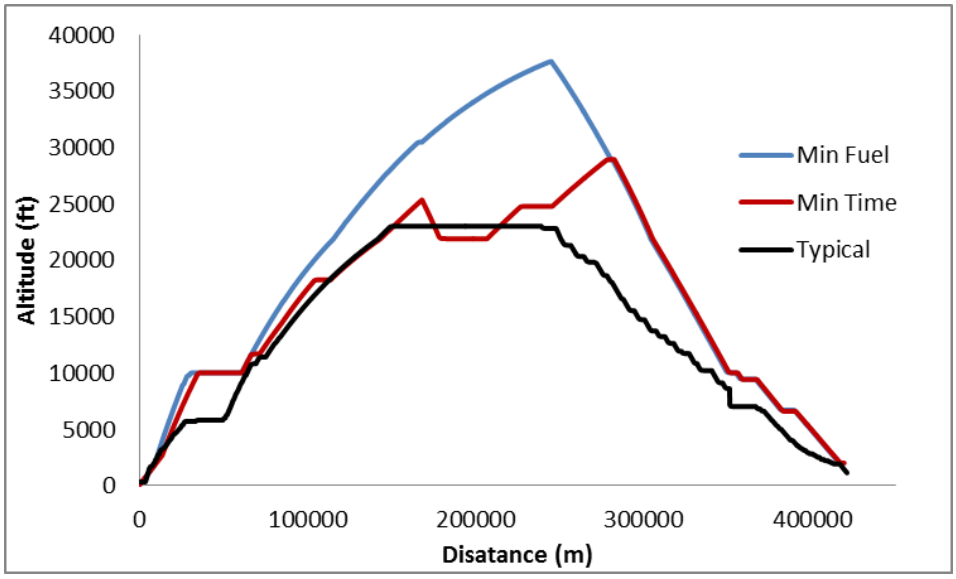

Fig. 6.31: Comparison of a Typical Airline Trajectory with Optimised Trajectories for Icing Encounter

Fig. 6.32 shows the speed variation with distance. As usual, the minimum fuel trajectory has lower speed profile than minimum time and typical trajectories. Because of this difference in speed profile, the fuel flow requirement was investigated.

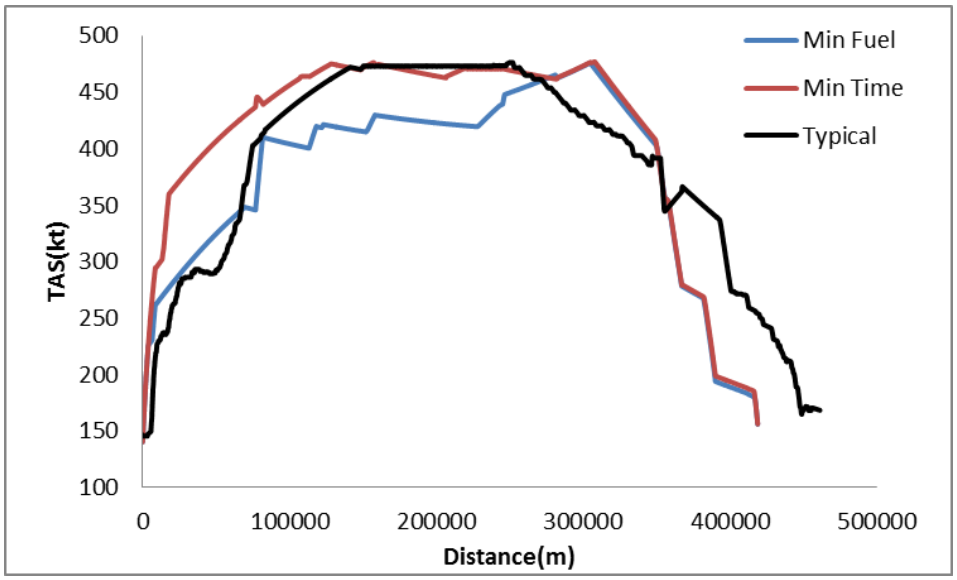

Fig. 6.32: TAS Comparison

Theoretically, IPS power demand is a function of air speed and altitude. Hence it can be seen that 200 km from LHR, the IPS was autonomously operated with rest to the minimum time trajectory. Fig. 6.33 shows bleed flow due to IPS comparison. Fig. 6.34 shows how the fuel flow to the engine based on the trajectory choice affect aircraft mass. Although, the initial mass of the aircraft in the typical trajectory is not known, same condition has been applied to it as the study case for ease of comparison. The result is as expected with minimum fuel trajectory having lower fuel flow requirement as the minimum time or the low altitude typical trajectory. In can be noted in Fig. 6.34 that min fuel trajectory saves more fuel (10.3%) than the typical and min time trajectory. This is because the min time trajectory is achieved through higher TAS as can be seen in Fig. 6.32. Although the typical trajectory is at similar TAS with the minimum fuel trajectory, it is at a lower altitude where air drag is highest.

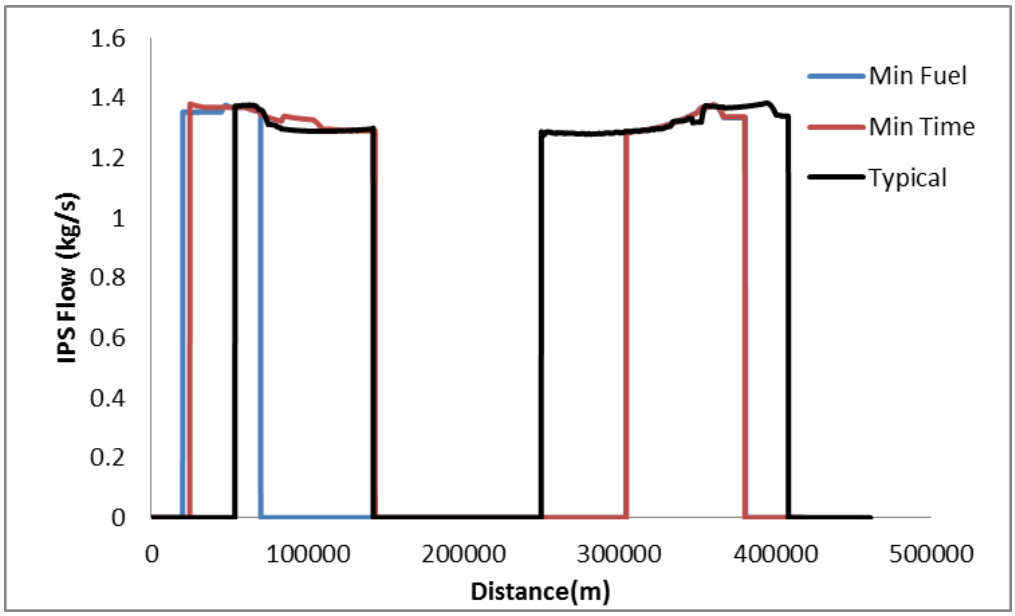

Fig. 6.33: Bleed Flow due to IPS Comparison

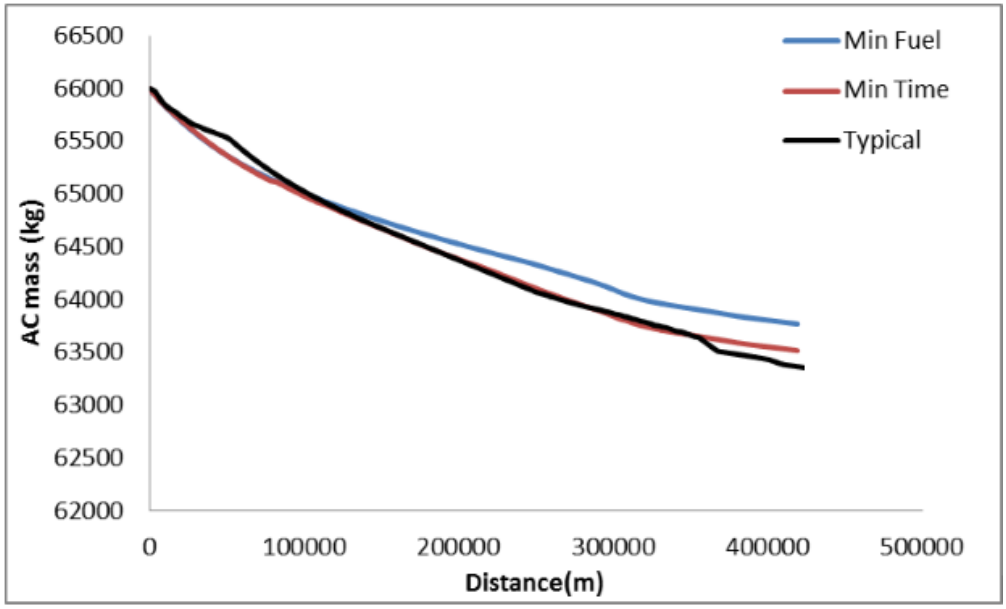

Fig. 6.34: Fuel Consumption Comparison

Commercial aircraft mission profile depends solely on the route, operator and aircraft type and sometimes weather interference. However, it can be noted from the solution of the GATAC trajectory optimisation that there are fuel savings and environmental benefits in flying icing optimised routes in comparison to a typical flight route between LHR to EGLL. Both British Airways and KLM airlines fly the route between 22,000 ft and 25,000 ft. Meanwhile, the most economic flight profile obtained from the GATAC optimization is a steady climb from LHR to 37,000 ft and cruising for about 5 minutes before gradual descent to EGLL. Considering the similarity of minimum time trajectory with the typical trajectory, the persistence of using lower altitudes by the regular operators of the route could be attributed to the flight schedule requirement. ATM constraints are also likely to be a factor.

6.4 3D Optimisations

6.4.1 Set up

The conditions for the 3D optimisation problem are shown on Table 6.8. The WP1 to WP9 are way points for the nominal trajectory (subject of optimisation). The artificial icing cloud was set between 12,000 ft to 18,500 ft. The 3D graphical reprentation of the 3D Pareto carpet plot shown in Fig. 6.40 represents the simulation based on the Table 6.8 set-up. The parametric variables in this case are CO_2, NOx and water vapour emissions; each as a function of fuel burn versus flight time optimisation. Fig. 6.40 (a), (b) and (c) show the impact of fuel burn vs flight time optimisation on CO_2, NOx and water vapour emissions. It can be seen that the emission trend is similar - even though the gradient is not same. This is because the threesome are products of same chemical

Table 6.8: 3D Extended Departure Route - Inputs to Optimiser

WP	**Latitude**	**Longitude**	**Altitude(ft) min/max**	**CAS(kt) min/max**
WP1	51 27 53.25 N	000 28 54.99 W	83	140
WP2	51 27 52.51 N	000 31 35.75 W	83/23,000	140/340
WP3	51 31 08.00 N	000 40 38.00 W	83/23,000	140/340
WP4	51 35 07.13 N	000 36 29.69 W	83/23,000	140/340
WP5	51 37 23.00 N	000 31 07.00 W	83/23,000	140/340
WP6	51 44 59.00 N	000 06 24.00 W	83/23,000	140/340
WP7	51 46 30.00 N	000 11 48.00 E	83/23,000	140/340
WP8	51 48 40.00 N	000 39 06.00 E	83/23,000	140/340
WP9	51 49 19.00 N	000 47 39.00 E	83/23,000	340

reaction which is the complete combustion of hydrocarbon in air.

As the focus is on fuel burn and emission reduction, the 3D minimum fuel trajectory was compared with the 2D minimum fuel trajectory referred to the reference trajectory. The graphical projections of the ground tracks generated by the simulation of the two cases are shown in Fig. 6.37. It can be observed that at the region of the in built artificial icing cloud, the optimiser selected different lateral track for the two cases. This suggests that lateral track has influence on fuel consumption as much as the vertical profile. Fig. 6.38 shows the two trajectories in a 3D format. The difference in the vertical and lateral tracking can clearly be seen. The 3D optimised trajectory climbs at a relatively steeper angle than the reference trajectory. The trajectories are projected in a real geographical space in Fig. 6.39 and Fig. 6.40. The graphs show how the aircraft climbs in relation to ground track. Fig. 6.41 shows how the aircraft climbs to 23,000 ft in icing conditions described above. The red rings represent the icing area, which is about 17.4 nm horizontally and 6,500 ft vertically. The aircraft in the reference trajectory accelerated from take-off to about 360 kt before maintaining a steady acceleration to the maximum cruise speed. In the 3D trajectory however, the aircraft accelerated at a rather lower

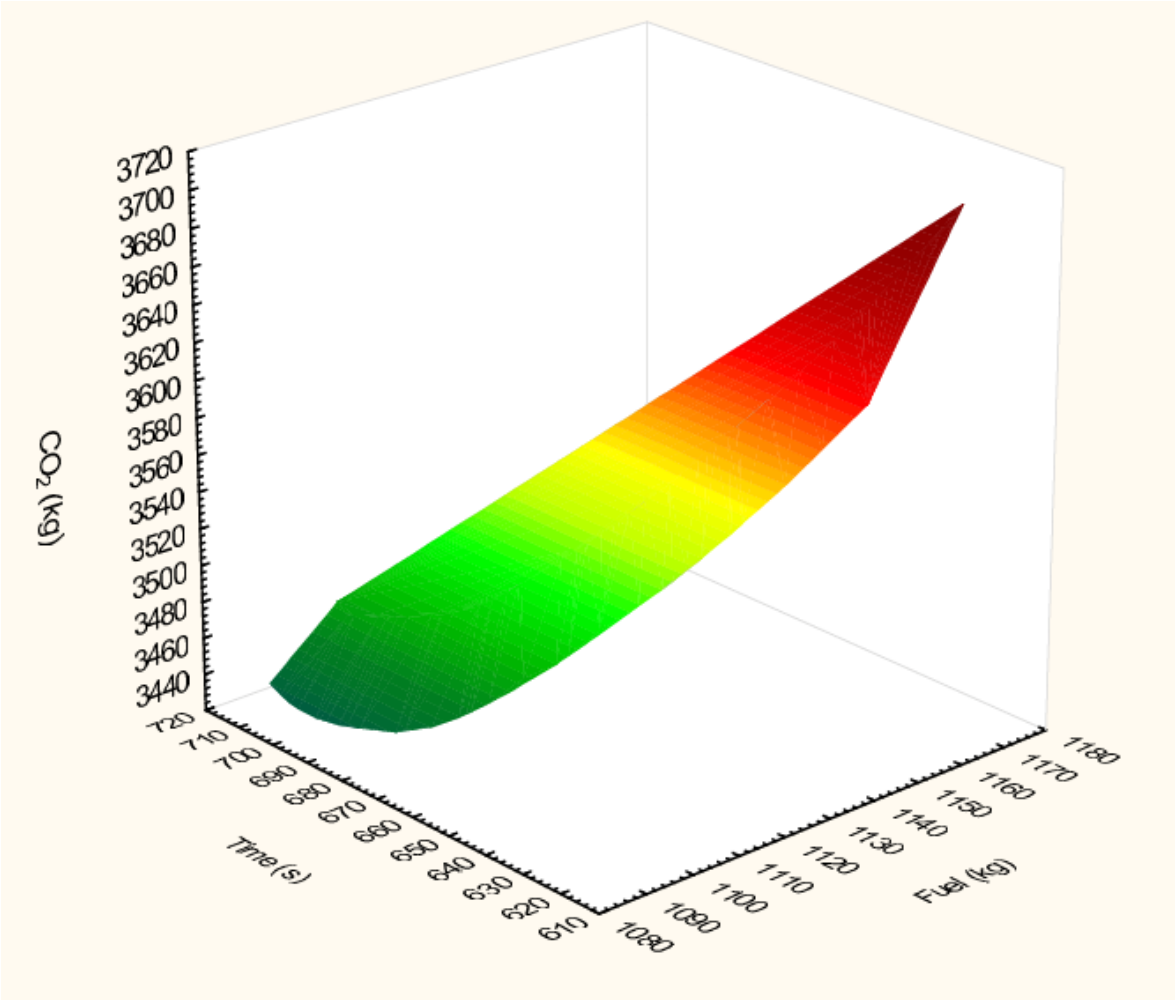

Fig. 6.35: 3D CO2 Pareto

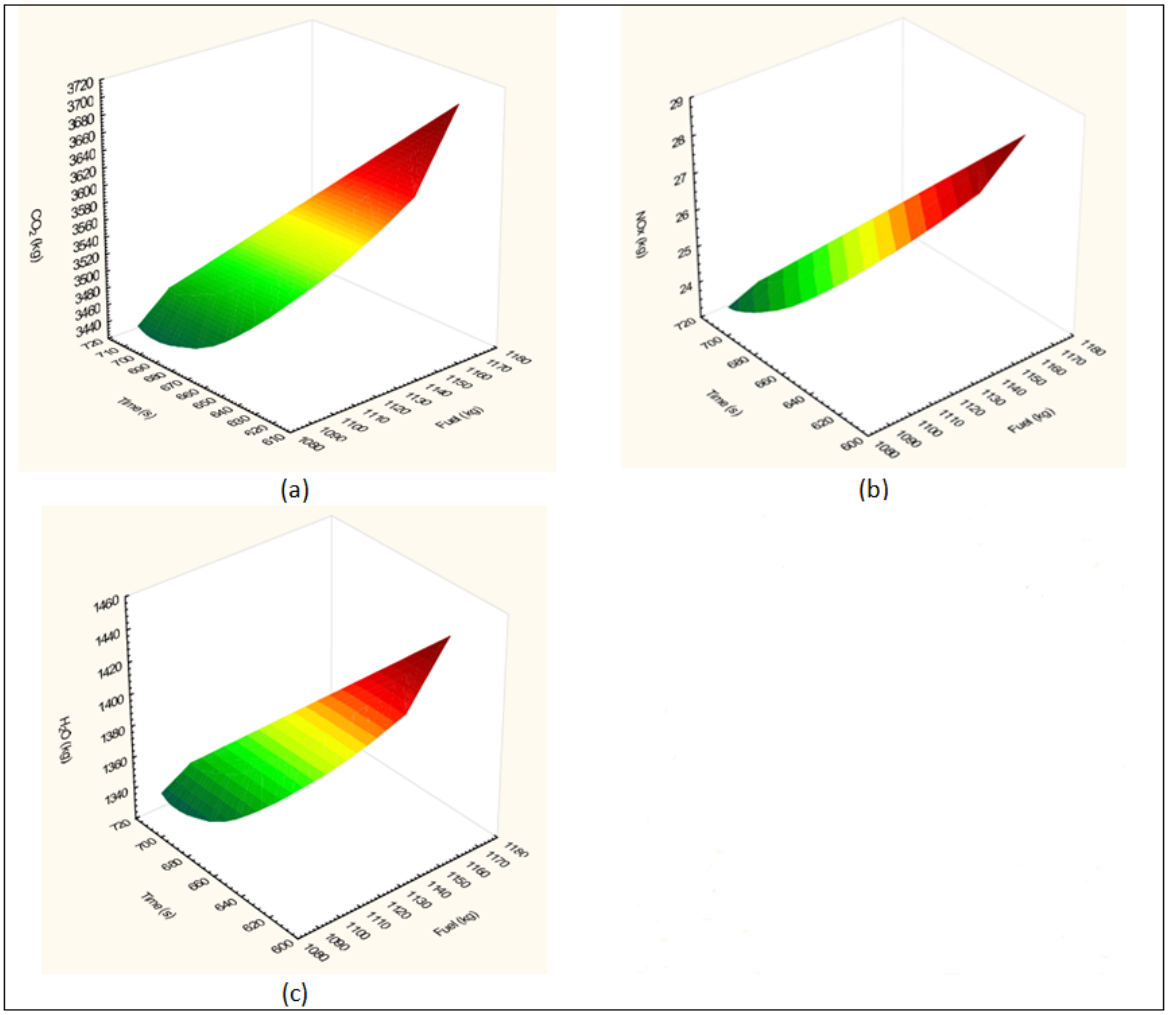

Fig. 6.36: 3D Solution of the Optimisation Case

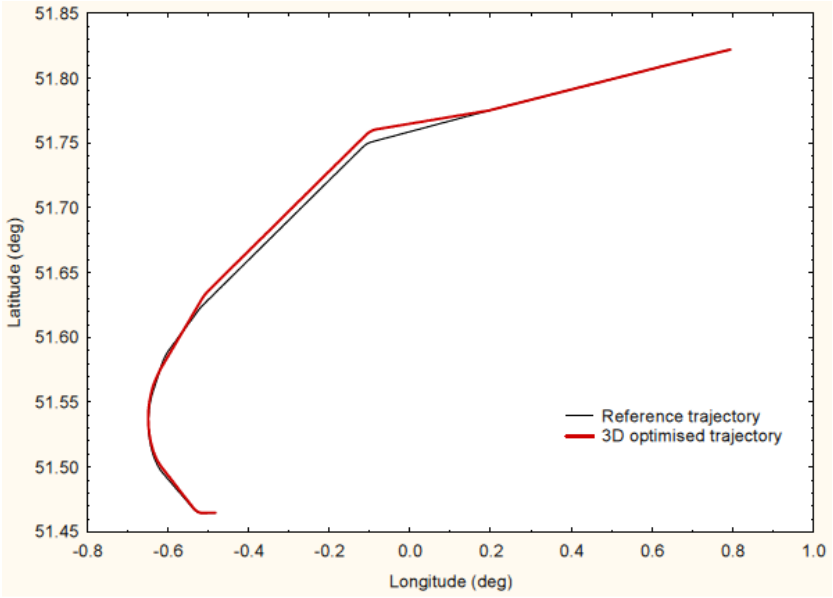

Fig. 6.37: Ground Track for the 3D Optimisation Case

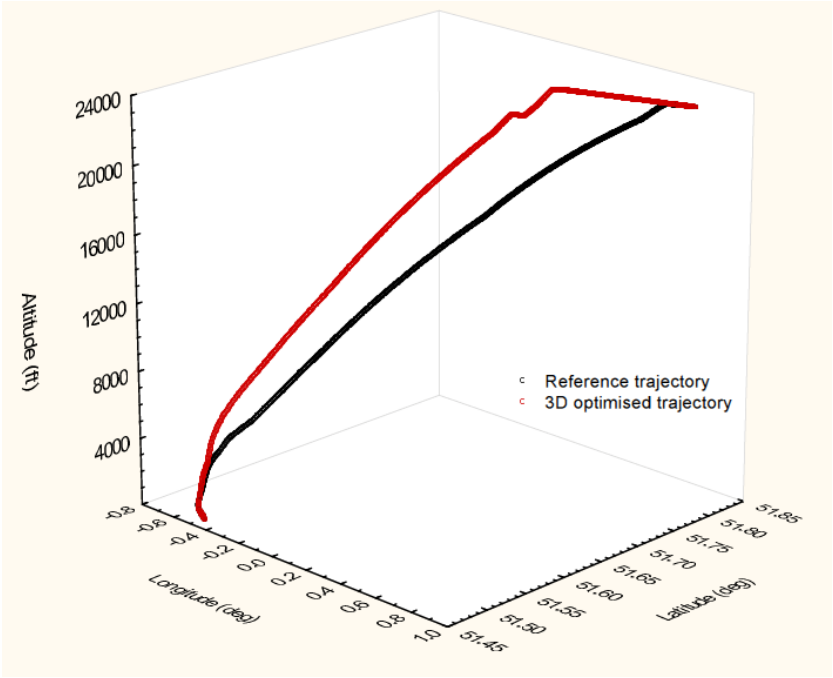

Fig. 6.38: 2D and 3D Trajectories Comparison

rate than in the reference trajectory. This is due the fact that the optimiser searches for minimum cost points in both the vertical and the lateral planes. This operational difference resulted in different bleed power demands as shown in Fig. 6.42.

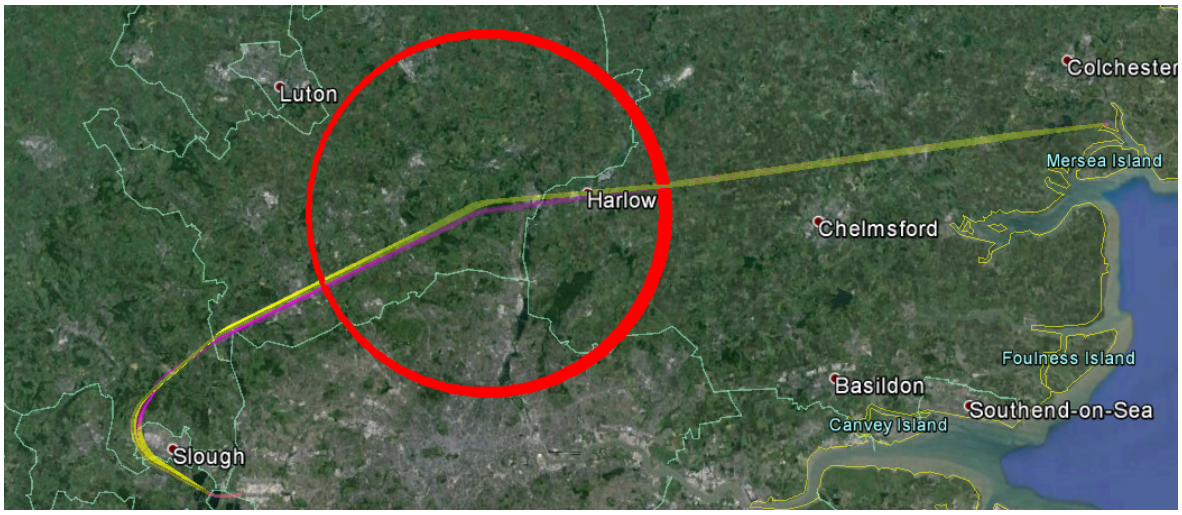

Fig. 6.39: The 2D and 3D Icing Optimised Trajectories Projected on the Air Space

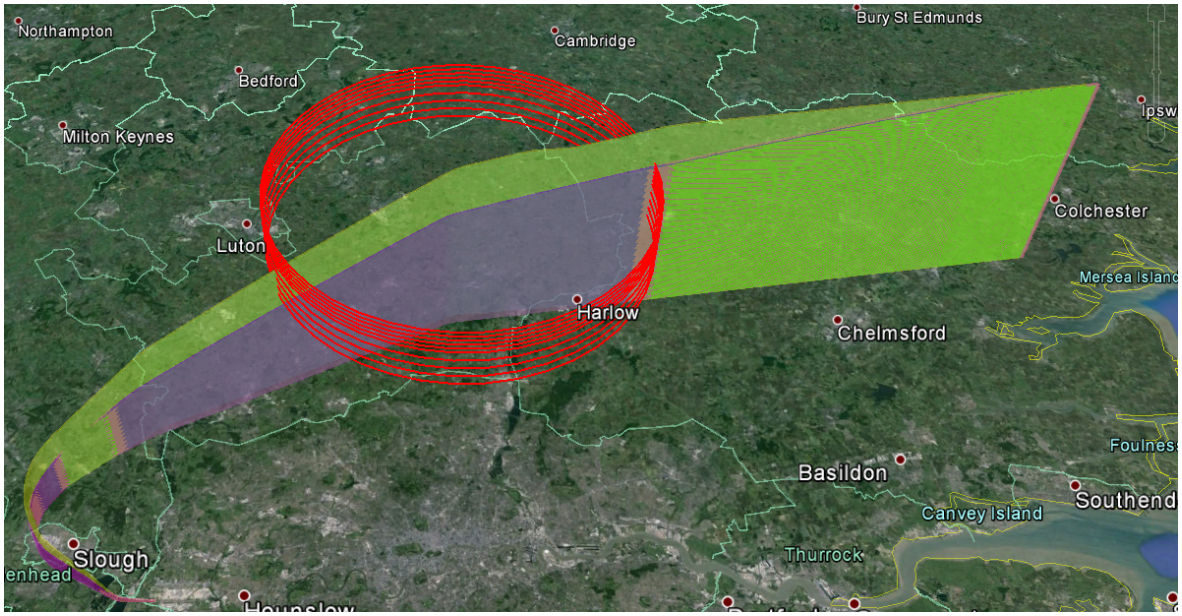

Fig. 6.40: A Zoom-in View of the 2D and 3D Icing Optimised Trajectories Projection on the Air Space

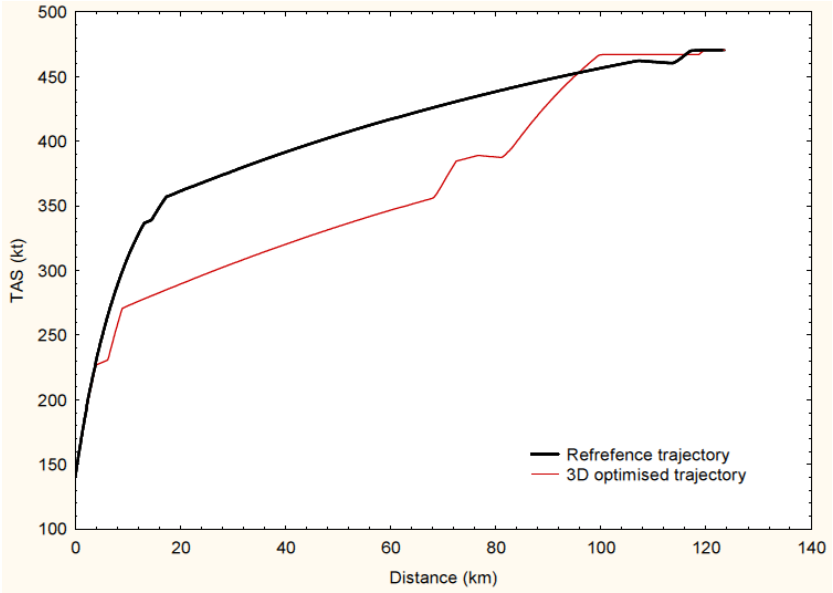

Fig. 6.41: True Air Speed 2D vs 3D Trajectories

The higher bleed power requirement related to the reference trajectory resulted in higher fuel flow rate as shown in 6.43. When translated into total fuel burn, the results show a fuel saving of about 6.3% can be achieved using the 3D optimised trajectory in relation to use of 2D optimised trajectory in an icing encounter. It can also be observed in Fig. 6.44 that as the range increases, the difference in terms of total fuel burn and associated emissions increase. The result show that 3D optimised trajectories saves more fuel consumption than the current 2D trajectories flown by commercial transport aircraft. This reduction will also reduce the GHG emissions due to air transport for reasons discussed in previous sections. It was established in the results presented earlier that fuel burn has a ripple effect on GHG emissions. The total CO_2, NOx and H_2O emissions are presented in Fig. 6.45, Fig. 6.46 and Fig. 6.47 respectively. In each case, the total emission generated by the reference trajectory outweighs that generated by the 3D optimised trajectory. This is expected because of the direct relationship between fuel burn and the primary greenhouse gases. It can however be noted in Fig. 6.48 that the

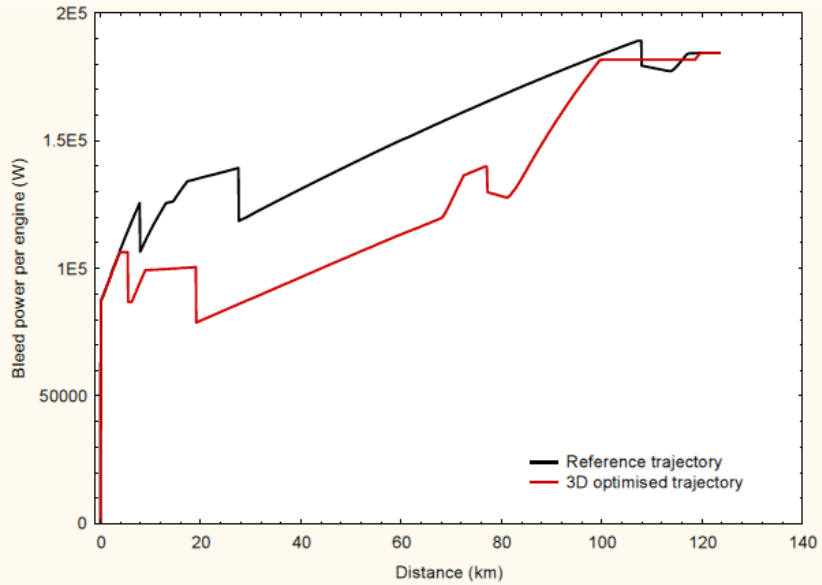

Fig. 6.42: Bleed Power Off-take per Engine Comparison: 3D Case

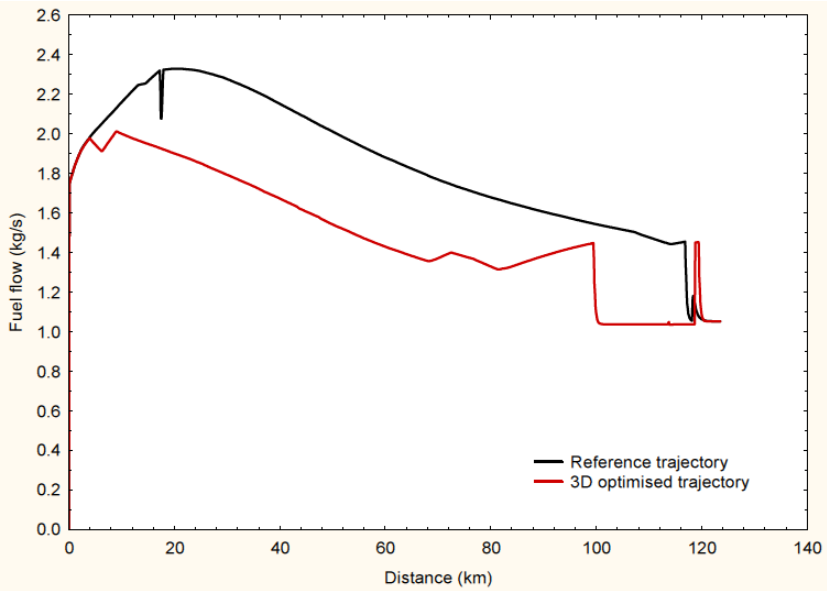

Fig. 6.43: Fuel Flow Comparison, 3D Case

3D optimised trajectory generated higher CO emission than the reference trajectory. This is possible due the unpredictability of incomplete combustion. Therefore, the CO result doe not affect the results of the primary greenhouse gas emissions. However, Fig. 6.49 shows that the reference trajectory generated more HC emission than the 3D

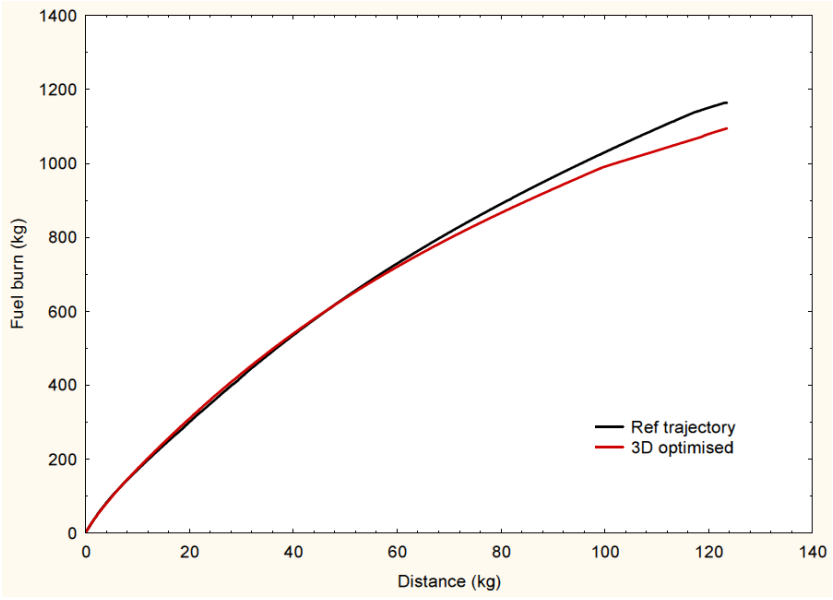

Fig. 6.44: Total Fuel Burn Comparison, 3D Case

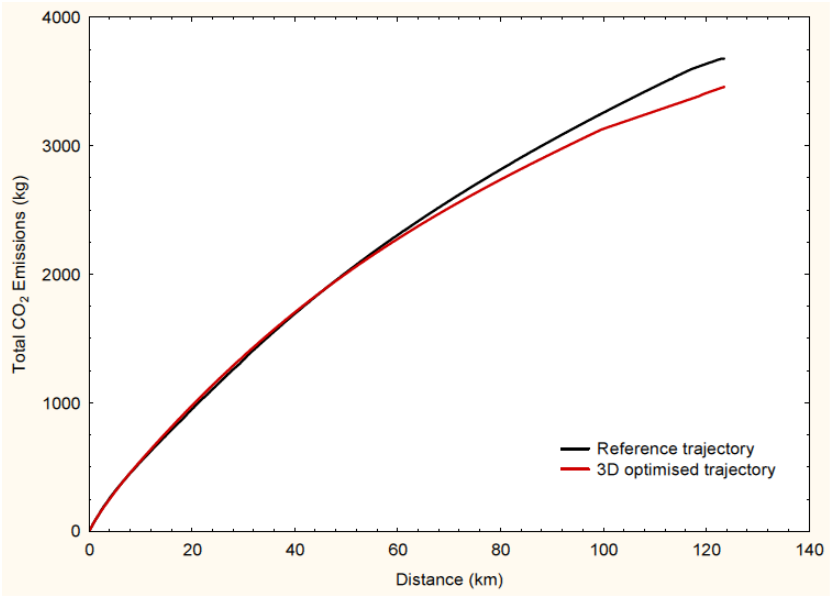

Fig. 6.45: Total CO_2 Emissions for the 3D Case

optimised trajectory as expected.

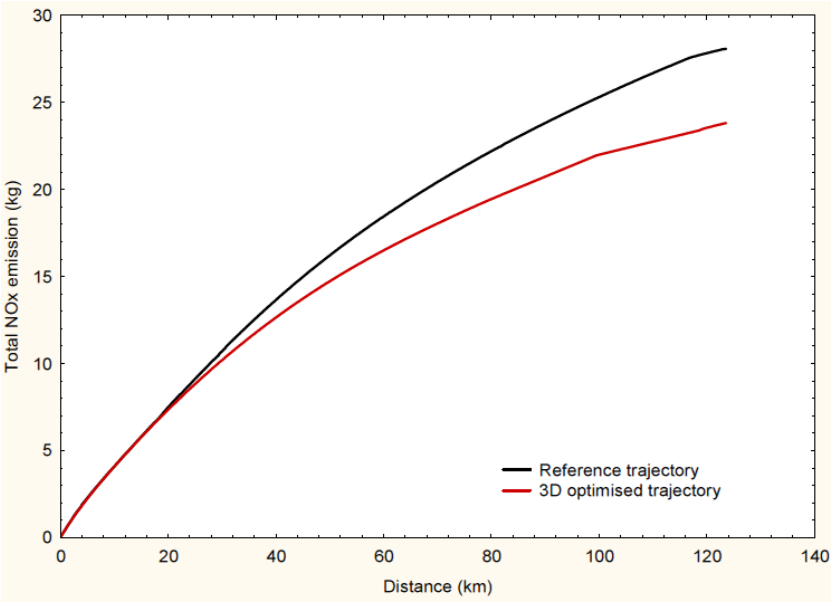

Fig. 6.46: Total Nox Emission Comparison

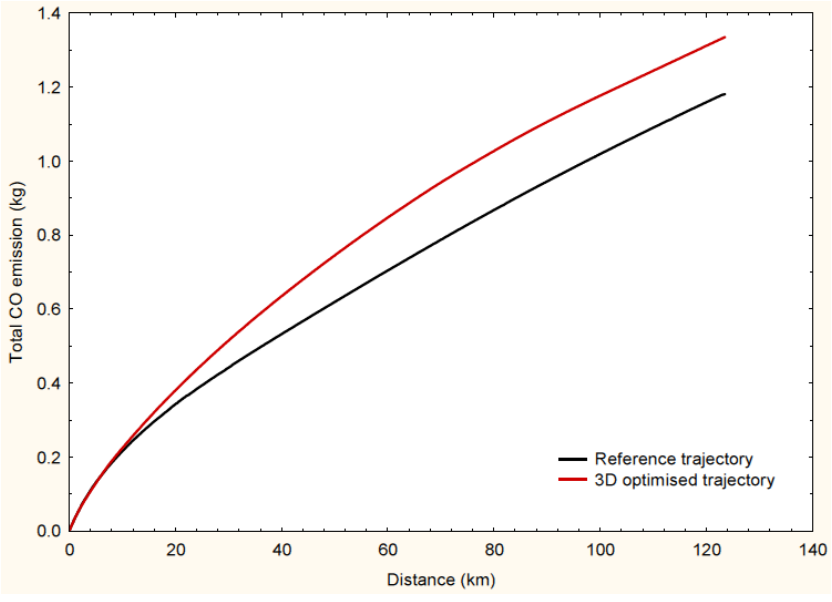

Fig. 6.48: Total CO Emissions for the 3D Case

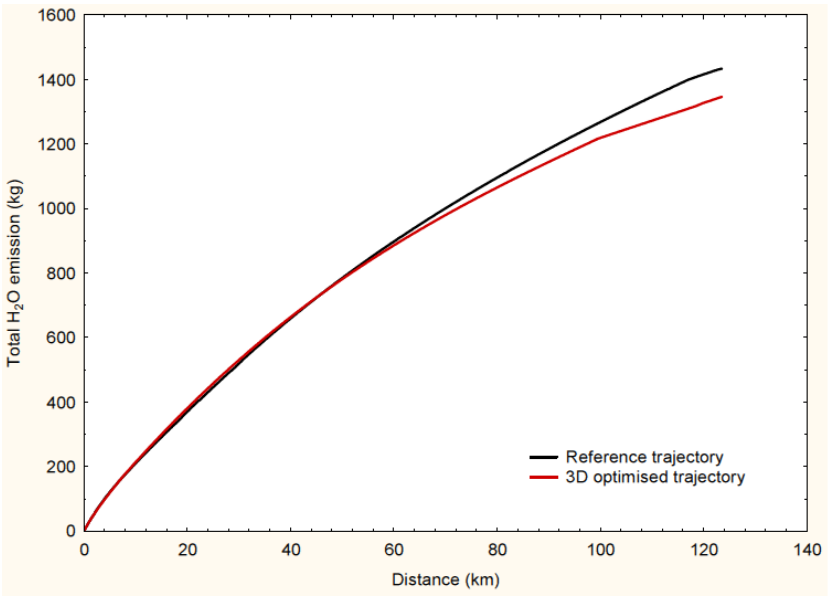

Fig. 6.47: Total H_2O Emissions for the 3D Case

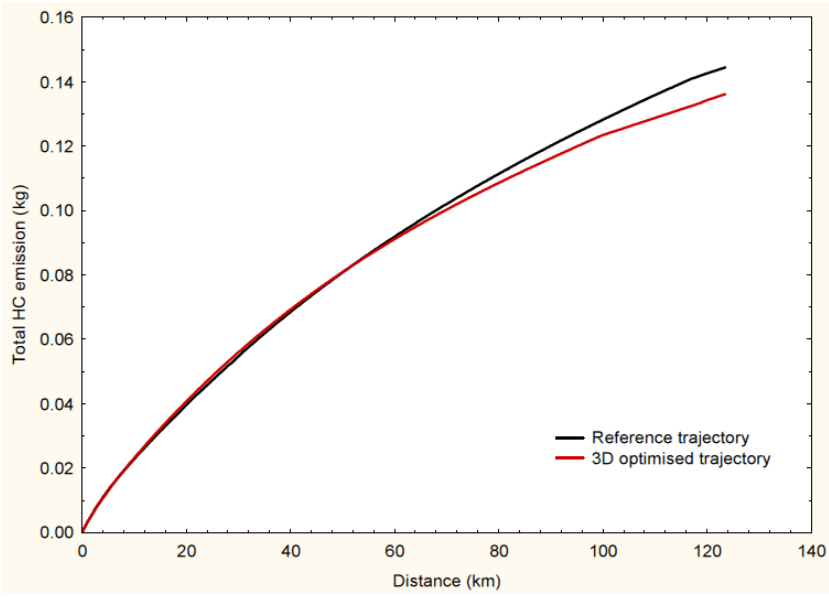

Fig. 6.49: Total HC Emissions for the 3D Case

6.4.2 Noise Optimisation

Noise is produced by the engine due high throttle setting during departures. This noise negatively affects the populations living around the airport by causing annoyance and or awakening. Thus, a noise optimisation case was ran to assess the impacts of flying minimum noise alternative routes on a densely populated areas. The same setting for the conventional departure was used with the addition of lateral movement. The population data around the Heathrow below the trajectory path within the greater London area was considered for the noise calculation. Fig. 6.50 presents the lateral profile comparison for the minimum fuel and the alternative minimum Noise Preferential Route (NPR). It can be seen that the minimum noise trajectory used a wider turn radius to angle itself to a northward alternative noise preferential route while the minimum fuel trajectory maintain the typical noise preferential root. Looking at the vertical profile in Fig. 6.52,

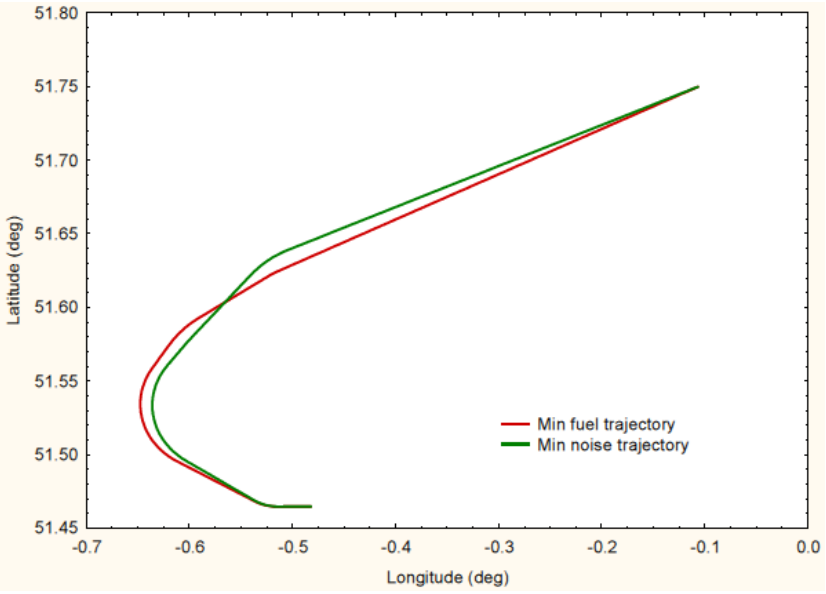

Fig. 6.50: Noise Ground Track for Minimum Fuel and Minimum Noise Trajectories

it can be observed that the alternative minimum noise trajectory flew at relatively lower altitude to reach the BPK SID, which marks the end of the departure. The difference

in the speed profile is not great as illustrated in Fig. 6.51. Much of the difference comes from the vertical and lateral profiles.

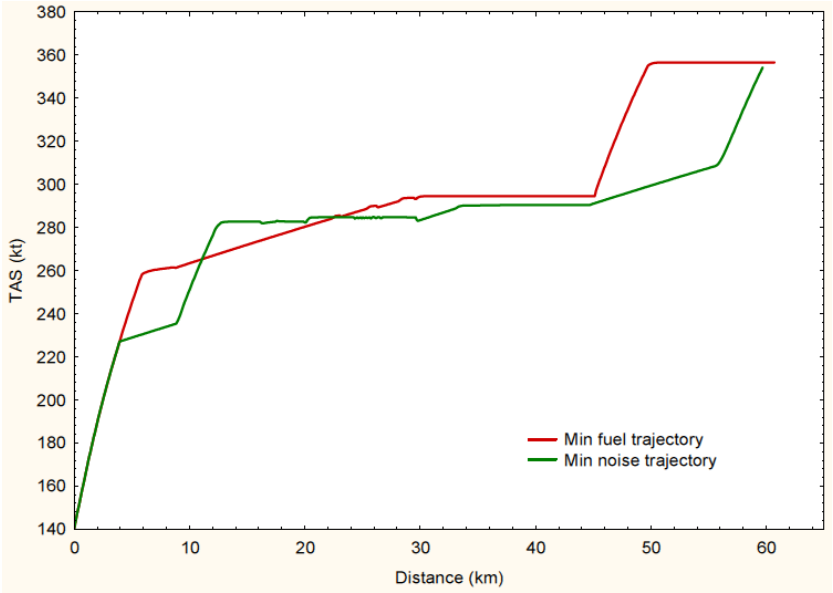

Fig. 6.51: True Air Speed Comparison for the Noise Case

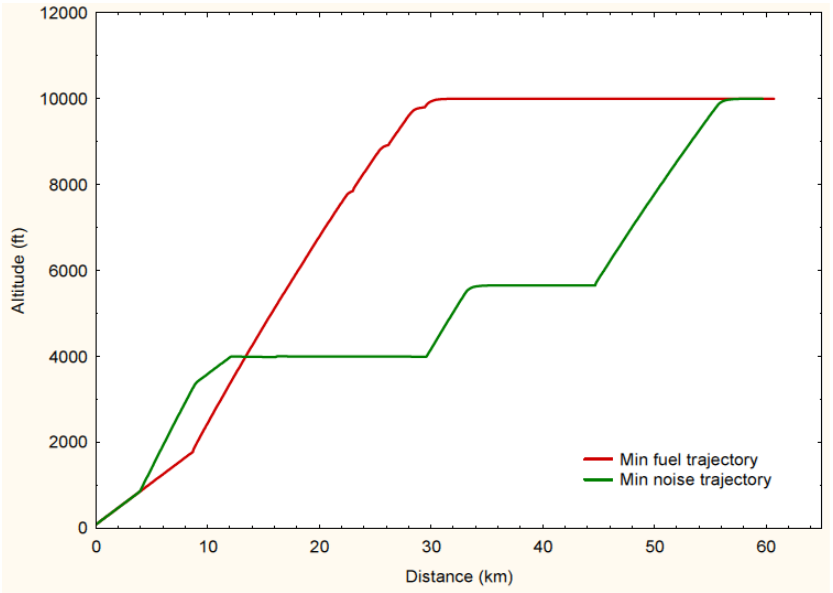

Fig. 6.52: Trajectories Comparison for the Noise Case

A 3D graphical projection of the minimum fuel trajectory over the greater London area

Fig. 6.53: Minimum Fuel Trajectory and Population Density, Noise Case

is shown in Fig. 6.53. The population density of the area is shown in colour codes, with deep red representing more than 2,000 people per grid point and deep green representing 0 people. The A marking shows the relative location of the Trafalgar Square in central London. Similarly, the noise optimised alternative route is presented on over the same are as illustrated in 6.54.

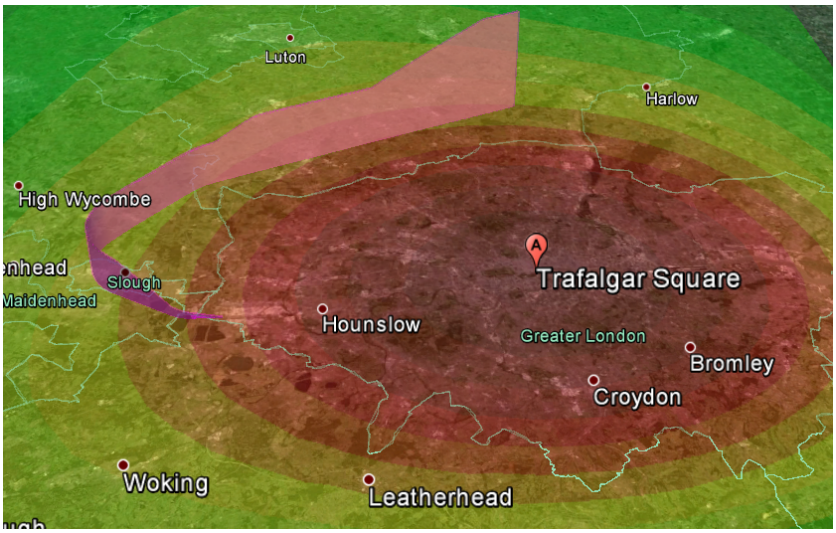

Fig. 6.54: Minimum Noise Trajectory

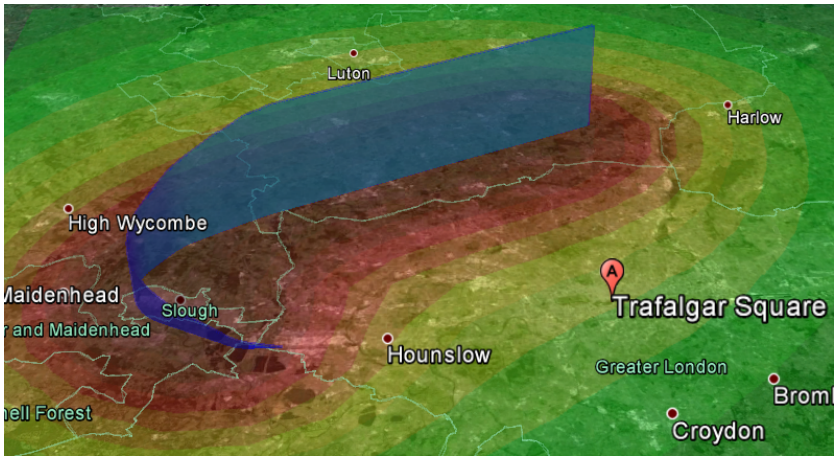

Fig. 6.55: Noise Contours for the Minimum Noise Trajectories

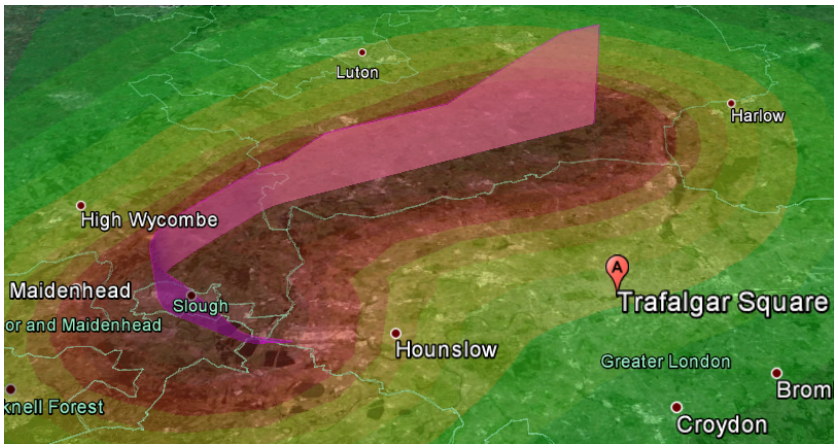

Fig. 6.56: Noise Contours for the Minimum Noise Trajectories

The respective noise generated by the minimum fuel and the minimum noise alternative routes are shown in Fig. 6.55 and Fig. 6.56. The deep red colour represents greater 60dBA and the deep green colour represents less than 16 dBA.

The noise evaluation of the minimum fuel trajectory indicates 8,752 awakenings whereas the minimum noise alternative trajectory indicates 6,049 awakenings with extra 17.84 kg of fuel burn as illustrated in Fig. 6.57. Overall, the result shows that the minimum noise route can significantly reduce the impact of aircraft noise in a densely populated areas through avoidance and mitigation. The minimum noise trajectory allows a 45% reduction of the awakening footprint with a 3% fuel penalty.

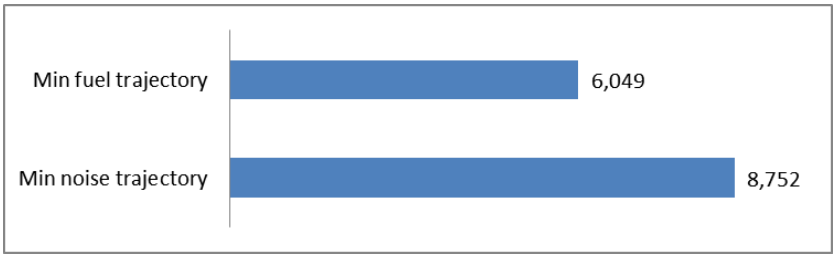

Fig. 6.57: Number of People Awaken in Each Trajectory

6.5 Chapter Summary

There are many parameters that can significantly influence the optimisation process. In this analysis however, the major parameters influencing trajectory optimisation have been considered based on the method described in section 3. The results obtained show that there is significant advantage in including the icing conditions in the optimisation set up for flights in known icing conditions. Currently, the two most critical problems affecting anti-icing system design are rating and sizing. In a new system rating is part and parcel of sizing whereas, in an existing system, rating is simply a measure of the system performance. By flying weather optimised trajectories such as the ones developed and simulated in this work, it was demonstrated that the overall fuel burn due to anti-icing operation can be reduced by up to 11%. Indirectly therefore, the method developed in this work would influence the design and production of anti-icing systems with small size (light weight) and lower power rating.

Chapter 7

Conclusions and Further Works

Chapter 7 presents the conclusions of a multi-objective and multi-disciplinary aircarft trajectory optimisation in the presence of icing conditions. The chapter draws conclusions from the objectives set out at the beginning of the thesis to the limitations of the methodology used. At the end of the chapter, recommendations are given for future work.

7.1 Conclusions

The ACARE targets the reduction of CO_2, NOx emissions and perceived noise by 75% and 90% and 65% respectively by the year 2050 referenced to a new aircraft flying in 2000. [50] The ACARE has also identified enablers which include radical changes in aviation since 2000, such as greener all-weather commercial air transport, more efficient next generation aircraft technologies and operation procedures for the protection of the environment. In line with these goals, a method is developed and used for the analysis of aircraft trajectory optimisation involving icing encounter using GATAC framework. This is an improvement in the approach to the trajectory optimisation problem since the current approach of representing only the aircraft dynamics and the engine fuel model neglects the effects of systems power off-takes. This is aimed at optimising trajectories and missions with aircraft systems in operation in order to demonstrate the environmental gains that can be achieved if such optimised flight profiles are flown.

Consequently, the primary objective of the work is to develop a cohesive method for managing in-flight icing in a future ATM environment that enables efficient flight planning. To achieve this objective, three major works were carried out in this project which includes development of anti-icing power simulation model, analysis of the effects of icing parameters on anti-icing energy and, the impacts of icing optimised trajectories on overall fuel consumption, noise and emissions. The current icing codes such as LEWICE and TRAJICE are complex; therefore, cannot be easily integrated into GATAC optimisation framework. In order to incorporate icing scenarios in the trajectory optimisation, a simplified icing model which focuses mainly on power requirement was developed using MATLAB/Simulink which was implemented in GATAC using dynamic link library. This allowed independent assessment of aircraft fuel burn penalties due to icing. The model also helped in the analysis of the icing parameters for the selection of the trajectory optimisation cases. This includes the determination of the boundaries of the parameters that mostly affect the anti-icing energy. Knowledge of these boundaries helped in determining the critical cases considered in the investigation of energy efficient trajectories. Finally, a trajectory optimisation study was carried out to assess the impacts of including icing conditions in the optimisation schemes. This is to allow the assessment of the effects of flying trajectories obtained with and without consideration to the icing conditions on fuel burn and associated emissions.

During the icing parameter analysis, it was observed that icing does occur at 0℃ ambient temperature but anti-icing may not be necessary except for low climb speeds. In the anti-icing power simulation, -30℃, 1.14 $2g/m^3$, $15\mu m$ gave the highest power requirement out of the 48 cases ran based on the Appendix C icing envelope. This means that, the lowest OAT (-40℃ IM conditions) does not necessarily produce the highest power

demand in low LWC or high aircraft speeds. From the trajectory optimisation simulations, it was observed that fuel penalty can get up to 3.7 % due to icing encounter in climb to cruise altitudes. It was found that a savings of bout 5.5% of which can be achieved using icing optimised trajectories. Considering that about 83,000 flights that take place globally and the significant number of those that fall under icing conditions, it would thus be desirable to incorporate en-route weather conditions such as icing in commercial transport aircraft trajectory planning. It was also observed that fuel penalty due to anti-icing operation can get up to 11% during arrival. This could be attributed to the lower total engine power settings associated with arrival segment. Because high power off-takes in lower throttle settings are more demanding than high throttle settings. This suggests that fuel penalty due to icing is not only dependent of icing conditions but engine power setting as well. Overall, it shows that there is more fuel saving on using icing optimised trajectories during arrival than any other flight segment.

In the multi-dimensional cases, it was observed that trajectories generated from 3D optimisation save more fuel than 2D optimised trajectories currently flown by commercial aircraft. Up to 0.7% of fuel burn due IPS operation can be saved by using 3D optimised trajectories in icing conditions. The minimum noise trajectory which is a 3D case allowed for a 45% reduction of the awakening footprint with a 3% fuel penalty. This shows that flying minimum noise optimised routes in addition to minimum NPR (see section 6.4.2 for details) can be applied for further mitigation of the impacts of aircraft noise upon densely populated areas.

It can be therefore concluded that, for an efficient anti-icing operation, consideration should be given to the secondary power bleed requirement throughout a vast flight envelope when deciding the off-takes limits. This is because the lowest icing temperature

does not necessarily give the highest power demand but rather a combination of many aircraft icing contributing factors. This is evident from the findings that fuel penalty due to IPS operation got up to 11% during arrival. It would therefore be desirable that at each flight phase, bleed extraction needs only to meet the combine airflow requirement for anti-icing and aircraft environmental control system. This would reduce excess fuel burn and emissions to the environment. It can also be concluded that flying icing optimised trajectories offers better fuel savings because of the inclusion of the icing profile in the FMS.

7.1.1 Contribution to Knowledge

This research contributes by developing a method structured to generate more efficient flight trajectories based on fuel consumption and environmentally related objectives. A multi-objective parameter synthesis of the optimisation space has been applied as a methodological platform for managing in-flight icing. To this end, a tool was developed to explore the aircraft trajectory optimisation space in real weather scenarios. The tool allowed an independent assessment of the methodology based on the three primary phases defining a commercial flight trajectory: departure, cruise and arrival. Hence, an objective evaluation of the performance of a large aircraft with respect to fuel burn and associated emissions has been performed which was hitherto not available in literature. The methodology by virtue of the results provides the basis to develop intelligent IPS which would influence the FMS to alter the flight plan for more efficient operation in icing conditions. Overall, the research contributes by combining two advanced concepts of efficient IPS with efficient aircraft operation to create a concept of controllable intelligent anti-icing operation in the future ATM environment.

7.1.2 Limitations of the Current Methodology

The fundamental limitation of the methodology employed in this work is that it is only practicable in an optimal free flights environment based on shared network-enabled information. To realise the full potentials of this method, flight operators must have access to current and planned routes to deal with congestion and other airspace constraints. These constraints might include scheduled times of use for special activity such as military, security or space operations. In addition, flight operators must continuously obtain an up-to-date planned and unplanned ATM restrictions, from ground operations to the intended flight trajectory and vice versa.

7.2 Further Works

The following further works are recommended:

- The author anticipates smart routing techniques to be used for efficient aircraft operations in the future. In that case, an intelligent IPS must be connected with the FMS receiving inputs from an on-board or remote weather source. The FMS using both the GPS and INS (Inertial Navigation System) to determine the aircraft position can pilot the aircraft based on the IPS algorithm through icing efficient trajectories. Therefore, future works should include integration of a real time weather data link for simulating real time trajectory optimisation in icing conditions. This conditions should represent the real weather encountered by the flying aircraft and used for flight guidance.

- Hybrid de-icing technology is a potential low energy ice protection system for the

next generation aircraft. Due to high power demand of thermal ice protection systems, future large transport systems may adopt hybrid anti-icing solutions. Therefore, the anti-icing power simulation tool should be upgraded to include hybrid (such as thermo-mechanical) ice protection systems. Potential research areas may start with the assessment of savings on fuel burn/emissions of hybrid de-icers using method developed in this work; and de-icer sizing and mechanism of operation for flying weather based optimised aircraft trajectories. The future aircraft is also thought to possess an electric power source. Therefore, a similar study using an all-electric-aircraft (AEA) model could also be undertaken in order to evaluate how this approach (one developed in this work) will fit into the AEA energy supply architecture.

- Using an operational bestselling aircraft (A320) model and the current icing standard (Appendix C) allowed a more realistic evaluation of the method developed in this work. Further benefits could be exploited using non-standard icing conditions (such as 200nm continuous icing encounter) operations. This would allow the evaluation of other possible icing cases that were not considered in this work. In addition, analyses such as the one carried out in this work should be applied to alternative aircraft with full protection (inclusive of tail-plane protection) and alternative standard (proposed Appendix D for SLD) for further evaluation of the method developed in this work. This would give a far more reaching trade-off between power consumption and flight performance using a potential future icing standard.

References

[1] E. F. Weener. Ntsb focus area - inflight icing. In *International Winter Operations Conference*, 5-6 October 2011 2011. xxi, 2

[2] R.G. Derwent I.L. Karol, H. Kelder and R.R. Friedl. Ipcc special report: Aviation and the global atmosphere - summary for policymakers. In *A Special Report of Working Groups I and III of the Intergovernmental Panel on Climate Change*, San Jose, Costa Rica, 12-14 Apr 1999. IPCC. xxi, xxix, 6, 7, 8, 10

[3] D. Pisani. Multi-parameter trajectory optimization using gatac. Msc thesis, Cranfield University, 2012. xxi, 12, 74

[4] G. Mingione and M. Barocco. Flight in icing conditions summary, 1997, French DGAC Icing Flight Manual. xxi, xxvii, 14, 15, 19, 20, 21, 40, 214

[5] WMO Commission for Aeronautical Meteorology. *Freezing Contamination: Aircraft Icing*, 2012 (accessed Jan 26, 2014). http://www.caem.wmo.int/_pdf/icing/icing_02_effects.pdf. xxi, 14, 18

[6] Clean Sky. Clean sky at a glanace: Bringing sustainable air transport closer. Technical report, Clean Sky JU, 2012. xxi, 26

[7] Vibro-meter. Ice detection sensor type ew 140. Technical Report 226-001, VIBRO-METER SA. xxi, 40, 41

[8] EC. *ON-Wing Ice Detection and Monitoring System*, 2012 (accessed April 17, 2013). http://ec.europa.eu/research/transport/projects/items/on_wings_en.html. xxi, 40, 41

[9] NASA and Innovative Dynamics Inc. *Ice Protection Sensor System*, (accessed January 19, 2013). http://sbir.gsfc.nasa.gov/SBIR/successes/ss/034text.html. xxi, 42

[10] M. O'Brien. *Chasing the Needles*, 2009 (accessed February 7, 2011). https://milesobrien.wordpress.com/2009/02/. xxii, 45

[11] SAE. Aerospace information report: Ice, rain, fog, and frost protection. Technical Report AIR1168/4, SAE Aerospace, 1990. xxii, 48, 49, 50, 53, 55, 104, 106, 108, 112, 113, 114

[12] B. L. Messinger. Equilibrium temperature of an unheated icing surface as a function of air speed. *Journal of The Aeronautical Sciences*, 20(1):29–42, 1953. xxii, 34, 52, 53

[13] J.J. Geraridi and B. Ingram. Electro-magnetic expulsion de-icing system, usa patent 2000, b64d 15/00, n.y., 244/134 r, 2000. xxii, 62, 63

[14] K. Al-Khalil. Thermo-mechanical expulsion deicing system - tmeds. Technical Report AIAA-2007-692, AIAA, 2007. xxii, 61, 64, 65

[15] GKN Aerospace. *Composite Aircraft Wing Research gets underway at GKN Aerospace*, 2011 (accessed April 25, 2011). http://www.gkn.com/aerospace/products-and-capabilities/Pages/default.aspx. xxii, 66

[16] G.A. Dimock R.W. Deters and M.S. Selig. Icing encounter flight simulator. *Journal of Aircraft*, 43(5), 2006. xxii, 69, 70

[17] M. B. Bragg, T. Basar, W. R. Perkins, M. S. Selig, P. G. Voulgaris, and J. M. Melody. Smart icing systems for aircraft icing safety. Technical Report AIAA 2002-0813, AIAA, 2002. xxii, 38, 69, 70

[18] SESAR. Single european sky atm research: The roadmap for sustatinable air traffic management: European atm master plan. Technical report, 2012. xxii, 78, 79

[19] E. Dimech; K. Chircop; M. Xuereb; R. Muscat and W. Camilleri. Systems for green operations (sgo) itd: Gatac v2 beta - user manual. Technical report, 2010. xxii, 85, 88

[20] S. Barley. Evaluation of small scale icing tunnel test results. In *SAE Aircraft Engine Icing International Conference 2007*. Airbus, 24-27, Sep 2007. xxii, 97

[21] Smart Cockpit. *A319/A320/A321 Ice and Rain Protection*, 2011 (accessed February 24, 2011). http://www.smartcockpit.com/aircraft-ressources/A320-Ice_and_Rain_Protection.html. xxii, 98

[22] D. T. Bowden, A. E. Gensemer, and C. A. Skeen. Engineering summary of airframe icing technical data. Technical Report FAA ADS-4, FAA, 1964. xxiii, xxvii, xxviii, 101, 102, 104, 133, 148, 220, 221, 222, 223

[23] R. W. Gent, N. P. Dart, and J. T. Cansdale. Aircraft icing. *The Royal Society*, (358):2873–2911, 2000. xxiv, 3, 13, 16, 33, 35, 36, 54, 132, 133

[24] FlightAware: Live flight tracking. http://uk.flightaware.com/live/flight/BAW442/history/20140414/1700Z/EGLL/EHAM/tracklog. Accessed: 2014-04-14. xxiv, 145

[25] *Unite Kingdom AIP: Standard Departure Chart - Instrument (SID) - ICAO*. xxviii, 226

[26] AIP Netherlands. *Schiphol Instrument Approach Chart*. http://www.bostonvirtualatc.com/charts/EHAM/IAP/EH_AD_2_EHAM_IAC_27_1_en.pdf. xxviii, 227

[27] CAA. *Aircraft Icing Handbook*. Canada Aviation Authority, Lower Hutt, New Zealand, 2000. xxix, 14, 15

[28] P. Verdin. An automatic multi-stepping approach for aircraft ice prediction, 2007. 1

[29] P. Appiah-Kubi. Us inflight icing accidents and incidents, 2006 to 2010, 2011. 1

[30] NTSB. National transportation safety board: Aviation accident statistics, 2011. 2

[31] I. Martinez. Aircraft environmental control in aircraft. Technical report, Isidoro Martinez, 2013. 2

[32] T. P. Ratvasky; B. P. Barnhart and S. Lee. Current methods for modeling and simulating icing effects on aircraft performance, stability and control. Technical report, NASA, 2008. 2

[33] ICAO. *2013 ICAO Air Transport Results Confirm Ruburst Passenger Demand, Sluggish Cargo Market*, 2013 (accessed February 3, 2014). http://www.icao.int/Newsroom/Pages/2013-ICAO-AIR-TRANSPORT-RESULTS-CONFIRM-ROBUST-PASSENGER-DEMAND,-SLUGGISH-CARGO-MARKET.aspx. 6

[34] SESAR. Single european sky atm research releases: Advancing atm modernisation, 2012. 6, 78

[35] G. Weiqun, R. Navatrane, D. Quaglia, Y. Yang, I. Madani, V. Sethi, H. Jia, K. Chircop, R. Sabatini, and D. Zammit-Mangion. Towards the development of a multi-disciplinaryi flight trajectory optimization tool - gatac. In *Proccedings of ASME Turbo Expo 2012, GT2012*. ASME, 11-15 June 2012 2012. 7

[36] C. Baukal. *Everything You Need to Know About NOx: Controlling and Minimising Pollutant Emissions is Critical for Meeting Air Quality*, 2005 (accessed Oct 6, 2014). http://www.dcl-inc.com/prod2.cfm?autoid=42&lg=En&gclid=CNSyrO-mwcUCFMatAodzglAUw. 9

[37] J.D. Schaffer. Flight trajectory optimization for an efficient air transport system. In *28th International Congress of the Aeronautical Sciences*, Brisbane, 23 - 28 September, 2012 1985. ICAS. 11, 74, 77

[38] Advisory Council for Aeronautics Research in Europe. Addendum to the strategic research agenda, 2008. Technical Report Brussels, ACARE, 2008. 11, 76

[39] C.P. Lawson. *Airframe Systems*. Msc avd course lecture notes, October 2008, Cranfield University, UK. 14

[40] A. Shinkafi and C. Lawson. Evaluating inflight ice protection methods for applications on next generation aircraft. *Journal of Aerospace Engineering and Technology*, (2231-038X), 2013. 16

[41] G. Mingione, V. Brandi, and B. Esposito. Ice accrertion prediction on multi-element airfoils. Technical Report AIAA-97-0177, AIAA, 1997. 16

[42] S. Altus. *Effective Flight Plans Can Help Airlines Economize*, 2015 (accessed Apri 20, 2015). http://www.boeing.com/commercial/aeromagazine/articles/qtr_03_09/pdfs/AERO_Q309_article08.pdf. 19

[43] R. Cassoni S. Thomas and C. MacArthur. Aircraft anti-icing and de-icing techniques and modelling. In *34th Aerospace Sciences Meeting Exhibite*. AIAA, 15-18 Sep 1996. 19, 103

[44] T. P. Ratvasky. Current methods modeling and simulating icing effects on aircraft performance, stability, control. *Journal of Aircraft*, 47(201):211. 19

[45] J. F. Van Zante and R. S. Thomas. Investigation of dynamic flight maneuvers with an iced tailplane. In *37th Aerospace Sciences Meeting Exhibite*. AIAA, 11-14 Jan 1999. 20

[46] R. K. Jeck. Icing design envelopes (14 cfr parts 25 and 29, appendix) converted to a distance-based format. Technical Report DOT/FAA/AR-00/30, FAA, 2002. 23, 135

[47] I. Moir and A. Seabridge. *Aircraft Systems Mechanical, Electrical, and Avionics Subsystems Integration*. Wiley, New Jersey, 3rd edition, 2008. 23

[48] B.C. Bernstein; T.P. Ratvasky and D.R. Miller. Freezing rain as an in-flight icing hazard. Technical report, 2012. 24

[49] M. Sammut, M. Xuereb, K. Chircop, W. Camilleri, E. Dimech, D. Karumbaiah, and H. Pervier. System for green operations (sgo) itd: Gatac v3 user manual. Technical report, Clean Sky, 2013. 27, 86

[50] European Commission. Flightpath 2050 europe's vision for aviation: Report of the high level group on aviation research. Technical report, EC, 2011. 29, 189

[51] FAA Aviation Administration. Nextgen implementation plan march 2012. Technical report, Federal Aviation Authority, 2012. 30

[52] AerTex. *Aircraft Icing Analysis Codes*, 2012 (accessed February 3, 2012). http://www.aerotex.co.uk/analysis_codes/analysis_codes.htm. 33, 37, 55

[53] C.L. Johnson. Wing loading, icing and associated aspects of modern transport design. *Journal of the Aeronautical Sciences*, 8(2), 1940. 33

[54] J.K. Hardy. Protection of aircraft against ice. Technical report, Research Assessment Exercise, 1946. 33

[55] J.O. Lewis and R.S. Ruggeri. Experimental droplet impingement on four bodies of revolution. Technical report, NACA, 1955. 34

[56] I. Longmuir and K.B. Blogett. A mathematical investigation of water droplet trajectories. Technical report, Army Air Forces, 1946. 34

[57] T.F. Gelder U. Von Glahn and W.H. Smyers Jr. A dye tracer technique for experimentally obtaining impingement characteristics of arbitrary bodies and a method for determining droplet size distribution. Technical report, NACA, 1955. 34

[58] W.H. Smyers Jr. T.F. Gelder and U. Von Glahn. Experimental droplet impingement on several two-dimensional airfoils with thickness ratios of 6 to 16 percent. Technical report, NACA, 1956. 34

[59] J. T. Cansdale and R. W. Gent. Ice accretion on aerofoil in two-dimensional compressible flow: A theoretical model. Technical Report RAE-TR-R82128, Royal Aircraft Establishment, 1983. 34, 54

[60] T.G. Myers. Extension to the messinger model for aircraft icing. *AIAA JOURNAL*, 39(2), 2001. 35

[61] S. Ozgen and M. Canibek. Ice accretion on multi-element airfoils using extended messinger model. *Heat and Mass Transfer*, (45):305–322, 2009. 35

[62] R. Hayashi and M. Yamamoto. Two- and three-dimensional validation of icing model. In *APCOM ISCM*. 5th Asia Pacific Congress on Computational Mechanics & 4th International Symposium on Computational Mechanics, 11-14 Dec 2013. 35, 53

[63] W.M. Leary. We freeze to please: A history of nasaâs icing research tunnel and the quest for flight safety. Technical report, NASA, 2002. 35

[64] Fluent Users Services Centre ANSYS. Fluent inroductory lectures, 2006. 36

[65] B. W. Wright, K. Al-Khalil, and D. Miller. Validation of nasa thermal ice protection computer codes part2 - lewice/thermal. Technical Report AIAA 97-0050, AIAA, 1997. 37, 125

[66] R. W. Gent. Trajice: A combined water doplet and ice accretion prediction code for aerofoils. Technical Report RAE TR 90054, RAE, 1994. 37

[67] R. Henry. Development of an electrothermal de-icing/anti-icing model. Technical Report ONERA TAP 92005, ONERA, 1992. 37

[68] BAE Systems. *3D Ice Prediction Tool - ICECREMO2*, 2011 (accessed january 30, 2012). http://www.baesystems.com/ProductsServices/ss_tes_atc_icecremo.html. 37

[69] Brahimi M.T. Tezok F. Paraschivoiu I. Morency, F. Hot air anti-icing system modelization in the ice prediction code canice. Technical Report AIAA 98-0192, AIAA, 1998. 37

[70] Newmerical Technologies Int. Fensap-ice inflight icing simulation system, 2009. 37

[71] R. Aykan C. Hajiyev and F. Caliskan. Aircraft icing detection, identification and reconfigurable control based on kalman filtering and neural networks. Technical Report AIAA 2005-6220, AIAA, 2005. 38, 68

[72] M.D. Johnson and K. Rokhsaz. Using artificial neural networks and self organizing maps for detection of airframe icing. In *Atmospheric Flight Mechanics Conference*, AIAA-2000-4099, Jun 2000. AIAA. 38

[73] A.E. Schuchard W.R. Perkins J.W. Melody, T. Basar and P. Voulgaris. Detection and classification of aircraft icing using neural networks. Technical Report AIAA 2000-0361, AIAA, 2000. 38

[74] H. Gao and J.L. Rose. Ice detection and classification on an aircraft wing with ultrasonic shear horizon guided waves. In *IEEE Transactions on Ultrasonics Ferroelectrics and Frequency Control*. IEEE, Mar 2009. 39

[75] J. van Hengst, R. Gent, D. Hammond, R. Seubert, and B. Wagner. Ice accretion and its effects on flight. *Advisory Group for Aerospace Research and Development*, (AGARD-AR-344):3–1–3–36, 1997. 42

[76] C. P. Lawson. Electrically powered ice protection systems for male uavs-requirements and integration challenges. Technical Report 25th International Congress of the Aeronautical Sciences, ICAS, 2006. 43

[77] Z. Goraj. An overview of the de-icing and anti-icing technologies with prospects for the future, icas 2004, 24th international congress of the aeronautical sciences, 2004. 44

[78] FAA Technical Centre. De-icing of aircraft turbine engine inlets, 1988 1988. 44

[79] T. F. Gelder; J. P. Lewis and L. K. Stanley. Icing protection for a turbojet transport airplane: Heating requirements, methods of protection, and performance penalties. Technical Report NACA TN 2866, NACA, 1953. 46

[80] K. M. AL-Khalil and M. G. Potapczuk. Numerical modelling of anti-icing systems and comparison to test results on a naca0012 airfoil. Technical Report AIAA-93-0170, AIAA, 1993. 46

[81] T.M. Wilson and S.C. Simhauser. *Electrothermal deicing system*, November 8 1995. EP Patent App. EP19,950,105,601. 46

[82] T. S. Jonathan. Microwave de-icing and anti-icing system for aircraft, 1997. 46

[83] R. B. Rutherford and R. L. Dudman. Zoned aicraft for de-icing system and method, 2001. 46, 47, 66

[84] O. Meier and D. Scholz. A handbook method for the estimation of power requirements for electrical de-icing systemms. Technical Report 161191, Hamburg University of Applied Sciences, 2010. 47, 57, 60, 66, 108

[85] Inc Innovative Dynamics. *Aircraft Deicing Systems*, 2010 (accessed December 12, 2010). http://www.idiny.com/deicing.html. 50

[86] E.A. Whalen; Andy P. Broeren and Michael B. Bragg. Characteristics of runback ice accretions and their aerodynamic effects. Technical Report DOT/FAA/AR-07/16, FAA, 2007. 50

[87] Jr. Al-Khalil; T.G. Keith and K.J. De Witt. Development of an anti-icing runback model. In *28th Aerospace Sciences Meeting*, Reno, Nevada, 8-11 Jan 1990. AIAA. 50

[88] N. Alegre. *Full-Scale Runback Ice: Accretion and Aerodynamic Study*. Phd thesis, December 2010, Cranfield University, UK. 50, 101

[89] V. F. Petrenko and R. W. Whitworth. *Physics of Ice*. Oxford University Press, Oxford, 1 edition, 1999. 55

[90] V. F. Petrenko, M. Higa, and Deresh L. Starostin, M. Pulse electrothermal de-icing. In Prinsenberg S. Chung, J.S., editor, *Proceedings of The Thirteenth (2003) International Offshore and Polar Engineering Conference*, volume 1, page 435, Honolulu, 25-30 May 2003 2003. The International Society of Offshore and Polar Engineers. 56, 57

[91] V. F. Petrenko, C. R. Sullivan, V. Kozlyuk, F. V. Petrenko, and V. Veerasamy. Pulse electrothermal de-icer (petd). *Cold Regions Science and Technology*, (65):70–78, 2011. 56, 57, 67

[92] P. Krammer and D. Scholz. Estimation of electrical power for deicing systems. Technical report, Hamburg University of Applied Sciences, 2009. 57, 59, 60, 108

[93] F.P. Incropera. Fundamentals of heat and mass transfer. In D.P. DeWitt, editor, *7th Edition,*. John Wiley & Sons, USA, 2011. 58

[94] O. Meier and D. Scholz. A handbook method for the estimation of power requirements for electrical de-icing systemms. Technical Report 161191, Hamburg University of Applied Sciences, 2010. 59, 60, 114

[95] J. J. Gerardi and B. I. Richard. Electro magnetic expulsive de-icing system. usa patent, b64d 15/00 ed., 244/134 r,, 2000. 61

[96] L.A. Haslim and R.D. Lee. Electro-expulsive separation system, 09 1987. 61

[97] R. A. Olson and M. R. Bridgeford. Electro-expulsive de-cicing system for aircraft and other applications. usa patent, b64d 15/12 ed., 244/134d, 2010. 61

[98] M. Qinglin. Aircraft icing and thermo-mechanical expulsion de-icing technology. Msc thesis, Cranfield University, 2010. 61, 125, 127

[99] G. C. Botura, D. Sweet, and D. Flosdorf. Development and demonstration of low power electrothermal de-icing system. Technical Report AIAA 2005-1460, AIAA, 2005. 65, 66

[100] P. Stoner, D. P. Christy, and D. B. Sweet. Low power, pulsed, electro-thermal ice protection system, 2007. 65

[101] W. G. Habashi. Recent progress in unifying cfd and in-flight icing simulation. Technical Report ICFD10-EG-30I11, ICFD, 2010. 66

[102] R. Moser and R. Gent. Analysis for the design and test of an ice protection system for a scoop intake. In *Proceedings of 2011 SAE International Conference on Aircraft and Engine Icing and Ground Deicing*, Chicago, 13-16 Jun 2011. SAE International, paper 2011-38-0055. 67

[103] US Army Research and Development Center. Progress in evaluating surface coatings for icing control at corps hydraulic structures. Technical Report ERCD/CRREL Technical Note 03-4, US Army Corps of Engineers, 2003. 67

[104] G. Fortin. Considerations on the use of hydrophobic, superhydrophobic or icephobic coatings as a part of the aircraft ice protection system. In *SAE 2013 Aerotech Congress and Exhibition*, 24-26 September 2013 2013. 67

[105] M. B. Bragg, T. Basar, W. R. Perkins, M. S. Selig, P. G. Voulgaris, and J. M. Melody. Smart icing systems for aircraft icing safety. Technical Report AIAA 2002-0813, AIAA, 2002. 68

[106] D. P. Raymer. *Enhancing Aircraft Conceptual Desing using Multi-Disciplinary Optimization*. PhD thesis, Royal Institute of Technology, Stockholm, 2002. 71, 73

[107] K. Patra. Multi-disciplinary aircraft trajectory optimisation using a hybrid based optimiser. Phd thesis, Cranfield University, 04 2014. 71, 72

[108] N. K. Wickramasinghe, A. Harada, and Y. Miyazawa. Multiple objective optimization with vector evaluated genetic algorithms. In *First International Conference on Genetic Algorithms and Their Applications*. Texas Instrument, Inc., Jun 1985. 71

[109] A.Mayer M. Erickson and J. Horn. Muiltiobjective optimization using nondominated sorting in genetic algorithms. *Evolutionay Computation*, 2(3):221–248, 2007. 71, 72

[110] N. K. Wickramasinghe, A. Harada, and Y. Miyazawa. Genetic algorithm for multiobjective optimization: Formulation, discussion and generation. In *5th International Conference on Genetic Algorithms*. Morgan Publishers Inc., 24-26 Jun 1993. 72

[111] A.Mayer M. Erickson and J. Horn. *The niched Pareto genetic algorithm 2 applied to the design of groundwater remediation system*. Springer, Verlag, Berlin Heidelberg, 2006. 72

[112] M. Laumanns E. Zitzler and L. Thiele. Spea2: Improving the strength pareto evolutionary algorithm. Technical report, Swiss Federal Institute of Technology (ETH), Zurich, 2001. 72

[113] C.A. Coello Coello A.G. Hernandez-Diaz, L.V. Sanatana-Quintero and J. Molina. Pareto-adaptive ε-dominance. *Evolutionay Computation*, 15(4):493–517, 2007. 72

[114] F. Xu J. Zhang and X. Fang. Decomposition of multi-objective evolutionary algorithm based on estimation of distribution. *Applied Mathematics Information Sciences, An International Journal*, 8(1):249–254, 2014. 72

[115] A. J. Calise. Extended energy management methods for flight performance optimization. *AIAA Journal*, 15(3):314–321, 1977. 74

[116] R. Howe-Veenstra. Commercial aircraft trajectory optimization and efficiency of air traffic control procedures. Msc thesis, The University of Minnesota, 2011. 74, 75, 76

[117] B. Sridhar and S. Grabbe. A practical approach for optimizing aircraft trajectories in winds. Technical report, IEEE, 2012. 74

[118] A. V. Romero. *Aircraft Trajectory Optimization Using Parametric Optimization Theory*. PhD thesis, Universidad de Sevilla, 2012. 74

[119] F. Mache. Decision-making for autonomous flight in icing conditions. Msc thesis, Cranfield University, 2011. 74

[120] S. Armanini. Autonomous decision-making for uav flight in icing conditions. Msc thesis, Cranfield University, 2012. 74

[121] H. Tang and J.E. Robinson. Tactical conflict detection in terminal airspace. *Journal of Guidance, Control, and Dynamics*, 34(2):403–413, 2011. 74

[122] U. Schumann. Volcanic, weather and climate effects on air transport. In *28th International Congress of the Aeronautical Sciences*, Brisbane, Australia, Sep 2012. Optimage Ltd. 75

[123] *ICAO Performance Based Navigation Programme, howpublished = http://www.icao.int/safety/pbn/Pages/default.aspx, note = accessed: 2014-02-25.* 76, 77

[124] ICAO. Performance based navigation. Technical report, 2012. 77

[125] H. Erzberger. Transforming the nas: The next genration air traffic control system. Technical Report NASA/TPâ2004-212828, NASA, Oct, 2004. 77

[126] P. Lee J. Mercer V. Battiste E. Palmer P. Thomas, T. Callantine and N. Smith. Co-operative air traffic management: Concept and transition. In *AIAA Guidance, Navigation, and Control Conference and Exhibit*. AIAA, 15-18 Aug 2005. 77

[127] FAA. Nextgen implementation plan. Technical report, Federal Aviation Administration, USA, 2013. 79

[128] A.A. Pitertsev and F.J. Yanovsky. Polarimetric approach to detection of probable aircraft icing zones. icing detection algorithms. In *Proceedings of the 4th European Radar Conference*, Munich, Germany, Oct 2007. EuMA. 83

[129] D.J. Brinker A.L. Reehorst and T.P. Ratvasky. Nasa icing remote sensing system comparisons from airs ii. Technical Report NASA/TMâ2005-213592, NASA, 2005. 83

[130] N.E. Antoine. *Aircraft Optimization for Minimal Environment Impact*. PhD thesis, Stanford University, 08 2004. 86

[131] N.E. Antoine and I.M. Kroo. Framework for aircraft conceptual design and environmental performance studies. *AIAA Journal*, 43(10):2100–2109, Oct 2005. 86

[132] T. Kipouros D. Jaeggi, G. Parks and J. Clarkson. *Aircraft Systems Mechanical, Electrical, and Avionics Subsystems Integration*. Springer-Verlag, Berlin Heidelberg, 2005. 86

[133] J. Gorce K. Jaffres-Runser and C. Comaniciu. *A Multiobjective Tabu Framework for the Optimization and Evaluation of Wireless Systems. In: Local Search Techniques: Focus on Tabu Search*. I-Tech, Vienna, 2008. 86

[134] J. E. B. Moss J. Cavazos, M. F.P. O Boyle (A. Mycroft, and A. Zeller (Eds.)). 15th international conference, cc 2006 held as part of the joint european conferences on theory and practice of software. In *A Special Report of Working Groups I and III of the Intergovernmental Panel on Climate Change*, Vienna, Austria, 30-31 Mar 2006. Springer. 86

[135] D. Quaglia. Multidisciplinary methods for evaluation and optimization of aircraft flight performance, 2014. 91, 92

[136] EUROCONTROL. Base of aircraft data (bada) aircraft performance modelling report. Technical Report 2009-009, EUROCONTROL, Bretigny-sur-Orge, 2009. 92

[137] R. Seresinhe and C. Lawson. Extended energy management methods for flight performance optimization. *Proceedings of the Institution of Mechanical Engineers, Part G: Journal of Aerospace Engineering*, 2014. 93

[138] M.B. Hocking. Passenger aircraft cabin air quality: trends, effects, societal costs, proposals. *Elsevier*, 45(4-5):703–704, 2000. 93

[139] FAA. Pilot guide: Flight in icing conditions. Technical Report 91-74A, FAA, 2007. 96

[140] UIUC Applied Aerodynamics Group. *UIUC Airfoil Database*, 2011 (accessed November 3, 2011). http://http://airfoiltools.com/search/index. 101

[141] B. Rouffie. Ice protection system for an all electric aircraft, 2003. 103

[142] D. T. Bowden; A. E. Gensemer and C. A. Skeen. Engineering summary of airframe icing technical data. Technical Report FAA ADS-4, FAA, 1964. 104

[143] SAE Aerospace. Ice, rain, fog, and frost protection. Technical Report AIR1168/4, Society of Automative Engineers, Inc, 1989. 107, 108, 118

[144] A. Al-Khalil, R. Hitzigrath, O. Philippi, and C. Bidwell. Icing analysis and test of a business jet engine inlet duct. In *38th Aerospace Sciences Meeting Exhibit*, 10-13 January 2000 2000. 114

[145] J.P. Lewis and T. Bowden. Preliminary investigation of cyclic de-icing of an airfoil using an external electric heater. Technical Report RM E51J30, NACA, 1952. 118

[146] A. Shinkafi and C. Lawson. Development of a tool for simulating aircraft performance for trajectory optimisation in the presence of icing conditions. *IMechE Part G: Journal of Aerospace Engineering*, xxx(xxx), 2014. 125

[147] M. J. Kilshaw. A comparative study of aircraft anti-icing and de-icing systems. Msc thesis, Cranfield University, 1975. 130

[148] Y. Cao and Q. Zhang. Numerical simulation of rime ice accretions on an aerofil using an eulerian method. *The Aeronautical Journal*, (3230):243–249, 2008. 134

[149] Federal Aviation Authority: Technical Centre. De-icing of aircraft turbine engine inlets, 1988 1988. 136

[150] D. Krumpak. Ice protection system for a new generation aircraft. Msc thesis, Cranfield University, 2010. 137

[151] NOAA National Weather Service. *Aircraft Digital Service*, 2012 (accessed February 18, 2014). https://mail.google.com/mail/u/0/?tab=wm#inbox. 138

[152] LHR. *Heathrow Official Airport Website: Departures*, 2013 (accessed June 09, 2014). http://www.heathrowairport.com/static/Heathrow_Noise/Downloads/PDF/Departures11.pdf. 148

[153] B.M Yutko and R.J. Hansmann. Approaches to representing aircraft fuel efficiency performance for the purpose of a commercial aircraft certification standard,. Technical Report ICAT-2011-05, MIT International Center for Air Transportation (ICAT), May, 2011. 148

[154] C. C. Ryerson. Remote sensing of in-flight icing conditions: Operational, meteorological, and technological considerations. Technical Report NASA/CR-2000-209938, NASA, 2000. 152

[155] S. Wesley. Saving fuel: It's a team sport. In *IATA 8th Maintenance Cost Conference - MCC 2012 Atlanta*. Airbus, 17-19 Oct 2012. 156

Appendix A

Certification Standards

A.1 Appendix C Envelope

A.2 Appendix D Envelope

A.3 Appendix O Envelope

A.3.1 Continuous Maximum Condition

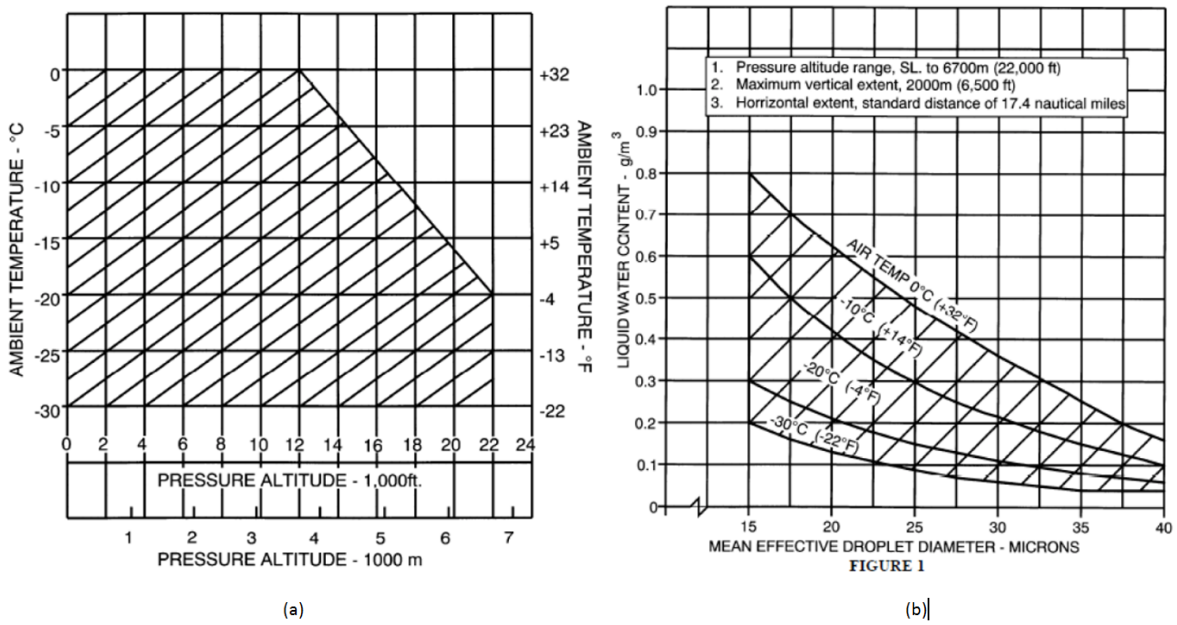

Fig. A.1: Appendix C definition: (a) CM, ambient temperature Vs pressure altitude, (b) CM, LWC Vs MVD for Stratiform clouds [4]

A.3.2 Intermittent Maximum Condition

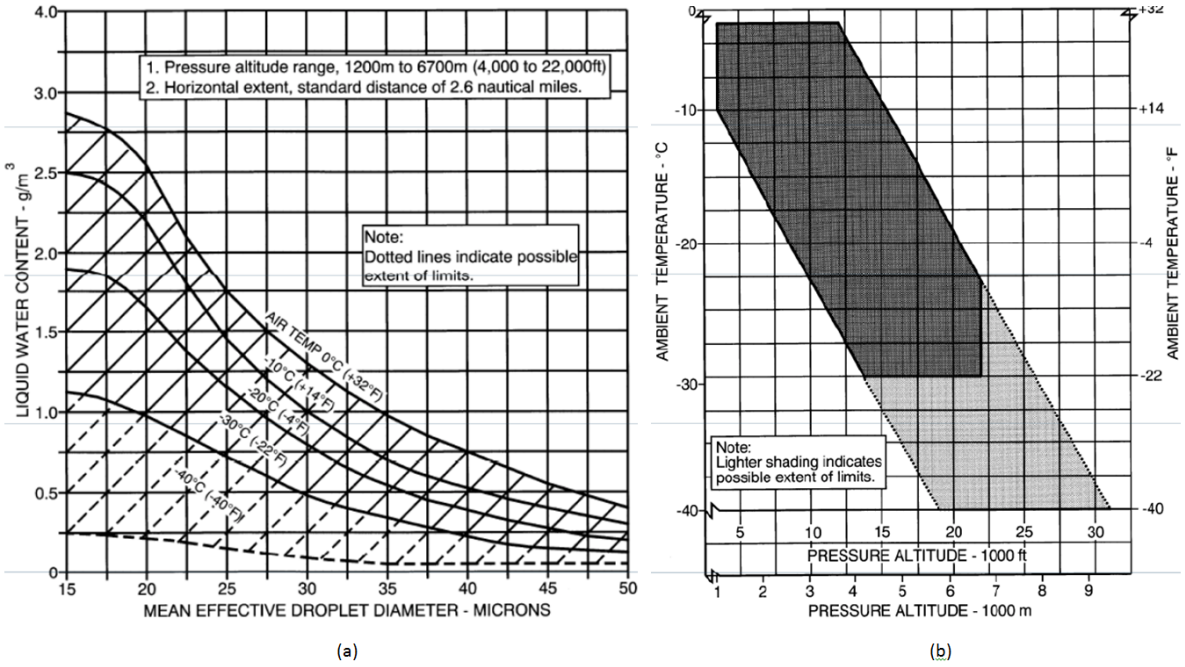

Fig. A.2: Appendix C definition: (a) IM, LWC Vs MVD, (b) IM, ambient temperature Vs pressure altitude

A.3.3 Proposed FAR Part 33 Appendix D

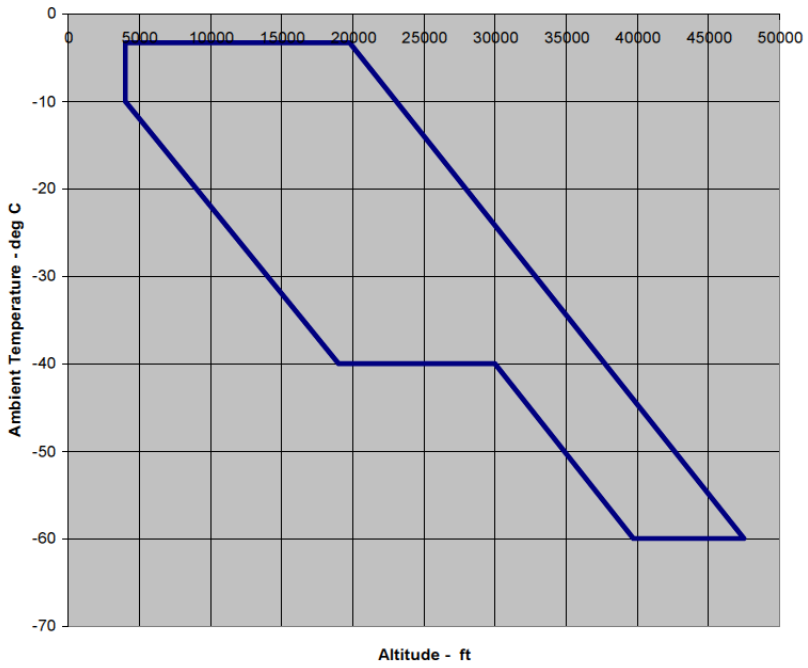

Fig. A.3: Proposed FAR Part 33 Appendix D

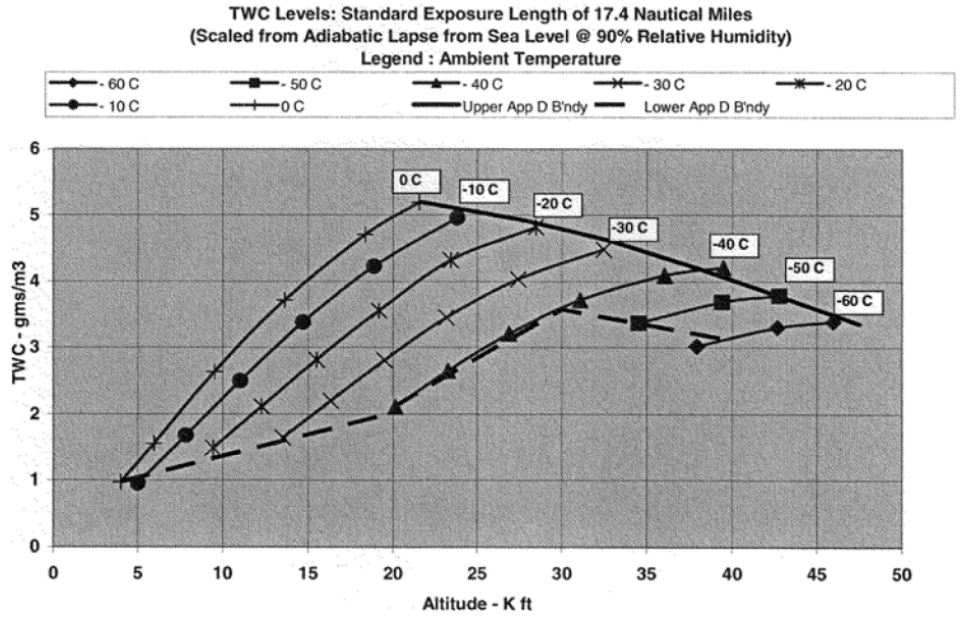

Fig. A.4: Plot of TWC levels over standard exposure length of 17.4nm

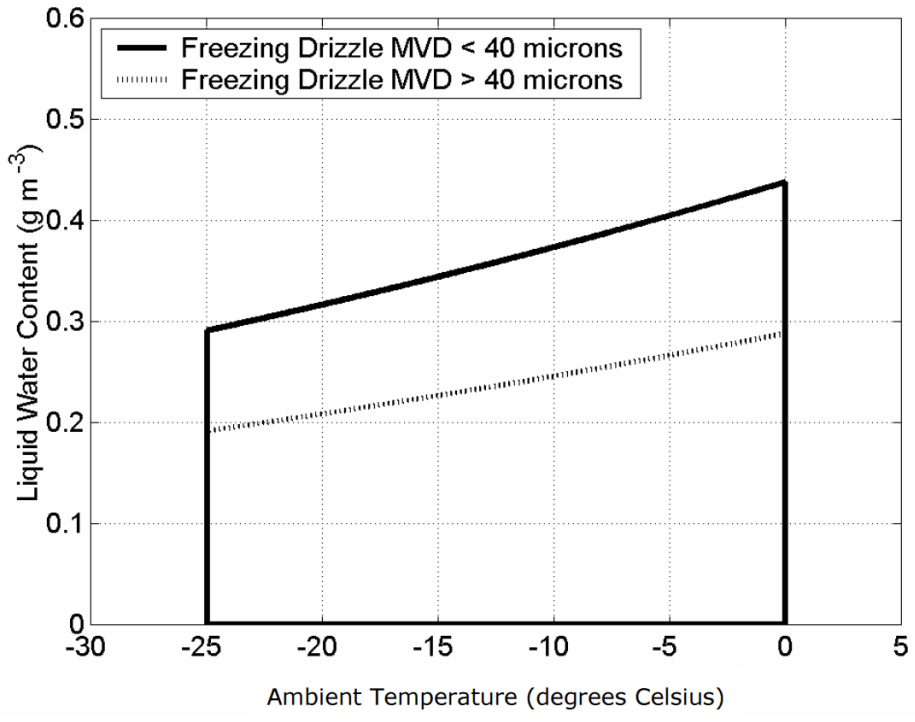

Fig. A.5: Appendx O, Freezing Drizzle, Liquid Water Content

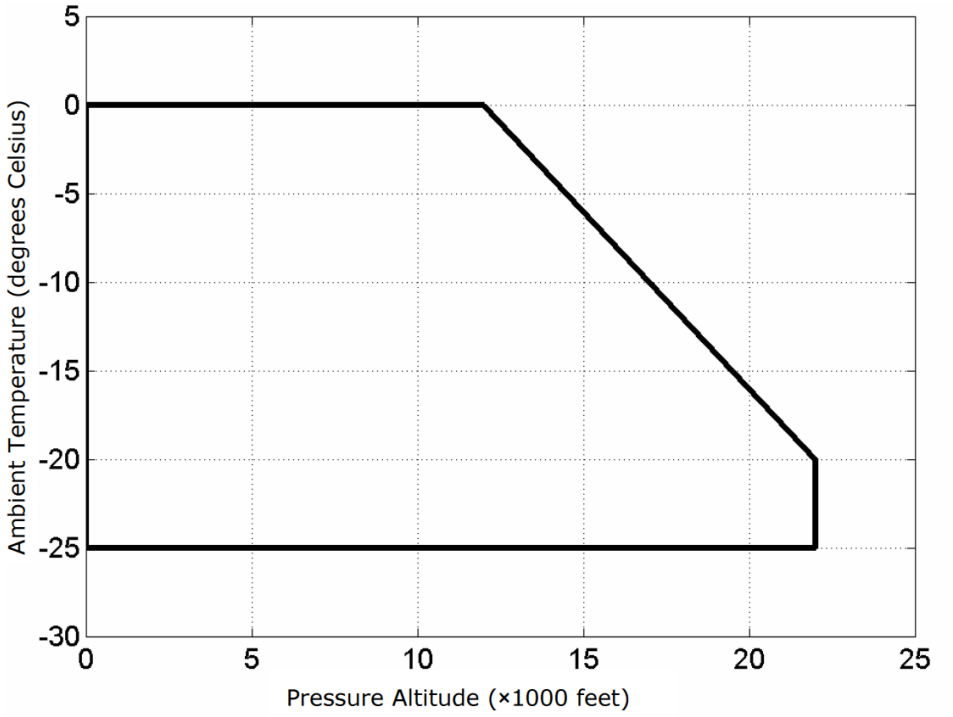

Fig. A.6: Ambient temperature Vs altitude range for Appendix O

Appendix B

Airframe Icing Technical Data Used

B.1 Projected Height of Different Aerofoils for Different Angles of Attack

B.2 Collection Efficiency Data

B.3 Upper Surface Impingement Limit Data

B.4 Lower Surface Impingement Limit Data

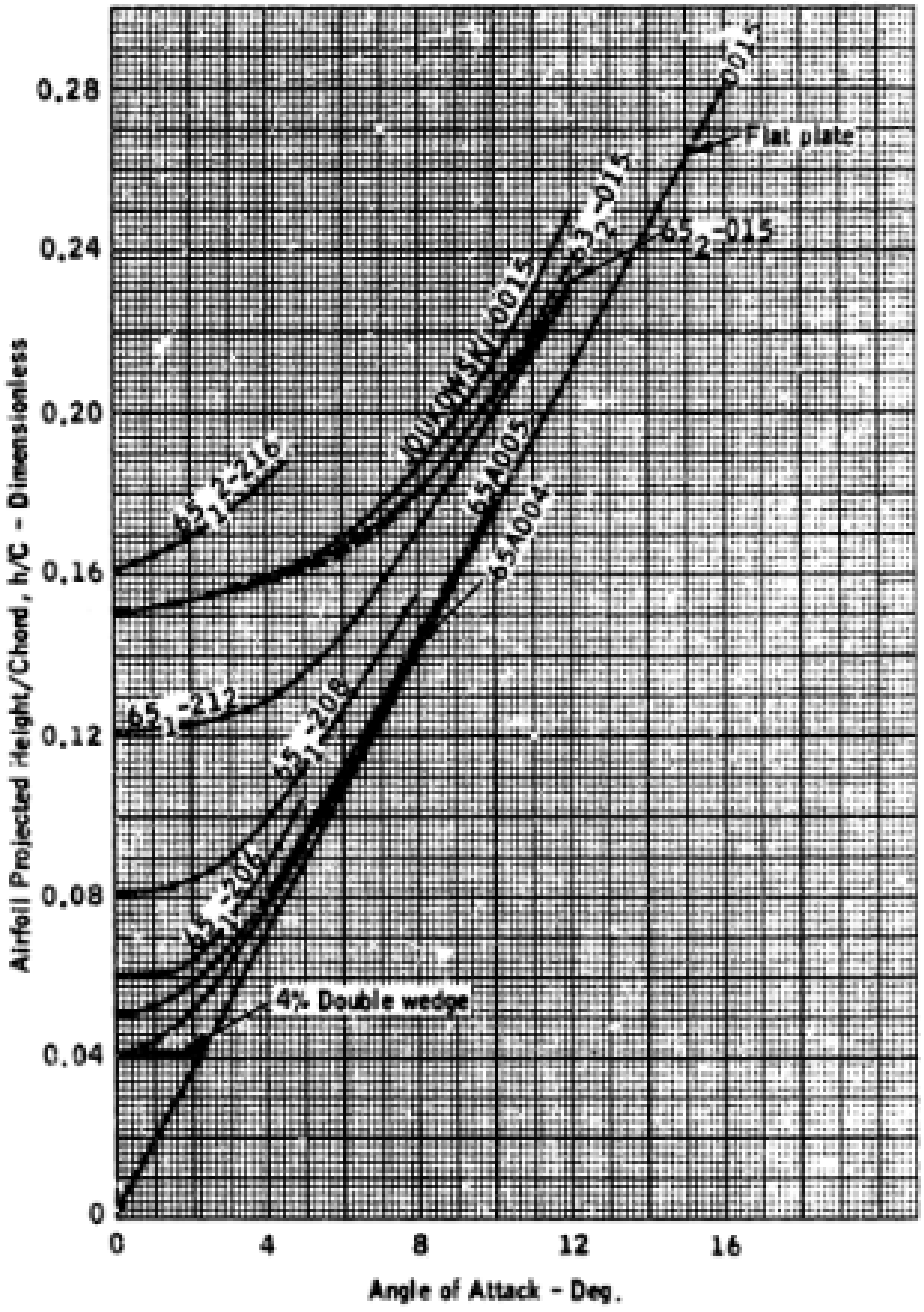

Fig. B.1: Projected Height of Several Airfoils Plotted Versus Angle of Attack [22]

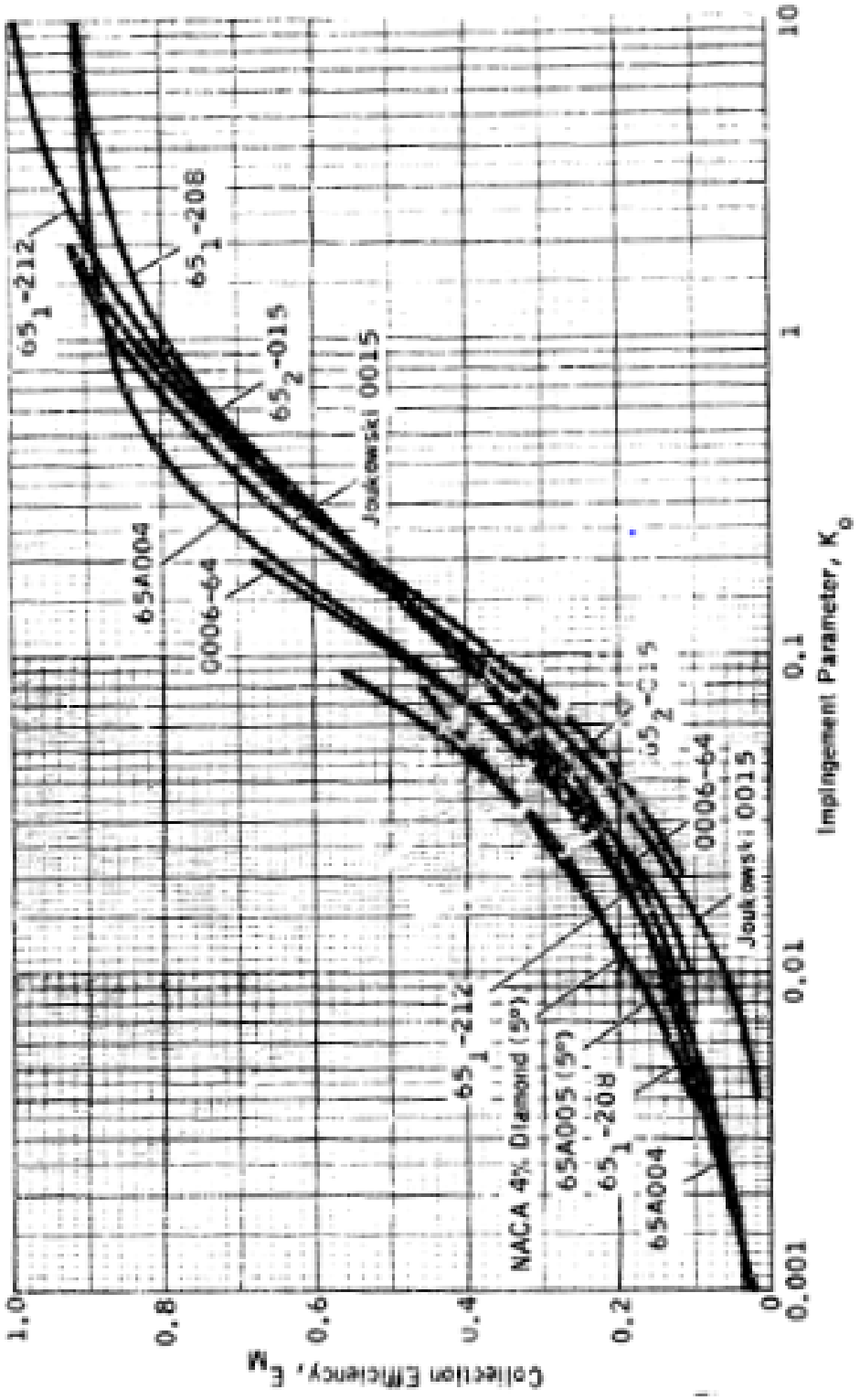

Fig. B.2: Collection Efficiency Versus K_0 Airfoils - Theoritical Data for α=4°[22]

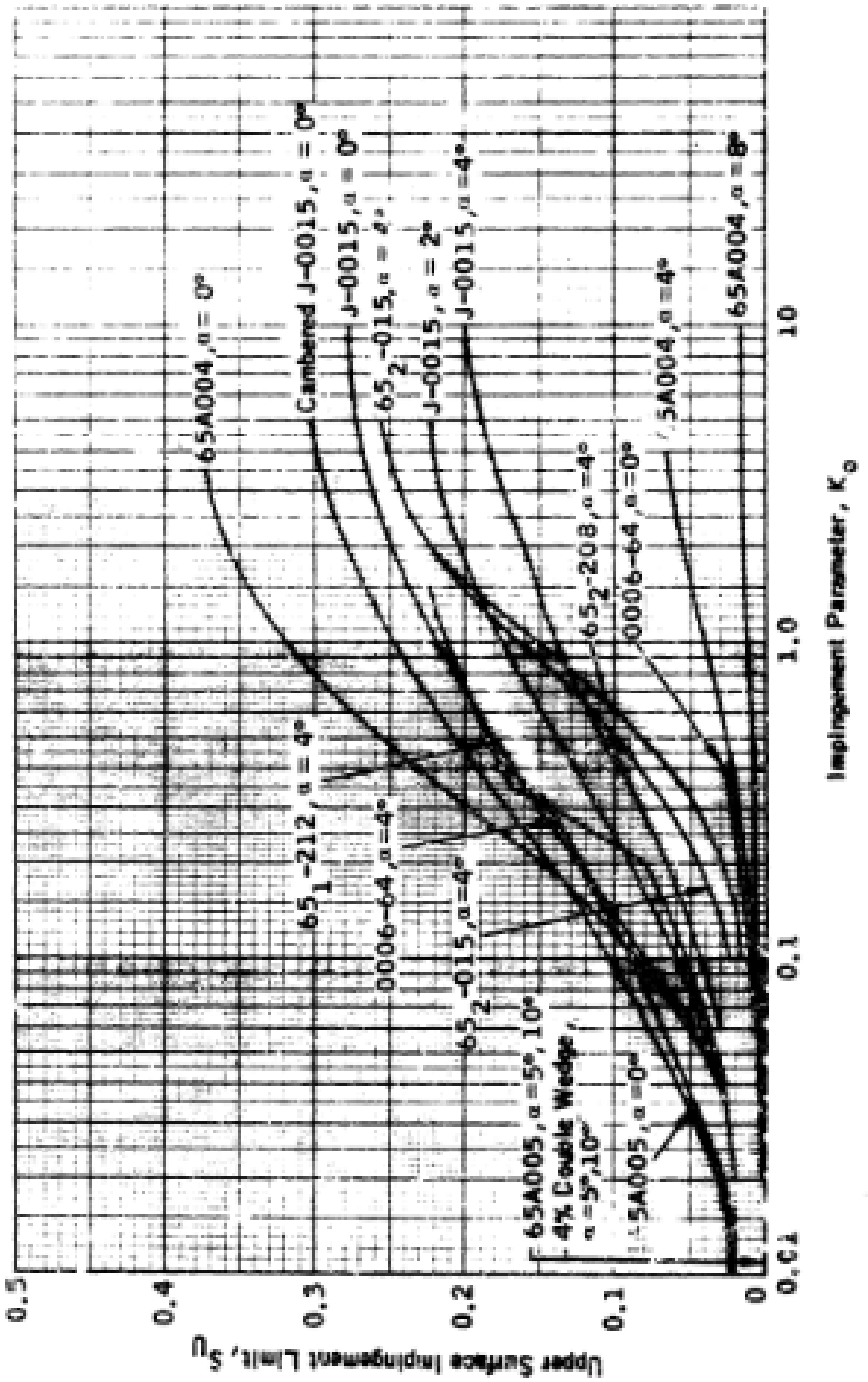

Fig. B.3: Impingement Limit on the Upper Surface of Several Airfoils Versus K_0 for $\alpha = 0, 2, 4, 5, 8 and 10°$(Theoretical Data) [22]

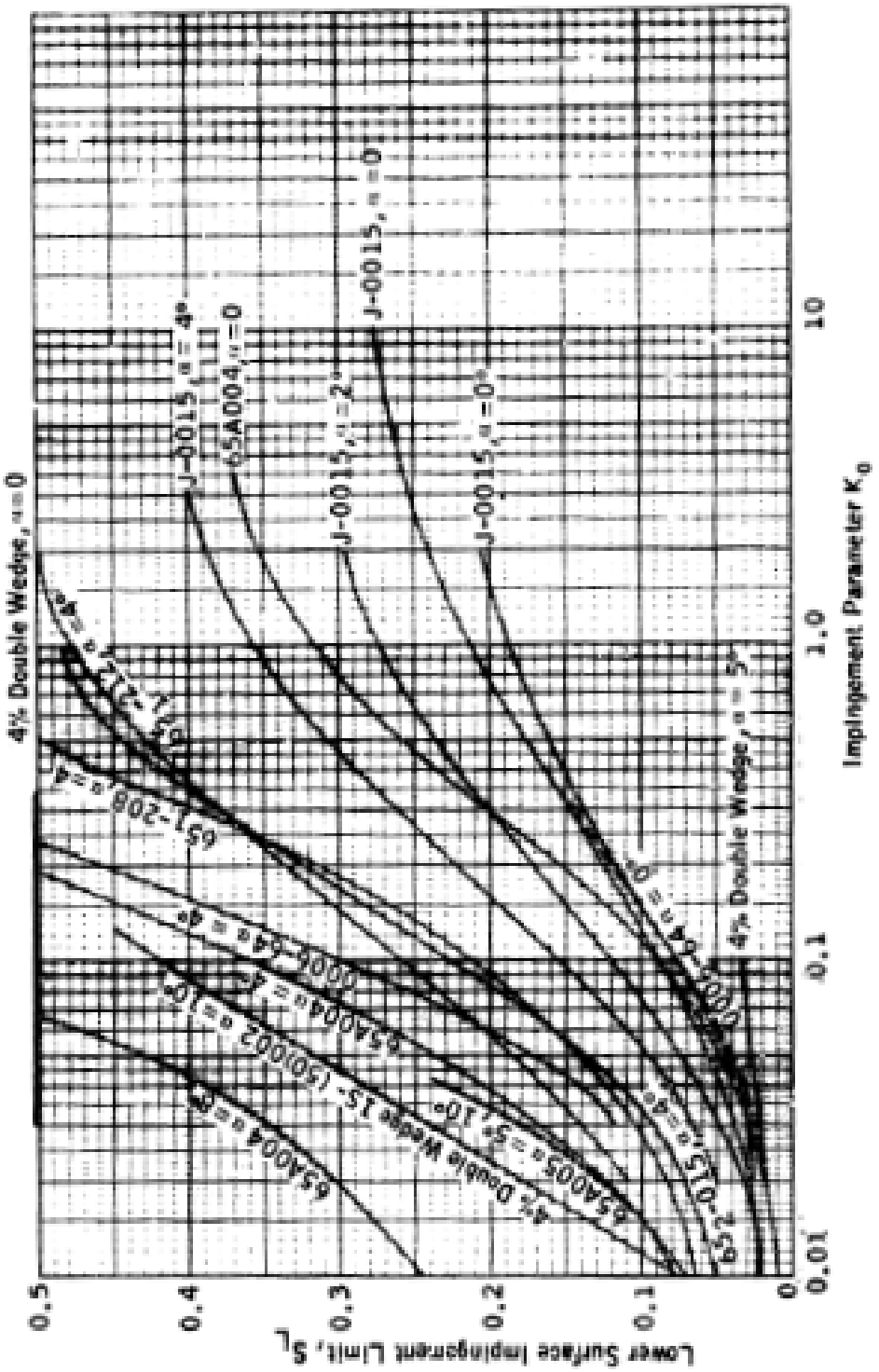

Fig. B.4: Impingement Limit on the Lower Surface of Several Airfoils Versus K_0 for $\alpha = 0, 2, 4, 5, 8 and 10°$(Theoretical Data) [22]

Appendix C

LHR Standard Instruments Departure/Arrival Charts

C.1 LHR/EGLL Standard Departure Chart

C.2 EHAM/AMS Standard Terminal Arrival Chart

STANDARD DEPARTURE CHART - INSTRUMENT (SID) - ICAO

DISTANCES IN NAUTICAL MILES
BEARINGS, TRACKS AND RADIALS ARE MAGNETIC
ALTITUDES AND ELEVATIONS ARE IN FEET

LONDON HEATHROW
BROOKMANS PARK 7F 7G 6J 5K

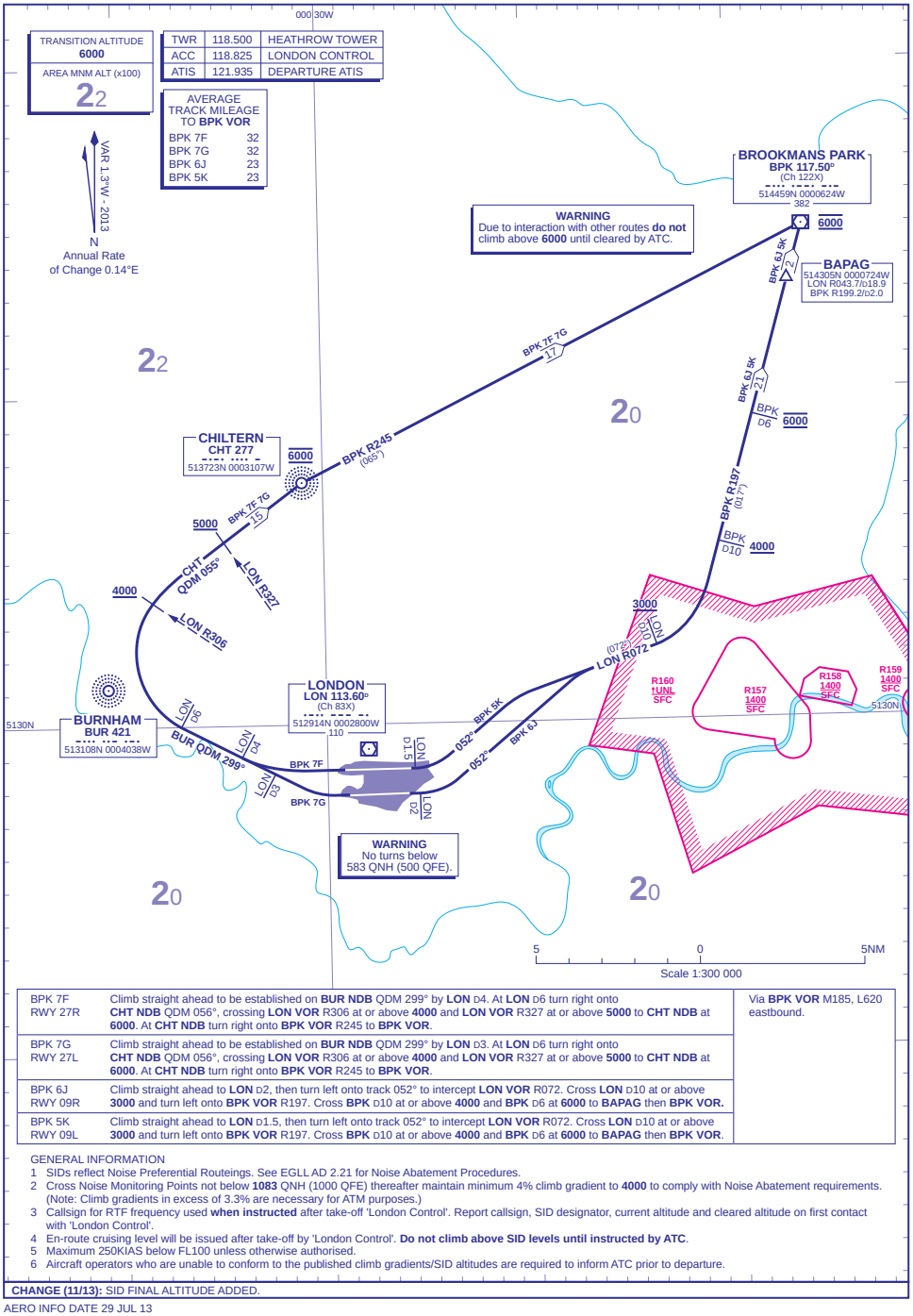

BPK 7F RWY 27R	Climb straight ahead to be established on **BUR NDB** QDM 299° by **LON** D4. At **LON** D6 turn right onto **CHT NDB** QDM 056°, crossing **LON VOR** R306 at or above **4000** and **LON VOR** R327 at or above **5000** to **CHT NDB** at **6000**. At **CHT NDB** turn right onto **BPK VOR** R245 to **BPK VOR**.	Via **BPK VOR** M185, L620 eastbound.
BPK 7G RWY 27L	Climb straight ahead to be established on **BUR NDB** QDM 299° by **LON** D3. At **LON** D6 turn right onto **CHT NDB** QDM 056°, crossing **LON VOR** R306 at or above **4000** and **LON VOR** R327 at or above **5000** to **CHT NDB** at **6000**. At **CHT NDB** turn right onto **BPK VOR** R245 to **BPK VOR**.	
BPK 6J RWY 09R	Climb straight ahead to **LON** D2, then turn left onto track 052° to intercept **LON VOR** R072. Cross **LON** D10 at or above **3000** and turn left onto **BPK VOR** R197. Cross **BPK** D10 at or above **4000** and **BPK** D6 at **6000** to **BAPAG** then **BPK VOR.**	
BPK 5K RWY 09L	Climb straight ahead to **LON** D1.5, then turn left onto track 052° to intercept **LON VOR** R072. Cross **LON** D10 at or above **3000** and turn left onto **BPK VOR** R197. Cross **BPK** D10 at or above **4000** and **BPK** D6 at **6000** to **BAPAG** then **BPK VOR**.	

GENERAL INFORMATION
1 SIDs reflect Noise Preferential Routeings. See EGLL AD 2.21 for Noise Abatement Procedures.
2 Cross Noise Monitoring Points not below **1083** QNH (1000 QFE) thereafter maintain minimum 4% climb gradient to **4000** to comply with Noise Abatement requirements. (Note: Climb gradients in excess of 3.3% are necessary for ATM purposes.)
3 Callsign for RTF frequency used **when instructed** after take-off 'London Control'. Report callsign, SID designator, current altitude and cleared altitude on first contact with 'London Control'.
4 En-route cruising level will be issued after take-off by 'London Control'. **Do not climb above SID levels until instructed by ATC**.
5 Maximum 250KIAS below FL100 unless otherwise authorised.
6 Aircraft operators who are unable to conform to the published climb gradients/SID altitudes are required to inform ATC prior to departure.

CHANGE (11/13): SID FINAL ALTITUDE ADDED.

AERO INFO DATE 29 JUL 13

Fig. C.1: LHR Standard Instruments Departure Chart [25]

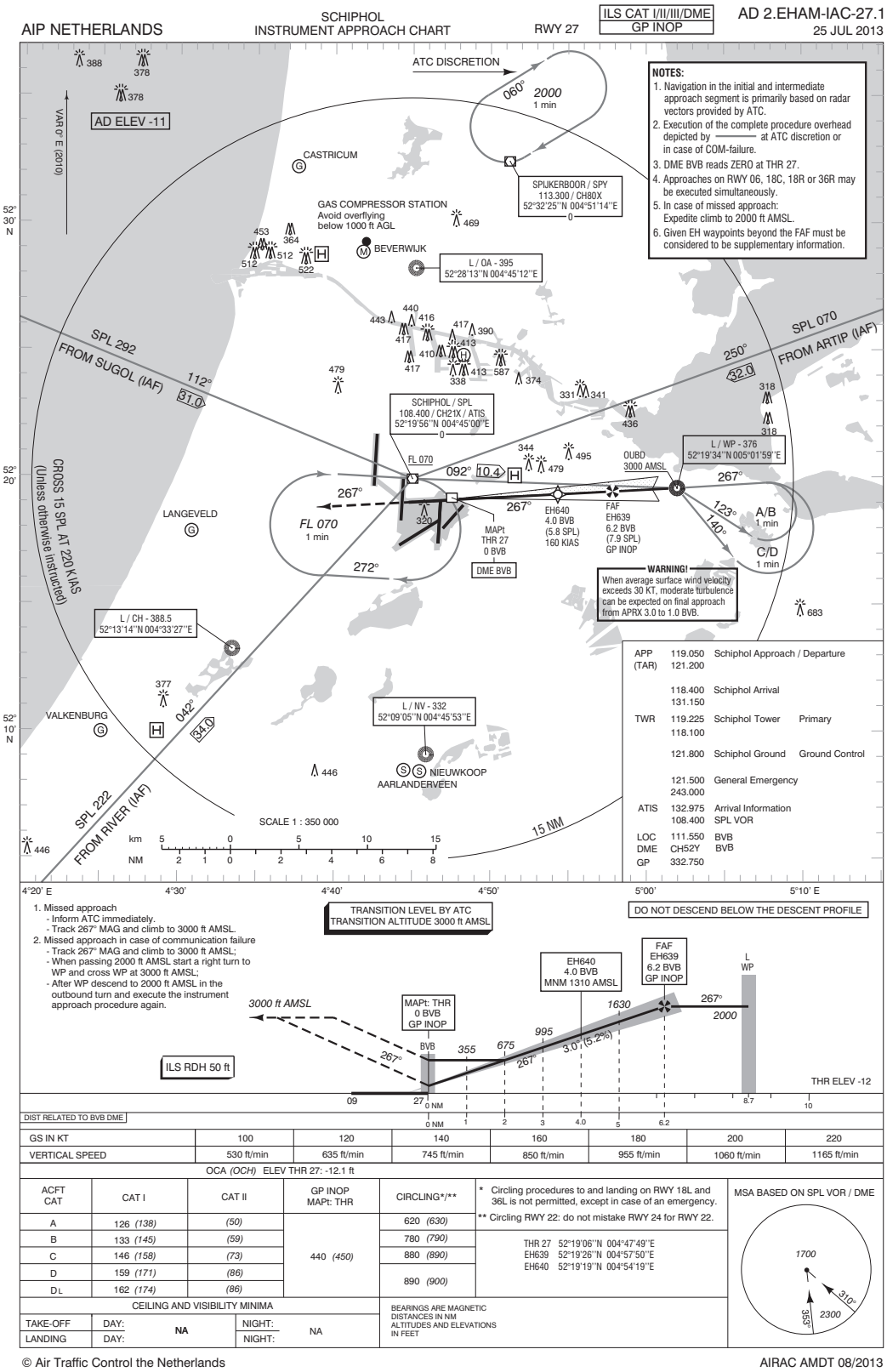

Fig. C.2: EHAM/AMS Standard Terminal Arrival Chart [26]

Appendix D

Benefits of the Research to the Nigerian Air Force

D.1 Nigerian Air Force Research and Development

The author is a member of the Nigerian Air Force (NAF) research and development team. He participated in the design and development of the AMEBO and GULMA UAVs. Research training at doctoral level in aircraft systems will advance the authors contribution in the numerous R&D projects in the NAF.

D.2 Contributions to the Aerospace Engineering in the NAF

The author has served for 16 years as an aircraft engineer in the NAF before embarking on the PhD training at Cranfield University. His field experience couple with the new skills acquired during the PhD training will be a great asset to the NAF. The author can serve as an aircraft engineering consultant in addition to his routine duties. In the field, over 70% of first line to third line maintenance work is on aircraft systems. He can import some of the field maintenance issues into AFIT research centre as researchable subjects. This will yield higher aircraft availability and operational capability.

D.3 Air Force Institute Technology Accreditation and Services

The author teaches Aircraft Systems/Airframe Technology, Computer Aided Design (CAD) and, Aviation/Airline Maintenance and Management at the Air Force Institute of Technology (AFIT), Kaduna, Nigeria. A doctoral degree in this area of Aerospace engineering is a requirement for accrediting Airframe Systems/Technology and other courses for graduate and postgraduate trainings at AFIT by the Nigerian University Commission (NUC) and the Nigerian Board for Technical Education (NBTE). With PhD training in aerospace engineering, the author will produce high level results and the quality of NAF aircraft engineers and technicians produce at AFIT will significantly increase. In addition, the experience acquired in Cranfield University while acting as teaching assistant will be of great benefit to the author's teaching career.

Appendix E

Publications and Reports by the Author

E.1 Journal Publications

1. Shinkafi, A. and Lawson, C. (2014), Development of a Tool for Simulating Aircraft Performance for Trajectory Optimisation in the Presence of Icing Conditions, Proceedings of the Institution of Mechanical Engineers, Part G: Journal of Aerospace Engineering, June 2015; vol. 229, 8: pp. 1464-1484., first published on October 10, 2014.

2. Shinkafi, A. and Lawson, C. (2014), "Enhanced Method of Conceptual Sizing of Aircraft Electro-Thermal De-icing System", International Journal of Mechanical, Aerospace, Manufacturing, Industrial Science and Engineering, vol. 8, no. 6, pp. 1004-1011.

3. Shinkafi, A. and Lawson, C. (2013), "Evaluating Inflight Ice Protection Methods for Applications on Next Generation Aircraft", Journal of Aerospace Engineering and Technology, , no. 2231-038X.

E.2 Conference

1. Seresinhe, R., Lawson, C., Shinkafi, A., Quaglia, D. and Madani, I. (2014), "Airframe Systems Power Off-take Modelling in More-Electric Large Commercial Aircraft for use in Trajectory Optimisation", 29th Conference of the International Council of the Aerospace, 7-12 Sep, St. Petersburg, ICAS, St. Petersburg, Russia.

E.3 Unpublished Internal Reports

1. Shinkafi, A. Atmospheric/Weather Model: Call for Proposal, JTI Clean Sky, SGO, November 2012

2. Shinkafi, A. Energy Management Model for Technology Evaluator (TE): Electrical Ice Protection Model Specification, Work Package 2.3.4.3, Clean Sky, 31 May 2011

3. Shinkafi, A. Energy Management Model for the SGO: Ice Protection System Model Requirements, WP3.1: O-3.1-40-a, Cleans Sky, Technology Evaluator, 03 February 2011

4. Shinkafi, A. Energy Management Model for the SGO: Bleed Ice Protection Model Specification, Work Package 2.3.4.3, Clean Sky, 09 January 2011

Appendix F

Author's Biography

Ahmed is an officer of the Nigerian Air Force (NAF) with the substantive rank of Group Captain. He is decorated with the Forces Service Star, Meritorious Service Star, Nigerian Golden Jubilee and the United Nations (UN) service medals. Ahmed obtained B.Eng (Mech), 2nd Class upper division from the Nigerian Defence Academy in 1994, and was commissioned into the NAF same time. He attended the junior staff course (JD50/2000) and senior division course (SC27) both at the Armed Forces Command and Staff College, Jaji, Nigeria. Ahmed attended the aeromedical equipment course and UN Junior Officers Course in the USA (1999) and Sweden (UNJOCII/2000) respectively. Ahmed has masters degree in Aerospace Vehicle Design (MSc AVD) with A-grade from Cranfield University, 2008/9. Ahmed has working experience on MiG-21 fighter jet, ABT-18 trainer aircraft and is type-rated on Do-228 light trasport aircraft. The major appointments held pertaining to engineering include, member NAF OLE project, lecturer AFIT, 2009 to date; Engineering Control Officer (ECO) 333 Log Gp, 2007-8; Assistant Force Communication Officer, UN mission in Sierra Leone (UNAMSIL), 2003-4; and Project Manager, Armed Forces/German Technical Assistance Group workshop Abuja from 2001-2. Ahmed teaches Aircraft Systems/Airframe Technology, Computer Aided Design (CAD) and, Aviation/Airline Maintenance and Management at the Air Force Institute of Technology (AFIT), Kaduna, Nigeria.

Ahmed participated in the design and production of the AMEBO and GULMA UAVs. After completing in house training courses, Ahmed was accorded 'Recognised Teacher' status by the Senior Appointments Committee of Cranfield University from 2010-16 which enables him to supervise and mark MSc theses. In addition to his PhD research work, Ahmed acted as teaching assistant for Computer Aided Design software (CATIA) in Aerospace Engineering Division in the period 2012 -14, and researcher in the EU Clean Sky programme from 2010 - 13. These two secondary duties improved Ahmed's understanding of advance aircraft systems design and application. The Clean Sky project was an opportunity for Ahmed to learn directly from industrial partners such as AIRBUS, THALES, NLR, DLR and EADS IW. Ahmed is a member of the Institution of Engineering and Technology (IET) with MIET designation, and a Chartered Engineer (CEng) registered by the UK Engineering Council (reg. no. 617900). Ahmed is also a prospective member of the Nigerian Society of Engineering.

Ahmed's hobbies include horse riding and playing Table Tennis. He was the president of the Cranfield University Table Tennis club from 2011-13. Ahmed received two awards from the Cranfield Students Association for his contribution and service to the club. He is happily married with children.